Journal Information

Maejo International Journal of Science and Technology (ISSN 1905-7873 © 2014), the international journal for preliminary communications in Science and Technology is the first peer-refereed scientific journal of Maejo University (www.mju.ac.th). Intended as a medium for communication, discussion, and rapid dissemination of important issues in Science and Technology, articles are published online in an open access format, which thereby gives authors the chance to communicate with a wide range of readers in an international community.

Publication Information

MIJST is published triannually. Articles are available online and can be accessed free of charge at http://www.mijst.mju.ac.th. Printed and bound copies of each volume are produced and distributed to selected groups or individuals.

Abstracting/Indexing Information

MIJST is covered and cited by Science Citation Index Expanded, SCOPUS, Journal Citation Reports/Science Edition, Zoological Record, Directory of Open Access Journals (DOAJ), CAB Abstracts, ProQuest, Google Scholar and EBSCO.

Contact Information

Editorial office: Maejo International Journal of Science and Technology (MIJST), 1st floor, Orchid Building, Maejo University, San Sai, Chiang Mai 50290, Thailand

Tel: +66-53-87-3880; Fax: +66-53-49-8133
E-mail: duang@mju.ac.th

MAEJO INTERNATIONAL JOURNAL OF SCIENCE AND TECHNOLOGY

MAEJO INTERNATIONAL JOURNAL OF SCIENCE AND TECHNOLOGY

The International Journal for the Publication of Preliminary Communications in Science and Technology

http://www.mijst.mju.ac.th
ISSN 1905-7873

MAEJO INTERNATIONAL JOURNAL
OF SCIENCE AND TECHNOLOGY

Volume 8, Issue 3 September-December 2014

CONTENTS

http://www.mijst.mju.ac.th
ISSN 1905-7873

http://www.mijst.mju.ac.th
ISSN 1905-7873

MAEJO INTERNATIONAL JOURNAL
OF SCIENCE AND TECHNOLOGY

Volume 8, Issue 3 September-December 2014

Author Index

Instructions for Authors

A proper introductory e-mail page containing the title of the submitted article and certifying its originality should be sent to the editor (Duang Buddhasukh, e-mail: duang@mju.ac.th). The manuscript proper together with a list of suggested referees should be attached in separate files. The list should contain at least 5 referees with appropriate expertise. Three referees should be non-native from 3 different countries. Each referee's academic/professional position, scientific expertise, affiliation and e-mail address must be given. The referees should not be affiliated to the same university/institution as any of the authors, nor should any two referees come from the same university/institution. The editorial team, however, retain the sole right to decide whether or not the suggested referees are approached.

Failure to conform to the above instructions will result in non-consideration of the submission.

Please also ensure that English and style is properly edited before submission. UK style of spelling should be used. Authors who would like to consult a professional service can visit www.proof-reading-service.com, www.editage.com, www.bioedit.co.uk (bioscience and medical papers), www.bioscienceeditingsolutions.com, www.scribendi.com, www.letpub.com, www.papersconsulting.com, www.stickleredit ing.com, Cambridge Proofreading (http://proofreading.org/), www.ProofreadingServices.com, www.horizonproofreaders.org, www.manuscript-proofreding.com, Quality Proofreading, Help.Plagtracker, www.ninjaessays.com/editing/, http://bid4papers.com/editing-services.html or www.enago.com.

Important : Manuscript with substandard English and style will not be considered.

Warning : Plagiarism (including self-plagiarism) may be checked for at *the last* stage of processing and, if detected, will result in a rejection and blacklisting.

Manuscript Preparation

Manuscripts must be prepared in English using a word processor. MS Word for Macintosh or Windows, and .doc or .rtf files are preferred. Manuscripts may be prepared with other software provided that the full document (with figures, schemes and tables inserted into the text) is exported to a MS Word format for submission. Times or Times New Roman font is preferred. The font size should be 12 pt and the line spacing 'at least 17 pt'. A4 paper size is used and margins must be 1.5 cm on top, 2.0 cm at the bottom and 2.0 cm on both left and right sides of the paper. Although our final output is in .pdf format, authors are asked NOT to send manuscripts in this format as editing them is much more complicated. Under the above settings, a manuscript submitted should not be longer than **15 pages** for a full paper or **20 pages** for a review paper.

A template file may be downloaded from the *Maejo Int. J. Sci. Technol*. homepage. (DOWNLOAD HERE)

Authors' full mailing addresses, homepage addresses, phone and fax numbers, and e-mail addresses homepages can be included in the title page and these will be published in the manuscripts and the Table of Contents. The corresponding author should be clearly identified. It is the corresponding author's responsibility to ensure that all co-authors are aware of and approve of the contents of a submitted manuscript.

A brief (200 word maximum) Abstract should be provided. The use in the Abstract of numbers to identify compounds should be avoided unless these compounds are also identified by names.

A list of three to five keywords must be given and placed after the Abstract. Keywords may be single words or very short phrases.

Although variations in accord with contents of a manuscript are permissible, in general all papers should have the following sections: Introduction, Materials and Methods, Results and Discussion, Conclusions, Acknowledgments (if applicable) and References.

Authors are encouraged to prepare Figures and Schemes in colour. Full colour graphics will be published free of charge.

Tables and Figures should be inserted into the main text, and numbers and titles supplied for all Tables and Figures. All table columns should have an explanatory heading. To facilitate layout of large tables, smaller fonts may be used, but in no case should these be less than 10 pt in size. Authors should use the Table option of MS Word to create tables, rather than tabs, as tab-delimited columns are often difficult to format in .pdf for final output.

Figures, tables and schemes should also be placed in numerical order in the appropriate place within the main text. Numbers, titles and legends should be provided for all tables, schemes and figures. Chemical structures and reaction schemes should be drawn using an appropriate software package designed for this purpose. As a guideline, these should be drawn to a scale such that all the details and text are clearly legible when placed in the manuscript (i.e. text should be no smaller than 8-9 pt).

For bibliographic citations, the reference numbers should be placed in square brackets, i.e. [ ], and placed before the punctuation, for example [4] or [1-3], and all the references should be listed separately and as the last section at the end of the manuscript.

Format for References

Journal :

1. D. Buddhasukh, J. R. Cannon, B. W. Metcalf and A. J. Power, "Synthesis of 5-n-alkylresorcinol dimethyl ethers and related compounds via substituted thiophens", *Aust. J. Chem*., **1971**, *24*, 2655-2664.

Text :

2. A. I. Vogel, "A Textbook of Practical Organic Chemistry", 3rd Edn., Longmans, London, **1956**, pp. 130-132.

Chapter in an edited text :

3. W. Leistritz, "Methods of bacterial reduction in spices", in "Spices: Flavor Chemistry and Antioxidant Porperties" (Ed. S. J. Risch and C-T. Ito), American Chemical Society, Washington, DC, **1997**, Ch. 2.

Thesis / Dissertation :

4. W. phutdhawong, "Isolation of glycosides by electrolytic decolourisation and synthesis of pentinomycin", *PhD Thesis*, **2002**, Chiang Mai University, Thailand.

Patent :

5. K. Miwa, S. Maeda and Y. Murata, "Purification of stevioside by electrolysis", *Jpn. Kokai Tokkyo Koho 79 89,066* **(1979).**

Proceedings :

6. P. M. Sears, J. Peele, M. Lassauzet and P. Blackburn, "Use of antimicrobial proteins in the treatment of bovine mastitis", Proceedings of the 3rd International Mastitis Seminars, **1995**, Tel-Aviv, Israel, pp. 17-18.

Websites :

7. S. Simon, "What is an odds ratio?", **2008**, http://www.childrensmercy.org/stats/definitions/or.htm (Accessed: October 2011).

Manuscript Revision Time

Authors who are instructed to revise their manuscript should do so within **45** days. Otherwise the revised manuscript will be regarded as a new submission.

Manuscript Processing Time

As a result of a large number of submissions, there may be a long delay in the evaluation or publication of a paper. A duration of at least 6-8 months between submission and acceptance (or rejection) can normally be expected.

Maejo International Journal of Science and Technology

ISSN 1905-7873
Available online at www.mijst.mju.ac.th

Full Paper

Phytoremediation of anthracene- and fluoranthene-contaminated soil by *Luffa acutangula*

Khanitta Somtrakoon [1, *], Waraporn Chouychai [2] and Hung Lee [3]

[1] Department of Biology, Faculty of Science, Mahasarakham University, Kantharawichai, Mahasarakham, Thailand 44150
[2] Biology Programme, Faculty of Science and Technology, Nakhonsawan Rajabhat University, Nakhonsawan, Thailand 60000
[3] School of Environmental Sciences, University of Guelph, Guelph, Ontario, N1G 2W1, Canada

* Corresponding author, e-mail: khanitta.s@msu.ac.th

Received: 18 September 2013 / Accepted: 26 August 2014 / Published: 4 September 2014

Abstract: Phytoremediation of soil contaminated with anthracene and fluoranthene, either alone or together, by ridge gourd (*Luffa acutangula*) was investigated through laboratory pot experiments in a greenhouse for 45 days. The initial concentration of anthracene or fluoranthene was 100 mg kg^{-1} when each was spiked alone. When spiked together, the initial concentration of each hydrocarbon was 50 mg kg^{-1}. The ridge gourd grew normally in anthracene-contaminated soil based on assessment of shoot growth at the end of the experiment. Fluoranthene spiked either alone or together with anthracene was toxic to the plant as shown by significantly reduced shoot and root growth, especially on day 45 after transplantation. Planting of ridge gourd was more effective in decreasing the amount of anthracene and fluoranthene from soil than un-planted control during the 45-day experiment. Only 0.5-1.8% and 3.1-14.1% of anthracene and fluoranthene respectively were detected in planted soil on day 45. In contrast, 27.7-48.2% and 46.9-73.8% of anthracene and fluoranthene respectively, spiked alone or together, remained in the control un-planted soil during the same period. The two aromatic hydrocarbons were neither detected in the shoot nor root tissue of the ridge gourd, which suggests that phytostimulation may be the most likely mechanism by which these hydrocarbons were removed from soil.

Keywords: phytoremediation, anthracene, fluoranthene, Cucurbitaceae, ridge gourd, *Luffa acutangula*

INTRODUCTION

The presence of polycyclic aromatic hydrocarbons (PAHs) in the environment is of serious concern due to their mutagenic and carcinogenic potential. The hydrophobicity of PAHs and their strong sorption onto the organic portion of soil particles contribute to their recalcitrance and persistence in the environment. While PAHs are found in air, water, soil and vegetation, soil and sediment are considered to be the ultimate sink of PAH contaminants in the environment [1, 2]. PAH contamination in soil increases the exposure risk of these compounds to living organisms. PAH contamination has been reported worldwide including Thailand. For example, the total concentration of PAHs bearing 3-7 rings was found to range between 6-8400 ng g^{-1} in surface sediment (dry weight) of the coastal and riverine areas in the Gulf of Thailand and the mouth of Chao Praya River [3]. Anthracene and fluoranthene are selected as model PAHs in this study due to their toxic effect on various organisms [4-6]. These PAHs are listed as hazardous pollutants by the United States Environmental Protection Agency (USEPA.) [1, 7].

Phytoremediation refers to the use of plants and their associated microorganisms to clean up polluted areas. This technique can be effective for the remediation of large areas contaminated with diffuse pollutants [7]. Some plants in Pocaceae and Leguminaosae have been tested with some degree of success for remediation of soil contaminated with anthracene, fluoranthene and other PAHs. For example, the residual fluoranthene in soil planted with ryegrass decreased from 88.7 to 26.4 mg kg^{-1} in 70 days [8]. Ryegrass also reduced the amount of anthracene and fluoranthene in a historically PAH-contaminated site from 6.0 to 2.2 and 103.5 to 38.6 mg kg^{-1} respectively, after 18 months of cultivation [9]. Leguminosae such as alfalfa and white clover significantly promoted the degradation of pyrene in soil: only 191.55 and 183.58 mg kg^{-1} (from initial concentration of 321.42 mg kg^{-1}) remained in soil after 70 days of cultivation with alfalfa and white clover respectively, as compared to 278.74 mg $kg^{-1}$of pyrene remaining in unplanted soil [10]. Some of the other plants used in PAH phytoremediation include *Mimosa monancistra*, *Festuca arundinacea*, *Psophocarpus tetragonolobus*, *Zea mays*, *Zostera marina* and *Vicia faba* [11-15]. The extent of PAH removal by planting usually was greater than the unplanted control, but the efficiency may vary depending on the plant species, soil texture, soil pH and type of PAHs.

Plants of the Cucurbitaceae family have been used to remediate some organic pollutants such as PCBs, DDT, DDE and heptachlor [16-18]. For example, *Lagenaria siceraria* cultivar Hyotan was shown to decrease heptachlor epoxide from 0.376 to 0.050 μg g^{-1} dry soil [16]. Somtrakoon et al. [15] reported that cucumber (*Cucumis sativus*) was effective in removing anthracene and fluoranthene from soil. However, this plant was not tolerant of their toxicity and died after 25-30 days of transplantation. Other plants in the Cucurbitaceae family such as *Cucurbita pepo* and *Legenaria siceraria* have also been observed to accumulate some soil contaminants such as anthracene, fluoranthene, heptachlor epoxide and dioxin-like compounds [16, 17, 19]. Although, the toxicity of PAHs on ridge gourd (*Luffa acutangula*), another plant in the Cucurbitaceae family, has been reported [20], to our knowledge it has not been used to remediate PAH-contaminated sites. In this study we therefore undertake to investigate the potential of ridge gourd for remediating PAH-contaminated soil.

MATERIALS AND METHODS

Soil Preparation

Soil with no previous history of anthracene and fluoranthene contamination as verified by GC-MS analysis (described below) was obtained from Kookaew Temple, Kantharawichai district, Mahasarakham province, Thailand. The soil was air dried at room temperature (29±1ºC) for at least 72 hr to constant weight before use. A sample of this soil was sent to Central Laboratory (Thailand) Co. for physical and chemical characterisation. It was of clay texture with a pH of 8.1 and electrical conductivity of 109.5 μs cm^{-1}, and contained 2.4% organic matter, 0.29% total nitrogen and 58.38 mg kg^{-1} available phosphorus.

About 20% of the soil was spiked with anthracene (98%, Fluka), fluoranthene (99%, Fluka) or a mixture of the two dissolved in dichloromethane. After thorough mixing, the solvent was allowed to evaporate inside a fume hood at room temperature (29±1°) for 48 hr. Then the spiked soil was added to the remaining 80% of unspiked soil and mixed thoroughly. The initial concentration of anthracene or fluoranthene in single-PAH-spiked soil was 100 mg kg^{-1}, while in mixed-PAH-spiked soil the concentration was 50 mg kg^{-1} of each. Finally, the spiked soil samples were transferred to pots.

Seedling Preparation

Commercial seeds of ridge gourd (*Luffa acutangula*) were obtained from Chia Tai Group Co., Bangkok. Seeds were rinsed with sterile distilled water and immersed in distilled water for 3 hr. They were then germinated in moist soil spiked with anthracene, fluoranthene or a mixture of the two in experimental pots and kept at 29±1° in a plant nursery which received natural sunlight. After 10 days, healthy plant seedlings with comparable sizes were picked and transplanted in pots with soil containing the same PAH or PAH combination as that used for germination.

Experimental Design

Pot experiments were performed in a plant nursery from March to May, 2012. In single and mixed PAH experiments, each pot containing spiked soil (1 kg dry weight) was planted individually with a 10-day-old seedling. Pots with ridge gourd seedlings in unspiked soil served as control. Other controls were soil spiked with anthracene, fluoranthene or their mixture but without any plants. Three independent replicates of each treatment were prepared in a completely randomised design and the total number of pots were 21. The detail of each treatment is described as follows:

1) Anthracene-spiked soil planted with ridge gourd - 3 pots
2) Fluoranthene-spiked soil planted with ridge gourd - 3 pots
3) Anthracene+fluoranthene-spiked soil planted with ridge gourd - 3 pots
4) Anthracene-spiked soil without ridge gourd planting - 3 pots (control for anthracene removal)
5) Fluoranthene-spiked soil without ridge gourd planting - 3 pots (control for fluoranthene removal)
6) Anthracene+fluoranthene-spiked soil without ridge gourd planting - 3 pots (control for anthracene and fluoranthene removal)
7) Unspiked soil planted with ridge gourd - 3 pots (control for plant growth)

All pots were supplemented periodically with sterile distilled water to maintain the water content of the soil at about 60% for 45 days. The placement of pots in the nursery was changed randomly every week. One gram (dry weight) each of the rhizospheric soil and bulk soil from planted soil were carefully collected on day 20 and 45 for analysis of anthracene and fluoranthene

concentrations by gas chromatography - mass spectrometry (GC-MS). Soil samples from unplanted control treatments were also collected and analysed. The plants from single and mixed PAH pots were sampled on day 20 and 45 to determine the length, fresh weight and dry weight of shoot (including leaves and stem) and root. During removal of the plants from soil, the root was shaken gently to dislodge any loose soil into the rest of the soil in the pot and this was referred to as the bulk soil. The rhizospheric soil referred to the soil which remained tightly bound to the root system, and it was removed from the plant root by shaking in a plastic bag after a short period of air drying (about 12 hr). The root debris in the collected rhizospheric soil was removed by sieving.

PAH Extraction and Analytical Procedures

One gram of dried, PAH-containing soil was mixed with anhydrous sodium sulfate powder in 1:1 ratio. Fluorene (purity 99%, Fluka) was then added as internal standard (50 μL of 200 mg L^{-1} fluorene stock solution prepared in dichloromethane). The mixture was extracted with 180 mL of dichloromethane for 8 hr in a Soxhlet extractor and the solution obtained was evaporated at 60^{o} to near dryness under reduced pressure. Anthracene and fluoranthene in the shoot and root of each plant were extracted in the same way. The shoot or root was dried in an incubator at 60° to constant weight before mixing with anhydrous sodium sulfate. Anthracene and fluoranthene concentrations in the dichloromethane extracts were determined using a gas chromatograph (Shimadzu GC AOC-5000) equipped with a mass spectroscopic detector (Shimadzu MS-QP2010) as described by Somtrakoon et al. [15].

Statistical Analysis

Per cent of each PAH remaining was expressed as the mean ± SD. One-way ANOVA was used to test for statistical significance among treatments. Subsequent multiple comparisons of means were performed using the Turkey comparison method. Statistical significance was accepted at $P<0.05$.

RESULTS

General Health of Ridge Gourd Grown in PAH-Contaminated Soil

In unspiked control pots, the ridge gourd grew well, flourished and produced fruits between day 40-45 of transplantation. In soil spiked with anthracene, fluoranthene or anthracene + fluoranthene, the ridge gourd grew, but did not produce fruits until about 45 days after transplantation. The toxic effects of these PAHs were mostly manifested in the reduced shoot length. The shoot length of ridge gourd grown in PAH-spiked soil was shorter than that grown in unspiked soil (Figures 1a and 1b).

Shoot Growth and Root Growth of Ridge Gourd

The ridge gourd showed delayed growth in PAH-spiked soils, as evidenced by the shorter length and lower fresh and dry weight of its shoots, compared to those of the control plants on day 20 (Table 1). In anthracene-spiked soil, however, the growth of the ridge gourd caught up such that by day 45, the shoot length was similar to that of the control plant grown in unspiked soil, and the shoot fresh and dry weights also increased to values approaching those of the control plant. In contrast, in soil spiked with fluoranthene or anthracene + fluoranthene, the shoot length remained significantly shorter than that of the control plant on day 45 (Table 1). The shoot length of ridge gourd grown in fluoranthene and anthracene+fluoranthene mixture was only 68.7 and 87.0 cm

respectively. In comparison, the shoot length of the control plant in unspiked soil was 106.2 cm. This is also reflected in the significantly lower shoot fresh weight (4.8 g and 5.6 g) and shoot dry weight (0.8 g and 0.8 g) of the plants grown for 45 days in soil with fluoranthene and anthracene+fluoranthene mixture respectively. In comparison, shoot fresh weight and dry weight of the control plant were 14.8 g and 2.6 g respectively) (Table 1).

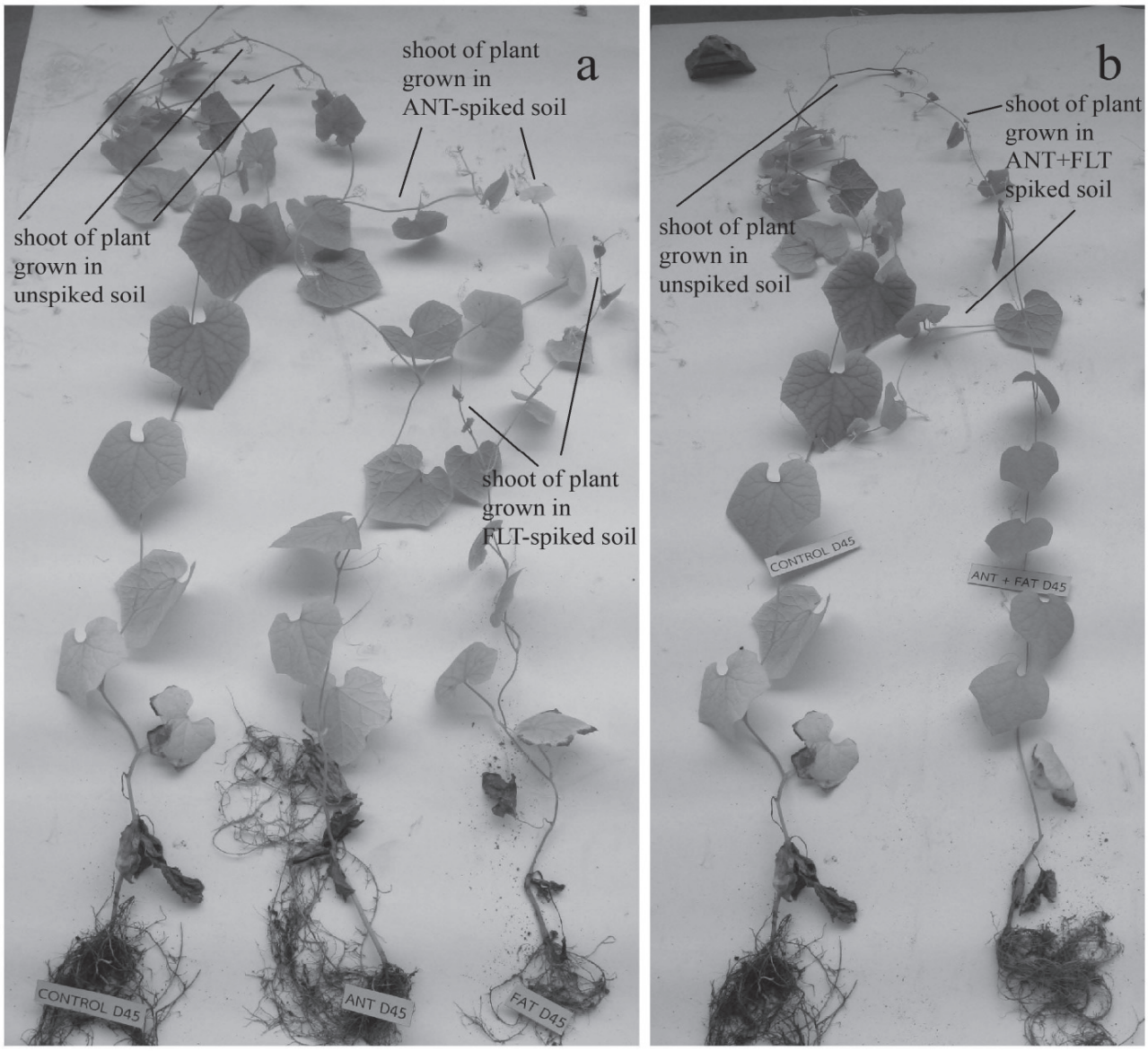

Figure 1. Comparative shoot growth of ridge gourd after 45 days of transplantation in: (a) unspiked soil (left), anthracene-spiked soil (middle), and fluoranthene-spiked soil (right); (b) unspiked soil (left) and anthracene+fluoranthene-spiked soil (right) (ANT = anthracene, FLT = fluoranthene)

Table 1. Shoot length, shoot fresh weight and shoot dry weight of ridge gourd grown in anthracene- and fluoranthene-spiked soil

Soil	Day 20			Day 45		
	Shoot length (cm)	Shoot fresh weight (g)	Shoot dry weight (g)	Shoot length (cm)	Shoot fresh weight (g)	Shoot dry weight (g)
Unspiked (control)	111.1 ± 3.8a	12.9 ± 0.9a	1.2 ± 0.2a	106.2 ± 2.1a	14.8 ± 3.0a	2.6 ± 0.4a
Anthracene-spiked	33.0 ± 2.2c	3.6 ± 1.2b	0.4 ± 0.1b	108.3 ± 3.0a	11.2 ± 0.1a	2.0 ± 0.3a
Fluoranthene-spiked	52.6 ± 2.8b	3.2 ± 0.5b	0.5 ± 0.1b	68.7 ± 8.8c	4.8 ± 0.4b	0.8 ± 0.1b
Anthracene+Fluoranthene-spiked	28.6 ± 3.0c	2.2 ± 0.8b	0.3 ± 0.0b	87.0 ± 5.8cb	5.6 ± 1.2b	0.8 ± 0.2b

Note: Different letters denote significant difference ($P<0.05$) in the same column.

Table 2. Root length, root fresh weight and root dry weight of ridge gourd grown in anthracene- and fluoranthene-spiked soil

Soil	Day 20			Day 45		
	Root length (cm)	Root fresh weight (g)	Root dry weight (g)	Root length (cm)	Root fresh weight (g)	Root dry weight (g)
Unspiked (control)	26.1 ± 1.1a	1.7 ± 0.5a	0.09 ± 0.1a	74.5 ± 18.4a	5.8 ± 1.3a	0.4 ± 0.1a
Anthracene-spiked	24.7 ± 1.2a	0.5 ± 0.1b	0.04 ± 0.0b	55.2 ± 2.9ab	2.9 ± 0.9b	0.2 ± 0.1ab
Fluoranthene-spiked	28.5 ± 2.3a	0.6 ± 0.2b	0.03 ± 0.0b	26.7 ± 6.6c	0.8 ± 0.1b	0.1 ± 0.1b
Anthracene+Fluoranthene-spiked	21.2 ± 5.7a	0.4 ± 0.0b	0.03 ± 0.0b	31.7 ± 2.0bc	1.5 ± 0.0b	0.1 ± 0.0b

Note: Different letters denote significant difference ($P<0.05$) in the same column.

The root of ridge gourd was adversely affected when the plant was grown in PAH-contaminated soil as compared to that of control plants grown in unspiked soil. This is readily seen in the low root weight (fresh and dry) of all the plants in PAH-spiked soil on both day 20 and 45 (Table 2). As for root length, the adverse effect of the PAHs was not apparent on day 20, but by day 45 the root length of all the plants grown in PAH-spiked soil was clearly shorter than that of the control plant in unspiked soil. The most severe effect is seen in the root length, root fresh weight and root dry weight of the plant grown in fluoranthene-spiked soil, which decreased to only 26.7 cm, 0.8 g and 0.1g respectively on day 45.

Anthracene and Fluoranthene in Plant Tissues

Anthracene and fluoranthene were not detected in any of the shoot and root samples of ridge gourd grown in PAH-spiked soil on day 20 or 45 (data not shown). The detection limit was 0.4 mg kg^{-1} for each PAH by GC.

Anthracene Removal from Soil

Planting of ridge gourd in anthracene-spiked soil led to its significant removal irrespective of whether the soil was spiked with anthracene alone or in combination with fluoranthene. The rapid removal of anthracene in the planted soil was seen on day 20 when more than 87% of the spiked anthracene was removed from both the bulk and rhizospheric soils (Table 3). By day 45,

only about 0.5-1.8% of the initial anthracene remained. Anthracene in the rhizospheric soil was removed to a slightly greater extent than that in the bulk soil. In unplanted control soil, about 28-48% of the initial anthracene remained on day 45 (Table 3).

Table 3. Percentages of anthracene remaining in soil planted with ridge gourd

Treatments	% of anthracene remaining	
	Day 20	Day 45
Control (unplanted, soil spiked with ANT)	104.9 ± 21.3a	48.2 ± 0.1a*
Planted, soil spiked with ANT		
Bulk soil	12.7 ±19.0b*	1.8 ± 0.4b*
Rhizospheric soil	4.7 ± 5.7b*	1.1 ± 1.1b*
Control (unplanted, soil spiked with ANT+FLT)	66.6 ± 25.0ab	27.7 ± 32.7ab*
Planted soil spiked with ANT+FLT		
Bulk soil	4.8 ± 2.9b*	1.2 ± 0.0b*
Rhizospheric soil	3.9 ± 0.9b*	0.5 ± 0.2b*

Note: Initial concentration of anthracene (ANT) was 100 mg kg^{-1} when spiked alone and 50 mg kg^{-1} when spiked together with fluoranthene (FLT).
Different letters show significant difference ($P<0.05$) between treatments on the same column.
* Value is significantly different ($P<0.05$) from that at day 0.

Table 4. Percentages of fluoranthene remaining in soil planted with ridge gourd

Soil	% Fluoranthene remaining	
	Day 20	Day 45
Control (unplanted, spiked with FLT)	82.8 ± 40.7a	73.8 ± 15.3a
Planted, spiked with FLT		
Bulk soil	16.1 ± 11.3b*	14.1 ± 4.6b*
Rhizospheric soil	15.0 ± 1.8b*	3.1 ± 1.4b*
Control (unplanted, spiked with ANT+FLT)	84.2 ± 19.7a	46.9 ± 32.2a*
Planted, spiked with ANT+FLT		
Bulk soil	9.3 ±4.4b*	7.9 ± 3.9b*
Rhizospheric soil	8.1 ± 0.5b*	5.5 ± 3.7b*

Note: Initial concentration of fluoranthene (FLT) was 100 mg kg^{-1} when spiked alone and 50 mg kg^{-1} when spiked together with anthracene.
Different letters show significant difference ($P<0.05$) between treatments on the same column.
* Value is significantly different ($P<0.05$) from that at day 0.

Fluoranthene Removal from Soil

Fluoranthene, whether spiked alone or in combination with anthracene, was also rapidly removed from soil planted with the ridge gourd, although the extent of removal was not as fast or great compared to that for anthracene. On day 20, 8.1-16.1% of the spiked fluoranthene remained in planted soil (Table 4). By day 45, the amount of fluoranthene remaining declined further to 3.1-14.1%. The percentages of fluoranthene removal from the rhizospheric and bulk soils were not significantly different. In unplanted soil spiked with fluoranthene alone, 82.8% and 73.8% of fluoranthene remained on day 20 and 45 respectively. With fluoranthene and anthracene, the corresponding values were 84.2 and 46.9%.

DISCUSSION

Both anthracene and fluoranthene have been reported to adversely affect shoot and root growth of waxy corn, sweet corn and rice seedlings, fluoranthene being more toxic than anthracene [21]. In our study a similar toxic effect of anthracene and fluoranthene was also apparent in the decreased shoot and root lengths of ridge gourd on day 45. Some plants in the Cucurbitaceae family have been shown to stimulate PAH biodegradation in the rhizosphere, while others were reported to accumulate PAHs in their tissues [19, 22]. For example, cucumber (*Cucumis sativus*) was shown to enhance the removal of anthracene and fluorene from PAH-spiked soil [15]. The amounts of anthracene and fluorene remaining in its rhizospheric soil were only 9.5% and 4.6% respectively of the initial concentration on day 30 after transplantation. In comparison, the amounts of the two PAHs remaining in unplanted control soil on day 30 were 76.1% and 60.8% respectively. However, the plant was very sensitive to these PAH contaminants and was less healthy when grown together with winged bean (*Z. mays*) and finally died between 25-30 days after transplantation. In a different study, the rhizospheric soil of plants in the Cucurbitaceae family was found to be effective in removing a total of 16 PAH compounds, which decreased to the lowest amount of 1118.6 mg kg^{-1} from 3306 mg kg^{-1} in the control soil [22]. In another study, zucchini (*Curcubita pepo* Ravaen) planted in soil obtained from a coal gasification plant enhanced the removal of several PAHs after 90 days. The plant led to high extent of removal of fluorene (41%), anthracene (50%), fluoranthene (55%), pyrene (64%), benz(e)pyrene (60%) and benzo(k)fluoranthene (74%) (cf. 87%, 12%, 13%, 3.8%, 0% and 2.4% respectively in unplanted soil) [23].

The enhanced removal of anthracene and fluoranthene by ridge gourd observed in this study follows the same trend as shown by other plants. Kim et al. [24] reported that 89.8%, 77% and 76.1% of anthracene (initial concentration = 660-670 mg/kg) were removed from soil planted for 63 days with alfalfa, barley and tall fescue respectively. In comparison, about 72.4% was removed from unplanted soil and 71.4% from soil planted with orchard grass. In another study, planting with willow for 12 weeks led to 84% removal of fluoranthene (initial concentration = 3.3 mg/kg) from creosote-contaminated soil (cf. 75% removal in unplanted soil) [25]. In our study, the amounts of anthracene and fluoranthene removed from soil planted with ridge gourd for 45 days were more than 98.2 and 85.9% respectively (initial concentration = 100 mg/kg), while in unplanted soil the amounts removed were, respectively, 51.8 and 26.2%. Based on this results, ridge gourd could be an effective plant for PAH phytoremediation. Further studies are needed using other PAHs and by varying their concentrations to assess the plant's PAH phytoremediation potential.

In this study anthracene and fluoranthene seem to have been degraded by competent microorganisms in the rhizospheric soil of ridge gourd as well as bulk soil. While no specific microbial analysis had been done, the availability of these microorganisms in the soil is suggested

by the removal of some anthracene and fluoranthene from unplanted soil in the control pots. In the presence of the plant, the per cent degradation of anthracene and fluoranthene increased. Given that anthracene and fluoranthene were not accumulated by the plant, its cultivation in PAH-spiked soil must have provided suitable conditions for stimulating the degradation of PAHs by indigenous microorganisms. Thus, the significant enhancement of anthracene and fluoranthene removal by ridge gourd points to the value of phytoremediation in stimulating microbial activity to clean up PAH-contaminated soil.

PAHs are commonly found in mixtures in the environment. The degradation of individual PAHs may be affected by the presence of other PAHs. Both synergistic and antagonistic effects during degradation of PAH mixtures have been reported [26]. For example, Somtrakoon et al. [27] observed that *Burkholderia* sp. VUN10013 could degrade anthracene but not fluoranthene when each was supplied as the sole carbon source. However, when both compounds were supplied together, the presence of anthracene stimulated the degradation of fluoranthene by strain VUN10013 and the presence of fluoranthene reduced the extent of anthracene degradation. In this instance, anthracene was thought to induce enzymes needed for the transformation of fluoranthene [27]. There are examples where the presence of one PAH may impede the degradation of another PAH. For example, *Pseudomonas* sp. strain *S Ant Mu5* was reported to degrade anthracene to a high extent when it was supplied as a sole carbon source, but the degradation of anthracene was lowered when it was supplied together with fluorene. It was speculated that the inhibition of anthracene degradation might be due to the formation of toxic metabolite(s) during fluorene degradation [28].

Plants in the Cucurbitaceae family have been reported to accumulate PAHs and other organic pollutants in their tissues. For example, the root and shoot tissues of *Cucurbita pepo* ssp. *pepo* cv. Raven could accumulate pyrene from soils with the amount accumulated ranging between 9.6-36.7 μg/plant [29], while *C. pepo* ssp. *pepo* cv. Gold Rush accumulated pyrene in both its shoot and root up to 16.0 μg g^{-1} and 1.7 μg g^{-1} respectively [30]. The vine of *Lagenaria siceraria* accumulated heptachlor epoxide with bioaccumulation factors of 1.0-5.2 [16]. *C. pepo* ssp. *texana* cv. Patty Green and *C. pepo* ssp. *pepo* cv. Black Beauty and Gold Rush also accumulated dioxin-like compounds [17], while *C. pepo* ssp. *pepo* cv. Black Beauty could accumulate anthracene and fluoranthene with bioaccumulation factors of 26.5 and 5.17 respectively [19]. Anthracene was reported to accumulate in lettuce and radish and the amount accumulated varied depending on the application method and plant species [31]. However, the ridge gourd in our study was not found to accumulate anthracene and fluoranthene.

CONCLUSIONS

Ridge gourd shows great promise of use in the phytoremediation of soil contaminated with anthracene and fluoranthene because of its ability to tolerate and grow in PAH-spiked soil. The enhanced degradation of anthracene and fluoranthene relative to that in control unplanted soil occurs in both the rhizospheric soil and bulk soil. Most of the anthracene and fluoranthene were effectively removed from soil during the 45-day experiment and the PAH degradation was most likely accomplished by competent microorganisms, in particular those residing in the rhizosphere. The precise mechanism(s) by which the ridge gourd can enhance the removal of anthracene and fluoranthene from soil warrants investigation.

ACKNOWLEDGEMENTS

We gratefully acknowledge financial support from the Faculty of Science, Mahasarakham University (Grant No MSU-SC-2557 019/57).

REFERENCES

1. S. Gan, E. V. Lau and H. K. Ng, "Remediation of soils contaminated with polycyclic aromatic hydrocarbons (PAHs)", *J. Hazard. Mater*., **2009**, *172*, 532-549.
2. J. Rezek, C. in der Wiesche, M. Mackova, F. Zadrazil and T. Macek, "Biodegradation of PAHs in long-term contaminated soil cultivated with European white birch (*Betula pendula*) and red mulberry (*Morus rubra*) tree", *Int. J. Phytoremediat*., **2009**, *11*, 65-80.
3. R. Boonyatumanond, G. Wattayakorn, A. Togo and H. Takada, "Distribution and origins of polycyclic aromatic hydrocarbons (PAHs) in riverine, estuarine, and marine sediments in Thailand", *Marine Pollut. Bull*., **2006**, *52*, 942-956.
4. M. E. Knuckles, F. Inyang and A. Ramesh, "Acute and subchronic oral toxicity of fluoranthene in F-344 rats", *Ecotoxicol. Environ. Safe*., **2004**, *59*, 102-108.
5. L. Palanikumar, A. K. Kumaraguru, C. M. Ramakritinan and M. Anand, "Biochemical response of anthracene and benzo[*a*]pyrene in milkfish *Chanos chanos*", *Ecotoxicol. Environ. Safe*., **2012**, *75*, 187-197.
6. E. Šepič, M. Bricejl and H. Leskovšek, "Toxicity of fluoranthene and its biodegradation metabolites to aquatic organisms", *Chemosphere*, **2003**, *52*, 1125-1133.
7. N. Weyens, D. van der Lelie, S. Taghavi and J. Vangronsveld, "Phytoremediation: Plant-endophyte partnerships take the challenge", *Curr. Opin. Biotechnol*., **2009**, *20*, 248-254.
8. Y. P. Jing, M. Q. Liu, Q. P. Yin, H. X. Li and F. Hu, "Effects of earthworms and ryegrass on the removal of fluoranthene from soil", *Pedosphere*, **2013**, *23*, 523-531.
9. J. Rezek, C. in der Wiesche, M. Mackova, F. Zadrazil and T. Macek, "The effect of ryegrass (*Lolium perenne*) on decrease of PAH content in long term contaminated soil", *Chemosphere*, **2008**, *70*, 1603-1608.
10. S. Wei and S. Pan, "Phytoremediation for soils contaminated by phenanthrene and pyrene with multiple plant species", *J. Soils Sediment*s, **2010**, *10*, 886-894.
11. D. Álvarez-Bernal, S. Contreras-Ramos, R. Marsch and L. Dendooven, "Influence of catclaw *Mimosa monancistra* on the dissipation of soils PAHs", *Int. J. Phytoremediat*., **2007**, *9*, 79-90.
12. S. A. Cheema, M. I. Khan, X. Tang, C. Zhang, C. Shen, Z. Malik, S. Ali, J. Yang, K. Shen, X. Chen and Y. Chen, "Enhancement of phenanthrene and pyrene degradation in rhizosphere of tall fescue (*Festuca arundinacea*)", *J. Hazard. Mater*., **2009**, *166*, 1226-1231.
13. S. Fan, P. Li, Z. Gong, W. Ren and N. He, "Promotion of pyrene degradation in rhizosphere of alfalfa (*Medicago sativa* L.)", *Chemosphere*, **2008**, *71*, 1593-1598.
14. M. H. Huesemann, T. S. Hausmann, T. J. Fortman, R. M. Thom and V. Cullinan, "In situ phytoremediation of PAH- and PCB-contaminated marine sediments with eelgrass (*Zostera marina*)", *Ecol. Eng*., **2009**, *35*, 1395-1404.
15. K. Somtrakoon, W. Chouychai and H. Lee, "Comparing anthracene and fluorene degradation in anthracene and fluorene-contaminated soil by single and mixed plant cultivation", *Int. J. Phytoremediat*., **2014**, *16*, 415-428.
16. S. Campbell, A. S. Arakaki and Q. X. Li, "Phytoremediation of heptachlor and heptachlor epoxide in soil by Cucurbitaceae", *Int. J. Phytoremediat*., **2009**, *11*, 28-38.

17. H. Inui, T. Wakai, K. Gion, Y. S. Kim and H. Eun, "Differential uptake for dioxin-like compounds by zucchini subspecies", *Chemosphere*, **2008**, *73*, 1602-1607.
18. M. L. W. Åslund, A. I. Lunney, A. Rutter and B. A. Zeeb, "Effects of amendments on the uptake and distribution of DDT in *Cucurbita pepo* spp. *pepo* plants", *Environ. Pollut*., **2010**, *158*, 508-513.
19. M. I. Mattina, M. Isleyen, B. D. Eitzer, W. Iannucci-Berger and J. C. White, "Uptake by cucurbitaceae of soil-borne contaminants depends upon plant genotype and pollutant properties", *Environ. Sci. Technol*., **2006**, *40*, 1814-1821.
20. K. Somtrakoon and W. Chouychai, "Phytotoxicity of phenanthrene and fluoranthene contaminated in soils on growth of *Luffa acutangula*", *J. Agric. Res. Extension*, **2013**, *30*, 1-11 (In Thai).
21. K. Somtrakoon and W. Chouychai, "Phytotoxicity of single and combined polycyclic aromatic hydrocarbons toward economic crops", *Russ. J. Plant Physiol*., **2013**, *60*, 139-148.
22. P. Oleszczuk and S. Baren, "Polyaromatic hydrocarbons in rhizosphere soil of different plants: Effect of soil properties, plant species, and intensity of anthropogenic pressure", *Commun. Soil Sci. Plant Anal.*,**2007**, *38*, 171-188.
23. N. Cofield, A. P. Schwab and M. K. Banks, "Phytoremediation of polycyclic aromatic hydrocarbons in soil: Part I. Dissipation of target contaminants", *Int. J. Phytoremediat*., **2007**, *9*, 355-370.
24. Y.-B. Kim, K.Y. Park, Y. Chung, K.-C. Oh and B. B. Buchnan, "Phytoremediation of anthracene contaminated soil by different plant species", *J. Plant Biol*., **2004**, *47*, 174-178.
25. J. Hultgren, L. Pizzul, M. P. Castillo and U. Granhall, "Degradation of PAH in a creosote-contaminated soil. A comparison between the effects of willows (*Salix Viminalis*), wheat straw and a nonionic surfactant", *Int. J. Phytoremediat*., **2010**, *12*, 54-66.
26. A. L. Juhasz and R. Naidu, "Bioremediation of high molecular weight polycyclic aromatic hydrocarbons: A review of the microbial degradation of benzo[*a*]pyrene", *Int. Biodeter. Biodegr*., **2000**, *45*, 57-88.
27. K. Somtrakoon, S. Suanjit, P. Pokethitiyook, M. Kruatrachue, H. Lee and S. Upatham, "Phenanthrene stimulates the degradation of pyrene and fluoranthene by *Burkholderia* sp. VUN10013", *World J. Microbiol. Biotechnol*., **2008**, *24*, 523-531.
28. M. Bochez, D. Blanchet, V. Bardin, F. Haeseler and J. P Vandecasteele, "Efficiency of defined strains and of soil consortia in the biodegradation of polycyclic aromatic hydrocarbon (PAH) mixtures", *Biodegradation*, **1999**, *10*, 429-435.
29. T. Kobayashi, R. R. Navarro, K. Tatsumi and Y. Imura, "Influence of compost amendment on pyrene availability from artificially spiked soil to two subspecies of *Cucurbita pepo*", *Sci. Total Environ*., **2008**, *404*, 1-9.
30. R. R. Navarro, H. Ichikawa, K. Morimoto and K. Tatsumi, "Enhancing the release and plant uptake of PAHs with a water-soluble purine alkaloid", *Chemosphere*, **2009**, *76*, 1109-1113.
31. J. K. Wieczorek and Z. J. Wieczorek, "Phytotoxicity and accumulation of anthracene applied to the foliage and sandy substrate in lettuce and radish plants", *Ecotoxicol. Environ. Safe*., **2007**, *66*, 369-377.

Maejo Int. J. Sci. Technol. **2014**, *8*(03), 232-239

Maejo International Journal of Science and Technology

ISSN 1905-7873

Available online at www.mijst.mju.ac.th

Communication

A sequential injection system for spectrophotometric determination of ketoconazole

Safwan M. Fraihat

Department of chemistry, College of Science, Aljouf University, Saudi arabia

E-mail: safwanf@yahoo.com

Received: 7 October 2013 / Accepted: 3 October 2014 / Published: 7 October 2014

Abstract: Sequential injection analysis (SIA) with spectrophotometric detection is used for a fast determination of ketoconazole in pure and pharmaceutical preparations. The developed method is based on oxidation of ketoconazole with cerium ion in an acidic medium, which leads to the formation of a coloured product that absorbs at a wavelength of 496 nm. Then automation of the method is developed using the SIA technique. All variables that affect the reaction response are studied and optimised using univariate and simplex optimisation. The method is applicable for the determination of ketoconazole in the range of 20-120 μg mL^{-1}.

Keywords: ketoconazole, sequential injection analysis, spectrophotometric determination, oxidation

INTRODUCTION

Ketoconazole (KC) is chemically known as *cis*-1-acetyl-4-[4-[[2-(2,4-dichlorophenyl)-2-(1*H*-imidazole-1-ylmethyl)-1,3-dioxolan-4-yl]methoxy]phenyl]piperazine. The drug is a highly effective broad-spectrum antifungal agent [1]. It is used to treat a wide variety of superficial and systemic mycoses [2] and has an advantage over other imidazole derivatives in producing adequate sustained blood levels following oral administration [3]. Different methods have been reported for its determination such as spectrophotometry [4-10], chromatography [11-16] and electrochemical method [17-22]. The oxidation of KC with Ce(IV) has not been extensively studied in the literature, thus warranting a comprehensive investigation of the reaction. Standard chromatographic methods of KC generic assay require elaborate and sophisticated instrumentation and have low sampling frequency. Some of the spectrophotometric methods require heating, extraction, a lengthy procedure and a long time for maximum colour development, but lack sensitivity, specificity and a wide dynamic range. Electrochemical methods sometimes suffer from interferences while chromatographic methods are time-consuming and require long procedures for filtration and

extraction. Sequential injection analysis (SIA) has been adopted for the assay of many pharmaceutical and environmental compounds due to many advantages over classical methods. Specifically it is reproducible, robust, reagent-saving and adaptable to different detecting systems [23, 24]. In this paper SIA is utilised along with spectrophotometric measurement to determine KC in pharmaceutical forms. The newly adopted method is validated by its application to the real dosage form of the drug.

MATERIALS AND METHODS

Chemicals and Reagents

A standard stock solution (0.20 mg mL^{-1}) of KC (Sigma) was prepared daily and ten standard working solutions (5-200 mg mL^{-1}) were prepared daily by dilution. Cerium(IV) solution (0.05M) was prepared from ceric ammonium sulphate trihydrate (AR grade) dissolved in 0.5M sulphuric acid. Appropriate working solutions were prepared by dilution. Extra-pure-grade sulphuric acid (95-98 %) was used to prepare a solution of 1.84 g L^{-1} used in this study.

Apparatus

The manifold used consists of SIA apparatus of FIALab 3500 (Medina, USA) combined with a fibre-optic spectrometer, a syringe pump equipped with PVC pumping tube, an 8-port multi-position valve, a fibre-optic Z-flow cell equipped with an LS-1 tungsten halogen lamp and a USB2000 spectrometer (Ocean Optics, USA). A schematic diagram of components of the manifold is shown in Figure 1.

ESR spectra were recorded with a JEOL JES-RE1X spectrometer using an aqueous flat sample cell at 293 K, g = 1.9930, with a microwave frequency of 9.4371 GHz, microwave power of 4.00 mW, sweep width of 5.000 mT and sweep time of 1.0 min.

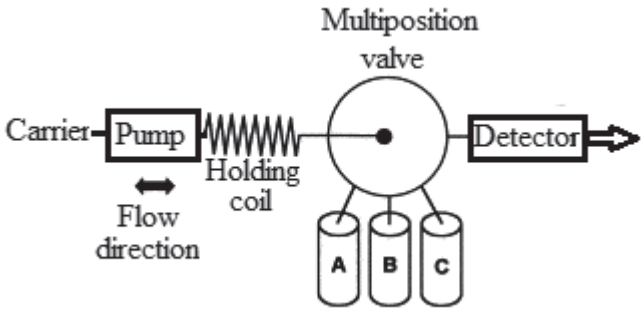

Figure 1. SIA manifold diagram: A = KC solution; B = Ce(IV) solution; C = Sulphuric acid solution

Method and Procedure

The analytical system control including control of the peristaltic pump and selection valve was achieved by FIALAB for Windows version 5.0 from FIAlab® (Medina, USA) using a compatible IBM personal computer.

SigmaPlot 2004 for Windows version 9.01 from Systat Software Inc. was employed for constructing kinetic curves and calculating linear regression equations.

The Chemometric Optimisation by Simplex programme was obtained from Elsevier Scientific Co. (Netherland) and utilised for the optimisation of variables using a compatible IBM personal computer.

To carry out the simplex optimization method, a super-modified simplex programme was employed to find optimum concentrations of both H_2SO_4 and Ce(IV) solutions for sequential injection determination of KC with Ce(IV). The boundary conditions for the two variables lineated in Table 1, together with the start and step values, were fed into the programme.

Table 1. Simplex computer programme parameters and boundaries considered for the optimisation

Parameter	$[H_2SO_4]$	[Ce(IV)]
Step	0.01	0.001
Start-step	0.01	0.001
Lower	0.001	0.0001
Upper	0.1	0.01

RESULTS AND DISCUSSION

The method is based on the reaction of KC with Ce(IV) in sulphuric acid medium. A red-coloured product that is believed to be a radical cation $KC^{\cdot+}$ [25] formed as a result of the loss of an electron from the piperazine ring of the KC molecule (Figure 2). The reaction is instantaneous and the product is stable for several hours. Absorption spectra showed that the oxidised form of KC has λ_{max} at 496 nm.

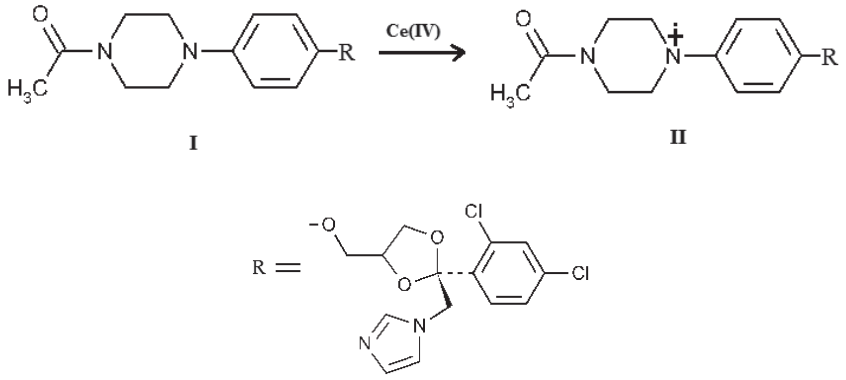

Figure 2. Proposed oxidation reaction of KC: I = KC; II = KC radical cation

It was reported earlier that KC reactions with metal ions proceed by either a complexation or an oxidation reaction [4, 19]. The KC oxidation reaction is accompanied by the formation of a radical cation during the oxidation process, which gradually decays via a chemical reaction to form some stable products. The presence of a radical accompanying the oxidation was confirmed by the ESR spectrum as shown in Figure 3, which illustrates the hyperfine structure of the resultant radical ion, reflecting the extent of delocalisation of the unpaired electron of $KC^{\cdot+}$.

At Ce(IV) concentration higher than 0.05M, the red colour of the product disappears, probably due to further oxidation of the radical formed in the first step of the reaction, producing a divalent cation in another step as shown below [20]:

$$KC \; -e \rightarrow \; KC^{\cdot+}$$
$$KC^{\cdot+} \; -e \rightarrow \; KC^{++}$$

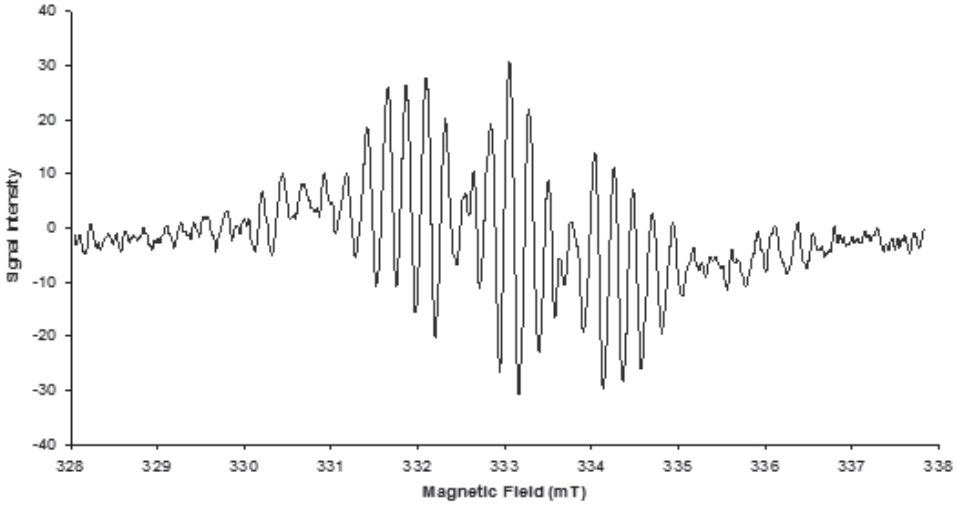

Figure 3. ESR spectrum of 100 µg mL^{-1} KC prepared in 100 mL of 0.078M H_2SO_4 mixed with 0.0013M Ce(IV) solution in 0.5M H_2SO_4

Preliminary investigation of the reaction indicates that the oxidation reaction is dependent on the acid and Ce(IV) concentrations as well as the flow rate. At acid concentration lower than 1.0×10^{-4} mol L^{-1}, the drug is not soluble. When Ce(IV) is prepared lower than 1.0×10^{-4} mol L^{-1}, the molar equivalency of Ce(IV) is limited enough to cover a wider dynamic range of the adopted method. Ce(IV) was found to be insoluble when prepared at a concentration higher than 1.0 mol L^{-1}. The concentrations mentioned above delineate the boundaries of both parameters to be considered in further optimisation procedure.

Univariant Optimisation Method

The univariant optimisation method was applied to examine the effect of each parameter, i.e. flow rate, sulphuric acid concentration and cerium(IV) concentration, on the absorbance. In this method all chemical and instrument parameters were kept constant while varying the concentration of the one being investigated. The effects of H_2SO_4 and Ce(IV) concentrations on the absorbance measured at 496 nm are given in Figure 4 and Figure 5 respectively. It is clear that the absorbance has a maximum value at the acid concentration of around 0.03 mol L^{-1} and the Ce(IV) concentration of around 0.005 mol L^{-1}.

For the flow rate, a number of experiments were carried out keeping the concentrations of sulphuric acid and cerium(IV) constant at 0.01 mol L^{-1} and 0.005 mol L^{-1} respectively while varying the flow rate in the range of 10-50 µL s^{-1} as shown in Figure 6. It was found that the variation of the flow rate not only affects the peak height but it also influences the shape of the peak due to dispersion. The optimum value of flow rate was taken at 30 µL s^{-1} for the sharp and intense peaks in order to enhance sensitivity and sampling frequency.

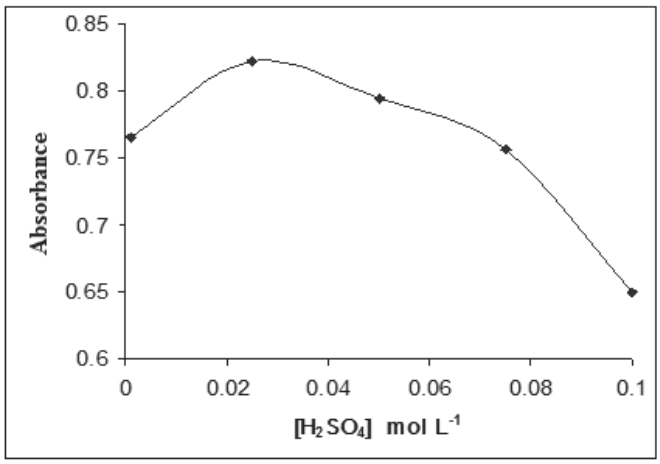

Figure 4. Absorbance as a function of $[H_2SO_4]$ ([Ce(IV)] = 0.005M, [KC] = 100 µg mL^{-1} and flow rate = 50 µL s^{-1})

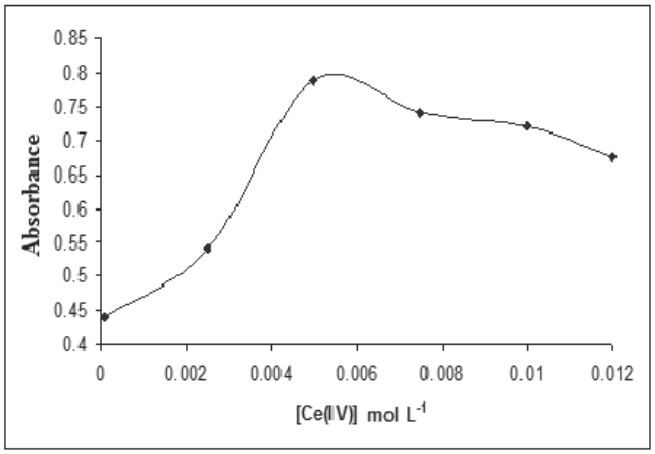

Figure 5. Absorbance as a function of [Ce(IV)] ($[H_2SO_4]$ = 0.003 M, [KC] = 100 µg mL-1 and flow rate =50 µL s^{-1})

Figure 7 shows the progress of the simplex, which indicates a gradual improvement in the response. Sixteen experiments were performed, enough to evaluate the proper conditions. Further investigations on the effects of other parameters such as injection volume and delay time on the absorbance indicated that the optimum operating conditions for KC assay were: $[H_2SO_4]$ = 0.00734 mol L^{-1} and [Ce(IV)] = 0.00176 mol L^{-1}, flow rate = 30 µL s^{-1} and injection volume = 180 µL.

Regression Data

To obtain the best and widest linear calibration curve for KC analysis, different KC standard solutions were prepared keeping concentrations of the other reactants constant at 0.00734 mol L^{-1} H_2SO_4 and 0.00176 mol L^{-1} Ce(IV). The volumes of Ce and KC solutions were 30 µL and 180 µL respectively and the flow rate was 30 µL s^{-1}. The calibration equation was obtained from the plot of absorbance of the coloured product at 496 nm and the absorbance of Ce(IV) solution at that wavelength. The regression data in Table 2 show that the linear dynamic range is 20-120 µg mL^{-1} with high sensitivity, low detection limit and a sampling rate of 120 h^{-1}.

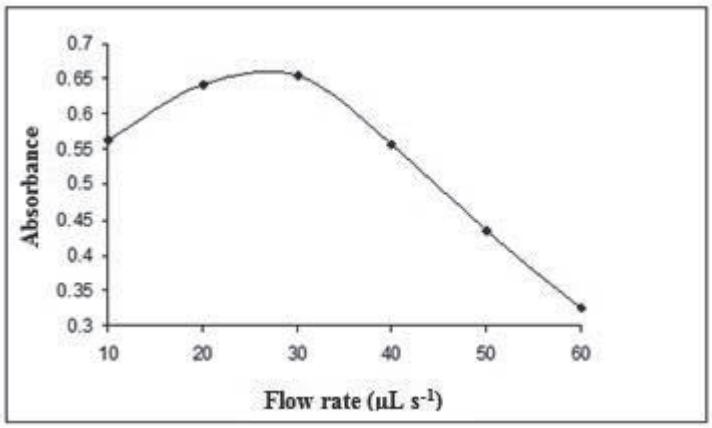

Figure 6. Absorbance as a function of flow rate ($[H_2SO_4]$ = 0.01mol L^{-1}, [Ce(IV)] = 0.005 mol L^{-1})

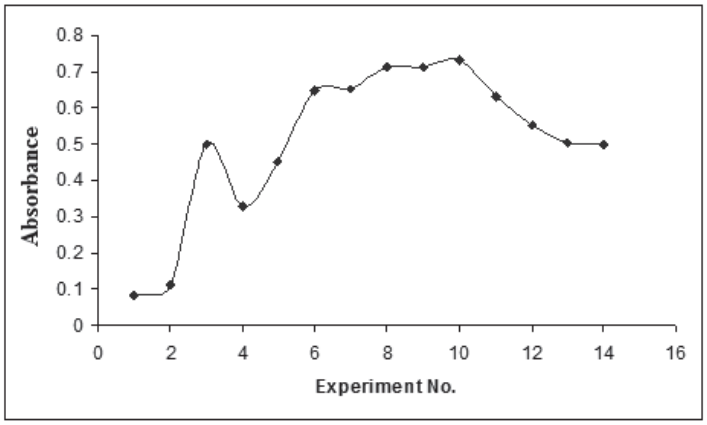

Figure 7. Absorbance progress of the simplex

Table 2. Regression data for SIA method for determination of KC

Wavelength (nm)	496
Concentration range (µg mL^{-1})	20-120
Correlation coefficient	0.997
Slope	0.00471
Intercept	0.0433
Sandell's sensitivity (µg cm^{-2})	0.0047
Detection limit (µg mL^{-1})	13.0
Relative standard deviation (RSD) %	11

Note: Detection limit = 3 Sb/slope; Sb = Standard deviation for blank using five replicates

Application

The effect of excipients in the dosage forms that may interfere with KC determination was studied by applying the proposed SIA method to some drug tablets from the market. The British Pharmacopoeia (BP) method [26] for the assay of KC tablets was also performed for the same batch samples.

Statistical comparison was performed by calculating the t-test of recovery data for two commercial forms of KC tablets. The results showed high accuracy and repeatability of the proposed method compared with the standard method as shown in Table 3.

Table 3. Results of KC determination in proprietary drugs

Drug	Supplier	KC content	Mean recovery ± RSD (%)* SIA method	BP method	t**
Nizoral tablet	JANSSEN	200 mg	95 ± 3.5%	96 ± 0.4%	0.26
	Samf, Sudan	100 mg	94 ± 3.5%	95 ± 0.4%	0.31

* Relative standard deviation for five replicates
** Student t-test value

CONCLUSIONS

The developed method for KC determination based on the oxidation reaction with cerium ion was successfully applied using the SIA system for analysis of commercial samples and the results were comparable with standard method.

REFERENCES

1. J. N. Delgado and W. A. Remers (Ed.), "Wilson and Gisvold's Textbook of Organic Medicinal and Pharmaceutical Chemistry", 9th Edn., Wiley, New York, **1991**.
2. J. Kowal, "The effect of ketoconazole on steroidogenesis in cultured mouse adrenal cortex tumor cells", *Endocrinol.*, **1983**, *112*, 1541-1543.
3. O. M. James and K. B. Sloan, "Structural features of imidazole derivatives that enhance styrene oxide hydrolase activity in rat hepatic microsomes", *J. Med. Chem.,* **1985**, *28,* 1120-1124.
4. N. A. El-Ragehv and Y. S. El-Saharty, "Investigation of ketoconazole copper(II) and cobalt(II) complexes and their spectrophotometric applications", *J. AOAC Int.*, **2001**, *84*, 563-568.
5. S. R. El-Shabouri, K. M. Emara P. Y. Khashaba and A. M. Mohamed, "Charge-transfer complexation for spectrophotometric assay of certain imidazole antifungal drugs", *Anal. Lett.*, **1998**, *31*, 1367-1385.
6. K. Kelani, L. I. Bebawy, L. Abdel-Fattah and A. K. S. Ahmad, "Spectrophotometric determination of some n-donating drugs using DDQ", *Anal. Lett.*, **1997**, *30*, 1843-1860.
7. R. T. Sane, R. V. Tendolkar, D. P. Gangal, K. D. Ladage and R. M. Kothurkar, "An extractive colorimetric method for the determination of ketoconazole from pharmaceutical preparations", *Indian J. Pharm. Sci.*, **1988**, *50*, 347-348.
8. M. A. Abounassif and B. M. El-Shazly, "D1-differential potentiometric and 1H-NMR spectrometric determination of ketoconazole and its formulations", *Anal. Lett.*, **1989**, *22*, 2233-2247.
9. F. Khalil and S. Hossein, "Separation and kinetic-spectrophotometric determination of ketoconazole from formulations using SDS-coated Al_2O_3 and $KMnO_4$ in alkaline-SDS micellar medium", *J. Chinese Chem. Soc.*, **2004**, *51*, 743-750.
10. K. Farhadi and R. Maleki, "Triiodide ion and alizarin red S as two new reagents for the determination of clotrimazole and ketoconazole", *J. Pharm. Biomed. Anal.*, **2002**, *30,* 1023-1033.

11. E. R. M. Kedor-Hackmann, M. M. F. Nery and M. I. R. M. Sanntoro, "Determination of ketoconazole in pharmaceutical preparations by ultraviolet spectrophotometry and high performance liquid chromatography", *Anal. Lett.*, **1994**, *27,* 363-376.
12. F. Alhaique, C. Anchisi, A. M. Fadda, A. M Maccioni and V. Travagli, "Miconazole, ketoconazole and liposomal preparations: A reserved-phase HPLC determination", *Acta Technol. Legis Med.*, **1993**, *4*, 169-175.
13. M. A. Al-Meshal, "Determination of ketoconazole in plasma and dosage forms by high-performance liquid chromatography and a microbiological method", *Anal. Lett.*, **1989**, *22*, 2249-2263.
14. A. S. Low and J. Wangboonskul, "An HPLC assay for the determination of ketoconazole in common pharmaceutical preparations", *Analyst*, **1999**, *124*, 1589-1593.
15. A. M. Di Pietra, V. Cavrini, V. Andriano and R. Gatti, "HPLC analysis of imidazole antimycotic drugs in pharmaceutical formulations", *J. Pharm. Biomed. Anal.*, **1992**, *10*, 873-879.
16. E. M. Abdel-Moety, F. I. Khattab, K. M. Kelani and A. M. Abou Al-Alamein, "Chromatographic determination of clotrimazole, ketoconazole and fluconazole in pharmaceutical formulations", *II Farmaco*, **2003**, *57*, 931-938.
17. Z. Fijalek, J. Chodkowski and M. Waraowna, "Polarographic examination of drugs derived from imidazol. I. Clotrimazole and Ketoconazole", *Acta Pol. Pharm.*, **1992**, *49*, 1-5.
18. T. Z. Peng, Q. Cheng and C. F. Yang, "Adsorptive behavior and electrochemical determination of the anti-fungal agent ketoconazole", *Fresenius J. Anal. Chem.*, **2001**, *370*, 1082-1086.
19. A. N. de Sousa Dantas, D. de Souza, J. E. S. de Lima, P. de Lima-Neto and A. N. Correia, "Voltammetric determination of ketoconazole using a polished silver solid amalgam electrode", *Electrochim. Acta*, **2010**, *55*, 9083-9089.
20. M. Shamsipur and K. Farhadi, "Electrochemical behavior and determination of ketoconazole from pharmaceutical preparations", *Electroanal.*, **2000**, *12*, 429-433.
21. M. Shamsipur and K. Farhadi, "Adsorptive stripping voltammetric determination of ketoconazole in pharmaceutical preparations and urine using carbon paste electrodes", *Analyst*, **2000**, *125*, 1639-1643.
22. M. Shamsipur and K. Farhadi, "Electroxidation of ketoconazole in acetonitrile and its determination in pharmaceutical preparations", *Chem. Anal.*, **2001**, *46*, 387-393.
23. A. M. S. Abulkibash, S. Fraihat and B. El Ali, "Flow injection determination of vitamin C in pharmaceutical preparations by differential electrolytic potentiometry", *J. Flow Inject. Anal.*, **2009**, *26*, 121-125.
24. S. M. A. Fraihat and A. M. S. Abulkibash, "Differential electrolytic potentiometry: A detector for flow injection/sequential analysis in complexation reactions", *Asian J. Chem.*, **2012**, *24*, 4847-4850.
25. M. A. Morsy, S. M. Sultan and H. Daffala, "Electron paramagnetic resonance method for the quantitative assay of ketoconazole in pharmaceutical preparations", *Anal. Chem.*, **2009**, *81*, 6991-6995.
26. Department of Health, "British Pharmacopoeia", HM Stationary Office, London, **1998**.

Maejo International Journal of Science and Technology

ISSN 1905-7873
Available online at www.mijst.mju.ac.th

Full Paper

Identification of *Pagasianodon gigas, P. hypophthalmus* and their hybrids using amplified fragment length polymorphism markers

Nantaporn Sutthi [1], Doungporn Amornlerdpisan [1], Supamit Mekchay [2] and Kriangsak Mengumphan [1,*]

[1] Faculty of Fisheries Technology and Aquatic Resources, Maejo University, Chiang Mai 50290, Thailand

[2] Department of Animal and Aquatic sciences, Faculty of Agriculture, Chiang Mai University, Chiang Mai 50200, Thailand

* Corresponding author, e-mail: *kriang1122sak@gmail.com*

Received: 18 August 2013 / Accepted: 29 September 2014 / Published: 9 October 2014

Abstract: Freshwater Pangasiid catfish species and hybrids are difficult to identify on the basis of morphological characteristics, especially for larvae and fingerlings. In this study, we identified genetic markers for Pangasiid catfish breeds, viz. *Pagasianodon gigas*, *Pagasianodon hypophthalmus* and their F_1 and F_2 hybrids. Twenty primer combinations were used to screen for specific amplified fragment length polymorphism (AFLP) markers. A total of 486 DNA bands were identified and 335 polymorphic bands were found to be segregated among these catfish types. The level of polymorphism detected using 20 different primer combinations ranged between 65.38-100%. Eleven distinct markers were found to be significantly associated with *P. gigas* (two markers), *P. hypophthalmus* (three markers), their F_1 hybrid (three markers) and F_2 hybrid (three markers). Using these markers, 100% of the individuals were accurately assigned to their correct species. These results demonstrate that AFLP markers can be used to genetically identify Pangasiid catfish species and hybrids.

Keywords: *Pagasianodon gigas, P. hypophthalmus*, Pangasiid catfish, AFLP markers, species identification, F_1 hybrid, F_2 hybrid

INTRODUCTION

Freshwater catfish from the Pangasiidae family represent an economically important protein source for local consumers in South-east Asia, including *Pangasius bocourti* in Vietnam [1], *P. djambal* in Indonesia [2] and *Pagasianodon hypophthalmus* in Thailand [3]. Adult Pangasiid catfish can be identified on the basis of morphology [4]; however, morphological characteristics are not enough to differentiate larvae and fingerlings from different species [5]. Most fish farmers also have

difficulties distinguishing between pure line and hybrid individuals. DNA-based techniques have been developed and proved to be analytically accurate in identifying species [6, 7]. These methods can help to identify and authenticate fish and seafood species. They include techniques such as restriction fragment length polymorphism (RFLP), single strand conformation polymorphism (SSCP), forensically informative nucleotide sequencing (FINS) and amplified fragment length polymorphism (AFLP). These methods have been used to identify of numerous fish species and other aquatic organisms [8] including gadoids [9, 10], flatfish [11, 12], salmonids [13, 14], scombroids [15, 16], sardines and anchovies [17-19], and mollusks [20, 21]. Mitochondrial DNA and nuclear ribosomal DNA fragments have recently been proposed as additional methods for species identification [22, 23].

AFLP was first described by Vos et al. [24]. It is essentially a fingerprinting technique that draws upon aspects of randomly amplified polymorphic DNA (RAPD) and RFLP techniques [25]. AFLP is the tool of choice when it comes to unravelling genetic information of complex traits, as it is a fast and inexpensive tool particularly suitable for screening the genome [25-27]. AFLP, like the RAPD technique, presents the advantages of being capable of differentiating among species even in the absence of prior knowledge of the DNA sequence. In addition, AFLP shows greater levels of polymorphism and reproducibility than does RAPD [28, 29]. However, many studies using AFLP have used the data to construct genetic linkage maps rather than to differentiate among species**.** In this study we investigate the potential of AFLP markers to identify and classify two Pangasiid catfish species and their two hybrids.

MATERIALS AND METHODS

Animal Samples

A total 16 individual catfish comprising *Pagasianodon gigas* (n = 4), *P. hypophthalmus* (n = 4), their F_1 hybrid (n = 4) and F_2 hybrid (n = 4) were cultured and collected as samples. The specimens were obtained from the hatcheries of the Plabuk Integrated Utilisation Project at the Faculty of Fisheries and Aquatic Resources, Maejo University.

DNA Extraction

Total genomic DNA was extracted from fish fin samples using phenol-chloroform extraction procedure adapted from that of Sambrook and Russel [30]. The samples were cut in small pieces and suspended in 700 μL of TNES-urea buffer (1mM Tris-HCL pH 8.0, 6 M NaCl, 0.5M EDTA pH 8.0, 10% sodium dodecyl sulphate, and 4M urea) with 4 μL of proteinase K solution (20 μg/mL) (Invitrogen, USA). After adding the proteinase K, the samples were incubated at 37°C overnight. An equal volume of phenol-chloroform (1:1 v/v) was added and the two phases were mixed until an emulsion formed. The two phases were separated by centrifugation at 10,000 rpm for 10 min. The aqueous supernatant solution was collected in fresh tubes. The phenol-chloroform extraction procedure was repeated twice. Sodium acetate (3.0M, pH 5.2) in 1/10 volume and equal volume of isopropanol were added to the collected supernatant and the samples were shaken gently until DNA precipitated. The precipitated DNA was washed twice with 70% ethanol and dried. Finally, the DNA was resuspended in Tris-EDTA buffer and kept at 4° until further use. The final DNA concentration from each sample was tested using a spectrophotometer (NanoDrop 2000, Thermo Fisher Scientific Inc.) and measured on 1% agarose-gel electrophoresis.

AFLP Marker Methodology

The AFLP assay was performed using the protocols described by Wimmers et al. [31]. The DNA of the 16 individual fish was analysed using the adapter and primer sequences shown in Table 1. In brief, 100 ng of genomic DNA was digested with two enzymes: FastDigest® *EcoR*I and *Taq*I restriction endonuclease (Fermentas, USA) following the manufacturer's instructions. The digested products were ligated to 50 µmols of *EcoR*I-Adapters and 50 µmols of *Taq*I-Adapters (Fermentas, USA) in 30 µL of a solution containing 6 U T4 DNA ligase **(**Fermentas, USA**)** and 46mM ATP (Fermentas, USA) and incubated overnight at 4° to ensure ligation. The concentration of the ligated DNA templates was adjusted to 10 ng/µL and diluted fivefold with distilled water for pre-selective amplification.

Table 1. AFLP primer combinations used to generate polymorphism markers between *P. gigas*, *P. hypophthalmus*, F_1 hybrid and F_2 hybrid (The combinations were randomly designed from *Tag*I and *EcoR*I nucleotide adapters.)

Combination	Primer-*EcoR*I	Primer-*Taq*I
1	5-GACTGCGTACCAATTC ACC -3	5-GATGAGTCCTGACCGA CAC -3
2	5-GACTGCGTACCAATTC ACC -3	5-GATGAGTCCTGACCGA CAT -3
3	5-GACTGCGTACCAATTC ACC -3	5-GATGAGTCCTGACCGA CGA -3
4	5-GACTGCGTACCAATTC ACC -3	5-GATGAGTCCTGACCGA CTG -3
5	5-GACTGCGTACCAATTC ACC -3	5-GATGAGTCCTGACCGA CGT -3
6	5-GACTGCGTACCAATTC ACG -3	5-GATGAGTCCTGACCGA CAC -3
7	5-GACTGCGTACCAATTC ACG -3	5-GATGAGTCCTGACCGA CAT -3
8	5-GACTGCGTACCAATTC ACG -3	5-GATGAGTCCTGACCGA CGA -3
9	5-GACTGCGTACCAATTC ACG -3	5-GATGAGTCCTGACCGA CTG -3
10	5-GACTGCGTACCAATTC ACG -3	5-GATGAGTCCTGACCGA CGT -3
11	5-GACTGCGTACCAATTC AAG -3	5-GATGAGTCCTGACCGA CAC -3
12	5-GACTGCGTACCAATTC AAG -3	5-GATGAGTCCTGACCGA CAT -3
13	5-GACTGCGTACCAATTC AAG -3	5-GATGAGTCCTGACCGA CGA -3
14	5-GACTGCGTACCAATTC AAG -3	5-GATGAGTCCTGACCGA CTG -3
15	5-GACTGCGTACCAATTC AAG -3	5-GATGAGTCCTGACCGA CGT -3
16	5-GACTGCGTACCAATTC AAC -3	5-GATGAGTCCTGACCGA CAC -3
17	5-GACTGCGTACCAATTC AAC -3	5-GATGAGTCCTGACCGA CAT -3
18	5-GACTGCGTACCAATTC AAC -3	5-GATGAGTCCTGACCGA CGA -3
19	5-GACTGCGTACCAATTC AAC -3	5-GATGAGTCCTGACCGA CTG -3
20	5-GACTGCGTACCAATTC AAC -3	5-GATGAGTCCTGACCGA CGT -3

The conditions for the pre-selectively amplified polymerase chain reaction (PCR) were as follows: 10 ng of genomic DNA, 1X *Taq* buffer [20 mM Tris-HCl, pH 8.4 and 50mM $(NH_4)_2SO_4$] (Fermentas, USA), 3.0mM $MgCl_2$, 0.25mM each of the four deoxynucleotide triphosphates (dNTPs) (Fermentas, USA), 0.25U *Taq* polymaerase (Fermentas, USA), 4 pmols of pre-selectively amplified *EcoR*I primer (E-A: 5′-GAC TGC GTA CCA ATT CA-3′) (Pacific Science, USA) and 4 pmols of pre-selectively amplified *Taq*I primer (T-C: 5′-GAT GAG TCC TGA CCG AC-3′) (Pacific Science,

USA) in a final volume of 25 μL. The PCR programme was: 3 min. at 94°, 20 cycles of 30 sec. each at 94°, 1 min. at 56° and 30 sec. at 72°, followed by 5 min. at 72°, and a final step at 4°. PCR products were analysed using 6% polyacrylamide-gel electrophoresis (120 V; 400 mA), stained with ethidium bromide. The pre-amplified products were diluted twentyfold with distilled water and then used as selectively amplified DNA templates.

For the selective amplification, 20 primer combinations were used in the following PCR reaction mix: 2.5 μL of diluted pre-selectively amplified products, 1X *Taq* buffer, 3.0mM $MgCl_2$, 0.25mM each of the four dNTPs, 0.25U *Taq* polymerase, 2 pmols of selectively amplified *Eco*RI primer (Pacific Science, USA) and 2 pmols of selectively amplified *Taq*I primer (Pacific Science, USA) in a total volume of 12.5 μL. A touchdown thermal protocol was used for the selective PCR amplification. The selectively amplified products were resolved on a 6% denatured polyacrylamide-gel electrophoresis with constant power (50W) for 3 hr. The AFLP fingerprints were visualised using silver staining.

Statistical Analysis

The individual samples were scored for the presence or absence of each AFLP band. Only polymorphic AFLP bands were analysed using the logistic regression model as follows:

$$\text{logit}(LP) = \text{In}\,(P_i/1\text{-}P_i) = \beta_0 + \beta_1 X_1 + \beta_2 X_2 + \ldots + \beta_n X_n + e \quad (1^*)$$

where LP = logistic probability of a catfish to be predicted as *P. gigas* or non - *P. gigas* (*P. hypophthalmus*, F_1 hybrid and F_2 hybrid)

β_0 = value of y-intercept

$\beta_1, \beta_2, \ldots, \beta_n$ = regression coefficient of molecular markers: $X_1, X_2 \ldots, X_n$

$X_1, X_2 \ldots, X_n$ = molecular markers: $X_1, X_2 \ldots, X_n$

e_{ij} = residual error term

The best-fit model was selected using a backward elimination regression, which tends to be the preferred method for performing exploratory analyses. The predicted probability to be assigned to *P. gigas* was used as follows:

$$P^*_i = e^{LP^*}/1 + e^{LP^*}$$

where P^*_i = predicted probability test of *P. gigas* species: if probability ≥ 0.5, it is *P. gigas* species; if probability < 0.5 it is non - *P. gigas* species.

e = value of exponential constant

LP^* = $\ln(P_i/1\text{-}P_i)$ from equation (1*)

The accuracy test of these markers was described by Wassertheil-Smoller [32]: accuracy = no. of correct assessments / no. of all assessments. Separate logistic regressions were done for other species (*P. hypophthalmus*, F_1 hybrid and F_2 hybrid) using equations similar to the above.

RESULTS AND DISCUSSION

The 20 primer combinations generated a total of 487 AFLP fragments from the 16 Pangasiid catfish individuals (Figure 1). The results showed 9-45 bands per primer combination and 335 markers covering a range of 65.38-100.0% (Table 2). A total of 335 polymorphic bands were used to analyse the association between markers and species assignment using logistic regression. Two markers were found to be significantly associated with *P. gigas*, whereas three markers helped

distinguish *P. hypophthalmus*, F_1 hybrid and F_2 hybrid (Table 3). The identification of *P. gigas*, *P. hypophthalmus*, F_1 hybrid and F_2 hybrid was 100% accurate using these markers (Table 4).

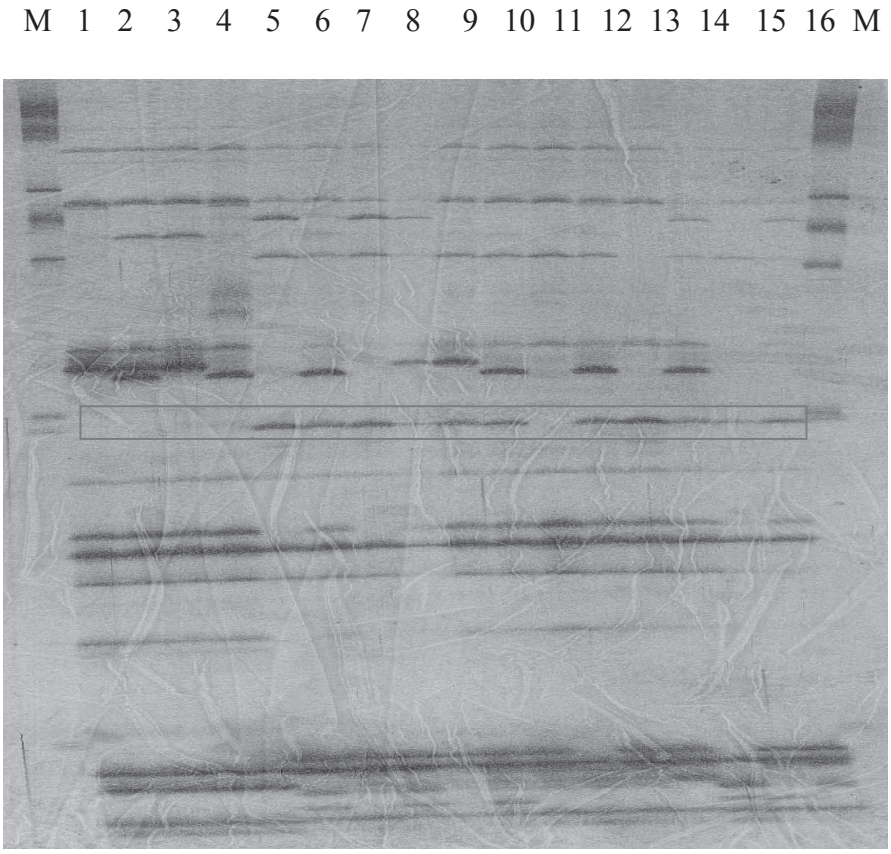

Figure 1. AFLP fingerprints of *P. gigas* (1-4), *P. hypophthalmus* (5-8), F_1 hybrids (9-12) and F_2 hybrids (13-16). DNA bands were amplified by primer E-ACC/ T-CTG. Red box = specific bands present in *P. hypophthalmus,* F_1 hybrids and F_2 hybrids but absent in *P. gigas*. M = DNA ladder 100 bp.

In a previous study, Sriphairoj et al. [33] identified species-specific markers for four economically important Pangasiid catfish, i.e. *P. gigas*, *P. hypophthalmus*, *Pangasius bocourti* and *Pangasius larnaudii*, using seven primers developed by means of AFLP. They used SSCP to screen for potential species-specific markers and only one marker (*PL8*) was shown to be conserved within species, and thus this could be useful for distinguishing among different species. However, these markers failed to separate hybrids of *P. gigas*, *P. hypophthalmus* and *Pangasius bocourti* from their parents. Thus, the present study extends these results by including additional markers. Our results have shown that these markers are also useful for distinguishing hybrids from their parental species.

AFLP markers can be assigned to single-locus markers such as sequence-characterised amplified regions (SCARs) as described by Xu et al. [34]. Kai et al. [35] used AFLP to distinguish three colour morphotypes, in which diagnostic AFLP loci were identified as well as loci with significant frequency differences. In the same way, Chong et al. [36] used AFLP to analyse Malaysian river catfish (*Mystus nemurus*) population in five geographical regions and found that AFLP was more efficient for the differentiation of sub-populations and for the identification of genotypes within the population than RAPD, although similar clusters of the population were

concluded with either analysis. Moreover, Zhang and Cai [14] used AFLP to develop a species-specific marker for rainbow trout. The marker was distinctly present in all the rainbow trout samples tested and was absent from all other Atlantic salmon samples. The species-specific SCAR could only be detected in the admixture containing 10-50% rainbow trout DNA in Atlantic salmon DNA for processed product in 10 replicates. Our results suggest that AFLP makers can be used to identify Pagasiid catfish and their F_1 and F_2 hybrids; however, further testing using more samples per species will be required to test the efficacy of this method. For further study, we plan to identify species-specific DNA fragments using sequencing and to develop DNA or SCAR markers for testing in a larger sample size.

Table 2. Estimation of average number of DNA bands in each primer, number of polymorphic bands and per cent polymorphic

Primer combination	No. of DNA bands in each primer	No. of polymorphic bands	% Polymorphic
1	15	14	93.33
2	21	17	80.95
3	18	16	88.88
4	24	22	91.66
5	14	12	85.71
6	9	7	77.77
7	26	25	96.15
8	12	12	100.00
9	23	23	100.00
10	20	20	100.00
11	25	19	76.00
12	34	26	76.47
13	15	15	100.00
14	45	32	71.11
15	35	33	94.28
16	26	17	65.38
17	37	27	72.97
18	21	20	95.23
19	35	23	65.71
20	32	26	81.25
Total	487	406	1,712.85
Average	24.35	20.30	85.64

Table 3. Estimated values of logistic regression, P-value and odds ratio for the identification of Pangasiid catfish

Species	Variant	Estimated logistic regression	P-value ($Pr>X^2$)	Odds ratio
P. gigas	Intercept	9.4032±55.065	0.3134	-
	2(E3-T3)	-17.5301±80.116	0.0253	<0.001
	26(E3-T5)	-18.7468±64.614	0.0006	<0.001
	% concordant = 100.0; % discordant 0.0; % tied = 0.0			
P. hypophthalmus	Intercept	-20.5324±44.481	0.0004	-
	2(E3-T3)	-15.6238±49.607	0.0472	<0.001
	132(E7-T20)	28.7925±62.553	0.0088	<0.001
	270(E15-T22)	13.9173±35.076	0.0455	<0.001
	% concordant = 100.0; % discordant 0.0; % tied = 0.0			
F_1 hybrid	Intercept	-40.2265±87.031	0.0004	-
	310(E15-T23)	16.2689±50.459	0.0285	<0.001
	326(E15-T23)	16.7919±44.716	0.0209	<0.001
	386(E16-T5)	15.3156±46.502	0.0254	<0.001
	% concordant = 91.7; % discordant 0.0; % tied = 8.3			
F_2 hybrid	Intercept	-7.6711±40.081	0.0004	
	32(E3-T5)	15.8337±52.644	0.0455	<0.001
	77(E3-T22)	-16.7655±50.935	0.0077	<0.001
	98(E7-T3)	16.4146±46.167	0.0158	<0.001
	% concordant = 100.0; % discordant 0.0; % tied = 0.0			

Table 4. Accuracy test of molecular markers for *P. gigas*, *P. hypophthalmus*, F_1 hybrid and F_2 hybrid

Molecular markers for *P. gigas*	Observed		% Correct
	P. gigas	Non - *P. gigas*	
P. gigas	4	0	100%
Non - *P. gigas*	0	12	100%
Molecular markers for *P. hypophthalmus*	Observed		% Correct
	P. hypophthalmus	Non - *P. hypophthalmus*	
P. hypophthalmus	4	0	100%
Non - *P. hypophthalmus*	0	12	100%
Molecular markers for F_1 hybrid	Observed		% Correct
	F_1 hybrid	Non - F_1 hybrid	
F_1 hybrid	4	0	100%
Non - F_1 hybrid	0	12	100%
Molecular markers for F_2 hybrid	Observed		% Correct
	F_2 hybrid	Non - F_2 hybrid	
F_2 hybrid	4	0	100%
Non - F_2 hybrid	0	12	100%

CONCLUSIONS

This study shows that AFLP markers can be used to differentiate Pangasiid catfish (*Pagasianodon gigas* and *P. hypophthalmus*) and their F_1 and F_2 hybrids from their parents. Consequently, this technique may help differentiate taxonomic units and identify genetic relationships between the Pangasiae species. The technique may also provide valuable information for breeding and conservation programmes as well as for ecological, evolutionary and traceability studies

ACKNOWLEDGEMENTS

We are grateful to Thailand Research Fund (TRF) for financial support through the Royal Golden Jubilee Ph.D. Program (PHD/ 0149/ 2554). We are grateful to the Plabuk Integration Knowledge Base, Faculty of Fisheries Technology and Aquatic Resources, Maejo University for providing fish samples. We wish to express our gratitude to the Centre of Excellence on Agricultural Biotechnology, Science and Technology Postgraduate Education and Research Development Office, Commission on Higher Education (AG-BIO/PERDO-CHE), Ministry of Education, as well as the Project of the Service and Technology Transfer of Agricultural Biotechnology Centre, Faculty of Agriculture, Chiang Mai University, for providing research facilities.

REFERENCES

1. L. T. Hung, B. M. Tam, P. Cacot and J. E. Lazard, "Larval rearing of the Mekong catfish *Pangasius bocourti* (Pangasiidae, Siluroidei): Substitution of *Artemia nauplii* with live and artificial feed", *Aquat. Living Resour.*, **1999**, *12*, 229-232.
2. M. Legendre, L. Pouyaud, J. Slembrouck, R. Gustiano, A. H. Kriatanto, J. Subagja, O. Komarudin, Sudarto and Maskur, "*Pangasius djambal*: A new candidate species for fish culture in Indonesia", *Indones. Agric. Res. Dev. J.*, **2000**, *22*, 1-14.
3. W. Tarnchalanukit, "Experimental hybridization between catfishes of the families Clariidae and Pangasiidae in Thailand", *Environ. Biol. Fish.*, **1986**, *16*, 317-320.
4. T. R. Roberts and C. Vidthayanon, "Systematic revision of the Asian catfish family Pangasiidae, with biological observations and descriptions of three new species", *Proc. Acad. Nat. Sci. Philad.*, **1991**, *143*, 97-144.
5. C. Vidthayanon and S. Rungthongbaisuree, "Taxonomy of Thai riverine catfishes family Schilbeidae and Pangasiidae", *Nat. Inland Fish. Inst., Dep. Fish. Technol. Pap.*, **1993**, *150*, 1-57 (in Thai).
6. J. B. Zhang, L. M. Huang and H. Q. Huo, "Larval identification of *Lutjanus* Bloch in Nansha coral reefs by AFLP molecular method", *J. Exp. Mar. Biol. Ecol.*, **2004**, *298*, 3-20.
7. F. Teletchea, "Molecular identification methods of fish species: Reassessment and possible applications", *Rev. Fish Biol. Fisher.*, **2009**, *19*, 265-293.
8. R. S. Rasmussen and M. T. Morrissey, "DNA-based methods for the identification of commercial fish and seafood species", *Compr. Rev. Food Sci. Food Safety*, **2008**, *7*, 280-295.
9. T. Akasaki, T. Yanagimoto, K. Yamakami, H. Tomonaga and S. Sato, "Species identification and PCR-RFLP analysis of cytochrome *b* gene in cod fish (order *Gadiformes*) products", *J. Food Sci.*, **2006**, *71*, 190-195.
10. P. Morán and E. Garcia-Vazquez, "Identification of highly prized commercial fish using a PCR-based methodology", *Biochem. Mol. Biol. Educ.*, **2006,** *34*, 121-124.
11. A. Sanjuan and A. S. Comesana, "Molecular identification of nine commercial flatfish species by polymerase chain reaction-restriction fragment length polymorphism analysis of a segment of the cytochrome b region", *J. Food Prot.*, **2002**, *65*, 1016-1023.
12. A. S. Comesana, P. Abella and A. Sanjuan, "Molecular identification of five commercial flatfish species by PCR-RFLP analysis of a 12S rRNA gene fragment", *J. Sci. Food Agric.*, **2003**, *83*, 752-759.
13. J. J. Dooley, H. D. Sage, M. A. Clarke, H. M. Brown and S. D. Garrett, "Fish species identification using PCR-RFLP analysis and lab-on-a-chip capillary electrophoresis: Application to detect white fish species in food products and an interlaboratory study", *J. Agric. Food Chem.*, **2005**, *53*, 3348-3357.
14. J. Zhang and Z. Cai, "Differentiation of the rainbow trout (*Oncorhynchus mykiss*) from Atlantic salmon (*Salmo salmar*) by the AFLP-derived SCAR", *Eur. Food Res. Technol.*, **2006**, *223*, 413-417.
15. H. S. Hsieh, T. J. Chai and D. F. Hwang, "Using the PCR-RFLP method of identify the species of different processed products of billfish meats", *Food Control*, **2007**, *18*, 369-374.
16. W. F. Lin and D. F. Hwang, "Application of PCR-RFLP analysis on species identification of canned tuna", *Food Control*, **2007,** *18*, 1050-1057.

17. M. Jérôme, C. Lemaire, V. Verrez-Bagnis and M. Etienne, "Direct sequencing method for species identification of canned sardine and sardine-type products", *J. Agric. Food Chem*., **2003**, *51*, 7326-7332.
18. F. J. Santaclara, A. G. Cabado and J. M. Vieites, "Development of a method for genetic identification of four species of anchovies: *E. encrasicolus, E. anchoita, E. ringens* and *E. japonicas*", *Eur. Food Res. Technol*., **2006**, *223*, 609-614.
19. Y. S. Lin, Y. P. Poh, S. M. Lin and C. S. Tzeng, "Molecular techniques to identify freshwater eels: RFLP analyses of PCR-amplified DNA fragments and allele-specific PCR from mitochondrial DNA", *Zool. Stud*., **2002**, *41*, 421-430.
20. I. Rego, A. Martínez, A. González-Tizón, J. Vieites, F. Leira and J. Méndez, "PCR technique for identification of mussel species", *J. Agric. Food Chem*., **2002**, *50*, 1780-1784.
21. S. Klinbunga, P. Pripue, N. Khamnamtong, N. Puanglarp, A. Tassanakajon, P. Jarayabhand, I. Hirono, T. Aoki and P. Menasveta, "Genetic diversity and molecular markers of the tropical abalone (*Haliotis asinina*) in Thailand", *Mar. Biotechnol. (NY)*, **2003**, *5*, 505-517.
22. L. Frézal and R. Leblois, "Four years of DNA barcoding: Current advances and prospects", *Infect. Genet. Evol*., **2008**, *8*, 727-736.
23. B. C. Victor, R. Hanner, M. Shivji, J. Hyde and C. Caldow, ″ Identification of the larval and juvenile stages of the Cubera Snapper, *Lutjanus cyanopterus*, using DNA barcoding ″, *Zootaxa*, **2009**, *2215*, 24-36.
24. P. Vos, R. Hogers, M. Bleeker, M. Reijans, T. van de Lee, M. Hornes, A. Frijters, J. Pot, J. Peleman, M. Kuiper and M. Zebeau, "AFLP: A new technique for DNA fingerprinting", *Nucl. Acids Res.*, **1995**, *23*, 4407-4414.
25. S. Bensch and M. Akesson, "Ten years of AFLP in ecology and evolution: Why so few animals?", *Mol. Ecol.*, **2005**, *14*, 2899-2914.
26. M. J. Blears, S. A. de Grandis, H. Lee and J. T. Trevors, "Amplified fragment length polymorphism (AFLP): A review of the procedure and its applications", *J. Ind. Microbiol. Biotechnol*., **1998**, *21*, 99-114.
27. U. G. Mueller and L. L. Wolfenbarger, "AFLP genotyping and fingerprinting", *Trends Ecol. Evol*., **1999**, *14*, 389-394.
28. P. Bossier, "Authentication of seafood products by DNA patterns", *J. Food Sci*., **1999**, *64*, 189-193.
29. Z. J. Liu and J. F. Cordes, "DNA marker technologies and their applications in aquaculture genetics", *Aquaculture*, **2004**, *238*, 1-37.
30. J. Sambrook and D. W. Russel, "Molecular Cloning: A Laboratory Manual", 3rd Edn., Cold Spring Harbor Laboratory, New York, **2001**, pp.631-632.
31. K. Wimmers, E. Murani, S. Ponsuksili, M. Yerle and K. Schellander, "Detection of quantitative trait loci for carcass traits in the pig by using AFLP", *Mamm. Genome*, **2002**, *13*, 206-210.
32. S. Wassertheil-Smoller, "Biostatistics and Epidermiology: A Primer for Health and Biomedical", 3rd Edn., Springer-Verlag, New York, **2004**, p.243.
33. K. Sriphairoj, S. Klinbu-nga, W. Kamonrat and U. Na-Nakorn, "Species identification of four economically important *Pangasiid* catfishes and closely related species using SSCP markers", *Aquaculture*, **2010**, *308*, S47-S50.

34. M. Xu, E. Huaracha and S. S. Korban, "Development of sequence-characterized amplified regions (SCARs) from amplified fragment length polymorphism (AFLP) markers tightly linked to the Vf gene in apples", *Genome*, **2001**, *44*, 63-70.
35. Y. Kai, K. Nakayama and T. Nakabo, "Genetic differences among three colour morphotypes of the black rockfish, *Sebastes inermis*, inferred from mtDNA and AFLP analyses", *Mol. Ecol.*, **2002,** *11*, 2591-2598.
36. L. K. Chong, S. G. Tan, K. Yusoff and S. S. Siraj, "Identification and characterization of Malaysian river catfish, *Mystus nemurus* (C&V): RAPD and AFLP analysis", *Biochem*. *Genet*., **2000**, *38*, 63-76.

Maejo International Journal of Science and Technology

ISSN 1905-7873
Available online at www.mijst.mju.ac.th

Full Paper

Molecular mechanisms of resveratrol-induced apoptosis in human pancreatic cancer cells

Napaporn Kaewdoungdee[1,*], Chariya Hahnvajanawong[2,*], Benjamart Chitsomboon[3], Wongwarut Boonyanugomol[2], Banchob Sripa[4], Kovit Pattanapanyasat[5] and Anirban Maitra[6]

[1] Department of Biotechnology, Bansomdejchaopraya Rajabhat University, Thailand
[2] Department of Microbiology, Centre of Excellence for Innovation in Chemistry and Liver Fluke and Cholangiocarcinoma Research Centre, Khon Kaen University, Thailand
[3] School of Biology, Suranaree University of Technology, Thailand
[4] Department of Pathology, Khon Kaen University, Thailand
[5] Office of Research and Development, Siriraj Hospital, Mahidol University, Thailand
[6] McKusick-Nathans Institute of Genetic Medicine, the Sol Goldman Pancreatic Cancer Research Centre CRB-2, Johns Hopkins University School of Medicine, Baltimore, USA
* Corresponding authors, e-mail: kaewdo@gmail.com; hchari@kku.ac.th

Received: 8 August 2013 / Accepted: 21 May 2014 / Published: 29 October 2014

Abstract: Resveratrol is a polyphenolic phytoalexin found at high concentrations in grapes, nuts, fruits and red wine with reported anti-carcinogenic effects. In this study, the molecular mechanism of resveratrol-induced apoptosis in human pancreatic cancer (Panc 2.03) cells is investigated. Resveratrol treatment of Panc 2.03 cells results in dose-dependent inhibition of cell growth and cells accumulated at the S phase transition of the cell cycle. The anti-proliferative effect of resveratrol is due to apoptosis as seen by the appearance of chromatin condensation, nuclear fragmentation, DNA ladder formation and increased annexin V-stained cells. The apoptotic process is induced by decreased *Bcl-2* expression concomitant with increased *Bax* expression, leading to an increase in the *Bax/Bcl-2* ratio and subsequent activation of caspase-9 and caspase-3. In addition, resveratrol treatment also decreases the *survivin* level and increases the apoptosis-inducing factor level in a dose-dependent manner. These results suggest that resveratrol induces apoptosis of Panc 2.03 cells, at least in part through a mitochondrial-associated intrinsic pathway in both caspase-dependent and independent manners. The present findings suggest that resveratrol has potential as a chemopreventive agent, and possibly as a therapeutic one against pancreatic cancer.

Keywords: pancreatic cancer (Panc 2.03) cell, resveratrol, apoptosis, S phase arrest, *Bcl-2*, *Bax*, *survivin,* apoptosis-inducing factor

INTRODUCTION

Pancreatic cancer is the eighth most common cause of cancer-related deaths worldwide [1, 2]. It has an extremely poor prognosis; the respective 1- and 5-year relative survival rates are 25% and 6%. Treatments for pancreatic cancer remain limited, as only localised cancer is considered suitable for surgery, radiotherapy or chemotherapy [3, 4]. Alternative modes of therapy are therefore needed. Efforts have been made to develop novel strategies including chemoprevention using dietary phytochemicals [4]. Resveratrol (*trans*–3, 4′, 5–trihydroxystilbene) is a natural polyphenolic phytoalexin present in grapes, nuts, berries, red wine and various plants [5, 6] with a variety of pharmacological properties, i.e. cardioprotective, neuroprotective, anti-oxidant, antiviral, anti-inflammatory, anti-mutagenic, anti-carcinogenic and anticancer activities [7-10].

The cell processes of growth arrest, apoptosis, proliferation or differentiation are highly regulated by numerous proteins and signalling pathways. Disturbance of these processes can avert cell death and lead to cancer [11]. Moreover, disruption of the apoptotic pathway can confer resistance among cancer cells to radiation and chemotherapy [12]. Pancreatic cancer is a multi-stage process caused by the accumulation of genetic changes of normal cells leading to disturbance in cell cycle regulation and continuous growth [13]. Others have reported resveratrol-induced cell cycle arrest and apoptosis through (a) up-regulation of p53 and p21, (b) down-regulation of Bcl-2 expression and (c) activation of caspase-3 in several pancreatic cancer cell lines [10, 14]. Since there has been no study of the growth inhibition by resveratrol of Panc 2.03 pancreatic cancer cells, we investigate the inhibition of proliferation and apoptotic induction by resveratrol in Panc 2.03 cells. The molecular mechanisms of resveratrol-induced proliferation arrest and apoptosis are also explored.

MATERIALS AND METHODS

Cell Culture

The human pancreatic adenocarcinoma cell line, Panc 2.03, was provided by Dr. E. M. Jaffee of the Sol Goldman Pancreatic Cancer Research Centre, Johns Hopkins University, Baltimore, MD, USA. Cells were cultured in RPMI 1640 (Gibco BRL, USA) supplemented with 10% heat-inactivated fetal bovine serum, 100 µg/mL streptomycin and 100 units/mL penicillin (Gibco BRL) in an incubator at 37°C with a humidified atmosphere containing 5% CO_2.

Cell Growth Inhibition Assay

The growth inhibitory effect of resveratrol was determined using the sulphorhodamine B assay. The Panc 2.03 cells ($2x10^3$ cells/well) were seeded in 96-well microtitre plates and incubated for 24 hr (day 0). The cells were treated with 2.5, 5, 10 and 20 µg/mL of resveratrol (Sigma-Aldrich, USA) in cell culture medium, and with 0.1% DMSO as the solvent control. The plates were incubated at 37°C for 48 hr (day 2). Cells were fixed with trichloroacetic acid and stained with 0.4% sulphorhodamine B. The bound dye was solubilised with Tris-base buffer. The absorbance (OD) was measured using an ELISA plate reader (Sunrise-TECAN, USA) at 510 nm. The percentage of cell viability was calculated using equation: % cell survival = [$OD_{\text{test sample day 2}} - OD_{\text{day 0}}$] x 100 /[$OD_{\text{control day 2}} - OD_{\text{day 0}}$]. The 50% inhibitory concentration (IC_{50}) was then determined.

Cell Cycle Distribution Assay

Cells ($1x10^6$) were plated in duplicate in 10-cm dishes (Corning, USA), then incubated at 37°C for 24 hr. They were cultured in complete medium or 0.1% DMSO or 10, 20, 40 and 80 μg/mL resveratrol for 48 hr. After treatment, the cells were washed with cold phosphate buffer saline, fixed in 70% ethanol at 4°C overnight, and then stained with 200 μL GUAVA® cell cycle reagent (GUAVA Technologies, USA) at room temperature (~26ºC) for 30 min. in the dark according to the manufacturer's instructions. The cell cycle distribution (using 10,000 cells per analysis) was analysed in 3 different experiments by a FACSCalibur flow cytometer (Becton Dickinson Bioscience, USA). The percentage distribution of cell cycle phases was analysed by CellQuest software (Becton Dickinson, NJ, USA).

Morphological Examination

Cells ($1x10^6$) were grown in a 25-mL flask at 37°C for 24 hr, then starved in medium containing 0.5% fetal bovine serum for another 24 hr prior to treatment with 0.1% DMSO or 40 μg/mL resveratrol for 48 hr. Cell morphological changes were observed under a bright-field inverted Nikon microscope. In preparation for the nuclear morphology study, the treated cells were washed with phosphate buffer saline, fixed with methanol, stained with 1 μg/mL 4,6-diamidino-2-phenylindole solution (Roche, Germany) at room temperature for 10 min. and observed under a Nikon fluorescent microscope.

The percentage of apoptotic cells was determined using an annexin V-FITC apoptosis detection kit (BD Pharmingen^{TM}, USA) [15]. The cells ($5x10^5$ cells/well) were seeded in a 6-well culture plate (Corning, USA) for 24 hr, starved for 24 hr and treated with 0.1% DMSO or 20, 40 and 80 μg/mL resveratrol. After treatment, both adherent and floating cells were harvested and then double-labelled with annexin V-FITC and propidium iodide for 15 min. Ten thousand events were analysed for each sample using flow cytometry on a FACSCalibur and CellQuest software (Becton Dickinson, NJ, USA) [15].

DNA Fragmentation Assay

DNA fragmentation was determined according to Herrmann et al. [16] with some modifications. After the cells ($1x10^6$) were cultured for 24 hr and starved in medium containing 0.5% fetal bovine serum for 24 hr, they were treated with 0.1% DMSO or 20, 40 and 80 μg/mL resveratrol or 10 μg/mL etoposide as a positive control for 48 hr. The fragmented DNA in cell lysate was purified using a QIAamp DNA Blood Mini Kit (Qiagen, Germany) according to the manufacturer's instructions. The DNA fragments were precipitated with ethanol, re-suspended in 50 μL of Tris EDTA buffer and analysed by 1.6% agarose gel electrophoresis.

Quantitative Real-time Reverse-transcription Polymerase Chain Reaction

Cells were treated with 0.1% DMSO or 40 μg/mL resveratrol for 12 and 24 hr. Total cellular RNA was extracted using TRIzol reagent (Invitrogen, USA) as per the manufacturer's instructions. The reverse-transcription reaction was carried out [17], and then real-time polymerase chain reaction (PCR) was performed for the indicated genes (*Bcl-2*, *Bax*, *survivin* and *GAPDH*) [17] in a 20-μL PCR mixture which contained first-strand cDNA, 5 *p*moles of each primer and 10 μL of 2×SYBR Green PCR Master Mix (Gene System Co., USA), employing an ABI 7500 Real-time PCR System (Applied Biosystems, USA).

The sequences for the specific primers used in the PCR are summarised in Table 1. The sequences of PCR products were obtained by direct sequencing. Each amplicon was then cloned into pGEM®-T vector (Promega, USA) in order to generate standard curves for target cDNA. The respective ratio of copy numbers of each target cDNA to *GAPDH* cDNA was reported as the mRNA level. The up- or down-regulation of gene expression was determined according to the ratio of fold-change in gene expression between the treated and control cells.

Table 1. Primer sequences used in real-time PCR analysis

Gene	Forward primer	Reverse primer
Bcl-2	5′TGGATGACTGAGTACCTGA3′	5′TGAGCAGAGTCTTCAGAGA3′
Survivin	5′AAGGCTGGGAGCCAGA3′	5′TGGCTCTTTCTCTGTCCA3′
Bax	5′AACCATCATGGGCTGGA3′	5′CGCCACAAAGATGGTCA3′
GAPDH	5′TCATCAGCAATGCCTCCTGCA3′	5′TGGGTGGCAGTGATGGCA3′

Protein Extraction and Western Blot Analysis

Cells ($2x10^6$) were treated with 0.1% DMSO or 10, 20, 40 and 80 μg/mL resveratrol for 48 hr, and then harvested and lysed in ice-cold RIPA buffer containing 50 mM Tris-HCl (pH 7.5), 150 mM NaCl, 1 mM dithiothreitol, 0.5% Nonidet P-40, 0.5% deoxycholate, 1 mM EDTA, 0.1% sodium dodesyl sulphate, 1 mM E-64, 2 mM phenylmethylsulphonyl fluoride and 2 mM leupeptin. After homogenisation and centrifugation at 13,000 *g,* 4ºC, for 30 min., the supernatant was collected as whole cell lysate and the protein concentration was determined using a Coomassie protein assay kit (Pierce Biotechnology Inc., USA). Equal amounts of proteins were separated by 10% SDS-polyacrylamide gel electrophoresis and transferred to Hybond ECL nitrocellulose membranes (Amersham Pharmacia Biotech, UK). After blocking, the membranes were incubated overnight with the primary antibodies against Bcl-2, Bax, survivin, apoptosis inducing factor (Santa Cruz Biotechnology, USA) or procaspase-9 and procaspase-3, activated caspase-9 (Cell Signaling, USA) or activated caspase-3, and β-actin (Sigma USA) at 4ºC. The membranes were then incubated at room temperature for 1 hr with the corresponding secondary antibodies, viz. horseradish peroxidase-conjugated goat anti-mouse IgG or goat anti-rabbit IgG antibodies (Santa Cruz Biotechnology, USA). The blots were detected with an enhanced chemiluminescence kit (Pierce Biotechnology, USA) and fluorogrammed with CL-XPosure film. The protein band intensity was quantified using Scion Image software. For every immunoblot, equal loading of protein was confirmed by stripping the blot and re-probing with β-actin antibody. The relative intensity was evaluated and normalised with β-actin.

Statistical Analysis

Values are presented as mean ± SE. The *Student's t*-test was performed to determine the significance between untreated control cells and the resveratrol-treated cells. Differences were considered significant at $p < 0.05$. All analyses were performed using SPSS version 10.0 (SPSS Inc., USA).

RESULTS AND DISCUSSION

Growth Inhibitory Effect of Resveratrol on Panc 2.03 Cells

We first determine the effect of resveratrol on the growth of Panc 2.03 cells *in vitro*. The respective cell survival rates among the Panc 2.03 cells treated with resveratrol at 2.5, 5, 10 and 20 μg/mL (11-87.6 μM) are 54, 50, 43 and 30% respectively (Figure 1). Similar to observations of a variety of pancreatic cancer cell lines, our study shows that after the 48-hr exposure to 2.5-20 μg/mL (11-87.6 μM) of resveratrol, Panc 2.03 cells exhibit marked growth inhibition in a dose-dependent manner (Figure 1). A similar dose range of 25-200 μM has been observed to inhibit the proliferation of various types of pancreatic cancer cell lines [18-20]. Panc 2.03 cells are relatively sensitive to the cytotoxic effects of resveratrol as suggested by the IC_{50} values of only 5 μg/mL (22 μM) against 51-100 μM reported for other types of pancreatic cancer cells (Panc-1, CFPAC-1, MIA Paca-2, AsPC-1, BxPC-3, S2-013 and CD 18 cells) [18-20].

The difference in the sensitivity of pancreatic cancer cell lines to mitomycin C partly depends on which gene(s) controls the Fanconi Anemia (FA) pathway [21]. Specifically, mutations in the FA genes *FANCC*, *FANCG* and *BRCA2* have been reported in pancreatic cancer cell lines [21, 22] and the FA-defective pancreatic cancer cell lines—Hs 766T (*FANCG*-mutated), PL 11 (*FANCC*-mutated) and CAPAN1 (*BRCA2*-mutated)—have an increased sensitivity to mitomycin C compared to the FA-proficient cell lines (Su 86.86 and MIA Paca-2) [21]. Mutations of *FANCC* and *FANCG* are not detected in Panc 2.03, Panc-1, CFPAC, MIA Paca-2, AsPC-1 and BxPC-3 cells [21]. Since mutations in *TP53* (p53) and *CDKN2A* (p16) have been reported in Panc 2.03, Panc-1, CFPAC, MIA Paca-2, AsPC-1 and BxPC-3 cell lines [23, 24], genetic defects in *TP53* and *CDKN2A* might explain the variation in sensitivity of all these cell lines to resveratrol.

Treatment of normal pancreatic duct cells with resveratrol results in a growth inhibitory effect with an IC_{50} value of 373.89 μM [10]. Thus, the growth inhibition by resveratrol in Panc 2.03 cells is ~17 times greater than in normal pancreatic duct cells, suggesting that resveratrol is selectively toxic against cancer cells. Further investigation into the molecular mechanism of the growth inhibition of this compound is therefore warranted.

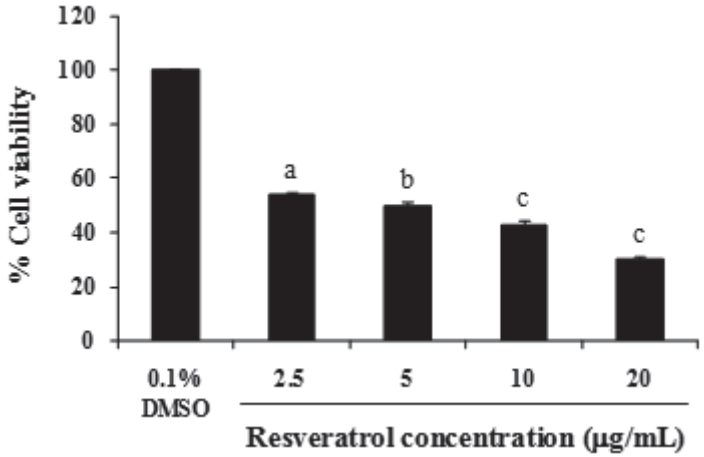

Figure 1. Effect of resveratrol on the growth of Panc 2.03 cells. Cells were treated with 0.1% DMSO or resveratrol at 2.5, 5, 10 and 20 μg/mL for 48 hr. Percent cell viability was determined using sulphorhodamine B assay. Mean ± SE represents 3 different experiments. (a: $p < 0.05$, b: $p < 0.01$, c: $p < 0.001$ vs. control)

Resveratrol Induces S Phase Cell Cycle Arrest in Panc 2.03 Cells

Perturbations of cell cycle progression can cause inhibition of cell growth. To study the mechanism of resveratrol-induced cell growth inhibition, the effect of resveratrol on cell cycle distribution is determined by flow cytometry. Resveratrol induces significant dose-dependent increase in the percentage of cells in the S phase (from 7% to 46%), while significantly decreasing the percentage of cells in the G0/G1 phase (from 78% to 47%) and the G2/M phase (from 10% to 6%) as compared with the DMSO-treated cells (Figure 2). Our results suggest that resveratrol induces cell cycle arrest in the S phase. The results support previous studies in which the ability of resveratrol to block the S/G_2 transition has been reported with CaCo-2 colon cancer cells [25]. Other investigators, however, have reported arrests in the G_1 phase with Panc-1, AsPC-1, capan-2 and colo 357 pancreatic cancer cells [14, 20]. The effects of resveratrol on cell cycle distribution may therefore vary depending on the source of tumour cells: Panc-1 and Panc 2.03 cells are derived from primary tumours, whereas AsPC-1 is from ascites [26]. Deregulation of cell cycle progression is the hallmark of several human tumours including pancreatic cancer. A variety of mutations in the cell-cycle-regulated genes, including the proto-oncogene K-*ras* and the tumour suppressor genes (*p53*, *p16* and *DPC4*), have been reported in many pancreatic cancer cell lines and patient tissues [13, 26]. It has been reported that Panc-1, Panc 2.03 and AsPC-1 cells contain mutant *p53* and *p16* genes, whereas capan-2 and colo 357 cells contain wild-type *p53* [14, 26]. It has also been reported that K-*ras* is mutated in Panc 2.03, Panc-1 and AsPC-1 cells [26]. Taken together, these results

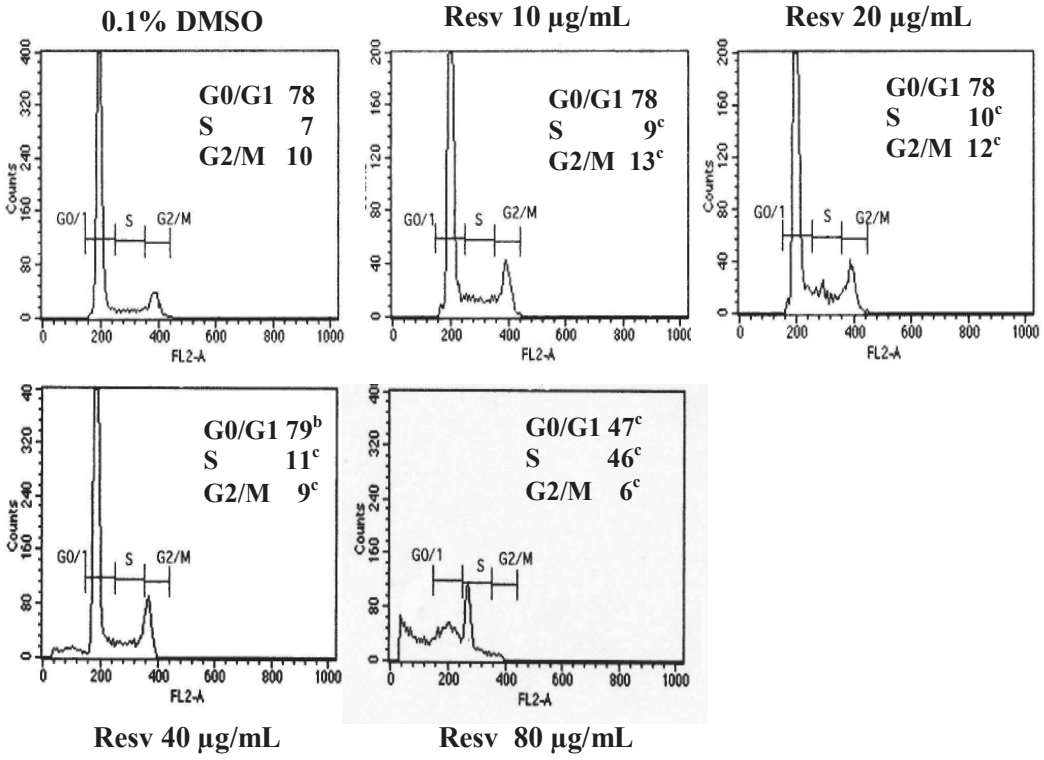

Figure 2. Effects of resveratrol on Panc 2.03 cell cycle distribution. Cells were treated with 0.1% DMSO or various concentrations of resveratrol (Resv) for 48 hr, then stained with GUAVA cell cycle reagent. Percentages of cells in G0/G1, S and G2/M phases of cell cycle were analysed by flow cytometry using CellQuest software. Respective mean ± SE was obtained from 3 independent experiments. (b: $p < 0.01$, c: $p < 0.001$ vs. DMSO-treated cells)

provide evidence that resveratrol induces cell cycle arrest in both *p53* wild-type and *p53* mutant pancreatic cancer cells. The discrepancy in the effects of resveratrol on the cell cycle distribution may be due to differences in the genetic profile of the respective cancer cells.

Apoptosis Induction by Resveratrol in Panc 2.03 Cell Line

The modulation of cell cycle distribution by resveratrol is closely linked to apoptotic cell death (i.e. G0/G1 phase arrest in capan-2, colo 357, Panc-1 and AsPC-1 pancreatic cancer cells) [14, 20]. To determine whether Panc 2.03 cell growth inhibition induced by resveratrol is due to apoptosis, the apoptosis characteristics were determined by several approaches. The typical morphology of apoptotic cells (i.e. cell shrinkage, rounding and membrane blebbing) was observed in the resveratrol-treated Panc 2.03 cells (Figure 3B), whereas no morphological changes were observed in the DMSO-treated cells (Figure 3A). Using 4,6-diamidino-2-phenylindole staining, the morphological changes in the nuclei (i.e. chromatin condensation and nuclear fragmentation, characteristic apoptotic features) were found in the resveratrol-treated cells (Figure 3D) but not in the DMSO-treated cells (Figure 3C). Subsequent visualisation of genomic DNA fragmentation, the hallmark of cell apoptosis in agarose gel electrophoresis, revealed that a 48-hr post-treatment of the Panc 2.03 cells with 20, 40 and 80 μg/mL resveratrol displayed a typical ladder pattern of the inter-nucleosomal DNA fragmentation [27] in a dose-dependent manner (Figure 3E).

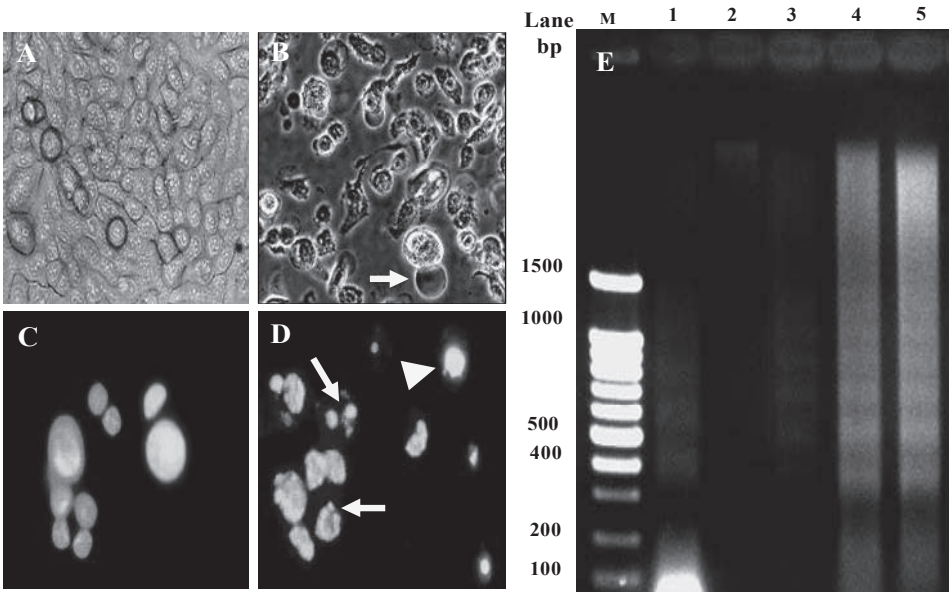

Figure 3. Induced apoptosis of Panc 2.03 cells by resveratrol and effects of resveratrol on morphological changes of Panc 2.03 cells (B and D). After treatment with 0.1% DMSO (A and C) and 40 μg/mL resveratrol (B and D) for 48 hr, cells were photographed by bright field microscope (A and B) or stained with 4,6-diamidino-2-phenylindole and photographed with a fluorescence microscope (C and D). Cells undergoing apoptosis with membrane blebbing are indicated by arrow (B). Nuclei of apoptotic cells show chromatin condensation (D, arrow head) and apoptotic bodies of nuclear fragmentation (D, arrow) (magnification ×400). DNA fragmentation of resveratrol-treated Panc 2.03 cells is evident (E). DNA was extracted from 10 μg/mL etoposide-treated cells (lane 1) or after treatment with 0.1% DMSO, 20, 40 and 80 μg/mL resveratrol (lane 2, 3, 4 and 5) for 48 hr, and then electrophoresed in 1.6% agarose and stained with ethidium bromide. Lane M represents 100 bp DNA markers

The apoptosis induction of Panc 2.03 cells was further confirmed by a flow cytometric analysis using annexin V and propidium iodide (PI) double staining. The percentage of apoptotic cells increased from 13% in 0.1% DMSO-treated cells to 40%, 44% and 53% in resveratrol-treated cells at 20, 40 and 80 μg/mL resveratrol respectively (Figure 4). The apoptosis induction capability of the highest treated group (80 μg/mL) was similar to the positive control, 20 μg/mL etoposide. Taken together, these results demonstrate that the growth inhibition of resveratrol on Panc 2.03 cells is mediated via apoptosis induction.

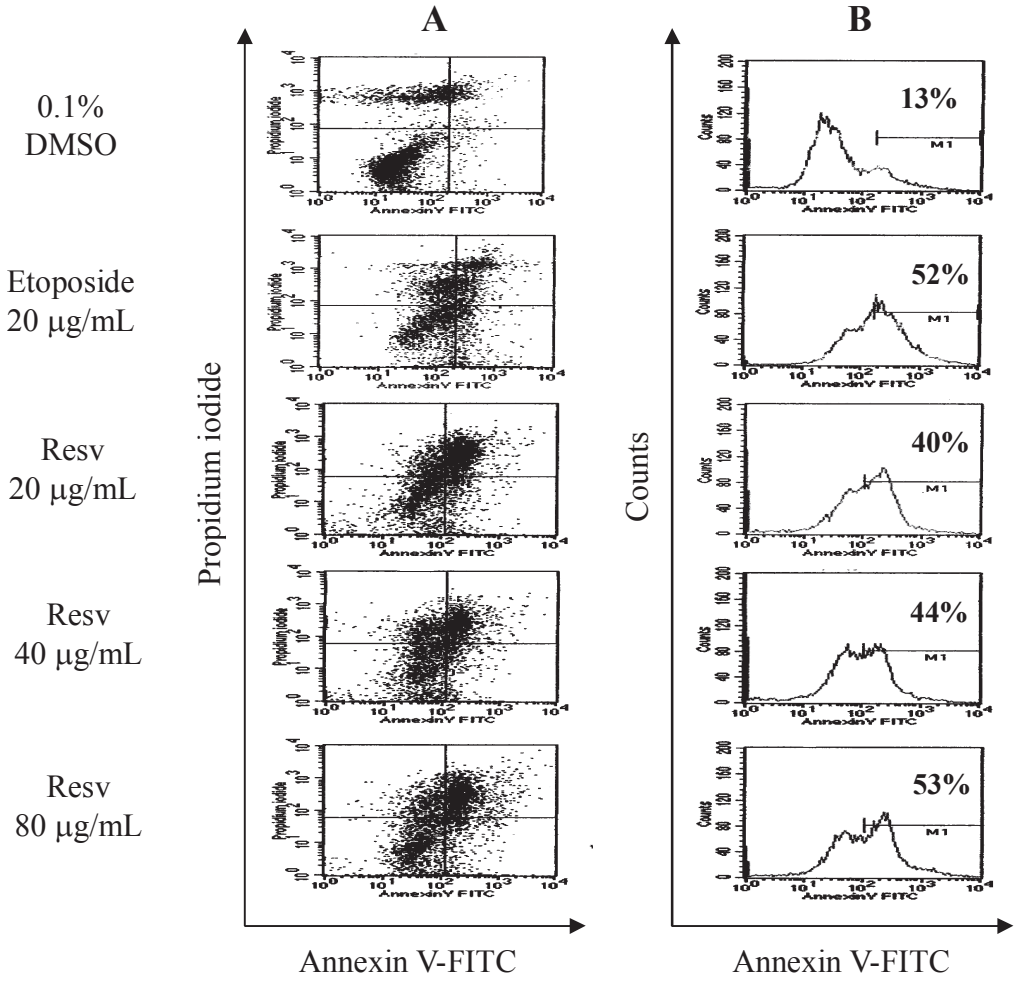

Figure 4. Flow cytometric analysis of cells undergoing apoptosis induced by resveratrol. Cells were cultured for 48 hr in 0.1% DMSO or 20 μg/mL etoposide (positive control) or indicated concentrations of resveratrol (Resv). (A) Apoptotic cells determined by Annexin V-FITC/PI double-staining assay: viable and non-apoptotic cells (lower left corner, annexin V^-/PI^-); early apoptotic cells (lower right corner, annexin V^+/PI^-); late apoptotic cells (upper right corner, annexin V^+/PI^+); necrotic cells (upper left corner, annexin V^-/PI^+). (B) Percentage of apoptotic cells quantified. Values represent average of 3 independent experiments.

Modulation of Resveratrol on Expressions of Apoptosis-Related Genes and Proteins

The apoptotic process is highly regulated at different levels through complex interactions of numerous genes and signalling proteins in response to various extracellular and intracellular stimuli. The apoptotic process can be specifically mediated by multiple pathways involving the

mitochondria/cytochrome C (intrinsic pathway), death receptors TNF, CD95 (extrinsic pathway) and granzyme B (cytotoxic T-cell product) [28].

The Bcl-2 family of proteins (Bax and Bcl-2) plays a crucial role in apoptosis by regulating the permeability of the mitochondrial membrane. Bax, in conjunction with other pro-apoptotic proteins, induces apoptosis by forming pores on the mitochondrial membrane, resulting in the leakage of cytochrome C and apoptosis-inducing factor from the membrane. In contrast, the Bcl-2 is an anti-apoptotic protein that helps to stabilise the integrity of the mitochondrial membrane by forming heterodimers with Bax and/or other apoptotic proteins and neutralise their apoptotic activity [29]. Over-expression of Bax can induce apoptosis by suppressing the activity of Bcl-2 [30]. The ratio of Bax/Bcl-2 is therefore a critical factor in determining the apoptotic destiny of cells under certain circumstances [29, 31].

In order to reveal the underlying mechanism of apoptotic execution, the kinetics of apoptosis-related gene expression of Panc 2.03 cells treated with resveratrol at 40 μg/mL were determined at 12-hr and 24-hr post-treatment using real-time PCR analysis. Resveratrol significantly decreased the *Bcl-2* (anti-apoptotic) gene expression, accompanied by a concomitant increase in *Bax* (pro-apoptotic) gene expression, in a time-dependent manner (Figure 5A). Compared to the control cells, *Bcl-2* gene expression was reduced 0.63- and 0.22-fold, whereas *Bax* gene expression was increased 1.79- and 4.56-fold at 12 hr and 24 hr respectively ($p < 0.001$). A marked increase in the *Bax* to *Bcl-2* ratio from 2.84 at 12 hr to 20.73 at 24 hr can be observed (Figure 5B).

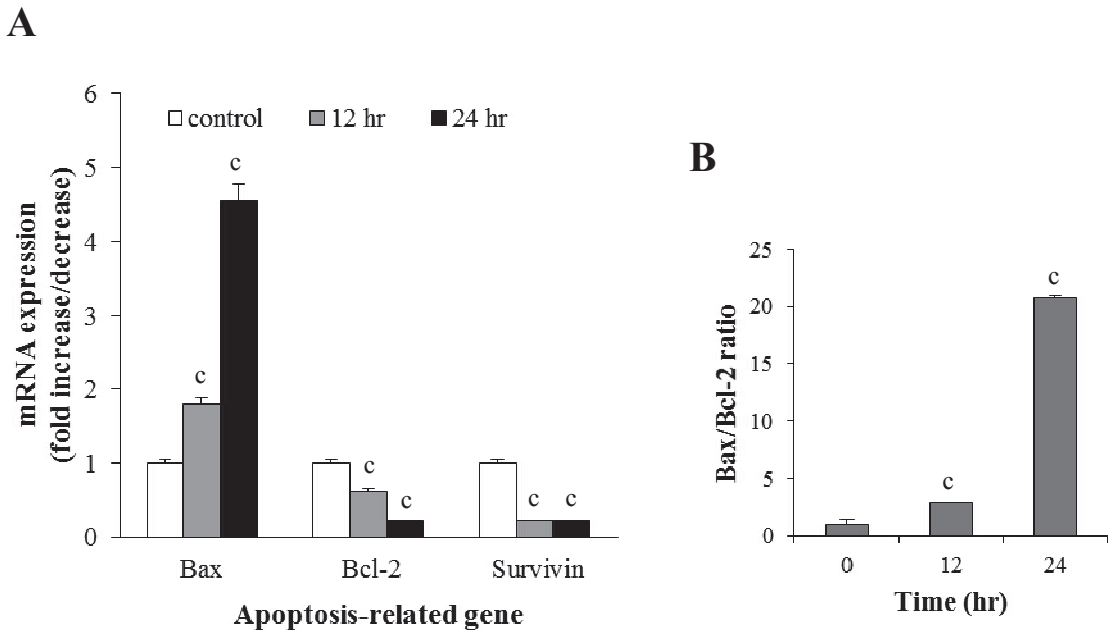

Figure 5. Effects of resveratrol on *Bax*, *Bcl-2* and *survivin* gene expressions of Panc 2.03 cells. Cells were treated with 0.1% DMSO (control) or resveratrol (40 μg/mL). (A) *Bax, Bcl-2* and *survivin* gene expressions were measured using real-time PCR at 12-hr and 24-hr post-treatment. Presented is the fold increase/decrease (mean ± SE) in mRNA expression vs. control, normalised with housekeeping gene glyceraldehyde-3-phosphate, of three independent experiments. (B) Bax/Bcl-2 ratio. (c: $p < 0.001$ vs. control)

The gene expression results, along with the Western blot analysis, demonstrates that the exposure of Panc 2.03 cells to 10, 20, 40 and 80 µg/mL of resveratrol for 48 hr results in a decrease in Bcl-2 protein expression, accompanied by an increase in Bax protein expression, in a dose-dependent manner (Figure 6). Our study reveals that resveratrol, at least in part, induces apoptotic Panc 2.03 cells by modulating the expression of the Bcl-2 family of proteins through the intrinsic (mitochondrial) apoptosis pathway. Moreover, the apoptosis-inducing factor released from the mitochondria can translocate into the nucleus and cause DNA fragmentation via a caspase-independent pathway [9, 28]. In this study, the dose-dependent increase of the apoptosis-inducing factor level in treated Panc 2.03 cells (Figure 6) suggests that the apoptotic execution can also be mediated via a caspase-independent mitochondrial pathway [32].

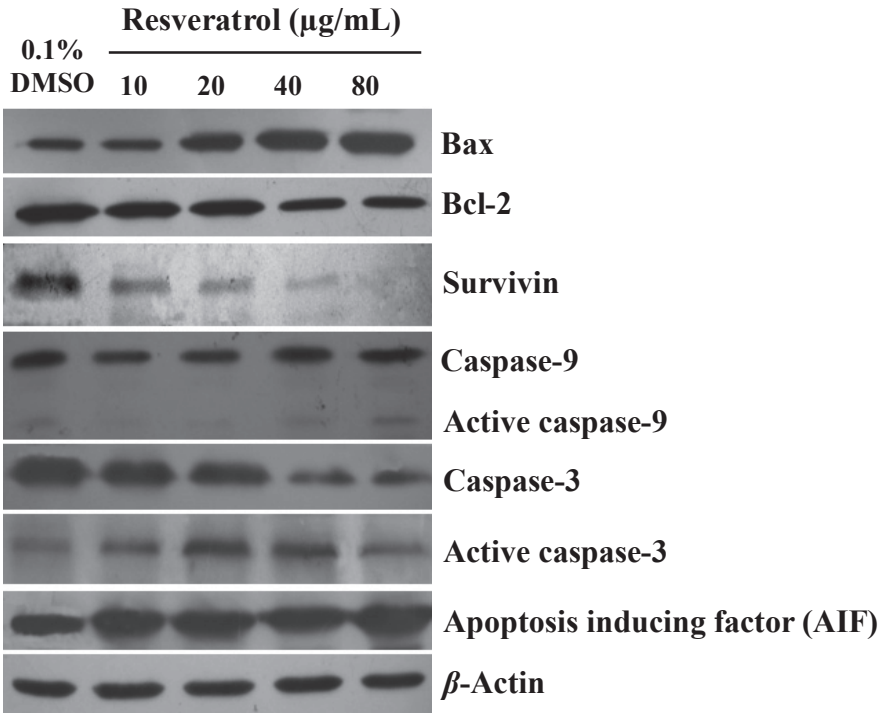

Figure 6. Effects of resveratrol on the expression of apoptosis-related proteins (determined by Western blot analysis) in Panc 2.03 cell. Cells were treated with 0.1% DMSO or the indicated doses of resveratrol for 48 hr.

A recent study [20] shows that resveratrol induces apoptosis in Panc-1, AsPC-1 and BxPC-3 pancreatic cancer cells, which might occur indirectly through the Hedgehog signalling pathway by the down-regulation of Gli1-targeted genes including *Ptc1*, *CCND1* and *Bcl-2*. In addition, resveratrol induces apoptosis by inhibiting miR-21 regulation of Bcl-2 expression in Panc-1, CFPAC-1 and MIA Paca-2 pancreatic cancer cells [10]. Our results likewise show that apoptosis induction of Panc 2.03 cells by resveratrol might be through the down-regulation of Bcl-2 expression.

In the mitochondrial apoptotic pathway, cytochrome C released from mitochondria activates caspase-9 and caspase-3, resulting in DNA fragmentation and apoptotic cell death [33]. Western blot analysis reveals that resveratrol decreases the procaspase-3 level in a dose-dependent manner (Figure 6). The down-regulation of procaspase-3 is accompanied by the up-regulation of active caspase-9 and caspase-3 in the treated groups. Our results suggest that apoptosis induction of Panc

2.03 cells by resveratrol is via the activation of caspase-9 and caspase-3. Our results agree to some extent with a study on capan-2 and colo 357 pancreatic cancer cells, in which resveratrol induces ERK phosphorylation, p21 up-regulation, p53 accumulation and caspase-3 activation, leading to cell cycle arrest and apoptotic cell death [14]. The mechanism of resveratrol-induced apoptosis mediated by cytochrome C release followed by caspase-3 activation has also been reported vis-à-vis other pancreatic cancer cell lines [34].

Survivin is a member of the inhibitor of apoptosis protein family of anti-apoptosis proteins. Since the binding of survivin to active caspase-3 and caspase-7 can inhibit apoptosis [35], the effects of resveratrol on the *survivin* gene and protein expression in Panc 2.03 cells were also examined. The real-time PCR analysis shows that resveratrol induces a dose-related decrease in *survivin* gene expression to a similar extent (about 0.22-fold decrease, $p < 0.001$) after 12-hr and 24-hr post exposure (Figure 5A). The modulation of *survivin* gene expression was subsequently confirmed by a dose-related decrease in survivin protein expression following a 48-hr exposure to 10, 20, 40 and 80 μg/mL of resveratrol (Figure 6). A decrease in survivin level may maintain caspase-3 in an active form, thereby increasing apoptotic cell death [35].

CONCLUSIONS

Our findings demonstrate that resveratrol inhibits the proliferation of Panc 2.03 cells *in vitro* by causing cell cycle arrest at the S phase and inducing apoptosis mediated, at least in part, via a mitochondrial apoptosis pathway in both caspase-dependent and independent manners. The molecular mechanisms involved are the up-regulation of the *Bax/Bcl-2* ratio, the activation of caspase-9 and caspase-3, the down-regulation of survivin and the up-regulation of the apoptosis-inducing factor. The variation in the mechanism of resveratrol-induced cell cycle arrest and apoptosis in different pancreatic cancer cell lines may be dependent on the genetic profile of the cells. Further study of the activity of resveratrol *in vivo* is needed to gain insights into its molecular mechanisms and guide its development for use in chemotherapy of pancreatic cancer.

ACKNOWLEDGEMENTS

This work was supported by research grants from: 1) the Office of National Research Council of Thailand through Bansomdejchaopraya Rajabhat University, 2) Suranaree University of Technology and 3) Centre of Excellence for Innovation in Chemistry, Commission on Higher Education, Khon Kaen University. The authors thank Mr. Bryan Roderick Hamman and Mrs. Janice Loewen-Hamman for assistance with the English language presentation.

REFERENCES

1. D. Hariharan, A. Saied and H. M. Kocher, "Analysis of mortality rates for pancreatic cancer across the world", *HPB (Oxford)*, **2008**, *10*, 58-62.
2. American Cancer Society, "Cancer Facts and Figures 2010", American Cancer Society Inc., Atlanta, **2010**, p.19.
3. D. Li, K. Xie, R. Wolff and J. L. Abbruzzese, "Pancreatic cancer", *Lancet*, **2004**, *363*, 1049-1057.
4. V. Heinemann, "Gemcitabine: Progress in the treatment of pancreatic cancer", *Oncology*, **2001**, *60*, 8-18.

5. J. K. Kundu and Y. J. Surh, "Molecular mechanisms underlying chemoprevention with resveratrol", *Cancer Prev. Res.*, **2005**, *10*, 89-98.
6. A. K. Joe, H. Liu, M. Suzui, M. E. Vural, D. Xiao and I. B. Weinstein, "Resveratrol induces growth inhibition, S-phase arrest, apoptosis, and changes in biomarker expression in several human cancer cell lines", *Clin. Cancer Res.*, **2002**, *8*, 893-903.
7. K. P. L. Bhat, J. W. Kosmeder and J. M. Pezzuto, "Biological effects of resveratrol", *Antioxid. Redox. Signal.*, **2001**, *3*, 1041-1064.
8. G. W. Osmond, C. K. Augustine, P. A. Zipfel, J. Padussis and D. S. Tyler, "Enhancing melanoma treatment with resveratrol", *J. Surg. Res.*, **2012**, *172*, 109-115.
9. J. H. Jang and Y. J. Surh, "Protective effect of resveratrol on beta-amyloid-induced oxidative PC12 cell death", *Free Rad. Biol. Med.*, **2003**, *34*, 1100-1110.
10. P. Liu, H. Liang, Q. Xia, P. Li, H. Kong, P. Lei, S. Wang and Z. Tu, "Resveratrol induces apoptosis of pancreatic cancers cells by inhibiting miR-21 regulation of BCL-2 expression", *Clin. Transl. Oncol.*, **2013**, *15*, 741-746.
11. S. Fulda and K. M. Debatin, "Resveratrol modulation of signal transduction in apoptosis and cell survival: A mini-review", *Cancer Detect. Prev.*, **2006**, *30*, 217-223.
12. S. W. Fesik, "Promoting apoptosis as a strategy for cancer drug discovery", *Nat. Rev. Cancer*, **2005**, *5*, 876-885.
13. G. Schneider and R. M. Schmid, "Genetic alterations in pancreatic carcinoma", *Mol. Cancer*, **2003**, *2*, 15.
14. J. H. Zhou, H. Y. Cheng, Z. Q. Yu, D. W. He, Z. Pan and D. T. Yang, "Resveratrol induces apoptosis in pancreatic cancer cells", *Chin. Med. J. (Engl.)*, **2011**, *124*, 1695-1699.
15. L. Casciola-Rosen, A. Rosen, M. Petri and M. Schlissel, "Surface blebs on apoptotic cells are sites of enhanced procoagulant activity: Implications for coagulation events and antigenic spread in systemic lupus erythematosus", *Proc. Natl. Acad. Sci. USA*, **1996**, *93*, 1624-1629.
16. M. Herrmann, H. M. Lorenz, R. Voll, M. Grunke, W. Woith and J. R. Kalden, "A rapid and simple method for the isolation of apoptotic DNA fragments", *Nucl. Acids Res.*, **1994**, *22*, 5506-5507.
17. N. Namwat, P. Amimanan, W. loilome, P. jearnaikoon, B. Sripa, V. Bhudisawasdi and W. Tassaneeyakul, "Characterization of 5-fluorouracil-resistant cholangiocarcinoma cell lines", *Chemotherapy*, **2008**, *54*, 343-351.
18. X. Z. Ding and T. E. Adrian, "Resveratrol inhibits proliferation and induces apoptosis in human pancreatic cancer cells", *Pancreas*, **2002**, *25*, 71-76.
19. L. Golkar, X. Z. Ding, M. B. Ujiki, M. R. Salabat, D. L. Kelly, D. Scholtens, A. J. Fought, D. J. Bentrem, M. S. Talamonti, R. H. Bell and T. E. Adrian, "Resveratrol inhibits pancreatic cancer cell proliferation through transcriptional induction of macrophage inhibitory cytokine-1", *J. Surg. Res.*, **2007**, *138*, 163-169.
20. W. Mo, X. Xu, L. Xu, F. Wang, A. Ke, X. Wang and C. Guo, "Resveratrol inhibits proliferation and induces apoptosis through the hedgehog signaling pathway in pancreatic cancer cell", *Pancreatol.*, **2011**, *11*, 601-609.
21. M. S. Van der Heijden, J. R. Brody, E. Gallmeier, S. C. Cunningham, D. A. Dezentje, D. Shen, R. H. Hruban and S. E. Kern, "Functional defects in the fanconi anemia pathway in pancreatic cancer cells", *Am. J. Pathol.*, **2004**, *165*, 651-657.

22. M. E. Moynahan, T. Y. Cui and M. Jasin, "Homology-directed DNA repair, mitomycin-c resistance, and chromosome stability is restored with correction of a Brca1 mutation", *Cancer Res.*, **2001**, *61*, 4842-4850.
23. M. Schutte, R. H. Hruban, J. Geradts, R. Maynard, W. Hilgers, S. K. Rabindran, C. A. Moskaluk, S. A. Hahn, I. Schwarte-Waldhoff, W. Schmiegel, S. B. Baylin, S. E. Kern and J. G. Herman, "Abrogation of the Rb/p16 tumor-suppressive pathway in virtually all pancreatic carcinomas", *Cancer Res.*, **1997**, *57*, 3126-3130.
24. M. S. Redston, C. Caldas, A. B. Seymour, R. H. Hruban, L. da Costa, C. J. Yeo and S. E. Kern, "p53 mutations in pancreatic carcinoma and evidence of common involvement of homocopolymer tracts in DNA microdeletions", *Cancer Res.*, **1994**, *54*, 3025-3033.
25. Y. Schneider, F. Vincent, B. Duranton, L. Badolo, F. Gosse, C. Bergmann, N. Seiler and F. Raul, "Anti-proliferative effect of resveratrol, a natural component of grapes and wine, on human colonic cancer cells", *Cancer Lett.*, **2000**, *158*, 85-91.
26. P. S. Moore, B. Sipos, S. Orlandini, C. Sorio, F. X. Real, N. R. Lemoine, T. Gress, C. Bassi, G. Kloppel, H. Kalthoff, H. Ungefroren, M. Lohr and A. Scarpa, "Genetic profile of 22 pancreatic carcinoma cell lines. Analysis of K-*ras*, *p53*, *p16* and *DPC4/Smad4*", *Virchows Arch.*, **2001**, *439*, 798-802.
27. M. M. Compton, "A biochemical hallmark of apoptosis: Internucleosomal degradation of the genome", *Cancer Metastasis Rev.*, **1992**, *11*, 105-119.
28. M. Andreeff, D. Goodrich and A. Pardee, "Cell proliferation, differentiation and apoptosis", in "Cancer Medicine" (Ed. R. Bast, D. Kufe, R. Pollock, R. Weichselbaum and J. Holland), B. C. Decker, Hamilton (Canada), **2000**, p.17-32.
29. V. G. Mbazima, M. P. Mokgotho, F. February, D. J. G. Rees and L. J. Mampuru, "Alteration of Bax-to-Bcl-2 ratio modulates the anticancer activity of methanolic extract of *Commelina benghalensis* (Commelinaceae) in Jurkat T cells", *Afr. J. Biotechnol.*, **2008,** *20*, 3569-3576.
30. D. M. Hockenbery, C. D. Giedt, J. W. O'Neill, M. K. Manion and D. E. Banker, "Mitochondria and apoptosis: New therapeutic targets", *Adv. Cancer Res.*, **2002**, *85*, 203-242.
31. H. B. Zhou, Y. Yan, Y. N. Sun and J. R. Zhu, "Resveratrol induces apoptosis in human esophageal carcinoma cells", *World J. Gastroenterol.*, **2003**, *9*, 408-411.
32. L. E. Broker, F. A. Kruyt and G. Giaccone, "Cell death independent of caspases: A review", *Clin. Cancer Res.*, **2005**, *11*, 3155-3162.
33. M. Bras, B. Queenan and S. A. Susin, "Programmed cell death via mitochondria: Different mode of dying", *Biochem. (Mosc).*, **2005**, *70*, 231-239.
34. M. Mouria, A. S. Gukovskaya, Y. Jung, P. Buechler, O. J. Hines, H. A. Reber and S. J. Pandol, "Food-derived polyphenols inhibit pancreatic cancer growth through mitochondrial cytochrome C release and apoptosis", *Int. J. Cancer*, **2002**, *98*, 761-769.
35. S. Shin, B. J. Sung, Y. S. Cho, H. J. Kim, N. C. Ha, J. I. Hwang, C. W. Chung, Y. K. Jung and B. H. Oh, "An anti-apoptotic protein human survivin is a direct inhibitor of caspase-3 and -7", *Biochem.*, **2001**, *40*, 1117-1123.

Maejo Int. J. Sci. Technol. **2014**, *8*(03), 264-278

Maejo International Journal of Science and Technology

ISSN 1905-7873
Available online at www.mijst.mju.ac.th

Full Paper

Levitin-Polyak well-posedness of inverse quasi-variational inequality with perturbations

Garima Virmani * **and Manjari Srivastava**

Department of Mathematics, University of Delhi, Delhi 110007, India

* Corresponding author, e-mail: garimavirmani86@gmail.com

Received: 20 November 2013/ Accepted: 13 October 2014/ Published: 30 October 2014

Abstract: Levitin-Polyak α-well-posedness for inverse quasi-variational inequality is investigated. We establish some metric characterisations of Levitin-Polyak α -well-posedness for inverse quasi-variational inequality problems having a unique solution and give some conditions under which the above problem is Levitin-Polyak α -well-posed by perturbations in the generalised sense.

Keywords: inverse quasi-variational inequality, Levitin-Polyak well-posedness by perturbations, metric characterisation

INTRODUCTION

Well-posedness is one of the most important concepts in the theory of optimisation and it has been studied extensively in the literature [1-8]. It plays a crucial role in the stability theory for optimisation problems, which guarantees that for an approximating solution sequence, there exists a subsequence which converges to a solution. The study of well-posedness for scalar minimisation problems was started by Tykhonov [1], according to whom the problem of minimising a function $h(x)$ over a closed convex set K is Tykhonov well-posed if it has a unique solution and every minimising sequence converges to the solution.

This type of well-posedness requires every minimising sequence to lie in the feasible set K. In many practical situations, the minimising sequence $\{x_n\}$ produced by a numerical optimisation method usually fails to be in K but $d_K(x_n) \to 0$ as $n \to \infty$. Such a sequence is called a generalised minimising sequence. Taking this into account, Levitin and Polyak [2] introduced a strengthening notion of Tykhonov well-posedness by requiring the convergence of every generalised minimising sequence to a unique solution, which is known as Levitin-Polyak (LP) well-posedness. Zolezzi [7, 8] also introduced a strengthening version of Tykhonov well-posedness by the name of extended well-posedness (also named well-posedness by perturbations) by embedding the original problem

into a family of perturbed problems depending on a parameter. This form of well-posedness establishes continuous dependence of the solution upon a parameter.

In recent years, the concepts of well-posedness have been generalised to various variational inequality problems [3, 9-19] and quasi-variational inequality problems [20-24]. The main motivation originates from the fact that a minimisation problem is equivalent to a variational inequality under convexity and differentiability assumptions. There is vast literature which relates the solutions of a minimisation problem and (generalised) variational inequality problem (see [25-28] and references therein). Lucchetti and Patrone [17] were the first to introduce the notion of well-posedness for a variational inequality. Lignola and Morgan [15] generalised the notion of well-posedness by perturbations to a variational inequality problem and established the equivalence between the well-posedness by perturbations of a variational inequality and the corresponding minimisation problem. Hu and Fang [12] and Hu et al. [29] studied the LP well-posedness of variational inequalities. Huang et al. [14] studied the LP well-posedness of variational inequality problems with functional constraints.

A new class of problems known as the inverse variational inequality (IVI) has been proposed and studied [30-34]. The IVI has broad applications in the market equilibrium problems in economics and normative flow control problems, appearing in transportation and telecommunication. The primary motivation of research on IVI originates from the transportation system operation and control policies. He et al. [33] demonstrated the applicability of constrained black-box variational inequality to the class of network equilibrium control problems by taking the spatial price equilibrium problem as an example. However, in some practical situations it is necessary to consider IVI models in which the constraint set is not constant. Hence a new class of problems known as the inverse quasi-variational inequality was introduced and studied recently by Aussel et al. [35]. This class of problems finds applications in road pricing problem in which the environmental impact problem due to traffic flow is taken into account to fix road taxes. Very recently, Hu and Fang [11] introduced and studied the well-posedness of IVI, which was further extended for Levitin-Polyak well-posedness by Hu and Fang [36].

Motivated by the above-mentioned research work, we establish some metric characterisations of LP α-well-posedness by perturbations. We derive some conditions under which the LP well-posedness by perturbations of an inverse quasi-variational inequality (IQVI) is equivalent to the existence and uniqueness of its solution. We also establish metric characterisations of LP α-well-posedness by perturbations in the generalised sense.

PRELIMINARIES

Let $f, h : \mathbb{R}^n \to \mathbb{R}^n$ be two continuous maps. Let $K : \mathbb{R}^n \to 2^{\mathbb{R}^n}$ be a set-valued map such that for each $x \in \mathbb{R}^n$, $K(x)$ is a closed convex set in $\mathbb{R}^n$. The IQVI associated with f, h and K denoted by IQVI(f, h, K) consists of:

Find $x^* \in \mathbb{R}^n$ such that $h(x^*) \in K(x^*)$ and

$$\langle f(x^*), y - h(x^*) \rangle \geq 0 \quad \forall \quad y \in K(x^*).$$

When h is the identity map on $\mathbb{R}^n$, then IQVI(f, h, K) reduces to the classical quasi-variational inequality.

When $K(x)$ is a constant set $\bar{K}$ on $\mathbb{R}^n$, then IQVI (f, h, K) reduces to inverse variational inequality IVI$(f, h, \bar{K})$.

Now, take f to be the identity map. We have

$$\text{IQVI}(h,K):\ \text{Find } x^* \in \mathbb{R}^n \text{ such that } h(x^*) \in K(x^*)$$
$$\text{and } \langle x^*, y - h(x^*)\rangle \geq 0 \quad \forall \quad y \in K(x^*).$$

Let L be a parametric normed space and $P \subset L$ be a closed ball with positive radius; $p^* \in P$ is a fixed point. Then the perturbed problem of $\text{IQVI}(h,K)$ is given by

$$\text{IQVI}_p(\tilde{h},K):\ \text{Find } x^* \in \mathbb{R}^n \text{ such that } \tilde{h}(p,x^*) \in K(x^*)$$
$$\text{and } \langle x^*, y - \tilde{h}(p,x^*)\rangle \geq 0 \quad \forall \quad y \in K(x^*)$$

where $\tilde{h} : P \times \mathbb{R}^n \to \mathbb{R}^n$ is such that $\tilde{h}(p^*,\cdot) = h$.

When $K(x^*) = K$, $\text{IQVI}_p(\tilde{h},K)$ reduces to the inverse variational inequality, the well-posedness of which has already been dealt with [11, 36].

Let T be the solution set of $\text{IQVI}_p(\tilde{h},K)$.

Now, we introduce some notations:

Definition 1. *Let $\{p_n\} \subset P$ with $p_n \to p^*$. A sequence $\{x_n\} \subset \mathbb{R}^n$ is called α-approximating sequence corresponding to $\{p_n\}$ for $\text{IQVI}_p(\tilde{h},K)$ if there exists a sequence $\varepsilon_n > 0$ with $\varepsilon_n \to 0$ such that $\tilde{h}(p_n,x_n) \in K(x_n)$ and*

$$\langle x_n, \tilde{h}(p_n,x_n) - y\rangle \leq \frac{\alpha}{2} \| \tilde{h}(p_n,x_n) - y \|^2 + \varepsilon_n \quad \forall \quad y \in K(x_n) \text{ and } n \in \mathbb{N}.$$

When $\alpha = 0$, we say that $\{x_n\}$ is an approximating sequence corresponding to $\{p_n\}$ for $\text{IQVI}_p(\tilde{h},K)$.

Definition 2. *Let $\{p_n\} \subset P$ with $p_n \to p^*$. A sequence $\{x_n\} \subset \mathbb{R}^n$ is called LP α-approximating* sequence c*orresponding to $\{p_n\}$ for $\text{IQVI}_p(\tilde{h},K)$ if there exists a sequence $\varepsilon_n > 0$ with $\varepsilon_n \to 0$ and $w_n \in \mathbb{R}^n$ with $w_n \to 0$ such that $\tilde{h}(p_n,x_n) + w_n \in K(x_n)$ and*

$$\langle x_n, \tilde{h}(p_n,x_n) - y\rangle \leq \frac{\alpha}{2} \| \tilde{h}(p_n,x_n) - y \|^2 + \varepsilon_n \quad \forall y \in K(x_n) \text{ and } n \in \mathbb{N}.$$

When $\alpha = 0$, we say that $\{x_n\}$ is LP approximating sequence corresponding to $\{p_n\}$ for $\text{IQVI}_p(\tilde{h},K)$.

Clearly every α-approximating sequence (corresponding to $\{p_n\}$) is LP α-approximating.

Definition 3. $\text{IQVI}_p(\tilde{h},K)$ *is α-well-posed by perturbations if* $\text{IQVI}_p(\tilde{h},K)$ *has a unique solution and for any sequence $\{p_n\} \subset P$ with $p_n \to p^*$, every α-approximating sequence corresponding to $\{p_n\}$ converges to the unique solution.*

If $\alpha_1 > \alpha_2 \geq 0$, then α_1-well-posedness by perturbations implies α_2-well-posedness by perturbations.

Definition 4. $\text{IQVI}_p(\tilde{h},K)$ is LP α-well-posed by perturbations *if* $\text{IQVI}_p(\tilde{h},K)$ *has a unique solution and for any sequence $\{p_n\} \subset P$ with $p_n \to p^*$, every LP α-approximating sequence corresponding to $\{p_n\}$ converges to the unique solution.*

When $p_n = p^*$, LP α-well-posedness by perturbations is called LP α-well-posedness.

Definition 5. $\mathrm{IQVI}_p(\tilde{h},K)$ *is* α*-well-posed by perturbations in the generalised sense if* $\mathrm{IQVI}_p(\tilde{h},K)$ *has a non-empty solution set and for any sequence* $\{p_n\}\subset P$ *with* $p_n \to p^*$, *every* α*-approximating sequence corresponding to* $\{p_n\}$ *has some subsequence which converges to some solution.*

Definition 6. $\mathrm{IQVI}_p(\tilde{h},K)$ *is LP* α*-well-posed by perturbations in the generalised sense if* $\mathrm{IQVI}_p(\tilde{h},K)$ *has at least one solution and for any sequence* $\{p_n\}\subset P$ *with* $p_n \to p^*$, *every LP* α*-approximating sequence corresponding to* $\{p_n\}$ *has some subsequence which converges to some solution.*

Definition 7. *A function* $h : \mathbb{R}^n \to \mathbb{R}^n$ *is said to be*

(i) monotone if $\langle h(x)-h(y), x-y\rangle \geq 0 \ \ \forall \ \ x,y\in\mathbb{R}^n$.

(ii) hemicontinuous if, for any $x,y\in\mathbb{R}^n$, $t \mapsto \langle hx+t(y-x), y-x\rangle$ *from* $[0,1]$ *to* $\mathbb{R}$ *is continuous at* 0^+.

Definition 8. *Let* A, B *be non-empty subsets of* $\mathbb{R}^n$. *The excess from* A *to* B *is defined by*

$$e(A,B)=\sup_{a\in A} d(a,B),$$

where $d(a,B)=\inf_{b\in B} \| a-b \|$.

Now, recall the notion of Mosco convergence. A sequence $(H_n)_n$ of subsets of E converges to a set H if

$$H=\liminf_n H_n = w\text{-}\limsup_n H_n,$$

where $\liminf H_n$ is the Painlevé-Kuratowski strong limit inferior and $w\text{-}\limsup H_n$ is the Painlevé-Kuratowski weak limit superior of a sequence $(H_n)_n$, i.e.

$$\liminf H_n = \{y\in E : \exists \ \ y_n \in H_n, n\in\mathbb{N} \ \text{ with } \ y_n \to y\}$$

and

$$w\text{-}\limsup H_n = \{y\in E : \exists \ \ n_k \uparrow +\infty, n_k\in\mathbb{N}, \exists \ \ y_{n_k}\in H_{n_k}, k\in\mathbb{N} \ \text{ with } \ y_{n_k} \rightharpoonup y\}.$$

If $H=\liminf H_n$, we call the sequence $(H_n)_n$ of subsets of E Lower Semi-Mosco which converges to a set H.

We state the following lemma which will be needed in the paper.

Lemma 1 [20]. *Let* $(H_n)_n$ *be a sequence of non-empty subsets of* E *such that*

(i) H_n *is convex* $\forall \ \ n\in\mathbb{N}$.

(ii) $H_0 \subseteq \liminf H_n$.

(iii) there exists $m\in\mathbb{N}$ *such that* $\bigcap_{n\geq m} H_n \neq \varnothing$.

Then for every $u_0 \in \operatorname{int} H_0$, *there exists a positive real number* δ *such that* $B(u_0,\delta)\subseteq H_n \ \ \forall \ \ n\geq m$.

If E *is a finite dimensional space, then assumption (iii) can be replaced by (iii)'* $\operatorname{int} H_0 \neq \varnothing$.

Now, consider the following approximating solution set of $\mathrm{IQVI}_p(\tilde{h},K)$:

For any $\varepsilon \geq 0$,

$$T_\alpha^p(\varepsilon) = \bigcup_{p\in B(p^*,\varepsilon)} \{x \in \mathbb{R}^n \ : \ d(\tilde{h}(p,x), K(x)) \le \varepsilon$$

$$\text{and } \langle x, \tilde{h}(p,x) - y\rangle \le \frac{\alpha}{2} \| \tilde{h}(p,x) - y \|^2 + \varepsilon \ \ \forall\, y \in K(x)\},$$

where $B(p^*,\varepsilon)$ denotes the closed ball centred at p^* with radius ε.

CASE OF A UNIQUE SOLUTION

In this section we investigate some metric characterisations of LP α-well-posedness with perturbations for $\text{IQVI}_p(\tilde{h}, K)$.

Theorem 1. *Let x^* be a solution of $\text{IQVI}_p(\tilde{h}, K)$. Then $\text{IQVI}_p(\tilde{h}, K)$ is LP α-well-posed by perturbations if and only if $\theta(\varepsilon) \to 0$ as $\varepsilon \to 0$, where $\theta(\varepsilon) = \sup\{\| x - x^* \| : x \in T_\alpha^p(\varepsilon)\}$ $\forall$ $\varepsilon \ge 0$.*

Proof: Let $\text{IQVI}_p(\tilde{h}, K)$ be LP α-well-posed by perturbations.

Then $x^* \in \mathbb{R}^n$ is the unique solution of $\text{IQVI}_p(\tilde{h}, K)$.

Let $\theta(\varepsilon) \not\to 0$ as $\varepsilon \to 0$. Then there exists $\delta > 0$ and a sequence $\{p_n\}$ such that $\text{IQVI}_p(\tilde{h}, K)$.

By definition of θ, there exists $x_n \in T_\alpha^p(\varepsilon_n)$ such that

$$\| x_n - x^* \| > \delta. \tag{1}$$

Since $x_n \in T_\alpha^p(\varepsilon_n)$, there exists $p_n \in B(p^*, \varepsilon_n)$ such that

$$d(\tilde{h}(p_n, x_n), K(x_n)) \le \varepsilon_n < \varepsilon_n + \frac{1}{n} \tag{2}$$

and

$$\left\langle x_n, \tilde{h}(p_n, x_n) - y \right\rangle \le \frac{\alpha}{2} \| \tilde{h}(p_n, x_n) - y \|^2 + \varepsilon_n \quad \forall\ y \in K(x_n). \tag{3}$$

Clearly, $p_n \to p^*$.

By (2), there exists $y_n \in K(x_n)$ such that $\| \tilde{h}(p_n, x_n) - y_n \| < \varepsilon_n + \frac{1}{n}$.

Take $w_n = y_n - \tilde{h}(p_n, x_n)$. Then

$$\tilde{h}(p_n, x_n) + w_n \in K(x_n) \text{ and } w_n \to 0. \tag{4}$$

By (3) and (4), $\{x_n\}$ is LP α-approximating sequence corresponding to $\{p_n\}$ for $\text{IQVI}_p(\tilde{h}, K)$ which is LP α-well-posed by perturbations.

Thus $\| x_n - x^* \| \to 0$, a contradiction to (1).

Conversely, let $\theta(\varepsilon) \to 0$ as $\varepsilon \to 0$. Then $x^* \in \mathbb{R}^n$ is the unique solution of $\text{IQVI}_p(\tilde{h}, K)$. If $\bar{x}$ $(\ne x^*)$ is another solution of $\text{IQVI}_p(\tilde{h}, K)$, then $\theta(\varepsilon) \ge \| x^* - \bar{x} \| > 0$ $\forall$ $\varepsilon \ge 0$, a contradiction.

Let $\{p_n\} \subset P$ with $p_n \to p^*$ and let $\{x_n\}$ be LP α-approximating sequence corresponding to $\{p_n\}$ for $\varepsilon_n = \max\{\| p_n - p^* \|, \| w_n \|, \varepsilon_n'\}$. Then there exists $w_n \in \mathbb{R}^n$ with $w_n \to 0$ and $\varepsilon_n > 0$ with $\varepsilon_n \to 0$ such that

$$\tilde{h}(p_n, x_n) + w_n \in K(x_n)$$

and

$$\left\langle x_n, \tilde{h}(p_n, x_n) - y \right\rangle \le \frac{\alpha}{2} \| \tilde{h}(p_n, x_n) - y \|^2 + \varepsilon_n \quad \forall\ y \in K(x_n) \ \ \forall\ n \in \mathbb{N}.$$

Taking $\delta_n = \| p_n - p^* \|$ and $\varepsilon_n' = \max\{\delta_n, \varepsilon_n, \| w_n \|\}$, we have $x_n \in T_\alpha^p(\varepsilon_n')$ with $\varepsilon_n' \to 0$.
Thus, $\| x_n - x^* \| \le \theta(\varepsilon_n') \to 0$.
Hence $\mathrm{IQVI}_p(\tilde{h}, K)$ is LP α-well-posed by perturbations.

The following example justifies the conclusion of Theorem 1.

Example 1. Let $X = \mathbb{R}$, $\tilde{h}(p,x) = x(1+|p|)$, $K(x) = \begin{cases} [0,\infty), & x \le 0 \\ (-\infty, 0), & x > 0 \end{cases}$, $P = [-1,1]$, $p^* = 0$, $\alpha = 2$.
Clearly, $x^* = 0$ is the solution of $\mathrm{IQVI}_p(\tilde{h}, K)$.
Let $A_\alpha^p(\varepsilon) = \{x \in \mathbb{R} : d(\tilde{h}(p,x), K(x)) \le \varepsilon\}$.
When $x \le 0$, $A_\alpha^p(\varepsilon) = \left[\frac{-\varepsilon}{1+|p|}, 0\right]$.
When $x > 0$, $A_\alpha^p(\varepsilon) = \left[0, \frac{\varepsilon}{1+|p|}\right]$.
Let

$$B_\alpha^p(\varepsilon) = \left\{x \in \mathbb{R} : \langle x, \tilde{h}(p,x) - y\rangle \le \| \tilde{h}(p,x) - y \|^2 + \varepsilon \quad \forall \quad y \in K(x)\right\}$$
$$= \left\{x \in \mathbb{R} : -\left[y - \left(\frac{2|p|+1}{2}\right)x\right]^2 + \frac{x^2}{4} \le \varepsilon \quad \forall \quad y \in K(x)\right\}.$$

When $x \le 0$,

$$B_\alpha^p(\varepsilon) = \left\{x \le 0 : -\left[y - \left(\frac{2|p|+1}{2}\right)x\right]^2 + \frac{x^2}{4} \le \varepsilon \ \forall\, y \ge 0\right\}.$$

When $x > 0$,

$$B_\alpha^p(\varepsilon) = \left\{x > 0 \ : -\left[y - \left(\frac{2|p|+1}{2}\right)x\right]^2 + \frac{x^2}{4} \le \varepsilon \quad \forall \quad y < 0\right\}.$$

Now,

$$T_\alpha^p(\varepsilon) = \bigcup_{p \in B(0,\varepsilon)} [A_\alpha^p(\varepsilon) \cap B_\alpha^p(\varepsilon)].$$

When $x \le 0$,

$$T_\alpha^p(\varepsilon) = \bigcup_{p \in B(0,\varepsilon)} \left(\left[\frac{-\varepsilon}{1+|p|}, 0\right] \cap B_\alpha^p(\varepsilon)\right)$$
$$= \bigcup_{p \in B(0,\varepsilon)} \left[\frac{-\varepsilon}{1+|p|}, 0\right] = [-\varepsilon, 0].$$

When $x > 0$,

$$T_\alpha^p(\varepsilon) = \bigcup_{p \in B(0,\varepsilon)} \left(\left[0, \frac{\varepsilon}{1+|p|}\right] \cap B_\alpha^p(\varepsilon)\right)$$
$$= \bigcup_{p \in B(0,\varepsilon)} \left(0, \frac{\varepsilon}{1+|p|}\right] = (0, \varepsilon].$$

Thus,

$$\theta(\varepsilon) = \{\sup \| x - x^* \| : x \in T_\alpha^p(\varepsilon)\}$$
$$= \sup_{x \in T_\alpha^p(\varepsilon)} |x| = \begin{cases} \varepsilon, & x \le 0 \\ \varepsilon, & x > 0 \end{cases}$$

and so $\theta(\varepsilon) \to 0$ as $\varepsilon \to 0$.

Hence the problem is LP α-well-posed by perturbations.

Next, we give a characterisation of LP α-well-posedness by perturbations using the approximate solution set $T_\alpha^p(\varepsilon)$.

Theorem 2. *Let K be a non-empty, convex-valued, set-valued map. Let $\tilde{h} : P \times \mathbb{R}^n \to \mathbb{R}^n$ be continuous. Assume the following:*
(i) K is non-empty convex-valued and for each sequence $\{x_n\}$ converging to x, the sequence $K(x_n)_n$ Lower Semi-Mosco converges to $K(x)$.
(ii) For every converging sequence $(x_n)_n$, there exists $m \in \mathbb{N}$ such that $\operatorname{int} \bigcap_{n \ge m} K(x_n) \neq \varnothing$.

Then $\mathrm{IQVI}_p(\tilde{h}, K)$ *is LP α-well-posed by perturbations if and only if $T_\alpha^p(\varepsilon) \neq \varnothing \ \forall \ \varepsilon > 0$ and* $\operatorname{diam} T_\alpha^p(\varepsilon) \to 0$ *as* $\varepsilon \to 0$.

Proof: Let $\mathrm{IQVI}_p(\tilde{h}, K)$ be LP α-well-posed by perturbations. Then $T_\alpha^p(\varepsilon) \neq \varnothing \ \forall \ \varepsilon > 0$.

On the contrary, assume diam $T_\alpha^p(\varepsilon) \not\to 0$ as $\varepsilon \to 0$. Then there exists a constant $\ell > 0$ and a sequence $\{\varepsilon_n\} \subset \mathbb{R}^+$ with $\varepsilon_n \to 0$ and $\{x_n^{(1)}\}, \{x_n^{(2)}\} \in T_\alpha^p(\varepsilon_n)$ such that

$$\| x_n^{(1)} - x_n^{(2)} \| > \ell \quad \forall \ n \in \mathbb{N} \tag{5}$$

As $\{x_n^{(1)}\} \in T_\alpha^p(\varepsilon_n)$, we have

$$d(\tilde{h}(p_n, x_n^{(1)}), K(x_n)) \le \varepsilon_n < \varepsilon_n + \frac{1}{n} \tag{6}$$

and

$$\left\langle x_n^{(1)}, \tilde{h}(p_n, x_n^{(1)}) - y \right\rangle \le \frac{\alpha}{2} \| \tilde{h}(p_n, x_n^{(1)}) - y \|^2 + \varepsilon_n \ \ \forall \ y \in K(x_n) \ \ \forall \ n \in \mathbb{N}. \tag{7}$$

By (6), there exists $\bar{x}_n^{(1)} \in K(x_n)$ such that

$$\| \tilde{h}(p_n, x_n^{(1)}) - \bar{x}_n^{(1)} \| < \varepsilon_n + \frac{1}{n}.$$

Let $w_n = \bar{x}_n^{(1)} - \tilde{h}(p_n, x_n^{(1)})$.

Thus, $\tilde{h}(p_n, x_n^{(1)}) + w_n = \bar{x}_n^{(1)} \in K(x_n)$ and $\| w_n \| = \| \bar{x}_n^{(1)} - \tilde{h}(p_n, x_n^{(1)}) \| \to 0$ as $n \to \infty$.

Thus, $\{x_n^{(1)}\}$ is LP α-approximating sequence corresponding to $\{p_n\}$ for $\mathrm{IQVI}_p(\tilde{h}, K)$.

Similarly, $\{x_n^{(2)}\}$ is LP α-approximating sequence corresponding to $\{p_n\}$ for $\mathrm{IQVI}_p(\tilde{h}, K)$.

So they both converge to the unique solution of $\mathrm{IQVI}_p(\tilde{h}, K)$, which is a contradiction to (5).

Conversely, let $T_\alpha^p(\varepsilon) \neq \varnothing \ \forall \ \varepsilon > 0$ and diam $T_\alpha^p(\varepsilon) \to 0$ as $\varepsilon \to 0$.

Let $\{p_n\} \subset P$ with $p_n \to p^*$, and let $\{x_n\}$ be LP α-approximating sequence for $\mathrm{IQVI}_p(\tilde{h}, K)$.

Then there exists $0 < \{\varepsilon_n'\} \downarrow 0$ and $w_n \in \mathbb{R}^n$ with $w_n \to 0$ such that $\tilde{h}(p_n, x_n) + w_n \in K(x_n)$ and

$$\left\langle x_n, \tilde{h}(p_n, x_n) - y \right\rangle \le \frac{\alpha}{2} \| \tilde{h}(p_n, x_n) - y \|^2 + \varepsilon_n' \ \ \forall \ y \in K(x_n) \ \ \forall \ n \in \mathbb{N}.$$

As $\tilde{h}(p_n, x_n) + w_n \in K(x_n)$, there exists $\bar{x}_n \in K(x_n)$ such that $\tilde{h}(p_n, x_n) + w_n = \bar{x}_n$.

Now, $d(\tilde{h},(p_n, x_n), K(x_n)) \leq \| \tilde{h}(p_n, x_n) - \bar{x}_n \| = \| w_n \| \to 0$.

Set $\varepsilon_n = \max\{\| p_n - p^* \|, \| w_n \|, \varepsilon_n'\}$. Thus, $\{x_n\} \in T_\alpha^p(\varepsilon_n)$.

Also, by hypothesis, $\{x_n\}$ is a Cauchy sequence and so it converges strongly to a point x. If x_1, x_2 are two distinct solutions of $\text{IQVI}_p(\tilde{h}, K)$, then $x_1, x_2 \in T_\alpha^p(\varepsilon) \quad \forall \quad \varepsilon > 0$ and $0 < \| x_1 - x_2 \| \leq \text{diam}\, T_\alpha^p(\varepsilon) \to 0$, a contradiction. We claim that x solves $\text{IQVI}_p(\tilde{h}, K)$. We prove this in the next two steps:

(a) $\tilde{h}(p^*, x) \in K(x)$.

For each $n \in \mathbb{N}$, choose $\tilde{h}(p_n, x_n') \in K(x_n)$ such that

$$\tilde{h}(p_n, x_n) - \tilde{h}(p_n, x_n') < d(\tilde{h}(p_n, x_n), K(x_n)) + \varepsilon_n \leq 2\varepsilon_n.$$

As $x_n \to x$ and $h(\cdot,\cdot)$ is continuous, we get $\tilde{h}(p_n, x_n) \to \tilde{h}(p^*, x)$.

Thus, it follows from above and $\varepsilon \to 0$ that

$$\tilde{h}(p_n, x_n') \to \tilde{h}(p^*, x).$$

Now,

$$\liminf K(x_n) = \{\tilde{h}(p^*, x) \in \mathbb{R}^n : \exists\, \tilde{h}(p_n, x_n') \in K(x_n), n \in \mathbb{N} \text{ with } \tilde{h}(p_n, x_n') \to \tilde{h}(p^*, x)\}.$$

Thus, $\liminf K(x_n) = K(x)$ and so $\tilde{h}(p^*, x) \in K(x)$.

(b) $\langle x, y - \tilde{h}(p^*, x)\rangle \geq 0 \quad \forall \quad y \in K(x)$.

Consider any $y \in K(x)$.

By Lower Semi-Mosco convergence, we have

$$K(x) \subseteq \liminf K(x_n).$$

By condition (ii) in the hypothesis applied to the constant sequence $x \quad \forall \quad n \in \mathbb{N}$ implies $\text{int}\, K(x) \neq \varnothing$.

Hence from Lemma 1, for $v \in \text{int}\, K(x)$, there exists $\delta > 0$ and $m \in \mathbb{N}$ such that $B(v, \delta) \subseteq K(x_n)$ $\forall \quad n > m$. Thus, $v \in K(x_n)$ for n sufficiently large.

As $\{x_n\}$ is LP α-approximating sequence for $\text{IQVI}_p(\tilde{h}, K)$, we have

$$\begin{aligned} \left\langle x, \tilde{h}(p^*, x) - y \right\rangle &= \lim \left\langle x_n, \tilde{h}(p_n, x_n) - y \right\rangle \\ &\leq \lim \left(\frac{\alpha}{2} \| \tilde{h}(p_n, x_n) - y \|^2 + \varepsilon_n \right) \\ &= \frac{\alpha}{2} \| \tilde{h}(p^*, x) - y \|^2 . \end{aligned}$$

Now, if $v \in K(x) \setminus \text{int}\, K(x)$, let $\{v_n\}$ be a sequence converging to v, whose point belongs to a segment contained in $\text{int}\, K(x)$.

Since $v_n \in \text{int}\, K(x) \quad \forall \quad n \in \mathbb{N}$, one has

$$\left\langle x_n, \tilde{h}(p_n, x_n) - v_n \right\rangle \leq \frac{\alpha}{2} \| \tilde{h}(p^*, x) - v_n \|^2 .$$

As h is continuous, this implies

$$\left\langle x, \tilde{h}(p^*, x) - v \right\rangle \leq \frac{\alpha}{2} \| \tilde{h}(p^*, x) - v \|^2, \quad v \in K(x).$$

As K is convex-valued, then $\forall\ y \in K(x)$, $t \in [0,1]$, $v_t = ty + (1-t)\tilde{h}(p^*, x) \in K(x)$.
Thus, $\langle x, \tilde{h}(p^*, x) - v_t \rangle \leq \frac{\alpha}{2} \| \tilde{h}(p^*, x) - v_t \|^2\ \forall\ y \in K(x), t \in [0,1]$.
Taking $t \to 0$, we get that x solves $\mathrm{IQVI}_p(\tilde{h}, K)$.

LP α-WELL-POSEDNESS BY PERTURBATIONS IN THE GENERALISED SENSE

In this section we investigate metric characterisations of LP α-well-posedness in the generalised sense for $\mathrm{IQVI}_p(\tilde{h}, K)$.

Theorem 3. *Let x^* be a solution of $\mathrm{IQVI}_p(\tilde{h}, K)$. Then $\mathrm{IQVI}_p(\tilde{h}, K)$ is LP α-well-posed by perturbations in the generalised sense if and only if T is non-empty and compact, and $e(T_\alpha^p(\varepsilon), T) \to 0$ as $\varepsilon \to 0$.*

Proof: Let $\mathrm{IQVI}_p(\tilde{h}, K)$ be LP α-well-posed by perturbations in the generalised sense. Then T is compact as when $\{x_n\}$ is any sequence in T and sequence $\{p_n\} \subset P$ with $p_n = p^*$, then $\{x_n\}$ is LP α-approximating sequence corresponding to $\{p_n\}$ for $\mathrm{IQVI}_p(\tilde{h}, K)$. So $\{x_n\}$ has a sub-sequence which converges to some point of T. Thus, T is compact.
If $e(T_\alpha^p(\varepsilon), T) \not\to 0$ as $\varepsilon \to 0$, then there exists $\ell > 0$, $\varepsilon_n > 0$ with $\varepsilon_n \downarrow 0$ and $x_n \in T_\alpha^p(\varepsilon_n)$ such that

$$x_n \notin T + B(0, \ell). \tag{8}$$

Since $x_n \in T_\alpha^p(\varepsilon_n)$, there exists $p_n \in B(p^*, \varepsilon_n)$ such that

$$d(\tilde{h}(p_n, x_n), K(x_n)) \leq \varepsilon_n < \varepsilon_n + \frac{1}{n}$$

and

$$\left\langle x_n, \tilde{h}(p_n, x_n) - y \right\rangle \leq \frac{\alpha}{2} \| \tilde{h}(p_n, x_n) - y \|^2 + \varepsilon_n \quad \forall\ y \in K(x_n).$$

As proved in Theorem 2, $\{x_n\}$ is LP α-approximating sequence corresponding to $\{p_n\}$ for $\mathrm{IQVI}_p(\tilde{h}, K)$, which is LP α-well-posed by perturbations in the generalised sense. Thus, there exists a sub-sequence $\{x_{n_k}\}$ of $\{x_n\}$ converging to some point of T. This contradicts (8).
Conversely, let T be compact and $e(T_\alpha^p(\varepsilon), T) \to 0$ as $\varepsilon \to 0$.
Let $\{p_n\} \subset P$ with $p_n \to p^*$, and let $\{x_n\}$ be LP α-approximating sequence corresponding to $\{p_n\}$.
Then there exists $w_n \in \mathbb{R}^n$ with $w_n \to 0$ and $0 < \varepsilon_n' \downarrow 0$ such that $\tilde{h}(p_n, x_n) + w_n \in K(x_n)$ and

$$\left\langle x_n, \tilde{h}(p_n, x_n) - y \right\rangle \leq \frac{\alpha}{2} \| \tilde{h}(p_n, x_n) - y \|^2 + \varepsilon_n' \quad \forall\ y \in K(x_n)\ \forall\ n \in \mathbb{N}.$$

Take $\varepsilon_n = \max\{\varepsilon_n', \| w_n \|, \| p_n - p^* \|\}$. Then $\varepsilon_n \to 0$ and $x_n \in T_\alpha^p(\varepsilon_n)$.
Thus, $d(x_n, T) \leq e(T_\alpha^p(\varepsilon_n), T) \to 0$.
Since T is compact, there exists $\bar{x}_n \in T$ such that $\| x_n - \bar{x}_n \| = d(x_n, T) \to 0$. Again, from the compactness of T, $\{\bar{x}_n\}$ has a sub-sequence $\{\bar{x}_{n_k}\}$ converging to $\bar{x} \in T$. Hence the corresponding sequence $\{x_{n_k}\}$ of $\{x_n\}$ converges to $\bar{x}$, proving that $\mathrm{IQVI}_p(\tilde{h}, K)$ is LP α-well-posed by perturbations in the generalised sense.

We now give the following example as an application of Theorem 3.

Example 2. Consider Example 1.

The solution set $T = \{0\}$ is compact and

$$T_\alpha^p(\varepsilon) = \begin{cases} [-\varepsilon, 0], & x \le 0 \\ (0, \varepsilon], & x > 0. \end{cases}$$

Thus, $e(T_\alpha^p(\varepsilon), T) \to 0$ as $\varepsilon \to 0$.

Hence the problem is LP α-well-posed by perturbations in the generalised sense.

Further, characterisation is given in terms of measure of non-compactness.

Theorem 4. *Let the assumptions be as in Theorem 2. Then* $\text{IQVI}_p(\tilde{h}, K)$ *is LP* α*-well-posed by perturbations in the generalised sense if and only if* $T_\alpha^p(\varepsilon) \neq \varnothing \ \forall \ \varepsilon > 0$ *and* $\mu(T_\alpha^p(\varepsilon)) \to 0$ *as* $\varepsilon \to 0$.

Proof: Let $\text{IQVI}_p(\tilde{h}, K)$ be LP α-well-posed by perturbations in the generalised sense. Then $T_\alpha^p(\varepsilon) \neq \varnothing \ \forall \ \varepsilon > 0$.

By Theorem 3, T is non-empty and compact, and $e(T_\alpha^p(\varepsilon), T) \to 0$ as $\varepsilon \to 0$.

For any $\varepsilon > 0$, we have

$$\begin{aligned} \mathcal{H}(T_\alpha^p(\varepsilon), T) &= \max\{e(T_\alpha^p(\varepsilon), T), e(T, T_\alpha^p(\varepsilon))\} \\ &= e(T_\alpha^p(\varepsilon), T). \end{aligned}$$

As T is compact, $\mu(T) = 0$.

Since $\forall \ n \in \mathbb{N}$, the following relation holds [37]:

$$\begin{aligned} \mu(T_\alpha^p(\varepsilon)) &\le 2\mathcal{H}(T_\alpha^p(\varepsilon), T) + \mu(T) \\ &= 2e(T_\alpha^p(\varepsilon), T) \to 0 \text{ as } \varepsilon \to 0. \end{aligned}$$

Conversely, let $T_\alpha^p(\varepsilon) \neq \varnothing \ \forall \ \varepsilon > 0$ and $\mu(T_\alpha^P(\varepsilon)) \to 0$ as $\varepsilon \to 0$.

Let $\{p_n\} \subset P$ be any sequence with $p_n \to p^*$, and let $\{x_n\}$ be LP α-approximating sequence for $\text{IQVI}_p(\tilde{h}, K)$.

Then there exists a sequence $\{\varepsilon_n'\} > 0$ with $\varepsilon_n' \downarrow 0$ and sequence $w_n \in \mathbb{R}^n$ with $w_n \to 0$ such that $\tilde{h}(p_n, x_n) + w_n \in K(x_n)$ and

$$\left\langle x_n, \tilde{h}(p_n, x_n) - y \right\rangle \le \frac{\alpha}{2} \| \tilde{h}(p_n, x_n) - y \|^2 + \varepsilon_n' \quad \forall \ y \in K(x_n) \ \forall \ n \in \mathbb{N}.$$

As K is non-empty, there exists $\bar{x}_n \in K(x_n)$ such that $\tilde{h}(p_n, x_n) + w_n = \bar{x}_n$.

Now, $d(\tilde{h}(p_n, x_n), K(x_n)) \le \| \tilde{h}(p_n, x_n) - \bar{x}_n \| = \| w_n \| \to 0$.

Set $\varepsilon_n = \max\{\| p_n - p^* \|, \| w_n \|, \varepsilon_n'\}$. Thus, $x_n \in T_\alpha^p(\varepsilon_n)$.

We claim that $e(T_\alpha^p(\varepsilon_n), T) \to 0$ as $\varepsilon \to 0$.

As $T_\alpha^p(\varepsilon_n) \neq \varnothing$, $\text{cl}(T_\alpha^p(\varepsilon_n))$ is non-empty and closed $\forall \ \varepsilon > 0$.

Thus, $\lim_{\varepsilon \to 0} \mu(\text{cl}(T_\alpha^p(\varepsilon))) = \lim_{\varepsilon \to 0} \mu(T_\alpha^p(\varepsilon)) = 0$.

Hence $\mathcal{H}(\text{cl}(T_\alpha^p(\varepsilon)), \bigcap_{\varepsilon > 0} \text{cl}(T_\alpha^p(\varepsilon))) \to 0$ as $\varepsilon \to 0$.

We now show that $T = \bigcap_{\varepsilon > 0} \text{cl}(T_\alpha^p(\varepsilon))$.

Obviously, $T \subset \bigcap_{\varepsilon>0} \text{cl}(T_\alpha^p(\varepsilon))$. For the reverse containment, let $x_0 \in \bigcap_{\varepsilon>0} \text{cl}(T_\alpha^p(\varepsilon))$. Then $d(x_0, T_\alpha^p(\varepsilon)) = 0 \ \forall \ \varepsilon > 0$.

Thus, given $\varepsilon_n > 0, \varepsilon_n \to 0 \ \forall \ n$, there exists $x_n \in T_\alpha^p(\varepsilon_n)$ such that $d(x_0, x_n) < \varepsilon_n$.
Hence $x_n \to x_0$ and $d(\tilde{h}(p_n, x_n), K(x_n)) \le \varepsilon_n$, and

$$\langle x_n, \tilde{h}(p_n, x_n) - y \rangle \le \frac{\alpha}{2} \| \tilde{h}(p_n, x_n) - y \|^2 + \varepsilon_n \quad \forall \ y \in K(x_n) \ \forall \ n \in \mathbb{N}.$$

By using the fact that $x_n \to x_0$, $\tilde{h}(\cdot,\cdot)$ is continuous and by condition (i) in the hypothesis, we obtain that $\tilde{h}(p^*, x) \in K(x)$.
Again by Theorem 2, we get $x_0 \in T$. Hence $\mathcal{H}(\text{cl}(T_\alpha^p(\varepsilon)), T) \to 0$ as $\varepsilon \to 0$ or $e(T_\alpha^p(\varepsilon), T) \to 0$ as $\varepsilon \to 0$.
Thus, we have $d(x_n, T) \le e(T_\alpha^p(\varepsilon), T) \to 0$ as $\varepsilon \to 0$.
T being compact, there exists $\bar{x}_n \in T$ such that

$$\| x_n - \bar{x}_n \| = d(x_n, T) \to 0.$$

Again, from compactness of T, $\{\bar{x}_n\}$ has a sub-sequence $\{\bar{x}_{n_k}\}$ converging to $\bar{x} \in T$. Hence the corresponding sub-sequence $\{x_{n_k}\}$ of $\{x_n\}$ converges to $\bar{x}$. Thus, $\text{IQVI}_p(\tilde{h}, K)$ is LP α-well-posed by perturbations in the generalised sense.

LP WELL-POSEDNESS AND UNIQUENESS

In this section we show that under suitable conditions, LP well-posedness by perturbations of an inverse quasi-variational inequality is equivalent to the existence and uniqueness of its solution.

Theorem 5. *Let K be a non-empty, convex-valued and set-valued map. Let $\tilde{h} : P \times \mathbb{R}^n \to \mathbb{R}^n$ be such that*
(i) $\tilde{h}(p,\cdot)$ is monotone $\forall \ p \in P$ and $\tilde{h}(p^*,\cdot)$ is hemicontinuous.
(ii) $\tilde{h}(\cdot, x)$ is continuous $\forall \ x \in \mathbb{R}^n$.
Then $\text{IQVI}_p(\tilde{h}, K)$ is LP well-posed by perturbations if and only if it has a unique solution.

Proof: The necessary condition holds true. For the sufficient condition, let $\text{IQVI}_p(\tilde{h}, K)$ has a unique solution x^*. Then $\tilde{h}(p, x^*) \in K(x^*)$ and

$$\langle x^*, y - \tilde{h}(p, x^*) \rangle \ge 0 \quad \forall \ y \in K(x^*). \tag{9}$$

Let $\{p_n\} \subset P$ be any sequence with $p_n \to p^*$ and $\{x_n\} \subset \mathbb{R}^n$ be LP approximating sequence corresponding to $\{p_n\}$ for $\text{IQVI}_p(\tilde{h}, K)$.

Then there exists a sequence $\{\varepsilon_n\} > 0$ with $\varepsilon_n \to 0$ and $w_n \in \mathbb{R}^n$ with $w_n \to 0$ such that $\tilde{h}(p_n, x_n) + w_n \in K(x_n)$ and

$$\langle x_n, \tilde{h}(p_n, x_n) - y \rangle \le \varepsilon_n \quad \forall \ y \in K(x_n) \ \forall \ n \in \mathbb{N}. \tag{10}$$

Take $u^* = (x^*, h(x^*))$ and $u_n = (x_n, \tilde{h}(p_n, x_n) + w_n) \ \forall \ n \in \mathbb{N}$.

If $\{u_n\}$ is unbounded, without loss of generality, we can suppose that $\| u_n \| \to +\infty$.

Set $t_n := \frac{1}{\|u_n - u^*\|}$ and

$$\begin{aligned} w_n &:= (z_n, g_n) = u^* + t_n(u_n - u^*) \\ &= \left(x^* + t_n(x_n - x^*), h(x^*) + t_n[\tilde{h}(p_n, x_n) + w_n - h(x^*)] \right). \end{aligned}$$

Without loss of generality, suppose $t_n \in (0,1]$ and $w_n \to w = (z,g) \in \mathbb{R}^n \times K(x^*)$.

Then $w = (z,g) \neq u^*$. For any $y \in K(x^*)$ and $x \in \mathbb{R}^n$, it follows that

$$\begin{aligned} &\left\langle \tilde{h}(p_n, x) - y, z - x \right\rangle + \left\langle g - y, x \right\rangle \\ &= \left\langle \tilde{h}(p_n, x) - y, z - z_n \right\rangle + \left\langle \tilde{h}(p_n, x) - y, z_n - x^* \right\rangle + \left\langle \tilde{h}(p_n, x) - y, x^* - x \right\rangle \\ &\quad + \left\langle g - g_{n,} x \right\rangle + \left\langle g_n - h(x^*), x \right\rangle + \left\langle h(x^*) - y, x \right\rangle \\ &= \{ \left\langle \tilde{h}(p_n, x) - y, z - z_n \right\rangle + \left\langle g - g_{n,} x \right\rangle \} + t_n \{ \left\langle \tilde{h}(p_n, x) - y, x_n - x \right\rangle + \left\langle \tilde{h}(p_n, x_n) + w_n - y, x \right\rangle \} \\ &\quad + (1 - t_n) \{ \left\langle \tilde{h}(p_n, x) - y, x^* - x \right\rangle + \left\langle h(x^*) - y, x \right\rangle \} \end{aligned} \tag{11}$$

As $\tilde{h}(p, \cdot)$ is monotone, it follows from (10) and (11) that

$$\begin{aligned} &\left\langle \tilde{h}(p_n, x) - y, z - x \right\rangle + \left\langle g - y, x \right\rangle \\ &\leq \left\langle \tilde{h}(p_n, x) - y, z - z_n \right\rangle + \left\langle g - g_{n,} x \right\rangle + t_n \{ \left\langle \tilde{h}(p_n, x_n) - y, x_n - x \right\rangle + \left\langle \tilde{h}(p_n, x_n) + w_n - y, x \right\rangle \} \\ &\quad + (1 - t_n) \{ \left\langle \tilde{h}(p_n, x) - y, x^* - x \right\rangle + \left\langle h(x^*) - y, x \right\rangle \} \\ &= \{ \left\langle \tilde{h}(p_n, x) - y, z - z_n \right\rangle + \left\langle g - g_{n,} x \right\rangle \} + t_n \{ \left\langle \tilde{h}(p_n, x_n) - y, x_n \right\rangle + \left\langle w_n, x \right\rangle \} \\ &\quad + (1 - t_n) \{ \left\langle \tilde{h}(p_n, x) - y, x^* - x \right\rangle + \left\langle \tilde{h}(x^*) - y, x \right\rangle \} \\ &\leq \{ \left\langle \tilde{h}(p_n, x) - y, z - z_n \right\rangle + \left\langle g - g_{n,} x \right\rangle \} + (1 - t_n) \{ \left\langle \tilde{h}(p_n, x) - y, x^* - x \right\rangle + \left\langle h(x^*) - y, x \right\rangle \} \\ &\quad + t_n \varepsilon_n + t_n \left\langle w_n, x \right\rangle \quad \forall\ x \in \mathbb{R}^n \quad \forall\ y \in K(x^*). \end{aligned}$$

Let $n \to \infty$; we get that

$$\begin{aligned} \left\langle h(x) - y, z - x \right\rangle + \left\langle g - y, x \right\rangle &= \left\langle \tilde{h}(p^*, x) - y, z - x \right\rangle + \left\langle g - y, x \right\rangle \\ &\leq \left\langle h(x) - y, x^* - x \right\rangle + \left\langle h(x^*) - y, x \right\rangle \\ &\leq \left\langle h(x^*) - y, x^* - x \right\rangle + \left\langle h(x^*) - y, x \right\rangle \\ &= \left\langle h(x^*) - y, x^* \right\rangle \quad \forall\ x \in \mathbb{R}^n \quad \forall\ y \in K(x^*). \end{aligned}$$

This together with (9) implies that

$$\left\langle h(x) - y, z - x \right\rangle + \left\langle g - y, x \right\rangle \leq 0 \quad \forall\ x \in \mathbb{R}^n \quad \forall\ y \in K(x^*). \tag{12}$$

For any $x' \in \mathbb{R}^n$ and $y' \in K(x^*)$, define $z(t) = z + t(x' - z)$ and

$$g(t) = g + t(y' - g) \quad \forall\ t \in [0,1].$$

Thus, (12) implies $\langle h(z(t)) - g(t), z - z(t) \rangle + \langle g - g(t), z(t) \rangle \leq 0$, i.e.

$$\langle h(z(t)) - g(t), z - x' \rangle + \langle g - y', z(t) \rangle \leq 0.$$

Let $t \to 0^+$, we get that

$$\langle h(z) - g, z - x' \rangle + \langle g - y', z \rangle \leq 0 \quad \forall x' \in \mathbb{R}^n \quad \forall y' \in K(x^*). \tag{13}$$

Letting $y' = g$ in (13) and $x' = z - \lambda r$, we get that $\lambda \langle h(z) - g, r \rangle \leq 0$, where λ is arbitrary and $r \in \mathbb{R}^n$ is also arbitrary. Thus,

$$h(z) = g \in K(x^*). \tag{14}$$

From (13) and (14), we get that $\langle h(z) - y', z\rangle \leq 0 \ \ \forall \ \ y' \in K(x^*)$, and so z solves IQVI$(\tilde{h}, K)$. Thus, $z = x^*$, which contradicts $(z, h(z)) \neq (x^*, h(x^*))$. So we can suppose that $\{u_n\}$ is bounded. Let $\{u_{n_k}\}$ be any sub-sequence of $\{u_n\}$ such that $u_{n_k} \to (\bar{x}, \bar{g})$ as $k \to \infty$. It is sufficient to show that $\bar{x}$ is a solution of IQVI$(\tilde{h}, K)$.

It follows from (10) that $\tilde{h}(p_{n_k}, x_{n_k}) + w_{n_k} \in K(x_{n_k})$ and

$$\langle x_{n_k}, \tilde{h}(p_{n_k}, x_{n_k}) - y_{n_k}\rangle \leq \varepsilon_{n_k} \qquad \forall\, y \in K(x_{n_k}) \ \ \forall\, k \in \mathbb{N}. \tag{15}$$

Let $k \to \infty$ in (15); we get that

$$\tilde{h}(p, \bar{x}) \in K(\bar{x})$$

and

$$\langle \bar{x}, \tilde{h}(p, \bar{x}) - y\rangle \leq 0 \quad \forall\, y \in K(\bar{x}).$$

Thus, $\bar{x}$ is a solution of IQVI$(\tilde{h}, K)$.

Remark 1. Theorem 5 generalises Theorem 4.1 of Hu and Fang [36], in which the equivalence of LP well-posedness and uniqueness of solution for the inverse variational inequality is derived.

CONCLUSIONS

We have established the Levitin-Polyak well-posedness for an inverse quasi-variational inequality and some metric characterisations have been given.

ACKNOWLEDGEMENTS

This research was funded by the Council of Scientific and Industrial Research, India (file number 09/045(1036)/2010-EMR-1). We are grateful to the anonymous referees and the editor for improving the paper.

REFERENCES

1. A. N. Tykhonov, "On the stability of the functional optimization problem", *USSR Comput. Math. Math. Phys*., **1966**, *6*, 28-33.
2. E. S Levitin and B. T. Poljak, "Convergence of minimizing sequences in conditional extremum problems", *Soviet Math. Dokl.*, **1966**, *7*, 764-767.
3. I. D. Prete, M. B. Lignola and J. Morgan, "New concepts of well-posedness for optimization problems with variational inequality constraints", *J. Inequal. Pure Appl. Math.*, **2003**, *4*, Article 5.
4. A. L. Dontchev and T. Zolezzi, "Well-posed Optimization Problems", Springer, Berlin, **1993**.
5. X. X. Huang and X. Q. Yang, "Generalized Levitin-Polyak well-posedness in constrained optimization", *SIAM J. Optim.*, **2006**, *17*, 243-258.
6. X. X. Huang and X. Q. Yang, "Levitin-Polyak well-posedness of constrained vector optimization problems", *J. Global Optim.*, **2007**, *37*, 287-304.
7. T. Zolezzi, "Well-posedness criteria in optimization with applications to the calculus of variations", *Nonlinear Anal. Theory Meth. Appl.*, **1995**, *25*, 437-453.
8. T. Zolezzi, "Extended well-posedness of optimization problems", *J. Optim. Theory Appl.*, **1996**, *91*, 257-266.
9. Y. P. Fang, N. J. Huang and J. C. Yao, "Well-posedness of mixed variational inequalities, inclusion problems and fixed point problems", *J. Global Optim.*, **2008**, *41*, 117-133.

10. Y. P. Fang, N. J. Huang and J. C. Yao, "Well-posedness by perturbations of mixed variational inequalities in Banach spaces", *Euro. J. Oper. Res.*, **2010**, *201*, 682-692.
11. R. Hu and Y. P. Fang, "Well-posedness of inverse variational inequalities", *J. Convex Anal.*, **2008**, *15*, 427-437.
12. R. Hu and Y. P. Fang, "Levitin-Polyak well-posedness of variational inequalities", *Nonlinear Anal. Theory Meth. Appl.*, **2010**, *72*, 373-381.
13. X. X. Huang and X. Q. Yang, "Levitin-Polyak well-posedness in generalized variational inequality problems with functional constraints", *J. Indus. Manag. Optim.*, **2007,** *3*, 671-684.
14. X. X. Huang, X. Q. Yang and D. L. Zhu, "Levitin-Polyak well-posedness of variational inequality problems with functional constraints", *J. Global Optim.*, **2009**, *44*, 159-174.
15. M. B. Lignola and J. Morgan, "Well-posedness for optimization problems with constraints defined by variational inequalities having a unique solution", *J. Global Optim.*, **2000**, *16*, 57-67.
16. M. B. Lignola, "Well-posedness and L-well-posedness for quasivariational inequalities", *J. Optim. Theory Appl.*, **2006**, *28*, 119-138.
17. R. Lucchetti and F. Patrone, "A characterization of Tykhonov well-posedness for minimum problems, with applications to variational inequalities", *Numer. Funct. Anal. Optim.*, **1981**, *3*, 461-476.
18. X. X. Huang and X. Q. Yang, "Levitin-Polyak well-posedness of vector variational inequality problems with functional constraints", *Numer. Funct. Anal. Optim.*, **2010**, *31*, 440-459.
19. X. B. Li and F. Q. Xia, "Levitin-Polyak well-posedness of generalized mixed variational inequality in Banach spaces", *Nonlinear Anal. Theory Meth. Appl.*, **2012**, *75*, 2139-2153.
20. J. W. Peng and J. Tang, "α-Well-posedness for quasivariational inequality problems", *Abstr. Appl. Anal.*, **2012**, *2012*, Art. ID 157532 (13 pages).
21. R. Hu, Y. P. Fang and N. J. Huang, "Characterizations of α-well-posedness for parametric quasivariational inequalities defined by bifunctions", *Math. Commun.*, **2010**, *15*, 37-55.
22. C. S. Lalitha and G. Bhatia, "Well-posedness for parametric quasivariational inequality problems and for optimization problems with quasivariational inequality constraints", *Optimization*, **2010**, *59*, 997-1011.
23. B. Jaing, J. Zhang and X. X. Huang, "Levitin-Polyak well-posedness of generalized quasivariational inequalities with functional constraints", *Nonlinear Anal. Theory Meth. Appl.*, **2009**, *70*, 1492-1503.
24. C. S. Lalitha and G. Bhatia, "Levitin-polyak well-posedness for parametric quasivariational inequality problem of the minty type", *Positivity*, **2012**, *16*, 527-541.
25. A. Jayswal, S. Choudhury and R. U. Verma, "Exponential type vector variational-like inequalities and vector optimization problems with exponential type invexities", *J. Appl. Math. Comput.*, **2014**, *45*, 87-97.
26. Q. H. Ansari, M. Rezaie and J. Zafarani, "Generalized vector variational-like inequalities and vector optimization", *J. Glob. Optim.*, **2012**, *53*, 271-284.
27. S. K. Mishra, S. Wang and K. K. Lai, "Role of α-pseudounivex functions in vector variational-like inequality problems", *J. Syst. Sci Complexity*, **2007**, *20*, 344-349.
28. R. Ferrentino, "Variational inequalities and optimization problems", *Appl. Math. Sci.*, **2007**, *47*, 2327-2343.

29. R. Hu, Y. P. Fang and N. J. Huang, "Levitin-Polyak well-posedness for variational inequalities and for optimization problems with variational inequality constraints", *J. Indus. Manag. Optim.*, **2010**, *6*, 465-481.
30. Q. M. Han and B. S. He, "A predict-correct projection method for monotone variant variational inequalities", *Chin. Sci. Bull.*, **1998**, *43*, 1264-1267.
31. B. S. He, "A Goldstein's type projection method for a class of variant variational inequalities", *J. Comput. Math.*, **1999**, *17*, 425-434.
32. B. S. He, "Inexact implicit methods for monotone general variational inequalities", *Math. Program.*, **1999**, *86*, 199-217.
33. B. S. He, X. Z. He and H. X. Liu, "Solving a class of constrained black-box inverse variational inequalities", *Euro. J. Oper. Res.*, **2010,** *204*, 391-401.
34. X. He and H. X. Liu, "Inverse variational inequalities with projection-based solution methods", *Euro. J. Oper. Res.*, **2011**, *208*, 12-18.
35. D. Aussel, R. Gupta and A. Mehra, "Gap functions and error bounds for inverse quasivariational inequality problems", *J. Math. Anal. Appl.*, **2013**, *407*, 270-280.
36. R. Hu and Y. P. Fang, "Levitin-Polyak well-posedness by perturbations of inverse variational inequalities", *Optim. Lett.*, **2013**, *7*, 343-359.
37. K. Kuratowski, "Topology", Vol. 1-2, Academic Press, New York, **1968**.
38. D. Kinderlehrer and G. Stampacchia, "An Introduction to Variational Inequalities and Their Applications", Academic Publishers, New York, **1980**.

Maejo Int. J. Sci. Technol. **2014**, *8*(03), 279-287

Maejo International Journal of Science and Technology

ISSN 1905-7873
Available online at www.mijst.mju.ac.th

Full Paper

The Fibonacci-Padovan sequences in finite groups

Sait Tas [1,*] **, Omur Deveci** [2] **and Erdal Karaduman** [1]

[1] Department of Mathematics, Faculty of Sciences, Atatürk University, 25240 Erzurum, Turkey

[2] Department of Mathematics, Faculty of Science and Letters, Kafkas University, 36100 Kars, Turkey

[*] Corresponding author, email: saittas@atauni.edu.tr

Received: 6 November 2013 / Accepted: 3 November 2014 / Published: 17 November 2014

Abstract: The Fibonacci-Padovan sequence modulo *m* was studied. Also, the Fibonacci-Padovan orbits of j-generator finite groups such that $2 \le j \le 5$ was examined. The Fibonacci-Padovan lengths of the groups Q_8, $Q_8 \times Z_{2m}$ and $Q_8 \times_{\varphi} Z_{2m}$ for $m \ge 3$, where Z is integer, were then obtained.

Keywords: Fibonacci-Padovan sequences, recurrence sequences, Fibonacci-Padovan orbits of finite groups, matrix

INTRODUCTION AND PRELIMINARIES

It is well known that linear recurrence sequences appear in modern research in many fields from mathematics, physics, computer science and architecture to nature and art [e.g. 1-10]. The study of recurrence sequences in groups began with an earlier work of Wall [11], who investigated the ordinary Fibonacci sequences in cyclic groups. The concept was extended to some special linear recurrence sequences by several authors [e.g. 12-21]. In this paper, we extend the theory to the Fibonacci-Padovan sequences.

A Fibonacci-Padovan sequence $\{a_n\}$ is defined [22] recursively by the equation

$$a_n = a_{n-1} + 2a_{n-2} - 2a_{n-3} + a_{n-5} \tag{1}$$

for $n \ge 5$, where $a_0 = 1, a_1 = 1, a_2 = 3, a_3 = 3, a_4 = 7$.

Kalman [23] mentioned that these sequences are special cases of a sequence which is defined recursively as a linear combination of the preceding *k* terms:

$$a_{n+k} = c_0 a_n + c_1 a_{n+1} + \mathrm{L} + c_{k-1} a_{n+k-1},$$

where $c_0, c_1, \mathrm{L}\ , c_{k-1}$ are real constants. Kalman [23] derived a number of closed-form formulas for the generalised sequence by companion matrix method as follows:

$$A_k = \left[a_{ij} \right]_{k\times k} = \begin{bmatrix} 0 & 1 & 0 & \mathrm{L} & 0 & 0 \\ 0 & 0 & 1 & \mathrm{L} & 0 & 0 \\ 0 & 0 & 0 & \mathrm{L} & 0 & 0 \\ \mathrm{M} & \mathrm{M} & \mathrm{M} & \mathrm{L} & \mathrm{M} & \mathrm{M} \\ c_0 & c_1 & c_2 & \mathrm{L} & c_{k-2} & c_{k-1} \end{bmatrix}. \tag{2}$$

Then by an inductive argument he obtained:

$$A_k^n \begin{bmatrix} a_0 \\ a_1 \\ \mathrm{M} \\ a_{k-1} \end{bmatrix} = \begin{bmatrix} a_n \\ a_{n+1} \\ \mathrm{M} \\ a_{n+k-1} \end{bmatrix}. \tag{3}$$

It is well known that a sequence, including that of group elements, is periodic if, after a certain point, it consists only of the repetition of a fixed sub-sequence. The number of elements in the repeating sub-sequence is the period of the sequence. For example, the sequence $a,b,c,d,e,b,c,d,e,b,c,d,e,\mathrm{L}$ is periodic after the initial element a and has period 4. A sequence of group elements is simply periodic with period *k* if the first *k* elements in the sequence form a repeating sub-sequence. For example, the sequence $a,b,c,d,e,f,a,b,c,d,e,f,a,b,c,d,e,f,\mathrm{L}$ is simply periodic with period 6.

Definition 1. For a finite generated group $G = \langle A \rangle$, where $A = \{a_1, a_2, ..., a_n\}$, the sequence $x_i = a_{i+1}$, $0 \le i \le n-1$, $x_{i+n} = \prod_{j=1}^{n} x_{i+j-1}$, $i \ge 0$ is called the Fibonacci orbit of G with respect to the generating set A, denoted by $F_A(G)$. If $F_A(G)$ is periodic, then the length of the period of the sequence is called the Fibonacci length of G with respect to the generating set A, written $LEN_A(G)$ [24].

FIBONACCI-PADOVAN SEQUENCES MODULO *m*

By (1) and (3), we can write

$$\begin{bmatrix} a_{n+1} \\ a_{n+2} \\ a_{n+3} \\ a_{n+4} \\ a_{n+5} \end{bmatrix} = \begin{bmatrix} 0 & 1 & 0 & 0 & 0 \\ 0 & 0 & 1 & 0 & 0 \\ 0 & 0 & 0 & 1 & 0 \\ 0 & 0 & 0 & 0 & 1 \\ 1 & 0 & -2 & 2 & 1 \end{bmatrix} \begin{bmatrix} a_n \\ a_{n+1} \\ a_{n+2} \\ a_{n+3} \\ a_{n+4} \end{bmatrix} \tag{4}$$

for the Fibonacci-Padovan sequence. Let us take

$$M=\left[m_{ij}\right]_{5\times 5}=\begin{bmatrix}0 & 1 & 0 & 0 & 0\\ 0 & 0 & 1 & 0 & 0\\ 0 & 0 & 0 & 1 & 0\\ 0 & 0 & 0 & 0 & 1\\ 1 & 0 & -2 & 2 & 1\end{bmatrix}.$$

which is said to be Fibonacci-Padovan matrix. By mathematical induction, it can be shown that, for $n\geq 0$,

$$M^n\begin{bmatrix}1\\1\\3\\3\\7\end{bmatrix}=\begin{bmatrix}a_n\\a_{n+1}\\a_{n+2}\\a_{n+3}\\a_{n+4}\end{bmatrix} \tag{5}$$

Reducing the Fibonacci-Padovan sequence by a modulus m, we can get the repeating sequence denoted by

$$\left\{a_n(m)\right\}=\left\{a_0(m),a_1(m),a_2(m),a_3(m),a_4(m),\text{L}\ ,a_i(m),\text{L}\ \right\}$$

where $a_i(m)\equiv a_i\pmod m$. It has the same recurrence relation as in (1).

Theorem 1. $\left\{a_n(m)\right\}$ is a simple periodic sequence.

Proof. Let $U=\left\{\left(x_1,x_2,\text{L}\ ,x_5\right)\middle|0\leq x_i\leq m-1\right\}$. Then we have $\left|U\right|=m^5$ being finite; that is, for any $j\geq 0$, there exists $i\geq j$ such that $a_{i+4}(m)\equiv a_{j+4}(m)$, $a_{i+3}(m)\equiv a_{j+3}(m)$, $a_{i+2}(m)\equiv a_{j+2}(m)$, $a_{i+1}(m)\equiv a_{j+1}(m)$ and $a_i(m)\equiv a_j(m)$. From the definition of the Fibonacci-Padovan sequence, we have $a_{n+5}=a_{n+4}+2a_{n+3}-2a_{n+2}+a_n$; that is, $a_n=a_{n+4}+2a_{n+3}-2a_{n+2}-a_{n+5}$. Then we can easily get that $a_{i-1}(m)\equiv a_{j-1}(m),a_{i-2}(m)\equiv a_{j-2}(m),\text{L}\ ,a_{i-j+1}(m)\equiv a_1(m),a_{i-j}(m)\equiv a_0(m)$, which implies that $\left\{a_n(m)\right\}$ is a simple periodic sequence.

Let $l(m)$ denote the smallest period of $\left\{a_n(m)\right\}$ and p is used for a prime number.

Example. We have $\left\{a_n(2)\right\}=\left\{1,1,1,1,1,0,1,0,1,0,0,1,1,0,0,0,1,0,0,0,0,1,1,1,1,1,\text{L}\ \right\}$, and then repeat. So we get $l(m)=21$.

For a given matrix $A=\left[a_{ij}\right]$ with a_{ij}'s being integers, $A\pmod m$ means that every entry of A is a reduced modulo m; that is, $A\pmod m\equiv\left(a_{ij}\pmod m\right)$. Let $\left\langle M\right\rangle_{p^u}=\left\{M^i\pmod{p^u}\middle|i\geq 0\right\}$ be a cyclic group and let $\left|\left\langle M\right\rangle_{p^u}\right|$ denote the order of $\left\langle M\right\rangle_{p^u}$. It is easy to see from (5) that $l\left(p^u\right)=\left|\left\langle M\right\rangle_{p^u}\right|$.

Theorem 2. Let t be the largest positive integer such that $l(p)=l\left(p^t\right)$. Then $l\left(p^\alpha\right)=p^{\alpha-t}\cdot l(p)$, for every $\alpha\geq t$.

Proof. Let q be a positive integer. Since $M^{l\left(p^{q+1}\right)}\equiv I\pmod{p^{q+1}}$; that is, $M^{l\left(p^{q+1}\right)}\equiv I\pmod{p^q}$, we get that $l\left(p^q\right)$ divides $l\left(p^{q+1}\right)$. On the other hand, writing $M^{l\left(p^q\right)}=I+\left(m_{ij}^{(q)}\cdot p^q\right)$, we have

$$M^{l\left(p^q\right)\cdot p}=\left(I+\left(m_{ij}^{(q)}\cdot p^q\right)\right)^p=\sum_{k=0}^{p}\binom{p}{k}\left(m_{ij}^{(q)}\cdot p^q\right)^k\equiv I\ \left(\mathrm{mod}\ p^{q+1}\right),$$

which yields that $l\left(p^{q+1}\right)$ divides $l\left(p^q\right)\cdot p$. Therefore, $l\left(p^{q+1}\right)=l\left(p^q\right)$ or $l\left(p^{q+1}\right)=l\left(p^q\right)\cdot p$, and the latter holds if and only if there is a $m_{ij}^{(q)}$ which is not divisible by p. Since $l\left(p^t\right)\neq l\left(p^{t+1}\right)$, there is an $m_{ij}^{(t+1)}$ which is not divisible by p; thus, $l\left(p^{t+1}\right)\neq l\left(p^{t+2}\right)$. The proof finishes by induction on t.

Theorem 3. If $m=\prod_{i=1}^{t}p_i^{e_i},\left(t\geq 1\right)$ where p_i's are distinct primes, then $l\left(m\right)=\mathrm{lcm}\left[l\left(p_i^{e_i}\right)\right]$.

Proof. The statement '$l\left(p_i^{e_i}\right)$ is the length of the period of $\left\{a_n\left(p_i^{e_i}\right)\right\}$' implies that the sequence $\left\{a_n\left(p_i^{e_i}\right)\right\}$ repeats only after blocks of length $u\cdot l\left(p_i^{e_i}\right),\ \left(u\in N\right)$, where N is natural number ; and the statement '$l\left(m\right)$ is the length of the period $\left\{a_n\left(m\right)\right\}$' implies that $\left\{a_n\left(p_i^{e_i}\right)\right\}$ repeats after $l\left(m\right)$ terms for all values i. Thus, $l\left(m\right)$ is of the form $u\cdot l\left(p_i^{e_i}\right)$ and since any such number gives a period of $\left\{a_n\left(m\right)\right\}$, then we get that $l\left(m\right)=\mathrm{lcm}\left[l\left(p_i^{e_i}\right)\right]$.

Let $l_{(a_1,a_2,\mathrm{L}\ ,a_5)}\left(p\right)$ denote the smallest period of the integer-valued recurrence relation $u_n=u_{n-1}+2u_{n-2}-2u_{n-3}+u_{n-5},\ u_1=a_1,u_2=a_2,\mathrm{L}\ ,u_5=a_5$ where each entry is a reduced modulo p. Then we have the following theorem.

Theorem 4. If $a_1,a_2,\mathrm{L}\ ,a_5,x_1,x_2,\mathrm{L}\ ,x_5\in Z$, where Z is integer, such that $\gcd\left(a_1,a_2,\mathrm{L}\ ,a_5,p\right)=1$ and $\gcd\left(x_1,x_2,\mathrm{L}\ ,x_5,p\right)=1$, then

$$l_{(a_1,a_2,\mathrm{L}\ ,a_5)}\left(p\right)=l_{(x_1,x_2,\mathrm{L}\ x_k)}\left(p\right).$$

Proof. Let $l\left(p\right)=\left|\left\langle M\right\rangle_p\right|=r$. From (4), it is clear that $\begin{bmatrix}u_{n+r}\\u_{n+r+1}\\u_{n+r+2}\\u_{n+r+3}\\u_{n+r+4}\end{bmatrix}=M^r\begin{bmatrix}u_n\\u_{n+1}\\u_{n+2}\\u_{n+3}\\u_{n+4}\end{bmatrix}$. So naturally

$\begin{bmatrix}u_{n+r}\\u_{n+r+1}\\u_{n+r+2}\\u_{n+r+3}\\u_{n+r+4}\end{bmatrix}\equiv\begin{bmatrix}u_n\\u_{n+1}\\u_{n+2}\\u_{n+3}\\u_{n+4}\end{bmatrix}\mathrm{mod}\ p$. This completes the proof.

Conjecture 1. If p is a prime, then there exists a σ with $0\leq\sigma\leq 5$ such that $\left|\left\langle M\right\rangle_p\right|$ divides $\left(p^6-p^\sigma\right)$.

Conjecture 2. If p is a prime such that $p>2$, then $\left|\left\langle M\right\rangle_p\right|$ is an even integer number. Table 1 lists some primes for which Conjectures 1 and 2 are true.

Table 1. Orders of the cyclic group $\langle M \rangle_p$

p	$\lvert\langle M\rangle_p\rvert$	$\lvert\langle M\rangle_p\rvert \mid (p^6 - p^\sigma)$
2	21	$\lvert\langle M\rangle_p\rvert \mid p^6 - 1$
3	104	$\lvert\langle M\rangle_p\rvert \mid p^6 - 1$
5	120	$\lvert\langle M\rangle_p\rvert \mid p^6 - p^3$, $\lvert\langle M\rangle_p\rvert \mid p^6 - p^4$
29	12194	$\lvert\langle M\rangle_p\rvert \mid p^6 - 1$, $\lvert\langle M\rangle_p\rvert \mid p^6 - p^3$
31	9930	$\lvert\langle M\rangle_p\rvert \mid p^6 - 1$, $\lvert\langle M\rangle_p\rvert \mid p^6 - p^3$
47	72224	$\lvert\langle M\rangle_p\rvert \mid p^6 - 1$
71	357910	$\lvert\langle M\rangle_p\rvert \mid p^6 - 1$, $\lvert\langle M\rangle_p\rvert \mid p^6 - p^3$
83	6888	$\lvert\langle M\rangle_p\rvert \mid p^6 - 1$, $\lvert\langle M\rangle_p\rvert \mid p^6 - p^2$, $\lvert\langle M\rangle_p\rvert \mid p^6 - p^4$
101	100	$\lvert\langle M\rangle_p\rvert \mid (p^6 - p^\sigma)$ for $0 \le \sigma \le 5$
211	210	$\lvert\langle M\rangle_p\rvert \mid (p^6 - p^\sigma)$ for $0 \le \sigma \le 5$
401	160800	$\lvert\langle M\rangle_p\rvert \mid p^6 - 1$, $\lvert\langle M\rangle_p\rvert \mid p^6 - p^2$, $\lvert\langle M\rangle_p\rvert \mid p^6 - p^4$
523	91176	$\lvert\langle M\rangle_p\rvert \mid p^6 - 1$, $\lvert\langle M\rangle_p\rvert \mid p^6 - p^2$, $\lvert\langle M\rangle_p\rvert \mid p^6 - p^4$
811	59267970	$\lvert\langle M\rangle_p\rvert \mid p^6 - 1$, $\lvert\langle M\rangle_p\rvert \mid p^6 - p^3$
1973	5125429148	$\lvert\langle M\rangle_p\rvert \mid p^6 - 1$
2221	365194662	$\lvert\langle M\rangle_p\rvert \mid p^6 - 1$, $\lvert\langle M\rangle_p\rvert \mid p^6 - p^3$
4657	2710956	$\lvert\langle M\rangle_p\rvert \mid p^6 - 1$, $\lvert\langle M\rangle_p\rvert \mid p^6 - p^2$, $\lvert\langle M\rangle_p\rvert \mid p^6 - p^4$
9473	44868864	$\lvert\langle M\rangle_p\rvert \mid p^6 - 1$, $\lvert\langle M\rangle_p\rvert \mid p^6 - p^2$, $\lvert\langle M\rangle_p\rvert \mid p^6 - p^4$
30137	454119384	$\lvert\langle M\rangle_p\rvert \mid p^6 - 1$, $\lvert\langle M\rangle_p\rvert \mid p^6 - p^2$, $\lvert\langle M\rangle_p\rvert \mid p^6 - p^4$

FIBONACCI-PADOVAN ORBITS OF FINITE GROUPS

Let G be a finite j-generator group and let X be the subset of $\underbrace{G \times G \times G \times \cdots \times G}_{j}$ such that $(x_0, x_1, \ldots, x_{j-1}) \in X$ if and only if G is generated by $x_0, x_1, \ldots, x_{j-1}$. We call $(x_0, x_1, \ldots, x_{j-1})$ a generating j-tuple for G.

Definition 2. The Fibonacci-Padovan orbits of finite groups with j-generating ($2 \le j \le 5$) are defined as follows:

i. Let G be a 2-generator group. For a generating pair $(x_0, x_1) \in X$, the Fibonacci-Padovan orbit $FP(G)_{x_0, x_1}$ is defined by the sequence $\{b_i\}$ of elements of G such that

$$b_0 = x_0,\ b_1 = x_1,\ b_2 = (b_0)^2 (b_1),\ b_3 = (b_0)^{-2} (b_1)^2 (b_2),\ b_4 = (b_1)^{-2} (b_2)^2 (b_3),$$
$$b_n = (b_{n-5})(b_{n-3})^{-2} (b_{n-2})^2 (b_{n-1}) \text{ for } n \ge 5.$$

ii. Let G be a 3-generator group. For a generating triplet $(x_0, x_1, x_2) \in X$, the Fibonacci-Padovan orbit $FP(G)_{x_0,x_1,x_2}$ is defined by the sequence $\{b_i\}$ of elements of G such that

$$b_0 = x_0,\ b_1 = x_1,\ b_2 = x_2,\ b_3 = (b_0)^{-2}(b_1)^2(b_2),\ b_4 = (b_1)^{-2}(b_2)^2(b_3),$$
$$b_n = (b_{n-5})(b_{n-3})^{-2}(b_{n-2})^2(b_{n-1}) \text{ for } n \geq 5.$$

iii. Let G be a 4-generator group. For a generating quadruplet $(x_0, x_1, x_2, x_3) \in X$, the Fibonacci-Padovan orbit $FP(G)_{x_0,x_1,x_2,x_3}$ is defined by the sequence $\{b_i\}$ of elements of G such that

$$b_0 = x_0,\ b_1 = x_1,\ b_2 = x_2,\ b_3 = x_3,\ b_4 = (b_1)^{-2}(b_2)^2(b_3),$$
$$b_n = (b_{n-5})(b_{n-3})^{-2}(b_{n-2})^2(b_{n-1}) \text{ for } n \geq 5.$$

iv. Let G be a 5-generator group. For a generating quintuplet $(x_0, x_1, x_2, x_3, x_4) \in X$, the Fibonacci-Padovan orbit $FP(G)_{x_0,x_1,x_2,x_3,x_4}$ is defined by the sequence $\{b_i\}$ of elements of G such that

$$b_0 = x_0,\ b_1 = x_1,\ b_2 = x_2,\ b_3 = x_3,\ b_4 = x_4,$$
$$b_n = (b_{n-5})(b_{n-3})^{-2}(b_{n-2})^2(b_{n-1}) \text{ for } n \geq 5.$$

The classic Fibonacci-Padovan sequence in the integers modulo m can be written as $FP(Z_m)_{0,1}$.

Theorem 5. A Fibonacci-Padovan orbit of a finite group which is generating ($2 \leq j \leq 5$) is simply periodic.

Proof. Let us consider the group G as a 4-generator group and let (x_0, x_1, x_2, x_3) be a generating quadruplet of G. If the order of G is n, there are n^5 distinct 5-tuples of elements of G. So at least one of the 5-tuples appears twice in the Fibonacci-Padovan orbit of G for the generating quadruplet (x_0, x_1, x_2, x_3); that is, the sub-sequence following these 5-tuples repeats. Hence the Fibonacci-Padovan orbit is periodic. Since the Fibonacci-Padovan orbit for the generating quadruplet (x_0, x_1, x_2, x_3) is periodic, there are positive integers i and j, with $i > j$, such that $b_{i+1} = b_{j+1}$, $b_{i+2} = b_{j+2}$, $b_{i+3} = b_{j+3}$, $b_{i+4} = b_{j+4}$ and $b_{i+5} = b_{j+5}$. By the defined relation of a Fibonacci-Padovan orbit, we know that

$$b_i = (b_{i+5})(b_{i+4})^{-1}(b_{i+3})^{-2}(b_{i+2})^2$$

and

$$b_j = (b_{j+5})(b_{j+4})^{-1}(b_{j+3})^{-2}(b_{j+2})^2.$$

Thus, $b_i = b_j$, and it follows that

$$b_{i-j} = b_{j-j} = b_0 = x_0,\ b_{i-j+1} = b_{j-(j-1)} = b_1 = x_1,$$
$$b_{i-j+2} = b_{j-(j-2)} = b_2 = x_2,\ b_{i-j+3} = b_{j-(j-3)} = b_3 = x_3.$$

So the Fibonacci-Padovan orbit $FP(G)_{x_0,x_1,x_2,x_3}$ is simply periodic. The proof for the 2-generator groups, the 3-generator groups and the 5-generator groups is similar to the above and is omitted.

We denote the periods of the orbits $FP(G)_{x_0,\ldots,x_k}$ with $1 \leq k \leq 4$ by $LFP(G)_{x_0,\ldots,x_k}$. From the definition, it is clear that the period of a Fibonacci-Padovan orbit of a finite group depends on the chosen generating set and the order for the assignments of $x_0,\ldots,x_k$ such that $1 \leq k \leq 4$.

Definition 3. Let G be a finite group. If there exists a Fibonacci-Padovan orbit of the group G such that every element of the group G appears in the sequence, then the group G is called Fibonacci-Padovan sequenceable.

We now address the periods of the Fibonacci-Padovan orbits of specific classes of finite groups. The usual notation $G_1 \times_\varphi G_2$ is used for the semidirect product of the group G_1 by G_2, where $\varphi : G_2 \to \mathrm{Aut}(G_1)$ is a homomorphism such that $b\varphi = \varphi_b$ and $\varphi_b : G_1 \to G_1$ is an element $\mathrm{Aut}(G_1)$.

The quaternion group Q_8 is defined by

$$Q_8 = \left\langle x, y : x^4 = e, y^2 = x^2, y^{-1}xy = x^{-1} \right\rangle;$$

the direct product $Q_8 \times Z_{2m}$ $(m \geq 3)$ is defined by

$$Q_8 \times Z_{2m} = \left\langle x, y, z : x^4 = e, y^2 = x^2, y^{-1}xyx = z^{2m} = [x,z] = [y,z] = e \right\rangle;$$

and the semidirect product $Q_8 \times_\varphi Z_{2m}$ $(m \geq 3)$ is defined by

$$Q_8 \times_\varphi Z_{2m} = \left\langle x, y, z : x^4 = e, y^2 = x^2, y^{-1}xyx = z^{2m} = e, z^{-1}xzx = e, z^{-1}yzy = e \right\rangle,$$

where, if $Z_{2m} = \langle z \rangle$, then $\varphi : Z_{2m} \to \mathrm{Aut}(Q_8)$ is a homomorphism such that $z\varphi = \varphi_z$; $\varphi_z : Q_8 \to Q_8$ is defined by $x\varphi_z = x$ and $y\varphi_z = y^{-1}$.

Theorem 6. $LFP(Q_8)_{x,y} = LFP(Q_8)_{y,x} = 42.$

Proof. $FP(Q_8)_{y,x}$ is

$$y, x, x^3, x^3, yx^3, y^3, xy, y, x^3y, e, y^3, x^3, yx, y^2, y^2, y^3, xy, y^2, e, e, y^3, x, x,$$
$$x, x, y^3x, y^3, xy^3, y, xy, y^2, y, x^3, yx, e, y^2, y, x^3y, e, e, e, y, x, x^3, x^3, yx^3, \mathrm{L},$$

which has period $LFP(Q_8)_{y,x} = 42$.

The proof for the orbit $FP(Q_8)_{x,y}$ is similar to the above and is omitted.

Remark 1. The quaternion group Q_8 is Fibonacci-Padovan sequenceable.

Theorem 7. The period of the Fibonacci-Padovan orbit of the direct product $Q_8 \times Z_{2m}$ $(m \geq 3)$ for each generating triplet is $\mathrm{lcm}\left[42, l(2m)\right]$.

Proof. Consider the Fibonacci-Padovan orbit $FP(Q_8 \times Z_{2m})_{x,y,z}$:

$$x, y, z^{a_0}, z^{a_1}, y^2z^{a_2}, x^3z^{a_3}, xyz^{a_4}, yxz^{a_5}, yxz^{a_6}, xyz^{a_7}, yz^{a_8}, x^3z^{a_9}, yz^{a_{10}},$$
$$xz^{a_{11}}, yz^{a_{12}}, y^2z^{a_{13}}, xz^{a_{14}}, xyz^{a_{15}}, yz^{a_{16}}, y^2z^{a_{17}}, z^{a_{18}}, x^3z^{a_{19}}, y^3z^{a_{20}}, x^2z^{a_{21}},$$
$$z^{a_{22}}, y^2z^{a_{23}}, xz^{a_{24}}, xyz^{a_{25}}, xyz^{a_{26}}, xyz^{a_{27}}, yxz^{a_{28}}, yz^{a_{29}}, x^3z^{a_{30}}, y^3z^{a_{31}}, xz^{a_{32}},$$
$$y^3z^{a_{33}}, z^{a_{34}}, x^3z^{a_{35}}, xyz^{a_{36}}, yz^{a_{37}}, z^{a_{38}}, z^{a_{39}}, xz^{a_{40}}, yz^{a_{41}}, z^{a_{42}}, z^{a_{43}}, y^2z^{a_{44}}, \mathrm{L}.$$

Using the above information, the sequence becomes:

$$b_0 = x, b_1 = y, b_2 = z, b_3 = z, b_4 = y^2z^3, \mathrm{L},$$
$$b_{42} = xz^{40}, b_{43} = yz^{41}, b_{44} = z^{42}, b_{45} = z^{43}, b_{46} = y^2z^{44}, \mathrm{L},$$
$$b_{42\cdot i} = xz^{42\cdot i-2}, b_{42\cdot i+1} = yz^{42\cdot i-1}, b_{42\cdot i+2} = z^{42\cdot i}, b_{42\cdot i+3} = z^{42\cdot i+1}, b_{42\cdot i+4} = y^2z^{42\cdot i+2}, \mathrm{L}.$$

The sequence can be said to form layers of length 42. So we need an i such that $b_{42i} = x, b_{42\cdot i+1} = y, b_{42\cdot i+2} = z, b_{42\cdot i+3} = z, b_{42\cdot i+4} = y^2z^3$. It is easy to see that the Fibonacci-Padovan orbit $FP\left(Q_8 \times Z_{2m}\right)_{x,y,z}$ has period $\text{lcm}\left[42, l\left(2m\right)\right]$.

The proof for other generating triplets is similar to the above and is omitted.

Theorem 8. The period of the Fibonacci-Padovan orbit of the direct product $Q_8 \times_\varphi Z_{2m}$ $\left(m \geq 3\right)$ for each generating triplet is $\text{lcm}\left[42, l\left(2m\right)\right]$.

Proof. Consider the Fibonacci-Padovan orbit $FP\left(Q_8 \times_\varphi Z_{2m}\right)_{y,x,z}$:

$$y, x, z^{a_0}, z^{a_1}, x^2z^{a_2}, y^3z^{a_3}, yxz^{a_4}, yxz^{a_5}, xyz^{a_6}, yxz^{a_7}, xz^{a_8}, yz^{a_9}, x^3z^{a_{10}},$$
$$y^3z^{a_{11}}, x^3z^{a_{12}}, z^{a_{13}}, yz^{a_{14}}, yxz^{a_{15}}, x^3z^{a_{16}}, z^{a_{17}}, y^2z^{a_{18}}, y^3z^{a_{19}}, x^3z^{a_{20}}, x^2z^{a_{21}},$$
$$x^2z^{a_{22}}, y^2z^{a_{23}}, yz^{a_{24}}, yxz^{a_{25}}, xyz^{a_{26}}, xyz^{a_{27}}, yxz^{a_{28}}, x^3z^{a_{29}}, y^3z^{a_{30}}, x^3z^{a_{31}}, y^3z^{a_{32}},$$
$$x^3z^{a_{33}}, x^2z^{a_{34}}, yz^{a_{35}}, yxz^{a_{36}}, x^3z^{a_{37}}, z^{a_{38}}, z^{a_{39}}, yz^{a_{40}}, xz^{a_{41}}, z^{a_{42}}, z^{a_{43}}, x^2z^{a_{44}}, \text{L}\ .$$

Using the above information, the sequence becomes:

$$b_0 = y, b_1 = x, b_2 = z, b_3 = z, b_4 = x^2z^3, \text{L}\ ,$$
$$b_{42} = yz^{40}, b_{43} = xz^{41}, b_{44} = z^{42}, b_{45} = z^{43}, b_{46} = y^2z^{44}, \text{L}\ ,$$
$$b_{42\cdot i} = xz^{42\cdot i-2}, b_{42\cdot i+1} = yz^{42\cdot i-1}, b_{42\cdot i+2} = z^{42\cdot i}, b_{42\cdot i+3} = z^{42\cdot i+1}, b_{42\cdot i+4} = x^2z^{42\cdot i+2}, \text{L}\ .$$

The sequence can be said to form layers of length 42. So we need an i such that $b_{42i} = y, b_{42\cdot i+1} = x, b_{42\cdot i+2} = z, b_{42\cdot i+3} = z, b_{42\cdot i+4} = x^2z^3$. It is easy to see that the Fibonacci-Padovan orbit $FP\left(Q_8 \times_\varphi Z_{2m}\right)_{y,x,z}$ has period $\text{lcm}\left[42, l\left(2m\right)\right]$.

The proof for other generating triplets is similar to the above and is omitted.

Remark 2. If $l\left(2m\right) < 2m$ and $42 \mid l\left(2m\right)$, the groups $Q_8 \times Z_{2m}$ and $Q_8 \times_\varphi Z_{2m}$ such that $m \geq 3$ are not Fibonacci-Padovan sequenceable (where, by $42 \mid l\left(2m\right)$, we mean that 42 divides $l\left(2m\right)$).

CONCLUSIONS

Examining the Fibonacci-Padovan sequence modulo m, we have defined the Fibonacci-Padovan orbits of j-generator finite groups for $2 \leq j \leq 5$. Furthermore, we have obtained the Fibonacci-Padovan lengths of the groups Q_8, $Q_8 \times Z_{2m}$ and $Q_8 \times_\varphi Z_{2m}$ for $m \geq 3$.

ACKNOWLEDGEMENT

This project (Project no. 2013-FEF-72) was supported by the Commission for the Scientific Research Projects of Kafkas University.

REFERENCES

1. P. G. Becker, "*k*-Regular power series and Mahler-type functional equations", *J. Number Theory*, **1994**, *49*, 269-286.
2. W. Bosma and C. Kraaikamp, "Metrical theory for optimal continued fractions", *J. Number Theory*, **1990**, *34*, 251-270.
3. M. S. El Naschie, "Deriving the essential features of the standard model from the general theory of relativity", *Chaos Solitons Fractals*, **2005**, *24*, 941-946.

4. M. S. El Naschie, "Stability analysis of the two-slit experiment with quantum particles", *Chaos Solitons Fractals*, **2005**, *26*, 291-294.
5. S. Falcon and A. Plaza, "*k*-Fibonacci sequences modulo m", *Chaos Solitons Fractals*, **2009**, *41*, 497-504.
6. A. S. Fraenkel and S. T. Kleinb, "Robust universal complete codes for transmission and compression", *Discrete Appl. Math.*, **1996**, *64*, 31-55.
7. B. K. Kirchoof and R. Rutishauser, "The phyllotaxy of costus (Costaceae)", *Bot. Gaz.*, **1990**, *151*, 88-105.
8. D. M. Mandelbaum, "Synchronization of codes by means of Kautz's Fibonacci encoding", *IEEE Trans. Inform. Theory*, **1972**, *18*, 281-285.
9. W. Syein, "Modelling the evolution of stelar archictecture in vascular plants", *Int. J. Plant Sci.*, **1993**, *154*, 229-263.
10. R. G. E. Pinch, "Distribution of recurrent sequences modulo prime powers", Proceedings of 5th IMA Conference on Cryptography and Coding, **1995**, Cirencester, UK.
11. D. D. Wall, "Fibonacci series modulo m", *Am. Math. Monthly*, **1960**, *67*, 525-532.
12. O. Deveci and E. Karaduman, "The generalized order-*k* Lucas sequences in finite groups", *J. Appl. Math.*, **2012**, DOI: 10.1155/2012/464580.
13. O. Deveci, "The *k-nacci* sequences and the generalized order-*k* Pell sequences in the semi-direct product of finite cyclic groups", *Chiang Mai J. Sci.*, **2013**, *40*, 89-98.
14. O. Deveci and E. Karaduman, "The cyclic groups via the Pascal matrices and the generalized Pascal matrices", *Linear Algebra Appl.*, **2012**, *437*, 2538-2545.
15. O. Deveci and E. Karaduman, "The Pell sequences in finite groups", *Util. Math.*, **2015**, *96* (in press).
16. O. Deveci, "The Pell-Padovan sequences and the Jacobsthal-Padovan sequences in finite groups", *Util. Math.*, in press.
17. S. W. Knox, "Fibonacci sequences in finite groups", *Fibonacci Quart.*, **1992**, *30*, 116-120.
18. K. Lü and J. Wang, "*k*-Step Fibonacci sequence modulo *m"*, *Util. Math.*, **2007**, *71*, 169-178.
19. E. Ozkan, H. Aydin and R. Dikici, "3-Step Fibonacci series modulo m", *Appl. Math. Comput.*, **2003**, *143*, 165-172.
20. V. W. de Spinadel, "The family of metallic means", *Visual Math.*, **1999**, *1*, 176-185.
21. V. W. de Spinadel, "The metallic means family and forbidden symmetries", *Int. Math. J.*, **2002**, *2*, 279-288.
22. N. D. Gogin and A. A. Myllari, "The Fibonacci-Padovan sequence and MacWilliams transform matrices", *Program. Comput. Softw.*, **2007**, *33*, 74-79.
23. D. Kalman, "Generalized Fibonacci numbers by matrix methods", *Fibonacci Quart.*, **1982**, *20*, 73-76.
24. C. M. Campbell and P. P. Campbell, "The Fibonacci length of certain centro-polyhedral groups", *J. Appl. Math. Comput.*, **2005**, *19*, 231-240.

Maejo International Journal of Science and Technology

ISSN 1905-7873
Available online at www.mijst.mju.ac.th

Full Paper

Control of *Fusarium* sp. on pineapple by megasonic cleaning with electrolysed oxidising water

Sirakan Khayankarn [1], Sanong Jarintorn [2], Nantinee Srijumpa [2], Jamnong Uthaibutra [1,3] and Kanda Whangchai [1, 3,*]

[1] Postharvest Technology Research Institute / Postharvest Technology Innovation Centre, Chiang Mai University, Chiang Mai 50200, Thailand
[2] Chiang Rai Horticultural Research Centre, Department of Agriculture, Chiang Rai, 57000, Thailand
[3] Department of Biology, Faculty of Science, Chiang Mai University, Chiang Mai 50200, Thailand

* Corresponding author, e-mail: kanda.w@cmu.ac.th; tel: +66-81-595-5690

Received: 8 August 2013 / Accepted: 15 August 2014 / Published: 9 December 2014

Abstract: The effects of megasonication (MS) with electrolysed oxidising (EO) water (MS/EO treatment) on *Fusarium* sp. which causes postharvest decay of pineapple cv. Phu Lae were investigated. Spore suspensions containing 10^5 conidia mL^{-1} and 1 cm mycelium discs of *Fusarium* sp. were subjected to MS (1 MHz) in EO water with available free chlorine at 100 ppm for 10 min., and compared with non-treated control samples. The MS/EO treatment completely inhibited spore germination and mycelial growth for 3 days and reduced fruit decay. Development of *Fusarium* sp. on de-crowned pineapple fruit was also investigated by scanning electron microscopy. The fungal growth was restricted on de-crowned pineapple fruit for 72 hr, following MS/EO treatment. The MS/EO treatment also enhanced the activity of two enzymes: phenylalanine ammonia lyase (PAL) and peroxidase (POD), which play important roles in plant defense responses.

Keywords: megasonication, electrolysed oxidising water, pineapple, *Fusarium* sp., pineapple, fruit decay, crown rot

INTRODUCTION

Pineapple is a commercially important crop in Thailand. A high incidence of postharvest diseases in pineapple is primarily caused by the fungi *Ceratocystis paradoxa* and *Fusarium* sp. The fungi preferentially penetrate wounds caused by de-crowning during postharvest handling, prior to export [1]. Several fungicides are presently used as postharvest treatments to control fruit-decay-causing fungi. Fungal decay of pineapple fruit may be controlled by dipping in Triabendazole or Benomyl and methyl bromide fumigation. However, these chemicals may also leave toxic residues and cause environmental pollution. Advanced oxidation techniques have been used as alternatives

to conventional fungicides for controlling plant diseases [2-4]. In a similar manner, our present study aims at testing a combination of megasonication (MS) by high-frequency ultrasound and electrolysed oxidising (EO) water to control postharvest fungal decay in de-crowned pineapple fruit.

Ultrasound refers to sound wave with frequency above those audible to humans [5]. It causes chemical and physical changes to biological structures (in a liquid medium) owing to the rapid formation and destruction of cavitation bubbles [6]. The potential use of ultrasound in food industry has been recognised since the 1970s [7]. Chemat et al. [8] stated that it can be used in food processing, preservation and extraction at 100-1000 kHz. In addition, using MS at 1 MHz can also reduce chlorpyrifos residue on bird's chili [9]. Ultrasound treatment significantly reduces spoilage and pathogenic microorganisms in fruits and vegetables [6]. Consequently, it has been used in postharvest treatments to reduce decay and to maintain the quality of fruits and vegetables.

EO water, an alternative to chlorinated water, was developed in Japan [10]. It has been studied for use in aquaculture [11], agricultural and food industrial processes [12, 13], as well as in postharvest disease control [14-16]. It is produced by electrolysing a dilute solution of sodium chloride, using an ion exchange membrane to separate the anode from the cathode. Water collected at the anode has unique oxidising properties due to its hypochlorous acid (HOCl) content and low pH [10].

Plants' defence-related enzymes such as phenylalanine ammonia lyase (PAL) and peroxidase (POD) are also involved in defence against pathogenic microorganisms. PAL, a key enzyme in the phenylpropanoid pathway, induces the synthesis of various fungitoxic phytoalexins [17]. POD is involved in the cross-linking of cell-wall components and the generation of antifungal metabolites [18]. These enzymes induce active defence mechanisms against pathogens [17]. In this study, which is a continuation of our previous experiments [19], the effects of MS and EO water on decay and elicitation of defence enzymes is also investigated.

MATERIALS AND METHODS

Fungal Culture

Fusarium sp. was obtained from the culture stock of the Department of Biology, Faculty of Science, Chiang Mai University. The fungi were cultured on potato dextrose agar (PDA) for 7 days at 25°C. A spore suspension was prepared by adding 10 mL of sterile distilled water to the *Fusarium* sp. cultured on a petri dish and the spores were transferred to 100 mL of sterile distilled water in a 250-mL conical flask. The suspension was shaken for 10 min. on an orbital shaker at 25° and filtered through two layers of sterile muslin. The spore suspension was diluted with sterile distilled water to a concentration of 10^5 spores mL^{-1} as determined by the haemacytometer.

Generation of EO Water and Megasonic Treatment

The conditions used in our previous work [19] were employed. To mention briefly, EO water was generated by electrolysis in a chamber with positively and negatively charged titanium electrodes coated with TiO_2 and separated by a polypropylene membrane. Water (12 litres) containing 5% NaCl was introduced into the system. The electrodes were then subjected to direct current of 8 A and 8 V from a DC power source. The pH was recorded with a pH/ion meter and the oxidation-reduction potential (ORP) was measured by a pH/ORP meter. The amount of free-chlorine concentration was determined by the N,N-diethyl-*p*-phenylenediamine test [20]. The EO water, with an initial free-chlorine concentration of 650 ppm, was diluted with distilled water to 100 ppm and used for the microbiological study within 5 hr.

For fungal study, spore suspensions or mycelium discs were sonicated in a megasonic polyethylene cylinder reactor, 10 cm in diameter, with an input power of 3W and a frequency of 1 MHz (Honda Electronics Co., Japan).

For fruit treatment, the fruits (up to 10 kg) were subjected to megasonic waves of 3W at a constant frequency of 1 MHz. The experiments were carried out in an ultrasonic 50-L water bath, dimensions: 44.5 × 51.5 × 35 cm (Honda Electronics Co., Japan).

Spore Survival and Mycelial Growth

One mL of a $1x10^5$ spore suspension or 1 cm of mycelium disc was placed in the megasonic chamber containing 9 mL of EO water (freshly prepared) with a free-chlorine concentration of 100 ppm and subjected to continuous MS at 1 MHz for 10 min. at room temperature. Subsequently, 0.1 mL of the treated spore suspension in EO water was added to 0.9 mL of 0.1N sodium thiosulfate. After well mixing, the spread-plate technique was applied; 0.1 mL of the solution was spread on a PDA plate. A mycelial disc was placed onto a PDA plate, which was then incubated at 27°. The fungal survival was expressed as the number of colony-forming units (cfu mL^{-1}) after incubation for 48 hr and the mycelial growth was recorded daily. Each treatment consisted of 9 replicates and the experiment was repeated twice independently. The control treatment consisted of a 1-mL spore suspension or 1 cm of mycelium disc in 9 mL of distilled water in place of EO water.

Disease Incidence and Quality Changes

The prepared spore suspension (0.1 mL) was artificially inoculated on the centre of de-crowned pineapple fruit. All treated fruits—two groups of 36 fruits each—were incubated at room temperature for 3 hr. The first group was immersed in the MS chamber with the dimension of 44.5 × 51.5× 35 cm, containing EO water with a free-chlorine concentration of 100 ppm, and subjected to continuous MS at 24W and a constant frequency of 1 MHz. The second group of pineapple fruits washed with distilled water were used as control. The treated fruits were then placed in a basket and air-dried. After that the fruits were covered with plastic bags and maintained at 13° for 20 days. Samples were taken at 5-day intervals during storage for decay monitoring. To determine changes in fruit quality, weight loss and pH were measured. Total soluble solids was determined with a digital refractometer (Atago, Model PAL-a, Japan) using 2-3 drops of juice obtained by squeezing the fruits [21]. Titratable acidity was assessed as outlined by AOAC [22]. Ascorbic acid was determined by dichloroindophenol method [23]. The experiment was repeated twice.

Disease Development

De-crowned pineapple fruits were inoculated with a $1x10^5$ spore suspension of *Fusarium* sp. and subjected to MS with EO water following the procedure mentioned above. De-crowned fruits treated with distilled water were used as control. To observe the varying stages of fungal penetration, fruit samples were taken at 12, 24, 48 and 72 hr after treatment. The samples were preserved in formaldehyde-acetic acid-alcohol solution. Pieces of 3-10 mm were cut out of the samples. After three rinses of 5 minutes each in sterile distilled water, the samples were mounted with carbon adhesion tape on a specimen holder and examined under a scanning electron microscope (KEYENCE VE-9800, Japan) at an acceleration voltage of 5 kV.

Plant's Defense-Related Enzymes

De-crowned pineapple fruits were inoculated with *Fusarium* sp. and subjected to MS/EO-water treatment as described above. On every five days of storage, healthy, non-infected areas of

the sampled fruit were separated, cut into small pieces, frozen in liquid nitrogen, freeze-dried and stored at -21° for enzyme assays. The sampling was done in triplicate. De-crowned fruits treated with distilled water were used as control.

For PAL assay, freeze-dried samples of de-crowned pineapple fruit (1.0 g) were homogenised with 10 mL of 150mM Tris buffer (pH 8.5). The homogenate was centrifuged at 12000 g for 30 min. at 4°. The supernatant was analysed for enzyme activity. The PAL assay system routinely consisted of the supernatant (1 mL), 50 mM L-phenylalanine (1 mL) and buffer (1 mL). The change in absorbance at 290 nm was monitored after 1 hr of reaction at 40°. Under these conditions, a change in absorbance of 0.01 was found to be equivalent to the production of 3.09 nmoles of cinnamic acid [17]. One unit of enzyme activity was defined as the production of 1 nmol cinnamic acid per hr.

For POD assay, the freeze-dried samples of de-crowned pineapple fruit (0.5 g) were homogenised with 20 mL of 0.10M sodium phosphate buffer (pH 7.0) containing 3mM ethylenediaminetetraacetic acid and 0.1 g of polyvinyl pyrrolidone. The homogenate was centrifuged at 12000 g for 20 min. at 4°. The supernatant was analysed for POD activity, which was determined spectrophotometrically at 470 nm [24]. The reaction medium contained 2.855 mL sodium phosphate buffer (0.10M, pH 7.0), 45 µL guaiacol (1%), 40 µL H_2O_2 (0.3%) and 60 µL supernatant. The absorbance was recorded at 470 nm and one unit of enzyme activity was defined as the amount causing an absorbance change of 0.01 per min.

The specific activity of the enzymes was expressed as units/ mg protein. Soluble protein content was determined using bovine serum albumin as standard [25].

RESULTS AND DISCUSSION

Spore Survival and Mycelial Growth

Spores treated with MS/EO water were completely inactivated (spore survival population = 0 log cfu mL^{-1}). In the control group spore survival was 7.88 log cfu mL^{-1}. The concentration of free chlorine in EO water was sufficient to reduce fungal growth. Of the chlorine compounds, hypochlorous acid is the most effective for disinfestation. It damages the microbial cell by oxidising nucleic acids and proteins, causing lethal damage [23]. The low pH in EO water sensitises the outer membrane of the cell, thereby allowing hypochlorous acid to enter the cell more efficiently. Similar results have been achieved with *Penicillium digitatum* after 1 min. exposure [27]. Other researchers also reported that it takes about 30 sec. or less to inhibit thin-walled fungi and 2 min. or more to inhibit thicker-walled species [3]. The reduction of spore survival by MS, on the other hand, is mainly due to free-radical attack resulting in physically disrupted cell membranes [28]. The effects of the combined treatment on mycelial growth are shown in Figure 1. Mycelial growth was delayed for 3 days, but after 5 days of storage the mycelium started to regrow. The mycelium structure was composed of a compact mass of hyphae and the ultrasonic wave might not have penetrated the inner mycelial matrix, leaving some parts protected from the high pressure and temperature effects of MS and from EO-water disinfection.

Disease Incidence and Quality Changes

The MS/EO-water treatment significantly inhibited decay incidence during the first 5 days ($p < 0.05$), and by the 10^{th} day the average disease incidence was 8.33%, compared with 66.67% for control (Figure 2). The combined treatment seems to effectively disinfect the fruit from pathogenic fungi through mechanical disruption of the microbial cells and disinfection by EO water. This result

is similar to those by other researchers. Ultrasound combined with EO water resulted in a greater reduction of the bacterial contamination of broccoli [29]. A combination of ultrasound and sanitisation enhanced removal of *Salmonella* and *Escherichia coli* O157:H7 on apple and lettuce [30]. The compression pressure generated by ultrasound might have facilitated the penetration of chemical oxidants through cellular membranes and the cavitation might have assisted in the disaggregation of the microorganisms, resulting in increased efficiency of the sanitisation treatment [31]. In our study MS with EO water seems to be applicable to pineapple handling systems due to its marked effect against fungal decay without any effect on fruit quality, as revealed by the results on weight loss, total soluble solids, titratable acidity, pH and ascorbic acid content (data not shown).

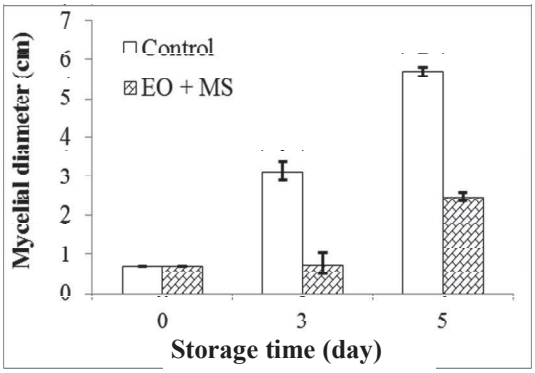

Figure 1. Mycelial disc growth diameter of *Fusarium* sp. on PDA plates, after being treated with MS/EO water, then incubated at 27 °C for 5 days

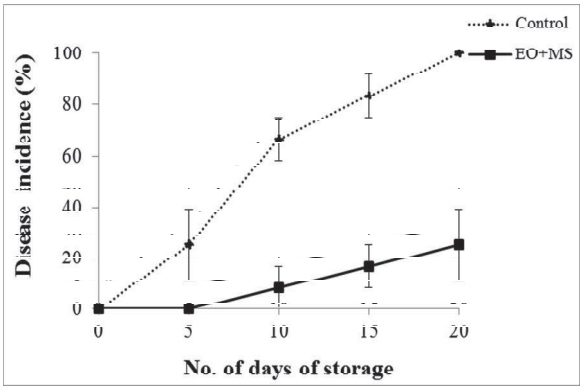

Figure 2. Effect of MS with EO water on disease incidence (% of infected fruits) of de-crowned pineapple during low-temperature storage for 20 days

Disease Development

The scanning electron micrograph of de-crowned pineapple in the control group showed germination of *Fusarium* sp. after 72-hr incubation. The germination of fungal spores was first observed in the control after 24 hr of storage whilst the MS/EO-water-treated fruits showed no sign of disease incidence (results not shown). After 72-hr incubation the treated samples still remained clear of fungal growth (Figure 3B) whilst the control group supported a high mass of fungal mycelia (Figure 3A). The combined treatment seems to effectively inhibit spore germination on de-crowned pineapple.

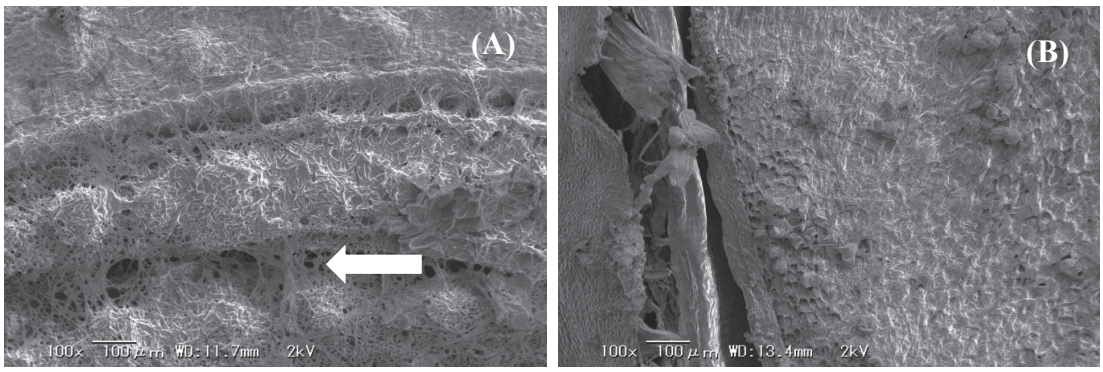

Figure 3. Scanning electron micrographs of de-crowned pineapple samples (4000 × magnification, 8-nm resolution) after 72-hr storage at 25° and 75-80% relative humidity: (A) development of *Fusarium* sp. in control sample (arrow indicates *Fusarium* sp. mycelia); (B) sample treated with MS/EO water

Plant Defence-Related Enzymes

The PAL level was found to increase rapidly and reach a peak after 10 days and then it gradually declined (Figure 4A). The PAL activity in the treated pineapple sample increased about 1.8-fold above that recorded for the control. The MS/EO-water treatment also increased the POD activity during storage as shown in Figure 4B. The mode of action of EO water and MS in inducing plant pathogen resistance is not yet fully understood. However, EO water has been reported to stress plants [32-34]. In lettuce, higher PAL levels were induced by stress from wounding plus ethylene [35]. In the present study we found that PAL and POD activities were induced by the MS/EO-water treatment, which may also induce enzyme responses to other kinds of stress including wounding and inoculation with *Fusarium* sp. as indicated in the control graphs in Figure 4.

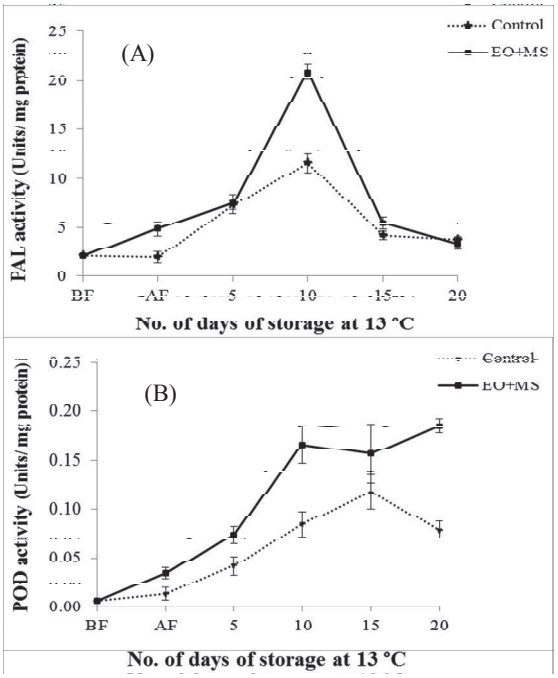

Figure 4. Effect of MS and EO water on activity (units/ mg protein) of PAL (A) and POD (B) in de-crowned pineapple fruit during storage at 13°C for 20 days **(**BF = before MS/EO-water treatment; AF = after MS/EO-water treatment)

CONCLUSIONS

The use of MS combined with EO water is recommended as a postharvest treatment of pineapple. The treatment significantly inhibits spore survival of *Fusarium* sp., prolonging the shelf life of pineapple by up to 20 days without affecting the fruit's quality. The antifungal effect of the treatment may also be due to the triggering activity of the plant's defence-related enzymes.

ACKNOWLEDGEMENTS

The funding for this work was provided by the Postharvest Technology Innovation Centre, Commission on Higher Education, Bangkok. The authors also thank the Postharvest Technology Research Institute, the Graduate School, Chiang Mai University for providing the laboratory facilities.

REFERENCES

1. Department of Agriculture, Fisheries and Forestry Biosecurity, Australia government, ″Provisional final import risk analysis report for the importation of fresh de-crowned pineapple (*Ananas comosus* (L.) Merr.) fruit from Malaysia″, **2012**, http://www.daff.gov.au/__data/assets/pdf_file/0004/2163973/Prov_final-malaysian_pineapplesIRA.pdf (Accessed: March 2014).
2. H. G. Sagong, H. L. Cheon, S. O. Kim, S. Y. Lee, K. H. Park, M. S. Chung, Y. J. Choi and D. H. Kang, ″Combined effects of ultrasound and surfactants to reduce *Bacillus cereus* spores on lettuce and carrots″, *Int. J. Food Microbiol*., **2013**, *160*, 367-372.
3. J. W. Buck, M. W. van Iersel, R. D. Oetting and C. Y. Hung, ″In vitro fungicidal activity of acidic electrolyzed oxidizing water″, *Plant Dis*., **2002**, *86*, 278-281.
4. J. F. Brilhante São José and M. C. Dantas Vanetti, ″Effect of ultrasound and commercial sanitizers in removing natural contaminants and *Salmonella enterica* Typhimurium on cherry tomatoes″, *Food Control*, **2012**, *24*, 95-99.
5. S. D. Jayasooriya, B. R. Bhandari, P. Torley and B. R. D'Arcy, ″Effect of high power ultrasound waves on properties of meat: A review″, *Int. J. Food Prop*., **2004**, *7*, 301-319.
6. X. Yuting, Z. Lifen, Z. Jianjun, S. Jie, Y. Xingqian and L. Donghong, ″Power ultrasound for the preservation of postharvest fruits and vegetables″, *Int. J. Agric. Biol. Eng*., **2013**, *6*,116-125.
7. P. Piyasena, E. Mohareb and R. C. McKellar, ″Inactivation of microbes using ultrasound: A review″, *Int. J. Food Microbiol.*, **2003**, *87*, 207-216.
8. F. Chemat, Z.E. Huma and M. K. Khan, ″Applications of ultrasound in food technology: Processing, preservation and extraction″, *Ultrason. Sonochem.*, **2011**, *18*, 813-835.
9. S. Pengphol, J. Uthaibutra, O. A. Arquero, N. Nomura and K. Whangchai, ″Reduction of residual chlorpyrifos on harvested bird chillies (*Capsicum frutescens* Linn.) using ultrasonication and ozonation″ , *Thai J. Agric. Sci.*, **2011,** *44*, 182-187.
10. H. Izumi, ″ Electrolyzed water as a disinfectant for fresh-cut vegetables″, *J. Food Sci*., **1999**, *64*, 536-539.
11. N. Whangchai, N. Nomura and M. Matsumura, ″Factors affecting phytoplankton removal by electro-oxidation of artificial seawater″, *Chiang Mai J. Sci*., **2003**, *30*, 255-259.
12. N. M. Grech and F. H. J. Rijkenberg, ″Injection of electronically generated chlorine into citrus microirrigation systems for the control of certain waterborne root pathogens″, *Plant Dis.*, **1992**, *76*, 457-461.

13. C. Kim, Y. C. Hung and R. E. Brackett, ″Efficacy of electrolyzed oxidizing (EO) and chemically modified water on different types of foodborne pathogens″, *Int. J. Food Microbiol*., **2000**, *61*,199-207.
14. M. I. Al-Haq, Y. Seo, S. Oshita and Y. Kawagoe, ″Disinfection effects of electrolyzed oxidizing water on suppressing fruit rot of pear caused by *Botryosphaeria berengeriana*″, *Food Res. Int.*, **2002**, *35*, 657-664.
15. K. S. Venkitanarayanan, G. O. Ezeike, Y. C. Hung and M. P. Doyle, ″Efficacy of electrolyzed oxidizing water for inactivating *Escherichia coli* 0157:H7, *Salmonella enteritidis*, and *Listeria monocytogenes*″, *Appl. Environ. Microbiol.*, **1999**, *65*, 4276-4279.
16. C. X. Hong, T. J. Michailides and B. A. Holtz, ″Effects of wounding, inoculum density, and biological control agents on postharvest brown rot of stone fruits″, *Plant Dis*., **1998**, *82*,1210 - 1216.
17. J. A. Saunders and J. W. McClure, ″The suitability of a quantitative spectrophotometric assay for phenylalanine ammonia-lyase activity in barley, buckwheat and pea seedlings″, *Plant Physiol*., **1974**, *54*, 412- 413.
18. M. Kozlowska, K. Fryder and B. Wolko, ″Peroxidase involvement in the defense response of red raspberry to *Didymella applanata* (Niessl/Sacc.) ″, *Acta Physiol. Plant***.**, **2001**, *23*, 303-310.
19. S. Khayankarn, J. Uthaibutra, S. Setha and K. Whangchai, ″Using electrolyzed oxidizing water combined with an ultrasonic wave on the postharvest diseases control of pineapple fruit cv. ‘Phu Lae’″, *Crop Protect.*, **2013**, *54*, 43-47.
20. A. T. Palin, ″Methods for the determination, in water, of free and combined available chlorine, chlorine dioxide and chlorite, bromine, iodine and ozone using diethyl-*p*-phenylene diamine (DPD)″ , *J. Inst. Water Eng*., **1967,** *21*, 537-547.
21. S. William (Ed.), ″Official Methods of Analysis of AOAC International″, 14th Edn., Association of Official Analytical Chemists, Inc., Arlington, **1984**, pp.4-5.
22. S. William (Ed.), ″Official Methods of Analysis of AOAC International″, 14th Edn., Association of Official Analytical Chemists, Inc., Arlington, **1984**, pp.522-533.
23. K. Helrich (Ed.), ″Official Methods of Analysis of AOAC International″, 15th Edn., Association of Official Analytical Chemists, Inc., Arlington, **1990**, pp.829- 830.
24. E. M. Yahia, G. Soto-Zamora, J. K. Brecht and A. Gardea, ″Postharvest hot air treatment effects on the antioxidant system in stored mature-green tomatoes″, *Postharvest Biol. Technol*., **2007**, *44*, 107-115.
25. O. H. Lowry, N. J. Rosebrough, A. L. Far and R. J. Randall, ″Protein measurement with the folin phenol reagent″, *J. Biol. Chem.*, **1951**, *193*, 265-275.
26. A. Acher, E. Fisher, R. Turnheim and Y. Manor, ″Ecologically friendly wastewater disinfection techniques″, *Water Res.*, **1997**, *31*, 1398-1404.
27. K. Whangchai, K. Saengnil, C. Singkamanee and J. Uthaibutra, ″Effect of electrolyzed oxidizing water and continuous ozone exposure on the control of *Penicillium digitatum* on tangerine cv. ‘Sai Nam Pung’ during storage″, *Crop Prot.*, **2010**, *29*, 386-389.
28. S. S. Phull, A. P. Newman, J. P. Lorimer, B. Pollet and T. J. Mason, ″The development and evaluation of ultrasound in the biocidal treatment of water″, *Ultrason. Sonochem.*, **1997**, *4*, 157-164.
29. Y-C. Hung, P. Tilly and C. Kim, ″Efficacy of electrolyzed oxidizing (EO) water and chlorinated water for inactivation of *Escherichia coli* O157:H7 on strawberries and broccoli″, *J. Food Qual.*, **2010**, *33*, 559-577.

30. T. S. Huang, C. L. Xu, K. Walker, P. West, S. Q. Zhang and J. Weese, ″Decontamination efficacy of combined chlorine dioxide with ultrasonication on apples and lettuce″, *J. Food Sci.*, **2006**, *71*, 134-139.
31. P. R. Gogate and A. M. Kabadi, ″A review of applications of cavitation in biochemical engineering/biotechnology″, *Biochem. Eng. J.*, **2009**, *44*, 60-72.
32. W. H. Flurkey and J. J. Jen, ″Peroxidase and polyphenol oxidase activities in developing peaches″, *J. Food Sci.*, **1978**, *43*, 1826-1828.
33. D. A. Jacobo-Velázquez, G. B. Martínez-Hernández, R. S. C. Del, C. M. Cao and L. Cisneros-Zevallos, ″Plants as biofactories: Physiological role of reactive oxygen species on the accumulation of phenolic antioxidants in carrot tissue under wounding and hyperoxia stress″, *J. Agric. Food Chem.*, **2011**, *59*, 6583-6593.
34. G. B. Martínez-Hernández, F. Artés-Hernández, P. A. Gómez, A. C. Formica and F. Artés, ″Combination of electrolysed water, UV-C and superatmospheric O_2 packaging for improving fresh-cut broccoli quality″, *Postharvest Biol. Technol.*, **2013**, *76*, 125-134.
35. G. Lopez-Galvez, M. E. Saltveit and M. I. Cantwell, ″Wound-induced phenylalanine ammonia lyase activity: Factors affecting its induction and correlation with the quality of minimally processed lettuces″, *Postharvest Biol. Technol.*, **1996**, *9*, 223-233.

Maejo International Journal of Science and Technology

ISSN 1905-7873
Available online at www.mijst.mju.ac.th

Full Paper

On asymptotic statistical equivalence of order α of generalised difference sequences

Mikail Et [1], Muhammed Cinar [2,*] and Murat Karakas [3]

[1] Department of Mathematics, Firat University, 23119, Elazig-Turkey
[2] Department of Mathematics, Mus Alparslan University, Mus-Turkey
[3] Department of Statistics, Bitlis Eren University, Bitlis-Turkey
[*] Corrseponding author, e-mail: muhammedcinar23@gmail.com

Received: 29 December 2013 / Accepted: 3 December 2014 / Published: 11 December 2014

Abstract : We introduce and examine the concepts of $\Delta_{uv}^{m}(\lambda)-$asymptotic statistical equivalence of order α, and strong $\Delta_{uv}^{m}(\lambda)-$asymptotic equivalence of order α of sequences**.** Also, we give some relations connected to these concepts.

Keywords: asymptotic equivalence, difference sequences, statistical convergence

INTRODUCTION

The concept of statistical convergence was introduced by Fast [1] and Schoenberg [2]. Later on it was further investigated from the sequence space point of view and linked with the summability theory by Belen and Mohiuddine [3], Colak [4, 5], Connor [6], Fridy [7], Gadjiev and Orhan [8], Gungor and Et [9], Gungor et al. [10], Isik [11], Kumar and Mursaleen [12], Mohiuddine et al. [13], Mursaleen [14, 15], Rath and Tripathy [16], Šalát [17] and many others. The idea of statistical convergence depends on the density of subsets of the set N of natural numbers. The density of a subset E of N is defined by

$$\delta(E)=\lim_{n\to\infty}\frac{1}{n}\sum_{k=1}^{n}\chi_E(k)\ ,$$

provided that the limit exists, where χ_E is the characteristic function of the set E. A sequence $x=(x_k)$ is said to be statistically convergent to L if for every $\varepsilon>0$, $\delta\left(\left\{k\in\mathsf{N}\ :\ |x_k-L|\geq\varepsilon\right\}\right)=0.$

The concept of asymptotically equivalent sequences was firstly introduced by Pobyvanets [18]. Since the last decades, asymptotically equivalent sequences have been studied by several authors [19-25]. In the present paper, using the generalised difference operator Δ^m and a non-decreasing sequence $\lambda=(\lambda_n)$ of positive real numbers such that $\lambda_{n+1}\leq\lambda_n+1$, $\lambda_1=1$, $\lambda_n\to\infty$

$(n \to \infty)$, we introduce $\Delta_{uv}^{m}(\lambda)$ – asymptotic statistical equivalence of order α and strong $\Delta_{uv}^{m}(\lambda)$ – asymptotic equivalence of order α of sequences, and give some relations connected to these concepts.

DEFINITIONS AND PRELIMINARIES

Let w be the set of all sequences of real or complex numbers, and ℓ_∞, c and c_0 be, respectively, the Banach spaces of bounded, convergent and null sequences $x=(x_k)$ with the usual norm $\|x\|=\sup|x_k|$. Let $\lambda=(\lambda_n)$ be a non-decreasing sequence of positive numbers tending to ∞ such that $\lambda_{n+1} \le \lambda_n + 1$, $\lambda_1 = 1$. The generalised de la Vallée-Poussin mean [26] is defined by

$$t_n(x) = \frac{1}{\lambda_n} \sum_{k \in I_n} x_k,$$

where $I_n = [n-\lambda_n+1, n]$ for $n = 1, 2, \ldots$. A sequence $x=(x_k)$ is said to be (V,λ) – summable to a number L if $t_n(x) \to L$ as $n \to \infty$. If $\lambda_n = n$, then (V,λ) – summability and strong (V,λ) – summability are reduced to $(C,1)$ – summability and $[C,1]$ – summability respectively. By Λ, we denote the class of all non-decreasing sequences of positive real numbers tending to ∞ such that $\lambda_{n+1} \le \lambda_n + 1$, $\lambda_1 = 1$.

The notion of difference sequence spaces was introduced by Kizmaz [27] and this concept was generalised by Et and Colak [28]. Later Et and Esi [29] generalised these sequence spaces to the following sequence spaces. Let $u=(u_k)$ be any fixed sequence of non-zero real numbers and let m be a non-negative integer. Then

$$X_u(\Delta^m) = \{x=(x_k) : (\Delta_u^m x_k) \in X\}$$

for $X = \ell_\infty$, c or c_0, where $m \in \mathsf{N}$, $\Delta_u^0 x = (u_k x_k)$, $\Delta_u^m x = (\Delta_u^{m-1} x_k - \Delta_u^{m-1} x_{k+1})$, and so $\Delta_u^m x_k = \sum_{i=0}^{m} (-1)^i \binom{m}{i} u_{k+i} x_{k+i}$. The sequence space $X_u(\Delta^m)$ is a Banach space normed by

$$\|x\|_\Delta = \sum_{i=1}^{m} |u_i x_i| + \|\Delta_v^m x_k\|_\infty$$

for $X = \ell_\infty$, c or c_0. It is noted that the sequence space $X_u(\Delta^m)$ is different from the sequence space $X(\Delta^m)$ and $X_u(\Delta^m) \cap X(\Delta^m) \ne \phi$, where $X(\Delta^m) = \{x=(x_k) : (\Delta^m x_k) \in X\}$. For this, let $X = \ell_\infty$ and choose $x = (k^{m-1})$ and $u = (k^2)$; then $x \in \ell_\infty(\Delta^m)$ but $x \notin \ell_{\infty u}(\Delta^m)$. Conversely if we choose $x = (k^{m+2})$ and $u = (k^{-2})$, then $x \in \ell_{\infty u}(\Delta^m)$ but $x \notin \ell_\infty(\Delta^m)$. Let X be any sequence space; if $x \in X_u(\Delta^m)$, then there exists one and only one $z=(z_k) \in X$ such that

$$x_k = u_k^{-1} \sum_{i=1}^{k-m} (-1)^m \binom{k-i-1}{m-1} z_i = u_k^{-1} \sum_{i=1}^{k} (-1)^m \binom{k+m-i-1}{m-1} z_{i-m}, \qquad (1)$$

$$z_{1-m} = z_{2-m} = \ldots = z_0 = 0$$

for sufficiently large k, for example $k > 2m$. We shall use the sequence which is defined in (1) to define the sequence in (2). Recently the difference sequence spaces have been studied [30-37].

MAIN RESULTS

In this section, we give the main results of this paper. In Theorem 1 we give the relationship between $\Delta_{uv}^{m}(\lambda)$ – asymptotic statistical equivalence of order α and $\Delta_{uv}^{m}(\mu)$ – asymptotic statistical

equivalence of order β of sequences. In Theorem 2 we give the relationship between strong $\Delta_{uv}^{m}(\lambda)-$asymptotic equivalence of order α and strong $\Delta_{uv}^{m}(\mu)-$asymptotic equivalence of order β of sequences. In Theorem 3 we give the relationship between $\Delta_{uv}^{m}(\lambda)-$asymptotic statistical equivalence of order α and strong $\Delta_{uv}^{m}(\mu)-$asymptotic equivalence of order β of sequences.

Two non-negative real-value sequences x and y are said to be $\Delta^{m}-$asymptotically equivalent provided that

$$\lim_{k}\frac{\Delta^{m}x_{k}}{\Delta^{m}y_{k}}=L$$

(denoted by $x\overset{\Delta^{m}}{\sim}y$).

Using the above expression we can make the following definition.

Definition 1. Let $\lambda\in\Lambda$ and $\alpha\in(0,1]$ be any real number. Two non-negative real-value sequences x and y are said to be $\Delta_{uv}^{m}(\lambda)-$asymptotically and statistically equivalent of order α provided that for every $\varepsilon>0$,

$$\lim_{n\to\infty}\frac{1}{\lambda_{n}^{\alpha}}\left|\left\{k\in I_{n}\ :\ \left|\frac{\Delta_{u}^{m}x_{k}}{\Delta_{v}^{m}y_{k}}-L\right|\geq\varepsilon\right\}\right|=0$$

(denoted by $x\overset{S_{\alpha}^{L}(\Delta_{uv}^{m}(\lambda))}{\sim}y$), where u and v are two non-negative real-value fixed sequences such that $u_{n}\neq0$ and $v_{n}\neq0$ for all $n\in\mathsf{N}$. For $\lambda_{n}=n$, we shall write $x\overset{S_{\alpha}^{L}(\Delta_{uv}^{m})}{\sim}y$ instead of $x\overset{S_{\alpha}^{L}(\Delta_{uv}^{m}(\lambda))}{\sim}y$ and in the special case $\alpha=1$, $\lambda_{n}=n$, $u_{n}=1$ and $v_{n}=1$ for all $n\in\mathsf{N}$, we shall write $x\overset{S^{L}(\Delta^{m})}{\sim}y$ (which is called $\Delta^{m}-$asymptotic statistical equivalence) instead of $x\overset{S_{\alpha}^{L}(\Delta_{uv}^{m}(\lambda))}{\sim}y$.

It is easy to see that if x and y are $\Delta^{m}-$asymptotically equivalent, then x and y are $\Delta^{m}-$asymptotically and statistically equivalent of order α, but the converse does not hold. For this, consider two sequences, $x=(x_{k})$ and $y=(y_{k})$, defined by

$$\left.\begin{aligned}\Delta^{m}x_{k}&=\begin{cases}0, & k\neq n^{3}\\ 1, & k=n^{3}\end{cases},\qquad n=1,2,...\\ \Delta^{m}y_{k}&=1,\quad \text{for all}\quad k.\end{aligned}\right\}\tag{2}$$

It is clear that x and y are $\Delta^{m}-$asymptotically and statistically equivalent of order α for $\alpha\in(\frac{1}{3},1]$, but they are not $\Delta^{m}-$asymptotically equivalent.

Definition 2. Let $\lambda\in\Lambda$ and $\alpha\in(0,1]$ be any real number. Two non-negative real-value sequences x and y are said to be strongly $\Delta_{uv}^{m}(\lambda)-$ asymptotically equivalent of order α provided that for every $\varepsilon>0$,

$$\lim_{n\to\infty}\frac{1}{\lambda_{n}^{\alpha}}\sum_{k\in I_{n}}\left|\frac{\Delta_{u}^{m}x_{k}}{\Delta_{v}^{m}y_{k}}-L\right|=0$$

(denoted by $x\overset{V_{\alpha}^{L}[\Delta_{uv}^{m}(\lambda)]}{\sim}y$). For $\lambda_{n}=n$, we shall write $x\overset{V_{\alpha}^{L}[\Delta_{uv}^{m}]}{\sim}y$ instead of $x\overset{V_{\alpha}^{L}[\Delta_{uv}^{m}(\lambda)]}{\sim}y$, and in the

special case $\alpha = 1,\ \lambda_n = n,\ u_n = 1$ and $v_n = 1$ for all $n \in \mathbb{N}$, we shall write $x \overset{V^L[\Delta^m]}{\sim} y$ (which is called strong Δ^m – asymptotic equivalence) instead of $x \overset{V_\alpha^L[\Delta_{uv}^m(\lambda)]}{\sim} y$.

Theorem 1. Let $\lambda, \mu \in \Lambda$ such that $\lambda_n < \mu_n$ for all $n \in \mathbb{N}$, and α and β be fixed real numbers such that $0 < \alpha \le \beta \le 1$. Also, let x and y be two non-negative sequences. Then each of the following assertions holds true:

i) If

$$\liminf_{n\to\infty} \frac{\lambda_n^\alpha}{\mu_n^\beta} > 0 \tag{3}$$

then $x \overset{S_\beta^L(\Delta_{uv}^m(\mu))}{\sim} y$ implies $x \overset{S_\alpha^L(\Delta_{uv}^m(\lambda))}{\sim} y$;

ii) If

$$\lim_{n\to\infty} \frac{\mu_n}{\lambda_n^\beta} = 1 \tag{4}$$

then $x \overset{S_\alpha^L(\Delta_{uv}^m(\lambda))}{\sim} y$ implies $x \overset{S_\beta^L(\Delta_{uv}^m(\mu))}{\sim} y$.

Proof. i) Suppose that $\lambda_n < \mu_n$ for all $n \in \mathbb{N}$ and $x \overset{S_\beta^L(\Delta_{uv}^m(\mu))}{\sim} y$. Then we can write

$$\left\{k \in J_n : \left|\frac{\Delta_u^m x_k}{\Delta_v^m y_k} - L\right| \ge \varepsilon\right\} \supset \left\{k \in I_n : \left|\frac{\Delta_u^m x_k}{\Delta_v^m y_k} - L\right| \ge \varepsilon\right\}$$

and so

$$\frac{1}{\mu_n^\beta}\left|\left\{k \in J_n : \left|\frac{\Delta_u^m x_k}{\Delta_v^m y_k} - L\right| \ge \varepsilon\right\}\right| \ge \frac{\lambda_n^\alpha}{\mu_n^\beta}\frac{1}{\lambda_n^\alpha}\left|\left\{k \in I_n : \left|\frac{\Delta_u^m x_k}{\Delta_v^m y_k} - L\right| \ge \varepsilon\right\}\right|$$

for all $n \in \mathbb{N}$, where $J_n = [n - \mu_n + 1, n]$. Hence we get $x \overset{S_\alpha^L(\Delta_{uv}^m(\lambda))}{\sim} y$.

ii) Let $x \overset{S_\alpha^L(\Delta_{uv}^m(\lambda))}{\sim} y$ and suppose that $I_n \subset J_n$ for all $n \in \mathbb{N}$. Then we can write

$$\begin{aligned}
&\frac{1}{\mu_n^\beta}\left|\left\{k \in J_n : \left|\frac{\Delta_u^m x_k}{\Delta_v^m y_k} - L\right| \ge \varepsilon\right\}\right| \\
&= \frac{1}{\mu_n^\beta}\left|\left\{n - \mu_n + 1 \le k \le n - \lambda_n : \left|\frac{\Delta_u^m x_k}{\Delta_v^m y_k} - L\right| \ge \varepsilon\right\}\right| \\
&\quad + \frac{1}{\mu_n^\beta}\left|\left\{k \in I_n : \left|\frac{\Delta_u^m x_k}{\Delta_v^m y_k} - L\right| \ge \varepsilon\right\}\right| \\
&\le \frac{\mu_n - \lambda_n}{\mu_n^\beta} + \frac{1}{\mu_n^\beta}\left|\left\{k \in I_n : \left|\frac{\Delta_u^m x_k}{\Delta_v^m y_k} - L\right| \ge \varepsilon\right\}\right|
\end{aligned}$$

$$\leq \frac{\mu_n - \lambda_n^\beta}{\lambda_n^\beta} + \frac{1}{\mu_n^\beta}\left|\left\{k \in I_n : \left|\frac{\Delta_u^m x_k}{\Delta_v^m y_k} - L\right| \geq \varepsilon\right\}\right|$$

$$\leq \left(\frac{\mu_n}{\lambda_n^\beta} - 1\right) + \frac{1}{\lambda_n^\alpha}\left|\left\{k \in I_n : \left|\frac{\Delta_u^m x_k}{\Delta_v^m y_k} - L\right| \geq \varepsilon\right\}\right|$$

for all $n \in \mathbb{N}$. Now, proceeding to the limit as $n \to \infty$ in the last inequality and using (4), we get $x \overset{S_\beta^L(\Delta_{uv}^m(\mu))}{\sim} y$. The following results are derivable easily from Theorem 1.

Corollary 1. Let $\lambda, \mu \in \Lambda$ be such that $\lambda_n < \mu_n$ for all $n \in \mathbb{N}$, and let x, y be two non-negative sequences. If condition (3) is satisfied, then

i) $x \overset{S_\alpha^L(\Delta_{uv}^m(\mu))}{\sim} y$ implies $x \overset{S_\alpha^L(\Delta_{uv}^m(\lambda))}{\sim} y$ for each $\alpha \in (0,1]$;

ii) $x \overset{S^L(\Delta_{uv}^m(\mu))}{\sim} y$ implies $x \overset{S_\alpha^L(\Delta_{uv}^m(\lambda))}{\sim} y$ for each $\alpha \in (0,1]$;

iii) $x \overset{S^L(\Delta_{uv}^m(\mu))}{\sim} y$ implies $x \overset{S^L(\Delta_{uv}^m(\lambda))}{\sim} y$.

Furthermore, if condition (4) is satisfied, then we get following corollary

i) $x \overset{S_\alpha^L(\Delta_{uv}^m(\lambda))}{\sim} y$ implies $x \overset{S_\alpha^L(\Delta_{uv}^m(\mu))}{\sim} y$ for each $\alpha \in (0,1]$;

ii) $x \overset{S_\alpha^L(\Delta_{uv}^m(\lambda))}{\sim} y$ implies $x \overset{S^L(\Delta_{uv}^m(\mu))}{\sim} y$ for each $\alpha \in (0,1]$;

iii) $x \overset{S^L(\Delta_{uv}^m(\lambda))}{\sim} y$ implies $x \overset{S^L(\Delta_{uv}^m(\mu))}{\sim} y$.

Theorem 2. Let $\lambda, \mu \in \Lambda$ such that $\lambda_n < \mu_n$ for all $n \in \mathbb{N}$, and α and β be fixed real numbers such that $0 < \alpha \leq \beta \leq 1$. Also, let x and y be two non-negative sequences. Then each of the following assertions holds true:

i) If condition (3) is satisfied, then $x \overset{V_\beta^L[\Delta_{uv}^m(\mu)]}{\sim} y$ implies $x \overset{V_\alpha^L[\Delta_{uv}^m(\lambda)]}{\sim} y$;

ii) Let $x, y \in \ell_{\infty u}(\Delta^m)$. If condition (4) is satisfied, then $x \overset{V_\alpha^L[\Delta_{uv}^m(\lambda)]}{\sim} y$ implies $x \overset{V_\beta^L[\Delta_{uv}^m(\mu)]}{\sim} y$,

where $\ell_{\infty u}(\Delta^m) = \{x = (x_k) : (\Delta_u^m x_k) \in \ell_\infty\}$.

Proof. i) Assume that $\lambda, \mu \in \Lambda$ such that $\lambda_n < \mu_n$ for all $n \in \mathbb{N}$ and that condition (3) holds. Since $I_n \subset J_n$, we have

$$\frac{1}{\mu_n^\beta}\sum_{k \in J_n}\left|\frac{\Delta_u^m x_k}{\Delta_v^m y_k} - L\right| \geq \frac{\lambda_n^\alpha}{\mu_n^\beta}\frac{1}{\lambda_n^\alpha}\sum_{k \in I_n}\left|\frac{\Delta_u^m x_k}{\Delta_v^m y_k} - L\right|$$

Since (3) holds and $x \overset{V_\beta^L[\Delta_{uv}^m(\mu)]}{\sim} y$, we get $x \overset{V_\alpha^L[\Delta_{uv}^m(\lambda)]}{\sim} y$.

ii) Let $x, y \in \ell_{\infty u}(\Delta^m)$ and suppose that condition (4) holds. Then there exists some $M > 0$ such that $\left|\frac{\Delta_u^m x_k}{\Delta_v^m y_k} - L\right| \leq M$ for all k, m. Then we can write

$$\frac{1}{\mu_n^\beta}\sum_{k\in J_n}\left|\frac{\Delta_u^m x_k}{\Delta_v^m y_k}-L\right|=\frac{1}{\mu_n^\beta}\sum_{k\in J_n-I_n}\left|\frac{\Delta_u^m x_k}{\Delta_v^m y_k}-L\right|+\frac{1}{\mu_n^\beta}\sum_{k\in I_n}\left|\frac{\Delta_u^m x_k}{\Delta_v^m y_k}-L\right|$$

$$\leq\left(\frac{\mu_n-\lambda_n}{\mu_n^\beta}\right)M+\frac{1}{\mu_n^\beta}\sum_{k\in I_n}\left|\frac{\Delta_u^m x_k}{\Delta_v^m y_k}-L\right|$$

$$\leq\left(\frac{\mu_n-\lambda_n^\beta}{\mu_n^\beta}\right)M+\frac{1}{\mu_n^\beta}\sum_{k\in I_n}\left|\frac{\Delta_u^m x_k}{\Delta_v^m y_k}-L\right|$$

$$\leq\left(\frac{\mu_n}{\lambda_n^\beta}-1\right)M+\frac{1}{\lambda_n^\alpha}\sum_{k\in I_n}\left|\frac{\Delta_u^m x_k}{\Delta_v^m y_k}-L\right|$$

for each $n\in\mathbb{N}$. Therefore $x \overset{V_\beta^L[\Delta_{uv}^m(\mu)]}{\sim} y$. Theorem 2 yields the following corollary.

Corollary 2. Let $\lambda,\mu\in\Lambda$ be such that $\lambda_n<\mu_n$ for all $n\in\mathbb{N}$, and let x, y be two non-negative sequences. If condition (3) is satisfied, then

i) $x \overset{V_\alpha^L[\Delta_{uv}^m(\mu)]}{\sim} y$ implies $x \overset{V_\alpha^L[\Delta_{uv}^m(\lambda)]}{\sim} y$ for each $\alpha\in(0,1]$;

ii) $x \overset{V^L[\Delta_{uv}^m(\mu)]}{\sim} y$ implies $x \overset{V_\alpha^L[\Delta_{uv}^m(\lambda)]}{\sim} y$ for each $\alpha\in(0,1]$;

iii) $x \overset{V^L[\Delta_{uv}^m(\mu)]}{\sim} y$ implies $x \overset{V^L[\Delta_{uv}^m(\lambda)]}{\sim} y$.

Furthermore, if condition (4) is satisfied, then we get the following corollary.

i) $x \overset{V_\alpha^L[\Delta_{uv}^m(\lambda)]}{\sim} y$ implies $x \overset{V_\alpha^L[\Delta_{uv}^m(\mu)]}{\sim} y$ for each $\alpha\in(0,1]$;

ii) $x \overset{V_\alpha^L[\Delta_{uv}^m(\lambda)]}{\sim} y$ implies $x \overset{V^L[\Delta_{uv}^m(\mu)]}{\sim} y$ for each $\alpha\in(0,1]$;

iii) $x \overset{V^L[\Delta_{uv}^m(\lambda)]}{\sim} y$ implies $x \overset{V^L[\Delta_{uv}^m(\mu)]}{\sim} y$.

Theorem 3. Let $\lambda,\mu\in\Lambda$ such that $\lambda_n<\mu_n$ for all $n\in\mathbb{N}$, and α and β be fixed real numbers such that $0<\alpha\leq\beta\leq 1$. Also, let x and y be two non-negative sequences. Then each of the following assertions holds true:

i) If condition (3) is satisfied, then $x \overset{V_\beta^L[\Delta_{uv}^m(\mu)]}{\sim} y$ implies $x \overset{S_\alpha^L(\Delta_{uv}^m(\lambda))}{\sim} y$;

ii) Let $x, y\in\ell_{\infty u}(\Delta^m)$. If condition (4) is satisfied, then $x \overset{S_\alpha^L(\Delta_{uv}^m(\lambda))}{\sim} y$ implies $x \overset{V_\beta^L[\Delta_{uv}^m(\mu)]}{\sim} y$.

Proof. i) For any two sequences, $x=(x_k)$ and $y=(y_k)$, we can write

$$\sum_{k\in J_n}\left|\frac{\Delta_u^m x_k}{\Delta_v^m y_k}-L\right| = \sum_{\substack{k\in J_n \\ \left|\frac{\Delta_u^m x_k}{\Delta_v^m y_k}-L\right|\geq\varepsilon}}\left|\frac{\Delta_u^m x_k}{\Delta_v^m y_k}-L\right| + \sum_{\substack{k\in J_n \\ \left|\frac{\Delta_u^m x_k}{\Delta_v^m y_k}-L\right|<\varepsilon}}\left|\frac{\Delta_u^m x_k}{\Delta_v^m y_k}-L\right|$$

$$\geq \sum_{\substack{k\in I_n \\ \left|\frac{\Delta_u^m x_k}{\Delta_v^m y_k}-L\right|\geq\varepsilon}}\left|\frac{\Delta_u^m x_k}{\Delta_v^m y_k}-L\right|$$

$$\geq \left|\left\{k\in I_n \ : \ \left|\frac{\Delta_u^m x_k}{\Delta_v^m y_k}-L\right|\geq\varepsilon\right\}\right|\varepsilon$$

so that

$$\frac{1}{\mu_n^\beta}\sum_{k\in J_n}\left|\frac{\Delta_u^m x_k}{\Delta_v^m y_k}-L\right| \geq \frac{1}{\mu_n^\beta}\left|\left\{k\in I_n \ : \ \left|\frac{\Delta_u^m x_k}{\Delta_v^m y_k}-L\right|\geq\varepsilon\right\}\right|\varepsilon$$

$$\geq \frac{\lambda_n^\alpha}{\mu_n^\beta}\frac{1}{\lambda_n^\alpha}\left|\left\{k\in I_n \ : \ \left|\frac{\Delta_u^m x_k}{\Delta_v^m y_k}-L\right|\geq\varepsilon\right\}\right|\varepsilon.$$

Hence $x \overset{V_\beta^L\left[\Delta_{uv}^m(\mu)\right]}{\sim} y$ implies $x \overset{S_\alpha^L\left(\Delta_{uv}^m(\lambda)\right)}{\sim} y$.

ii) Suppose that $x \overset{S_\alpha^L\left(\Delta_{uv}^m(\lambda)\right)}{\sim} y$ and $x, y \in \ell_{\infty u}\left(\Delta^m\right)$. Then there exists some $M>0$ such that $\left|\frac{\Delta_u^m x_k}{\Delta_v^m y_k}-L\right|\leq M$ for all k, m. Then for every $\varepsilon>0$ we can write

$$\frac{1}{\mu_n^\beta}\sum_{k\in J_n}\left|\frac{\Delta_u^m x_k}{\Delta_v^m y_k}-L\right| = \frac{1}{\mu_n^\beta}\sum_{k\in J_n-I_n}\left|\frac{\Delta_u^m x_k}{\Delta_v^m y_k}-L\right| + \frac{1}{\mu_n^\beta}\sum_{k\in I_n}\left|\frac{\Delta_u^m x_k}{\Delta_v^m y_k}-L\right|$$

$$\leq \left(\frac{\mu_n-\lambda_n}{\mu_n^\beta}\right)M + \frac{1}{\mu_n^\beta}\sum_{k\in I_n}\left|\frac{\Delta_u^m x_k}{\Delta_v^m y_k}-L\right|$$

$$\leq \left(\frac{\mu_n-\lambda_n^\beta}{\mu_n^\beta}\right)M + \frac{1}{\mu_n^\beta}\sum_{k\in I_n}\left|\frac{\Delta_u^m x_k}{\Delta_v^m y_k}-L\right|$$

$$= \left(\frac{\mu_n}{\lambda_n^\beta}-1\right)M + \frac{1}{\mu_n^\beta}\sum_{\substack{k\in I_n \\ \left|\frac{\Delta_u^m x_k}{\Delta_v^m y_k}-L\right|\geq\varepsilon}}\left|\frac{\Delta_u^m x_k}{\Delta_v^m y_k}-L\right|$$

$$+\frac{1}{\mu_n^\beta}\sum_{\substack{k\in I_n \\ \left|\frac{\Delta_u^m x_k}{\Delta_v^m y_k}-L\right|<\varepsilon}}\left|\frac{\Delta_u^m x_k}{\Delta_v^m y_k}-L\right|$$

$$\leq \left(\frac{\mu_n}{\lambda_n^\beta}-1\right)M + \frac{M}{\lambda_n^\alpha}\left|\left\{k\in I_n \ : \ \left|\frac{\Delta_u^m x_k}{\Delta_v^m y_k}-L\right|\geq\varepsilon\right\}\right|+\varepsilon$$

for all $n\in\mathbb{N}$. Using (4), we obtain that $x \overset{V_\beta^L\left[\Delta_{uv}^m(\mu)\right]}{\sim} y$ whenever $x \overset{S_\alpha^L\left(\Delta_{uv}^m(\lambda)\right)}{\sim} y$. Corollary 3 below is easily proven by applying Theorem 3.

Corollary 3. Let $\lambda, \mu\in\Lambda$ be such that $\lambda_n<\mu_n$ for all $n\in\mathbb{N}$, and let x, y be two non-negative sequences. If condition (3) is satisfied, then

i) $x \overset{V_\alpha^L[\Delta_{uv}^m(\mu)]}{\sim} y$ implies $x \overset{S_\alpha^L(\Delta_{uv}^m(\lambda))}{\sim} y$ for each $\alpha \in (0,1]$;

ii) $x \overset{V^L[\Delta_{uv}^m(\mu)]}{\sim} y$ implies $x \overset{S_\alpha^L(\Delta_{uv}^m(\lambda))}{\sim} y$ for each $\alpha \in (0,1]$;

iii) $x \overset{V^L[\Delta_{uv}^m(\mu)]}{\sim} y$ implies $x \overset{S^L(\Delta_{uv}^m(\lambda))}{\sim} y$.

Furthermore, if condition (4) is satisfied, then we get following corollary.

i) $x \overset{S_\alpha^L(\Delta_{uv}^m(\lambda))}{\sim} y$ implies $x \overset{V_\alpha^L[\Delta_{uv}^m(\mu)]}{\sim} y$ for each $\alpha \in (0,1]$;

ii) $x \overset{S_\alpha^L(\Delta_{uv}^m(\lambda))}{\sim} y$ implies $x \overset{V^L[\Delta_{uv}^m(\mu)]}{\sim} y$ for each $\alpha \in (0,1]$;

iii) $x \overset{S^L(\Delta_{uv}^m(\lambda))}{\sim} y$ implies $x \overset{V^L[\Delta_{uv}^m(\mu)]}{\sim} y$.

CONCLUSIONS

The results obtained in this study are more general than those reported in the literature. We get several results giving particular values to the numbers m, α, β and the sequences λ, μ, u and v. If we take $\lambda_n = \mu_n$ for all $n \in \mathsf{N}$, then we can write the above theorems without conditions (3) and (4).

REFERENCES

1. H. Fast, "Sur la convergence statistique", *Colloq. Math*., **1951,** *2*, 241-244.
2. I. J. Schoenberg, "The integrability of certain functions and related summability methods", *Amer. Math. Monthly*, **1959**, *66*, 361-375.
3. C. Belen and S. A. Mohiuddine, "Generalized weighted statistical convergence and application", *Appl. Math. Comput.*, **2013**, *219*, 9821-9826.
4. R. Colak, "Statistical Convergence of Order α. Modern Methods in Analysis and Its Applications", Anamaya Pub., New Delhi, **2010**, pp.121-129.
5. R. Colak, "On $\lambda-$statistical convergence", Proceedings of Conference on Summability and Applications, **2011**, Istanbul, Turkey, p.4.
6. J. S. Connor, "The statistical and strong $p-$Cesaro convergence of sequences", *Analysis*, **1988**, *8*, 47-63.
7. J. A. Fridy, "On statistical convergence", *Analysis*, **1985**, *5*, 301-313.
8. A. D. Gadjiev and C. Orhan, "Some approximation theorems via statistical convergence", *Rocky Mount. J. Math*., **2002,** *32*, 129-138.
9. M. Güngör and M. Et, "Δ^m-strongly almost summable sequences defined by Orlicz functions", *Indian J. Pure Appl. Math*., **2003**, *34*, 1141-1151.
10. M. Güngör, M. Et and Y. Altin, "Strongly $(V_\sigma, \lambda, q)-$summable sequences defined by Orlicz functions", *Appl. Math. Comput*., **2004,** *157*, 561-571.
11. M. Işık, "Strongly almost $(w, \lambda, q)-$summable sequences", *Math. Slovaca*, **2011**, *61*, 779-788.
12. V. Kumar and M. Mursaleen, "On (λ, μ)-statistical convergence of double sequences on intuitionistic fuzzy normed spaces", *Filomat*, **2011,** *25*, 109-120.

13. S. A. Mohiuddine, A. Alotaibi and M. Mursaleen, "Statistical convergence through de la Vallée-Poussin mean in locally solid Riesz spaces", *Adv. Difference Equa*., **2013**, doi:10.1186/1687-1847-2013-66.
14. M. Mursaleen, "λ – statistical convergence", *Math. Slovaca*, **2000**, *50*, 111-115.
15. M. Mursaleen, C. Çakan, S. A. Mohiuddine and E. Savaş, "Generalized statistical convergence and statitical core of double sequences", *Acta Math. Sinica*, **2010** , *26*, 2131-2144.
16. D. Rath and B. C. Tripathy, "On statistically convergent and statistically Cauchy sequences", *Indian J. Pure Appl. Math.*, **1994** , *25*, 381-386.
17. T. Šalát, "On statistically convergent sequences of real numbers", *Math. Slovaca*, **1980**, *30*, 139-150.
18. I. P. Pobyvanets, "Asymptotic equivalence of some linear transformations defined by a nonnegative matrix and reduced to generalized equivalence in the sense of Cesàro and Abel", *Mat. Fiz.*, **1980**, *28*, 83-87.
19. M. Başarır and S. Altundağ, "On asymptotically equivalent difference sequences with respect to a modulus function", *Ricerche mat*., **2011**, *60*, 299-311.
20. T. Bilgin, "f – Asymptotically lacunary equivalent sequences", *Acta Univ. Apulensis Math. Inform*., **2011**, *28*, 271-278.
21. N. L. Braha, "On asymptotically Δ^m – lacunary statistical equivalent sequences", *Appl. Math. Comput*., **2012**, *219*, 280-288.
22. A. Esi, "On Δ – asymptotically statistical equivalent sequences", *Appl. Math. Inform. Sci*., **2010,** *4*, 183-189.
23. M. Et, N. L. Braha, M. Cinar and M. Karakas, "On Δ_λ^m – Asymptotically statistical equivalent of order α of sequences", *Tamkang J. Math.* (under review).
24. M. S. Marouf, "Asymptotic equivalence and summability", *Int. J. Math. Math. Sci*., **1993**, *16*, 755-762.
25. R. F. Patterson, "On asymptotically statistical equivalent sequences", *Demonstratio Math*., **2003**, *36*, 149-153.
26. L. Leindler, **"**Über die verallgemeinerte de la Vallée-Poussinsche summierbarkeit allgemeiner orthogonalreihen", *Acta Math. Acad. Sci. Hungar.*, **1965,** *16*, 375-387.
27. H. Kizmaz, "On certain sequence spaces", *Canad. Math. Bull*., **1981**, *24*, 169-176.
28. M. Et and R. Colak, "On generalized difference sequence spaces", *Soochow J. Math*., **1995**, *21*, 377-386.
29. M. Et and A. Esi, "On Köthe-Toeplitz duals of generalized difference sequence spaces", *Bull. Malaysian Math. Sci. Soc*., **2000**, *23*, 25-32.
30. B. Altay and F. Başar, "On the fine spectrum of the difference operator Δ on c_0 and c", *Inform. Sci*., **2004**, *168*, 217-224.
31. Ç. A. Bektaş, M. Et and R. Colak, "Generalized difference sequence spaces and their dual spaces", *J. Math. Anal. Appl.,* **2004**, *292*, 423-432.
32. R. Colak, H. Altinok and M. Et, "Generalized difference sequences of fuzzy numbers", *Chaos Solitons Fract.*, **2009,** *40*, 1106-1117.
33. M. Et, H. Altinok and Y. Altin, "On some generalized sequence spaces", *Appl. Math. Comput*., **2004**, *154*, 167-173.

34. M. Et, "Strongly almost summable difference sequences of order m defined by a modulus", *Studia Sci. Math. Hungar*., **2003**, *40*, 463-476.
35. M. Et, A. Alotaibi and S. A. Mohiuddine, "On (Δ^m, I)-statistical convergence of order α", *Sci. World J.*, **2014**, Art. ID 535419.
36. E. Malkowsky, M. Mursaleen and S. Suantai , "The dual spaces of sets of difference sequences of order *m* and matrix transformations", *Acta Math. Sinica,* **2007,** *23*, 521-532.
37. M. Mursaleen, R. Colak and M. Et, "Some geometric inequalities in a new Banach sequence space", *J. Inequal. Appl.*, **2007**, Art. ID 86757.

Maejo International Journal of Science and Technology

ISSN 1905-7873
Available online at www.mijst.mju.ac.th

Full Paper

Label-free DNA detection by loop-mediated isothermal amplification coupled with quartz crystal microbalance sensor

Watcharee Boonlue [1,*], Nuntaree Chaichanawongsaroj [2] and Mana Sriyudthsak [1, 3]

[1] Biomedical Engineering Programme, Faculty of Engineering, Chulalongkorn University, Phyathai Road, Pathumwan, Bangkok 10330, Thailand
[2] Department of Transfusion Medicine and Clinical Microbiology, Faculty of Allied Health Sciences, Chulalongkorn University, Phyathai Road, Pathumwan, Bangkok 10330, Thailand
[3] Department of Electrical Engineering, Faculty of Engineering, Chulalongkorn University, Phyathai Road, Pathumwan, Bangkok 10330, Thailand
* Corresponding author, e-mail: boonlue.watcharee@gmail.com

Received: 21 November 2014 / Accepted: 4 December 2014 / Published: 15 December 2014

Abstract: Loop-mediated isothermal amplification (LAMP) and quartz crystal microbalance (QCM) sensors were used for DNA detection. Porcine DNA as DNA template was amplified and QCM sensors were then used to measure the changes in frequency in positive and negative samples. Mathematical models were employed to extract features from the sensor recordings by fitting the frequency-time plots using polynomial functions. The polynomial function coefficients of the plots gave valuable information for sample classification. Radar graphs and principle component analysis (PCA) were also applied to samples using these coefficients. Both the radar graphs and the PCA indicated differences between the sample groups when using coefficients of high-order functions.

Keywords: label-free DNA detection, DNA amplification, quartz crystal microbalance, loop-mediated isothermal amplification, DNA

INTRODUCTION

DNA detection is applied in many scientific fields such as medicine (treatment, prevention, etc.), forensic science (paternity test, personal identity, etc.) [1], DNA identity testing (GMOs, illegal organism, etc.) [2, 3] and agriculture (food, genetic resources, etc.) [4]. Devices for analysing DNA during screening tests have gained increasing attention over the past decades. Attempts have been made to improve the performance of the sensing devices to attain several desirable features such as high sensitivity, portability for on-site utilisation, low cost and simple protocols and

equipment. This study proposes a label-free, inexpensive and simple method for classifying DNA samples using quartz crystal microbalance (QCM) sensors together with the loop-mediated isothermal amplification (LAMP) method.

QCM is commonly applied in various kinds of analysis, for example gas detection [5, 6], chemical sensing [7, 8] and bio-sensing [9, 10]. It has many advantages over other sensors, such as its small size, low sample volume requirement and capacity to be implemented in real-time measurements. It can also be used as a label-free sensor with a reasonably high resolution. The resonant frequency of the QCM decreases when there is an increase in mass or viscosity of the sample. The detection of DNA using QCM can be performed by measuring the mass change with immobilised probes on the QCM surface when the target DNA hybridises [11, 12]. Attempts have been made to increase the sensitivity of the sensor by labelling the DNA with colloidal gold [13, 14] or magnetic beads [15] to amplify the change in mass. However, these methods are complicated and require sophisticated procedures and expertise.

Tsortos and co-workers [16] reported a relationship between the length of DNA and its viscosity. They found that the longer the DNA is, the higher its viscosity gets. This implies that different lengths and shapes of DNA lead to different viscosities. Since the DNA concentration is extremely low in most specimens, amplification is normally required before measurement. Polymerase chain reaction (PCR) is a common and well-known technique for amplifying DNA. Since DNA products from the PCR have the same length from the beginning to the end of the process, the viscosity of the specimen is directly proportional to the amount of the products. Recently, a number of reports have shown that the LAMP technique is able to detect viral DNA and RNA from different types of samples from both humans and animals [17-19]. LAMP is a unique DNA amplification method according to Notomi and colleagues [20]. An interesting point of this technique is its primer binding pattern. It produces various lengths of DNA and a cauliflower-like structure and involves the use of the strand displacement activity of DNA polymerase enzyme that can work at the same temperature as that used for the primer annealing. Compared with PCR, which uses three temperature steps for denaturing, annealing and extension, this is another unique characteristic of LAMP, which can amplify the target DNA at a single temperature. Recently, Hatano and colleagues [21] used a disposable pocket warmer with a styrofoam box as the heat source in LAMP without consuming electricity. This demonstrates the feasibility of using LAMP in field work. It is estimated that LAMP can amplify DNA by up to 10^9-10^{10} times in an hour at a single temperature. Owing to the structure and length of LAMP products described above, it is believed that LAMP can induce more changes in viscosity than other methods. This can be handled by analysing LAMP products with the QCM. In this paper, the use of the QCM sensor in classifying positive and negative samples before and after amplification by LAMP is reported.

MATERIALS AND METHODS

Reagents

The stock buffer for LAMP reactions was 10X ThermoPol reaction buffer from New England BioLabs (USA). The working buffer was prepared by diluting this buffer to 1X with deionised water. Four specific primers for porcine DNA detection were designed by Transfusion Medicine Laboratory, Allied Health Sciences, Chulalongkorn University [22]. The lengths of FIP, BIP, F3 and B3 primers were 38, 36, 18 and 18 bp respectively. The target DNA length was 169 bp. All the primers were synthesised by BioDesign Co. (Thailand). The stock buffer (TBE buffer) for gel electrophoresis was 0.9M Tris-borate -0.02M EDTA (pH 8).

DNA Sample Preparation

Porcine genomic DNA was used as the DNA template. Extraction and separation of the porcine DNA template was performed using Wizard® Genomic DNA Purification Kit (Promega, USA) [23]. Pork muscle from the supermarket was extracted for genomic DNA following the mouse tail protocol [23]. Except in DNA precipitation, isopropanol incubation was extended to 12 hr.

Test Samples

Positive and negative samples were investigated. The positive sample contained 10 ng/µL of porcine genomic DNA template and was labelled as 'Pos'. The negative sample contained 10 ng/µL of *Salmonella* genomic DNA template or deionised water and was labelled as 'Neg'. The sample before application of LAMP was labelled as 'Pre' while that after LAMP application was labelled as 'Post'. Four types of samples under investigation were: (1) positive sample before application of LAMP (Pos-Pre), (2) negative sample before application of LAMP (Neg-Pre), (3) positive sample after application of LAMP (Pos-Post), and (4) negative sample after application of LAMP (Neg-Post).

LAMP

LAMP was carried out in a total volume of 25 µL. The LAMP reaction solution contained 0.4 µM FIP, 0.4 µM BIP, 0.2µM F3, 0.2µM B3, 0.8M betaine (Aldrich Chemical, Germany), 1.4mM dNTP (Invitrogen, Germany), 8U of *Bst* DNA polymerase (New England Biolabs, USA), 20mM Tris-HCl, 10mM KCl, 10mM $(NH_4)_2SO_4$, 8mM $MgSO_4$, 0.1% Triton X-100 and 1 µL of a test sample. In the DNA amplification process, the LAMP reaction solutions were incubated at 60°C for 60 min. in a water bath and then heated at 80°C for 2 min. to terminate the reaction. The LAMP products were then analysed by gel electrophoresis. All four types of samples mentioned above were further analysed by QCMs.

Gel Electrophoresis

A 1.5% agarose gel was prepared using 1.5 g of agar powder (Patanasin Enterprise Ltd, Thailand) in 100 mL of 0.5X TBE buffer solution. The DNA products from LAMP were loaded and run under a constant voltage of 100 volts for 60 min. The gel was stained with SYBR Gold (Invitrogen, Germany) and observed under a UV transilluminator.

QCM Sensors

QCM discs (12 MHz) with a diameter of 12 mm were purchased from Tai Tien Electronics Co. (Thailand). Each disc was coated with layers of chromium and gold electrodes on both sides. First, 50 nm of chromium layer was deposited on both sides of the QCM discs and then 200 nm of gold layer was deposited on the chromium layer. The diameter of the electrode was 4 mm, giving an area of 0.126 cm^2. The disc was then mounted onto a holder and the contact was made with a silver paste. The electrode surface was subjected to hydrophobic treatment by dipping in 0.5% octadecyltrichlorosilane (Fluka, Switzerland) in toluene for 10 min. The sensors were rinsed with ethanol and dried with nitrogen gas before use. More than 30 QCMs with temperature coefficients of less than 10 Hz/°C were selected for further study.

Frequency Measurement

To measure the resonant frequency of QCM sensors, a laboratory-made measuring system was constructed. The system was composed of an 8-channel measuring circuit capable of making simultaneous measurements by up to 8 sensors. The frequency measuring circuit was a conventional Colpitts oscillator with high speed CMOS-TTL as described by Somboon et al. [24]. The oscillation frequency of the QCM was counted using the 8-bit CMOS microcontroller PIC16F628A. The data from all sensors were transferred to a personal computer through a communication interface driver (MAX232). The system was installed in a temperature-controlled chamber during the measurements. The temperature of the chamber was maintained at 29±1°C.

Data Collection

Figure 1 shows a scheme for classifying the samples using QCM. First, the resonant frequencies (f_0) of all blank QCMs were measured and recorded as the background value. Before amplification, positive and negative samples were taken and loaded onto the QCMs. These samples were named Pos-Pre and Neg-Pre respectively. The changes in frequency due to differences in sample composition before amplification were monitored and recorded.

The remaining positive and negative samples were subjected to LAMP. After the reaction was stopped, each sample was loaded onto the QCM. These positive and negative samples after amplification were called Pos-Post and Neg-Post respectively. The changes in frequency of the QCMs were monitored and compared with the samples before amplification to investigate the effect of the amplification.

All measurements were performed by loading a 20-µL sample onto one side of the QCM surface while the other side was left exposed to the air. The changes in frequency after sample loading were monitored and recorded with time until the oscillation stopped.

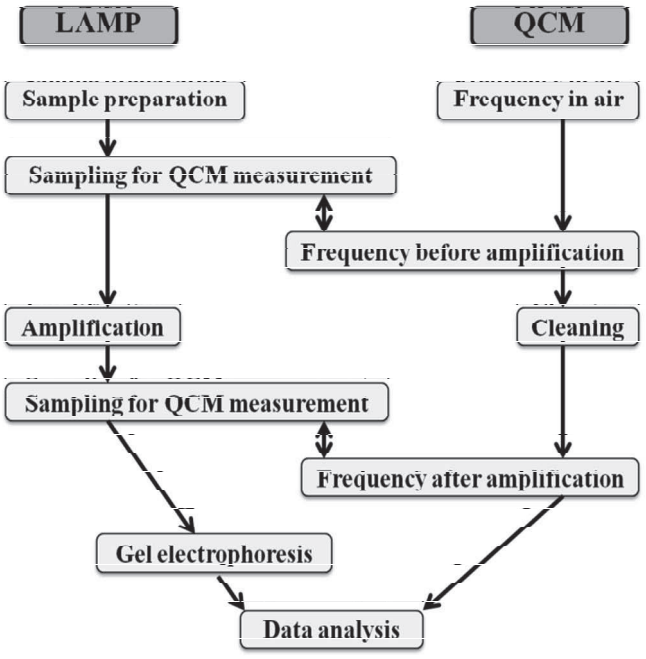

Figure 1. Scheme of QCM sensor for LAMP product detection

Data Analysis

Samples that could not be assessed by gel electrophoresis were excluded from data analysis. Consequently, only 38 samples remained for data analysis as follows: Pos-Pre (n=10), Neg-Pre (n=4), Pos-Post (n=15) and Neg-Post (n= 9).

The four groups of data were classified by comparing the frequency-time plots. Curve fittings were performed on the frequency-time plots using linear, 2nd order polynomial, 3rd order polynomial and 4th order polynomial functions. The coefficients obtained from the 2nd step were then used for the classification by radar plots. Finally, principal component analysis (PCA) was employed to analyse the selected coefficient data.

RESULTS AND DISCUSSION

Validation of LAMP Method

After completing the DNA amplification, the LAMP products were assessed by gel electrophoresis. No bands from the negative samples both before (Neg-Pre) and after (Neg-Post) amplification were detected. Positive samples before amplification (Pos-Pre) also displayed no bands. Although they contained dNTP, primers and DNA template, the amplification did not take place and thus there were no detectable bands. The bands were detected only in the positive samples after LAMP (Pos-Post) as shown in Figure 2. Long-strip bands were observed, showing that various lengths of DNA fragments were produced.

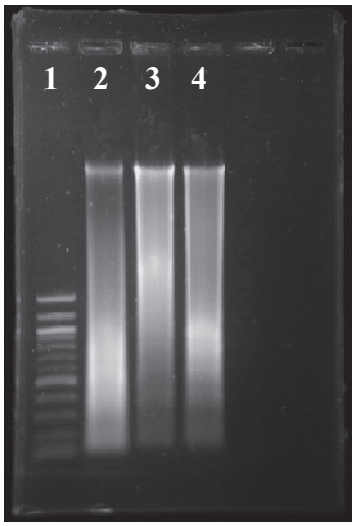

Lane 1 = 100 bp marker
Lane 2 = LAMP product from 10 ng/µL Pork DNA template (DNA template diluted from 336 ng/µL)
Lane 3 = LAMP product from 10 ng/µL Pork DNA template (DNA template diluted from 293 ng/µL)
Lane 4 = LAMP product from 10 ng/µL Pork DNA template (DNA template diluted from 445 ng/µL)

Figure 2. Typical gel electrophoresis pattern of positive samples with DNA template after LAMP (Pos-Post)

Frequency-Time Plots

Figure 3 shows typical frequency-time plots of the four sample groups. The temperature fluctuation during the experiment (2 hr) was less than ±1°C; thus, the change in frequency of QCM was not affected by temperature. All four sample groups gave similar responses as follows. At the beginning of the experiment ('a'-'b'), the frequency of QCM was quite stable. During this range of 'a'-'b', the QCM was exposed to air and the frequency recorded at this region was used as the background frequency. A step change in frequency occurred after the sample was loaded (at 'b') onto the sensor surface. This happened within 10 sec. Shortly afterward, the frequency gradually

decreased about 1500 Hz and then an abrupt drop in frequency was observed until the oscillation stopped at point 'c'. The frequency data in the range 'b'-'c' were utilised to characterise Neg-Pre and Pos-Pre samples.

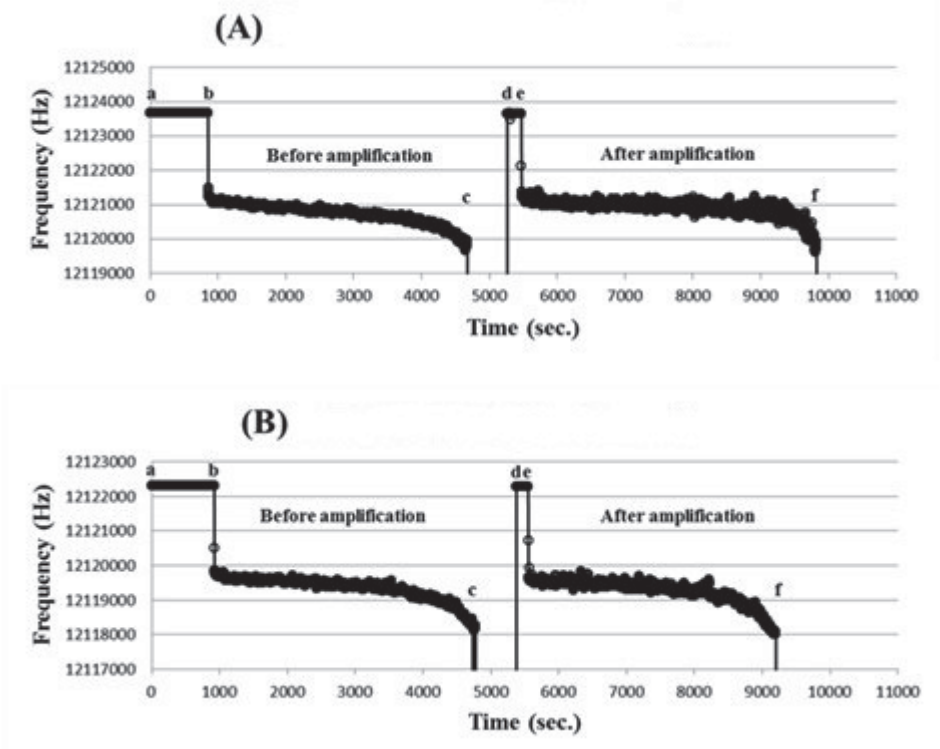

Figure 3. Typical frequency-time plots for samples before and after amplification: (A) negative samples; (B) positive samples

The QCMs were cleaned between each measurement. The four sample groups, after LAMP, were again loaded onto the QCMs. The range 'd'-'e' shows the plot before the loading of the sample subjected to LAMP. In this range, as in range 'a'-'b', the frequency was very stable. The LAMP sample was loaded at point 'e'. A sharp drop of frequency at point 'e' and a gradual decrease in the range 'e'-'f' were observed, similar to that observed at point 'b' and range 'b'-'c'. The data in the range 'e'-'f' were utilised to characterise the Neg-Post and Pos-Post samples. The abrupt change in frequency at the points 'b' and 'e' was the result of sample loading onto the QCM. According to Sauerbrey [25] and Kanazawa and Gordon [26], when the mass, the concentration or the viscosity at the electrode surface increases, the QCM frequency will decrease. The slow change in the ranges 'b'-'c' and 'e'-'f' might be due to a slow precipitation of the sample components on the QCM. Fang and co-workers [27] reported that the DNA appears on the surface of a solution with a low DNA concentration. As the concentration increases, the DNA forms a long chain and penetrates into the solution. After LAMP amplification, a positive sample should have various lengths of DNA fragments. Long-chain DNA fragments are then expected to penetrate into the solution. During evaporation, the long-chain DNA interacts more with the surface electrode than does the pre-LAMP DNA. Indeed, this can be observed from the frequency-time plot (Figure 3), where both the frequency change rate and frequency change value at the point 'f' of the amplified solution (Pos-Post) were higher than those of the negative samples (Neg-Post) and samples before

amplification (Pos-Pre and Neg-Pre). However, it is difficult to distinguish the differences between positive and negative samples before and after amplification using only simple observation.

Data Analysis

Comparison between each group of samples

On detailed examination of Figure 3, it was noticed that the frequency-drop rate of the positive samples (Pos-Pre and Pos-Post) is higher than that of the negative ones (Neg-Pre and Neg-Post). This implies that it is feasible to use this information to distinguish the negative samples from the positive samples. To classify the sample groups, a time-frequency-drop plot was made for each sample group (Figure 4) Since an abrupt change in frequency was observed for 20 sec. after loading the sample at points 'b' and 'e', the data obtained 20 sec. after loading were not used. The data used in the plots were taken after this 20-sec. period. The mean time taken for frequency change of up to 1300 Hz in all the sample groups were used.

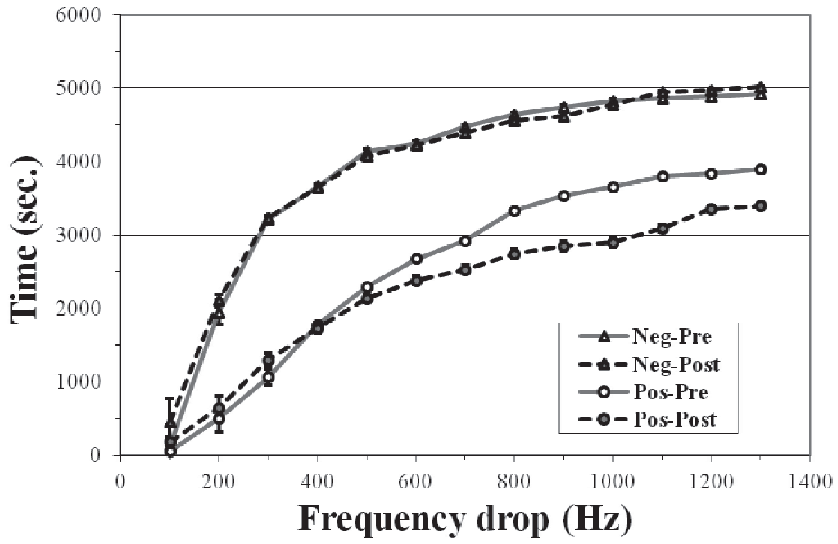

Figure 4. Time-frequency-drop plots for positive and negative samples before and after amplification

It should be noted that the per cent coefficient of variation (% CV) was quite high for the frequency change of less than 500 Hz as shown in Figure 4. However, it was less than 35 Hz for the frequency changes greater than 500 Hz in negative samples (Neg-Pre and Neg-Post) and positive samples before amplification (Pos-Pre), while it was in the range of 40-230 Hz for positive sample after amplification (Pos-Post). The high % CV or fluctuation in the Pos-Post samples could have resulted from the movement of the amplified DNA chains. Moreover, it is obvious that the overall frequency change rates of the negative samples, both Neg-Pre and Neg-Post, were lower than those of the positive ones (Pos-Pre, Pos-Post). The changes in frequency of the negative samples (Neg-Pre and Neg-Post) were very slow at the beginning (~13 sec/Hz) and higher after 1 hr (~1 sec/Hz). No differences were observed between the negative samples before and after amplification. However, the positive samples (Pos-Pre and Pos-Post) showed a rapid change from ~5 sec/Hz to ~1 sec/Hz from the beginning to 1 hr later respectively. This rapid change might have been due to the DNA template being added to the positive samples and also to the amplified DNA products by LAMP producing various long chains of DNA. According to Tsortos and co-workers [16], longer

chains of DNA induce higher viscosity, which leads to a faster drop in frequency. This can be observed in Figure 4, where the positive sample after amplification (Pos-Post) took about 3300 sec. for a frequency drop of 1300 Hz, while the positive sample before amplification (Pos-Pre) and the negative samples before (Neg-Pre) and after (Neg-Post) LAMP took 3800, 4900 and 4900 sec. respectively for this drop.

Classification using radar graphs

Although it is possible to distinguish the positive and negative samples groups (Figure 4), it is still difficult to classify individual samples due to variation. In our attempt to classify individual samples, mathematical models were applied to categorise the four groups of samples. Curve fitting using 4 polynomial functions, namely linear function ($y = a_0 + a_1t$), 2^{nd}-order ($y = a_0 + a_1t + a_2t^2$), 3^{rd}-order ($y = a_0 + a_1t + a_2t^2 + a_3t^3$) and 4^{th}-order polynomial functions ($y = a_0 + a_1t + a_2t^2 + a_3t^3 + a_4t^4$) was used on frequency-time plots. Means of coefficients (a_i) and coefficient of determination (R^2) were used in the analysis. The ratio of the coefficient before amplification to that after amplification for each sample was calculated and shown in Table 1. All the variables are defined as follows.

a_i' = a_i (Post) / a_i (Pre)

a_i' = ratio of coefficient before and after amplification for each polynomial coefficient at order i and R^2

a_i(Post) = means of coefficients in each polynomial order for sample after amplification

a_i (Pre) = means of coefficients in each polynomial order for sample before amplification

i = order of coefficient

For a clearer representation, the data were plotted as radar charts (Figure 5). Positive and negative samples could not be separated using linear and 2^{nd}-order polynomial functions. However, they could be clearly separated using 3^{rd}- and 4^{th}-order polynomial functions. Thus, it is possible to identify whether a sample has DNA template by comparing coefficient a_i'. Values of a_2', a_3' and a_3', a_4' for the 3^{rd}- and 4^{th}-order polynomial functions respectively significantly increased in the positive sample. This indicates that as time passes, the change in frequency is dominated by higher order coefficients. Thus, a certain time period is necessary in determining the frequency-time plot to achieve successful classification. In this case 3000 seconds (~50 min.) was needed for the classification.

Principal component analysis (PCA)

PCA was also applied to classify the samples. However, when the same data set was used as in the previous analysis, the samples could not be visually classified. The data used in the feature extraction for PCA was therefore slightly modified. The data set used in PCA was collected when the frequency change was larger than 200 Hz after sample loading at the points 'b' and 'e' (Figure 3). The procedure for coefficient extraction was the same as that for radar graph analysis. The data from the coefficient extraction for each sample were plotted in the PCA feature space. Figure 6 shows PCA scores in 2-dimenational feature space of PC1 vs. PC2, PC1 vs. PC3 and PC2 vs. PC3. PCA scores plot of PC1 vs. PC2 shows quite a good separation between positive and negative samples, although one of the samples is the outlier (Figure 6A). The separation of positive samples before (Pos-Pre) and after (Pos-Post) amplification is clearly observed, while the separation of

negative samples before (Neg-Pre) and after (Neg-Post) amplification cannot be achieved. The PCA score plot of PC2 vs. PC3 in Figure 6C also shows that the group of positive samples after amplification (Pos-Post) can be isolated from the others, as was the case in the PC1 vs. PC2 plot. This confirms that the target DNA was successfully amplified in the positive samples during the LAMP process and no amplification occurred in the negative samples. However, it should be noted that it is difficult to group the samples using PCA score plot of PC1 vs. PC3. This implies that even though the score of PC2 is not the highest, it plays an important role in grouping the samples as shown in Figures 6A and 6C.

Table 1. Mathematical values obtained from all groups of samples

Function	Sample	R^2	a_0	a_1	a_2	a_3	a_4
Linear	Neg-Pre	0.60	-2228	-0.38			
	Neg-Post	0.65	-2297	-0.50			
	Neg-Post/Neg-Pre(a_i')	**1.09**	**1.03**	**1.33**			
	Pos-Pre	0.65	-2371	-0.39			
	Pos-Post	0.67	-2489	-0.53			
	Pos-Post/Pos-Pre (a_i')	**1.03**	**1.05**	**1.34**			
2nd-Order	Neg-Pre	0.79	-2491	0.41	-3.75E-04		
	Neg-Post	0.84	-2588	0.53	-6.63E-04		
	Neg-Post/Neg-Pre(a_i')	**1.06**	**1.04**	**1.28**	**1.77**		
	Pos-Pre	0.83	-2611	0.33	-4.00E-04		
	Pos-Post	0.83	-2735	0.40	-7.23E-04		
	Pos-Post/Pos-Pre (a_i')	**1.01**	**1.05**	**1.23**	**1.81**		
3rd-Order	Neg-Pre	0.87	-2288	-0.81	1.15E-03	-5.25E-07	
	Neg-Post	0.90	-2387	-0.87	1.54E-03	-1.13E-06	
	Neg-Post/Neg-Pre(a_i')	**1.04**	**1.04**	**1.08**	**1.34**	**2.14**	
	Pos-Pre	0.89	-2442	-0.65	8.75E-04	-5.00E-07	
	Pos-Post	0.89	-2570	-0.86	1.92E-03	-1.48E-06	
	Pos-Post/Pos-Pre (a_i')	**1.00**	**1.05**	**1.32**	**2.20**	**2.95**	
4th-Order	Neg-Pre	0.89	-2400	0.30	-1.35E-03	1.65E-06	-5.25E-10
	Neg-Post	0.92	-2494	0.35	-1.86E-03	2.75E-06	-1.38E-09
	Neg-Post/Neg-Pre(a_i')	**1.03**	**1.04**	**1.16**	**1.38**	**1.67**	**2.62**
	Pos-Pre	0.91	-2539	0.22	-9.50E-04	7.75E-07	-3.85E-10
	Pos-Post	0.90	-2661	0.17	-1.44E-03	2.65E-06	-2.05E-09
	Pos-Post/Pos-Pre (a_i')	**1.00**	**1.05**	**0.80**	**1.51**	**3.42**	**5.31**

Note: R^2= coefficient of determination; a_0= mean of polynomial coefficient at order 0; a_1= mean of polynomial coefficient at order 1; a_2= mean of polynomial coefficient at order 2; a_3= mean of polynomial coefficient at order 3; a_4= mean of polynomial coefficient at order 4; a_i'= ratio of coefficient before and after the amplification for each polynomial coefficient at order i and R^2; E = times ten raised to the power of the value of the exponent

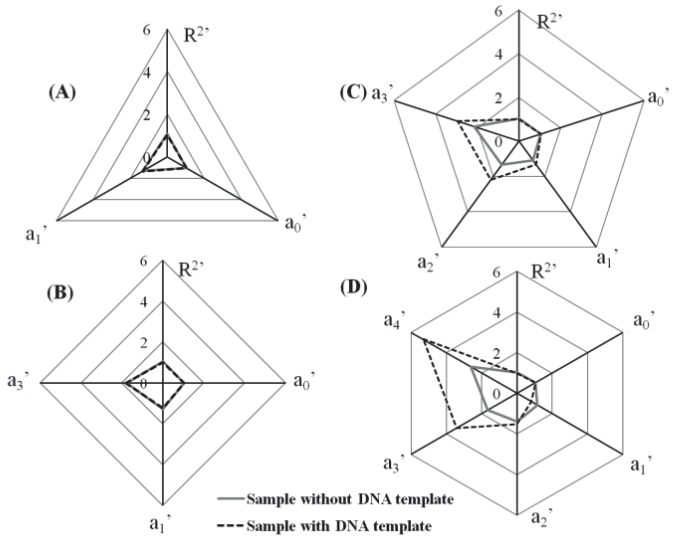

Figure 5. Rader charts of ratio of coefficients before and after amplification from positive and negative samples using four mathematical models: (A) linear; (B) 2nd-order polynomial; (C) 3rd-order polynomial; (D) 4th-order polynomial

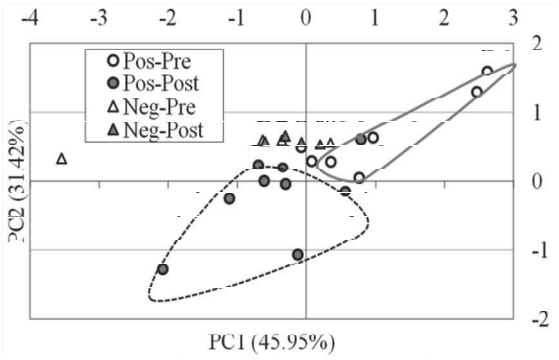

(A) PCA scores of samples in PC1 vs. PC2 feature space

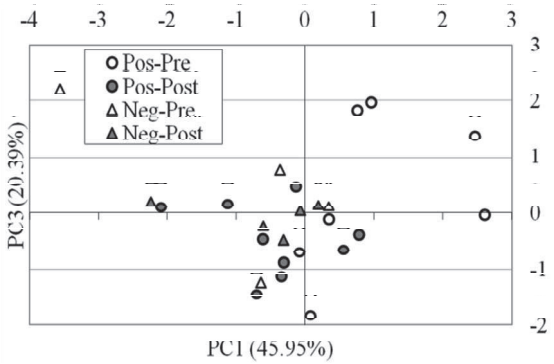

(B) PCA scores of samples in PC1 vs. PC3 feature space

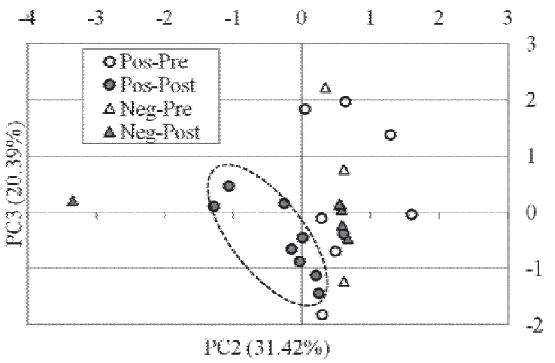

(C) PCA scores of samples in PC2 vs. PC3 feature space

Figure 6. PCA of the four groups of samples: (A) PCA scores of samples in PC1 vs. PC2 feature space; (B) PCA scores of samples in PC1 vs. PC3 feature space; (C) PCA scores of samples in PC2 vs. PC3 feature space

CONCLUSIONS

This study shows the feasibility of separating positive and negative samples both before and after amplification by LAMP using QCM sensor. This label-free technique can amplify target DNA at a single temperature without the need of a thermocycler and demonstrates an effective method for qualitative DNA detection using a combination of LAMP and QCM, together with simple mathematical functions.

ACKNOWLEDGEMENTS

This research was financially supported by the Chulalongkorn University Centenary Academy Development Project. Dr. Pakpum Somboon is gratefully acknowledged for kindly commenting on the PCA. The University Development Commission at the Ministry of University Affairs is thanked for W.B.'s scholarship.

REFERENCES

1. F. Frances, A. Castello and F. Verdu, "Testing the recoverability of grass DNA transferred to textiles for forensic purpose", *Maejo Int. J. Sci. Technol.*, **2010**, *4*, 462-467.
2. A. Suwanposri, P. Yukphan, Y. Yamada and D. Ochaikul, "Identification and biocellulose production of *Gluconacetobacter* strains isolated from tropical fruits in Thailand", *Maejo Int. J. Sci. Technol.*, **2013**, *7*, 70-82.
3. J. Jairin, S. Teangdeerith, P. Leelagud, K. Phengrat, A. Vanavichit and T. Toojinda, "Physical mapping of *Bph3*, a brown planthopper resistance locus in rice", *Maejo Int. J. Sci. Technol.*, **2007**, *1*, 166-177.
4. R. Charoensook, C. Knorr, B. Brenig and K. Gatphayak, "Thai pigs and cattle production, genetic diversity of livestock and strategies for preserving animal genetic resources", *Maejo Int. J. Sci. Technol.*, **2013**, *7*, 113-132.
5. C. K. O'Sullivan and G. G. Guilbault, "Commercial quartz crystal microbalances—theory and applications", *Biosens. Bioelectron.*, **1999,** *14*, 663-670.
6. P. Si, J. Mortensen, A. Kornolov, J. Denborg and P. J. Moller, "Polymer coated quartz crystal microbalance sensors for detection of volatile organic compounds in gas mixtures", *Anal. Chim. Acta,* **2007**, *597*, 223-230.
7. F. Caruso, D. N. Furlong and P. Kingshott, "Characterization of ferritin adsorption onto gold", *J. Colloid Interf. Sci.*, **1997**, *186*, 129-140.
8. S. Suematsu, Y. Oura, H. Tsujimoto, H. Kanno and K. Naoi, "Conducting polymer films of cross-linked structure and their QCM analysis", *Electrochim. Acta*, **2000**, *45*, 3813-3821.
9. M. A. Cooper and V. T. Singleton, "A survey of the 2001 to 2005 quartz crystal microbalance biosensor literature: Applications of acoustic physics to the analysis of biomolecular interactions", *J. Mol. Recognit.*, **2007**, *20*, 154-184.
10. H. Ogi, H. Nagai, Y. Fukunishi, T. Yanagida, M. Hirao and M. Nishiyama, "Multichannel wireless-electrodeless quartz-crystal microbalance immunosensor", *Anal. Chem.*, **2010**, *82*, 3957-3962.
11. G. Garcia-Martinez, E. A. Bustabad, H. Perrot, C. Gabrielli, B. Bucur, M. Lazerges, D. Rose, L. Rodriguez-Pardo, J. Farina, C. Compere and A. A. Vives, "Development of a mass sensitive quartz crystal microbalance (QCM)-based DNA biosensor using a 50 MHz electronic oscillator circuit", *Sensors*, **2011**, *11*, 7656-7664.
12. F. Caruso, E. Rodda, D. N. Furlong and V. Haring, "DNA binding and hybridization on gold and derivatized surfaces", *Sensor Actuat. B–Chem.*, **1997**, *41*, 189-197.

13. M. Lazerges, H. Perrot, N. Zeghib, E. Antoine and C. Compere, "*In situ* QCM DNA-biosensor probe modification", *Sensor Actuat. B–Chem.*, **2006**, *120*, 329-337.
14. I. Mannelli, M. Minunni, S. Tombelli and M. Mascini, "Quartz crystal microbalance (QCM) affinity biosensor for genetically modified organisms (GMOs) detection", *Biosens. Bioelectron.*, **2003**, *18*, 129-140.
15. H. Tsai, Y. Lin, H. W. Chang and C. B. Fuh, "Integrating the QCM detection with magnetic separation for on-line analysis", *Biosens. Bioelectron.*, **2008**, *24*, 485-488.
16. A. Tsortos, G. Papadakis and E. Gizeli, "The intrinsic viscosity of linear DNA", *Biopolymers*, **2011**, *95*, 824-832.
17. M. Parida, S. Sannarangaiah, P. K. Dash, P. V. L. Rao and K. Morita, "Loop mediated isothermal amplification (LAMP): A new generation of innovative gene amplification technique; perspectives in clinical diagnosis of infectious diseases", *Rev. Med. Virol.*, **2008**, *18*, 407-421.
18. M. A. Bakheit, D. Torra, L. A. Palomino, O. M. M. Thekisoe, P. A. Mbati, J. Ongerth and P. Karanis, "Sensitive and specific detection of *Cryptosporidium* species in PCR-negative samples by loop-mediated isothermal DNA amplification and confirmation of generated LAMP products by sequencing", *Vet. Parasitol.*, **2008**, *158*, 11-22.
19. S. Mitarai, M. Okumura, E. Toyota, T. Yoshiyama, A. Aono, A. Sejimo, Y. Azuma, K. Sugahara, T. Nagasawa, N. Nagayama, A. Yamane, R. Yano, H. Kokuto, K. Morimoto, M. Ueyama, M. Kubota, R. Yi, H. Ogata, S. Kudoh and T. Mori, "Evaluation of a simple loop-mediated isothermal amplification test kit for the diagnosis of tuberculosis", *Int. J. Tuberc. Lung Dis.*, **2011**, *15*, 1211-1217.
20. T. Notomi, H. Okayama, H. Masubuchi, T. Yonekawa, K. Watanabe, N. Amino and T. Hase, "Loop-mediated isothermal amplification of DNA", *Nucl. Acids Res.*, **2000**, *28*, e63.
21. B. Hatano, T. Maki, T. Obara, H. Fukumoto, K. Hagisawa, Y. Matsushita, A. Okutani, B. Bazartseren, S. Inoue, T. Sata and H. Katano, "LAMP using a disposable pocket warmer for anthrax detection, a highly mobile and reliable method for anti-bioterrorism", *Jpn. J. Infect. Dis.*, **2010**, *63*, 36-40.
22. P. Mahamad, "Development of porcine detection in food products by loop-mediated isothermal amplification in food", *MS Thesis*, **2006**, Chulalongkorn University, Thailand.
23. Promega Corporation, "WiZard® Genomic DNA Purification Kit Technical Manual", **2012**, http://www.promega.com/resources/protocols/technical-manuals/0/wizard-genomic-dna-purification-kit-protocol/ (Accessed: 19 June 2012).
24. P. Somboon, B. Wyszynski and T. Nakamoto, "Realization of recording a wide range of odor by utilizing both of transient and steady-state sensor responses in recording process", *Sensor Actuat. B–Chem.*, **2007**, *124*, 557-563.
25. G. Sauerbrey, "Verwendung von schwingquarzen zur wägung dünner schichten und zur mikrowägung", *Z. Phys.*, **1959**, *155*, 206-222.
26. K. K. Kanazawa and J. G. Gordon II, "Frequency of a quartz microbalance in contact with liquid", *Anal Chem*., **1985**, *57*, 1770-1771.
27. X. Fang, B. Li, E. Petersen, Y. S. Seo, V.A. Samuilov, Y. Chen, J. C. Sokolov, C. Y. Shew and M. H. Rafailovich, "Drying of DNA droplets", *Langmuir*, **2006**, *22*, 6308-6312.

Maejo International Journal of Science and Technology

ISSN 1905-7873
Available online at www.mijst.mju.ac.th

Full Paper

Protective coordination of main and backup overcurrent relays with different operating modes of active superconducting current controller

Ahmad Ghafari *, Morteza Razaz, Ghodratollah Seifossadat and Mohsen Hosseinzadeh Soreshjani

Department of Electrical Engineering, Shahid Chamran University of Ahvaz, Ahvaz, Iran

* Corresponding author, e-mail: ghafari.ieee@gmail.com

Received: 11 January 2014 / Accepted: 23 December 2014 / Published: 24 December 2014

Abstract: Active superconducting current controllers (ASCCs) are new generation of series compensators, which can also be categorised as fault current limiters because of their ability to decrease the fault current continuously. Although the performance of the ASCCs in different operating modes introduces a limiting impedance in series with the network, it can degrade the operation of the overcurrent relays (OCRs). In this paper the ASCC modelling and its control strategy for fault detection and converter operation is investigated. The simulation of a typical three-phase ASCC shows the effect of the ASCC on fault current limiting and confirms the operation of the control system. The impact of different modes of ASCC on the operation of the main and backup OCRs is studied through the simulation of a typical distribution system. Simulation results confirm that the protective coordination of different modes of the ASCC is achieved by modifying both the time dial and pickup current parameters of the OCRs.

Keywords: current controller, fault current limiters, main and backup protection, over-current relay, power distribution system, superconducting devices

INTRODUCTION

The recent growth of electrical energy demand and the rapid development of the power systems have increased short-circuit phenomena which can damage circuit breakers and other equipment. The application of fault current limiters (FCLs) can be regarded as an effective solution for this issue [1]. Several researches have introduced and evaluated different types of FCLs. For example, the resistive, magnetic-shield, high-temperature superconducting, saturated iron-core, and shunt superconducting FCL types have been presented and examined [2-5]. In general, these types

of FCLs have a low resistance against the line current under the normal state, but they suddenly represent a large resistance against the current when a fault occurs.

The active superconducting current controller (ASCC) as a new generation of series compensations is a combination of superconductor technology and power electronic devices [6]. This type of superconducting FCL can decrease the fault current continuously at different levels. In addition, it can also be implemented in the hybrid alternating-current-to-direct-current (AC-DC) power supply systems [7-8]. In spite of the aforementioned advantages, the ASCC may deteriorate the operation of employed over-current relays (OCRs). It stands to reason that reducing the fault current increases the trip time of the OCR and may deteriorate the transient stability of the network. The ASCC has been applied to reduce the fault current in the presence of a transformer rating of 100 megavolt-amperes to a level of normal current when a 45-megavolt-ampere transformer is used [9]. Although the protective coordination of the main relay has been considered [9], there seems to be no study of the protective coordination of both the main and backup OCRs. Thus, the main aim of this work is to analyse the protective coordination of the main and backup OCRs with adjustment of both the ASCC and OCR parameters to obtain a state of ASCC setting that can achieve simultaneously its most current-limiting capability and protective coordination.

NOTATIONS

L_1, M_S : Self- and mutual-inductances of ASCC
U_A, I_A : Superconducting transformer phase-A primary voltage and current in a transmission system
U_a, I_a : Superconducting transformer phase-A secondary voltage and current in a transmission system.
U_{SA} : Voltage source of phase A
Z_1, Z_2 : Line and load impedances
$I_{Af\text{-}withASCC}$, $I_{Af\text{-}noASCC}$: Fault current with and without ASCC
$I_{Af\text{-}1}$, $I_{Af\text{-}2}$, $I_{Af\text{-}3}$: Fault current in modes 1, 2 and 3
$Z_{ASCC\text{-}1}$, $Z_{ASCC\text{-}2}$, $Z_{ASCC\text{-}3}$: Limiting impedance of ASCC in modes 1, 2 and 3
K : Coefficient constant
$Z_{ASCC\text{-}F}$, $Z_{ASCC\text{-}N}$: Limiting impedance of ASCC in fault and normal states
Z_T^1, Z_T^2, Z_T^0 : Equivalent impedance of positive, negative and zero sequences
Z_{ASCC}^1, Z_{ASCC}^2, Z_{ASCC}^0 : ASCC impedance of positive, negative and zero sequences
C_1, C_2 : Split DC link capacitors
L_d , C_d : Filtering inductance and capacitor
i_d, i_q, i_0 : Instantaneous system current in synchronous reference frame
$i_{d\text{-}ref}$, $i_{q\text{-}ref}$, $i_{0\text{-}ref}$: Steady-state system current in synchronous reference frame
Δi : Amplitude of error between the instantaneous and steady-state current
A, B, P : Constants of a relay
TD : Time Dial of OCR
M : Multiple of current
I_{input}, I_p : Fault current and pickup current of OCR
ω : Angular frequency of source voltage
j : Index of imaginary numbers, which is equal to the square root of -1

CONFIGURATION AND MODELLING

Structure and Principle of ASCC

The ASCC structure for a typical three-phase circuit (Figure 1) consists of three superconducting transformers and one three-phase pulse-width-modulation (PWM) converter. In the normal state, the limiting impedance of the ASCC is adjusted to zero, but in the fault conditions it is increased through controlling the output current of the converter. Consequently, the fault current is limited to different levels [10-13].

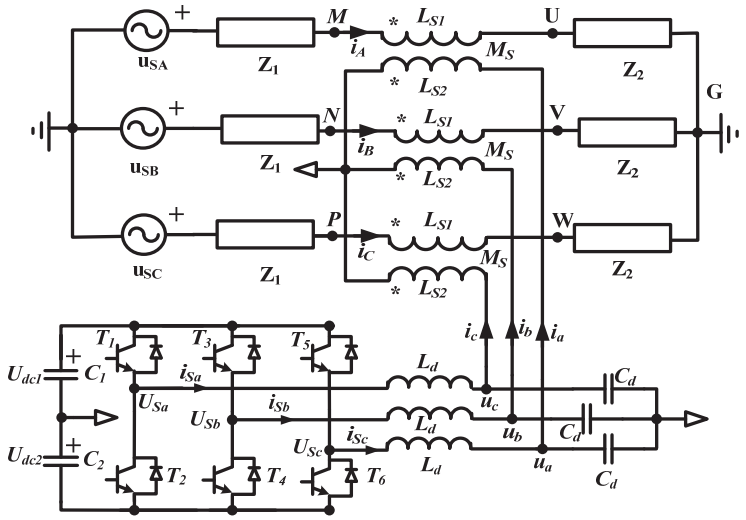

Figure 1. Structure of a three-phase ASCC

In this paper, phase A shown in Figure 1 is studied for the sake of simplicity of modeling, and the other two phases can be analysed in the same way. The primary voltage of the superconducting transformer is expressed as follows [6, 11-13].

$$U_A = j\omega L_{S1} I_A - j\omega M_S I_a \tag{1}$$

where L_{S1} is defined as:

$$L_{S1} = L_1 + M_S \tag{2}$$

In the normal state, I_a should be adjusted as:

$$I_a = \frac{L_{S1}}{M_S} I_A = \frac{L_{S1}}{M_S}\left(\frac{U_{SA}}{Z_1 + Z_2}\right) \tag{3}$$

When a fault occurs, the fault current without ASCC and with ASCC is defined as:

$$I_{Af-noASCC} = \frac{U_{SA}}{Z_1} \tag{4}$$

$$I_{Af-withASCC} = \frac{U_{SA} + j\omega M_S I_a}{Z_1 + j\omega L_{S1}} \tag{5}$$

In addition, the limiting impedance of ASCC (Z_{ASCC}) is defined as:

$$Z_{ASCC} = \frac{U_{Af}}{I_{Af}} = j\omega L_{S1} - \frac{j\omega M_S I_a (Z_1 + j\omega L_{S1})}{U_{SA} + j\omega M_S I_a} \tag{6}$$

Based on (5), three different modes are defined for the operation of ASCC [6-8]:

Mode 1: I_a is kept at the original setting, and

$$I_{Af-1} = \frac{U_{SA} + j\omega L_{S1} I_A}{Z_1 + j\omega L_{S1}} \tag{7}$$

$$Z_{ASCC-1} = \frac{Z_2(j\omega L_{S1})}{Z_1 + Z_2 + j\omega L_{S1}} \tag{8}$$

Mode 2: The amplitude of I_a is set at zero, and

$$I_{Af-2} = \frac{U_{SA}}{Z_1 + j\omega L_{S1}} \tag{9}$$

$$Z_{ASCC-2} = j\omega L_{S1} \tag{10}$$

Mode 3: I_a is adjusted so that the measured angle between u_{SA} and $j\omega M_s I_a$ is equal to 180°, and this is obtained by setting $j\omega M_s i_{2a} = -Ku_{SA}$. In this mode, the limiting impedance is defined as:

$$I_{Af-3} = \frac{U_{SA} - \omega M_S |I_a|}{Z_1 + j\omega L_{S1}} \tag{11}$$

$$Z_{ASCC-3} = \frac{K}{1-K} Z_1 + \frac{1}{1-K} j\omega L_{S1} \tag{12}$$

In order to investigate the ASCC performance for asymmetric faults, it is assumed that a phase-A-to-ground fault occurs. The limiting impedance of phase A is therefore adjusted to the fault state impedance of modes 1, 2 and 3, and the limiting impedance for other phases is kept at its normal state. The voltage and current equations are thus expressed as:

$$V^{abc} = Z^{abc} I^{abc} \tag{13}$$

where

$$Z^{abc} = \begin{bmatrix} Z_{ASCC-F} & 0 & 0 \\ 0 & Z_{ASCC-N} & 0 \\ 0 & 0 & Z_{ASCC-N} \end{bmatrix}.$$

The zero-, positive- and negative-sequence components of phase A are obtained as:

$$Z^{012} = \frac{1}{3}\begin{bmatrix} 1 & 1 & 1 \\ 1 & a & a^2 \\ 1 & a^2 & a \end{bmatrix}\begin{bmatrix} Z_{ASCC-F} & 0 & 0 \\ 0 & Z_{ASCC-N} & 0 \\ 0 & 0 & Z_{ASCC-N} \end{bmatrix}\begin{bmatrix} 1 & 1 & 1 \\ 1 & a^2 & a \\ 1 & a & a^2 \end{bmatrix} \tag{14}$$

where $a = 1\angle 120°$, $a^2 = 1\angle 240°$.

If a single-phase fault occurs, the fault current of positive, negative and zero sequences will be equal, and they are calculated as:

$$I_F^0 = I_F^1 = I_F^2 = \left(\frac{U_{SA}}{Z_T^1 + Z_T^2 + Z_T^0 + 3Z_f}\right) \tag{15}$$

In (15), Z_T^1, Z_T^2 and Z_T^0 are the equivalent impedance of positive, negative and zero sequences, which are defined as:

$$\begin{cases} Z_T^1 = Z_S + Z_{Tr} + Z_{ASCC}^1 \\ Z_T^2 = Z_S + Z_{Tr} + Z_{ASCC}^2 \\ Z_T^0 = Z_S + Z_{Tr} + Z_{ASCC}^0 \end{cases} \quad (16)$$

The fault current of positive, negative and zero sequences (I^1_F, I^2_F and I^0_F) for two-phase and two-phase-to-ground faults are obtained by (17) and (18) respectively:

$$\begin{cases} I_F^0 = 0 \\ I_F^1 = -I_F^2 = \left(\dfrac{\dot{U}_{SA}}{Z_T^1 + Z_T^2 + Z_f} \right) \end{cases} \quad (17)$$

$$\begin{cases} I_F^0 = 0 \\ I_F^1 = -I_F^2 = \left(\dfrac{\dot{U}_{SA}}{Z_T^1 + \dfrac{Z_T^2 \left(Z_T^0 + aZ_f \right)}{Z_T^2 + Z_T^0 + aZ_f}} \right) \end{cases} \quad (18)$$

Control Strategy for Fault Detection and Voltage Source Converter

The control strategy for fault detection is illustrated in Figure 2. For the sake of simplicity of the design, the currents are expressed in the synchronous reference frame. In order to detect the normal and fault conditions, instantaneous currents (i_d, i_q and i_0) and steady-state currents ($i_{d\text{-}ref}$, $i_{q\text{-}ref}$ and $i_{0\text{-}ref}$) are compared. If $\Delta i > \Delta i_{threshold}$, a fault occurs, and the ASCC provides the required compensating voltage to control the fault current level [1].

In addition, the control system diagram of a three-phase converter is shown in Figure 3. The reference current signals ($i_{abc\text{-}ref}$) are determined based on the operating state of the main circuit and the current-limiting mode of the ASCC. Consequently, the reference currents and voltages are calculated. Finally, the voltage reference signals of the converter can be obtained by *dq0-abc* transformation [11].

Distribution System

In a number of research work [14-17], the system used by the Korea Electric Power Corporation was chosen for investigation in the presence of superconducting fault current limiters since it contains both main and backup protections. So this system is selected here as the case study. The ASCC employed in this system is depicted in Figure 4. R_1-R_5 are OCRs that protect the related feeders of the distributed system, and R_6 is used not only as the main protection for the transformer, but also as the backup protection for R_1 - R_5. In turn, R_7 is employed as the backup protection for R_6. The parameters of the distribution system, along with the initial settings of the OCRs, are shown in Table 1 [16].

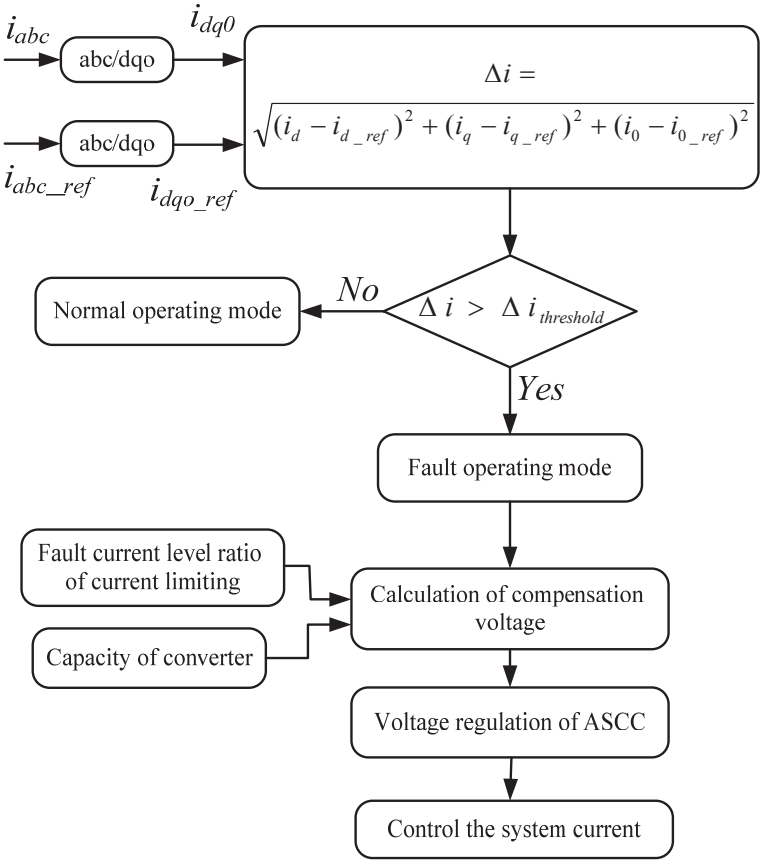

Figure 2. Control strategy for fault detection

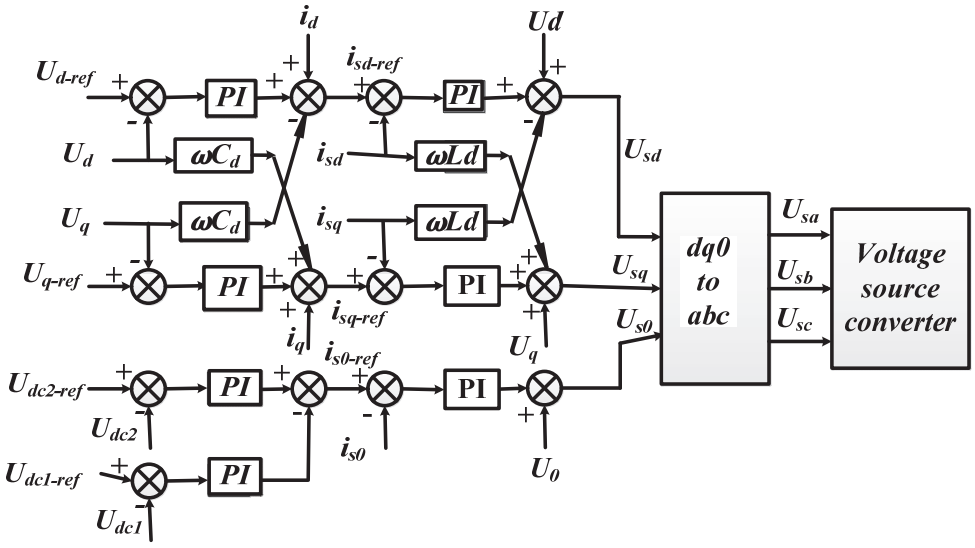

Figure 3. Control strategy for a three-phase pulse-width-modulation converter

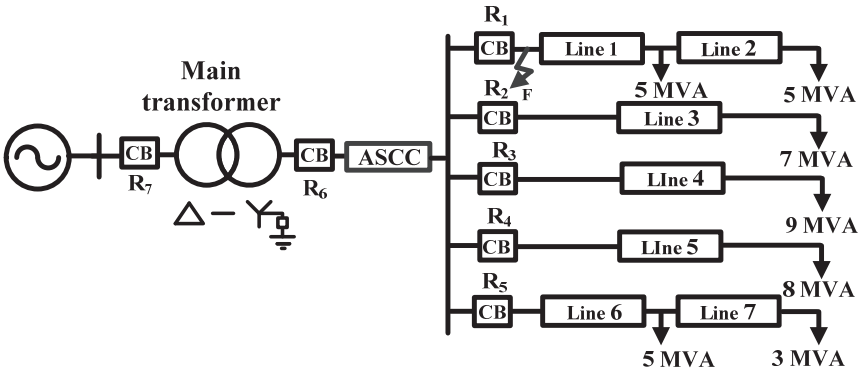

Figure 4. Schematic configuration of the distribution system

Table 1. Detailed specifications of distribution system and OCR

Configuration components	Specification
Source	154 (KV) , 1.75%
Transformer	154/22.9 (KV), 100 (MVA) , j 20(%)
Distribution line	Z_0=8.68+j22.86 (%) , (100MVA) Z_1=Z_2 =3.48+j7.44 (%) , (100MVA)
Loads	Feeder1: 10 (MVA) , pf=0.95 Lag Feeder2: 7(MVA) , pf=0.95 Lag Feeder3: 9 (MVA) , pf=0.95 Lag Feeder4: 8 (MVA) , pf=0.95 Lag Feeder5: 8 (MVA) , pf=0.95 Lag
OCR	Load current: 1.13 (KA_{rms}) Full load current: 1.51 (KA_{rms}) Pick-up current of time delay operation: 2.1 (KA_{rms}) Level: 1
	Parameters of very-inverse-type OCR: *A*=3.88, *B*=0.0963, *P*=2, *TD*=0.4
Superconducting FCL parameters	L_{s1}=L_{s2}=5 (mH), M_s=4 (mH)

Modelling of OCR

For the modelling purpose, the operational equations of OCR are obtained as follows [16]:

$$Time_{trip} = (\frac{A}{M^P - 1} + B) * TD \quad (19)$$

$$M = \frac{I_{input}}{I_{pickup}} \quad (20)$$

where *A*, *B* and *P* are determined based on the type of relays. According to (20), I_{input} is equal to the fault current and I_{pickup} is one of the setting parameters of OCR. *TD* is another setting parameter of OCR. By adjusting *TD* and I_{pickup} through analysis of the time-current curve, the protective coordination of ASCC with OCR is obtained for different current limiting modes. According to (7) - (11), the operational equations of OCR without ASCC and in the presence of ASCC are obtained as follows:

$$\begin{cases} (Time_{trip})_{WITHOUT-ASCC} = (\dfrac{A}{(\dfrac{U_{SA}}{Z_1 I_{pick-up}})^P - 1} + B) * TD \\ (Time_{trip})_{ASCC-1} = (\dfrac{A}{(\dfrac{U_{SA} + j\omega L_{S1} I_A}{(Z_1 + j\omega L_{S1}) I_{pick-up}})^P - 1} + B) * TD \\ (Time_{trip})_{ASCC-2} = (\dfrac{A}{(\dfrac{U_{SA}}{(Z_1 + j\omega L_{S1}) I_{pick-up}})^P - 1} + B) * TD \\ (Time_{trip})_{ASCC-3} = (\dfrac{A}{(\dfrac{U_{SA} - \omega M_S |I_a|}{(Z_1 + j\omega L_{S1}) I_{pick-up}})^P - 1} + B) * TD \end{cases} \quad (21)$$

Equations (21) show that reducing the fault current increases the trip time of OCR so that ASSC with mode 3 provides the largest trip time of OCR (i.e. $(Time_{trip})_{ASCC-3} > (Time_{trip})_{ASCC-2} > (Time_{trip})_{ASCC-1}$). This increase in the relay operation may therefore deteriorate the transient stability. For this reason, the protective coordination between ASCC and OCR for the whole modes of ASCC is inevitable, and this is performed through the setting of OCR parameters.

SIMULATIONS AND RESULTS

In order to evaluate the effect of different modes of ASCC on current limiting, a simulation of the three-phase circuit shown in Figure 1 was performed. In addition, to study the protective coordination of the main and backup relays by considering all different modes of ASCC, a simulation of the distribution system depicted in Figure 4 was also carried out.

Current Limiting Test

To assess the performance of the three aforementioned modes of ASCC on current limiting, the model shown in Figure 1 with parameters as in Table 2 was simulated in MATLAB. In order to evaluate and compare the effects of different modes of ASCC on current limiting, the fault current waveforms with and without ASCC are compared (Figure 5), which shows that ASCC can reduce the fault current as expected. In addition, by adjusting the phase angle of output current of the converter to 90° (i. e. mode 3), the maximum effect of fault-current limiting is obtained.

Table 2. Parameters of simulated system

Parameter	Value
$[U_{SA}, U_{dc}]$	[220,600] (V)
Z_1	0.19 + 2.16 i (Ω)
Z_2	15 + 2 i (Ω)
F	50 (Hz)
$Ls_1=Ls_2$	10 (mH)
$[M_s, L_f]$	[9, 6] (mH)
$C_1=C_2$	2000 (μF)
C_f	30 (μF)

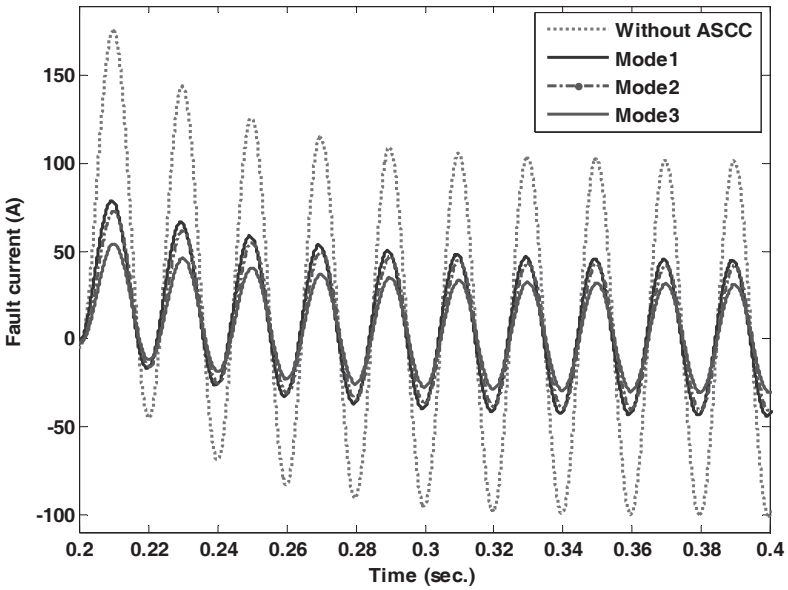

Figure 5. Comparison of fault current characteristics

By supposing the operation of ASCC in mode 3, the voltage and current reference signals of the converter under different conditions, viz. normal state, three-phase fault and single-phase fault, are shown in Figure 6. Figure 6a shows the reference currents of the normal state. The reference current of phase A can be obtained based on equation (3), and reference currents of the other phases (B and C) are the same as that of phase A due to symmetrical conditions ($I_{a\text{-}ref}$=15.7□-15.3°, $I_{b\text{-}ref}$= 15.7□-135.3° and $I_{c\text{-}ref}$=15.7□104.3°). In Figure 6b, the reference current of phase A is 15.7□ 90° since the ASCC operates in mode 3. Consequently, due to a symmetrical fault, $I_{b\text{-}ref}$ and $I_{c\text{-}ref}$ are equal to 15.7□-30° and 15.7□-150° respectively. In Figure 6c, as a result of the operation of ASCC in mode 3, the current of phase A is 15.7□ 90°, and because of an unsymmetrical fault, $I_{b\text{-}ref}$ = 15.7□-135.3° and $I_{c\text{-}ref}$=15.7□104.3° are obtained similar to the normal state. In addition, when the single-phase fault occurs, the AC components of DC link voltage of the converter (U_{dc1} and U_{dc2}) are opposite to each other, and the total DC voltage is kept at the level of 600 V.

Figure 7 depicts the current and voltage waveforms of the superconducting transformer in the presence of the ASCC. Interval t = 0.2-0.23 sec. is the time for detecting the fault for the operation of the converter, and the line current is reduced to 44.38 A since the ASCC operates in mode 1. Similarly, from t = 0.23 sec. to 0.4 sec., by setting the phase angle of compensating current (I_a) to 90°, defined as mode 3, the fault current is reduced to 30.76 A. It is notable that when a fault occurs, the fault current is suddenly reduced to a suitable level when the ASCC with its original setting operates in mode 1. After fault detection, based on the converter's control strategy, the ASCC operates in mode 3, causing the maximum effect on current limiting. In other words, the operating modes of the ASCC are selected based on the reference signals.

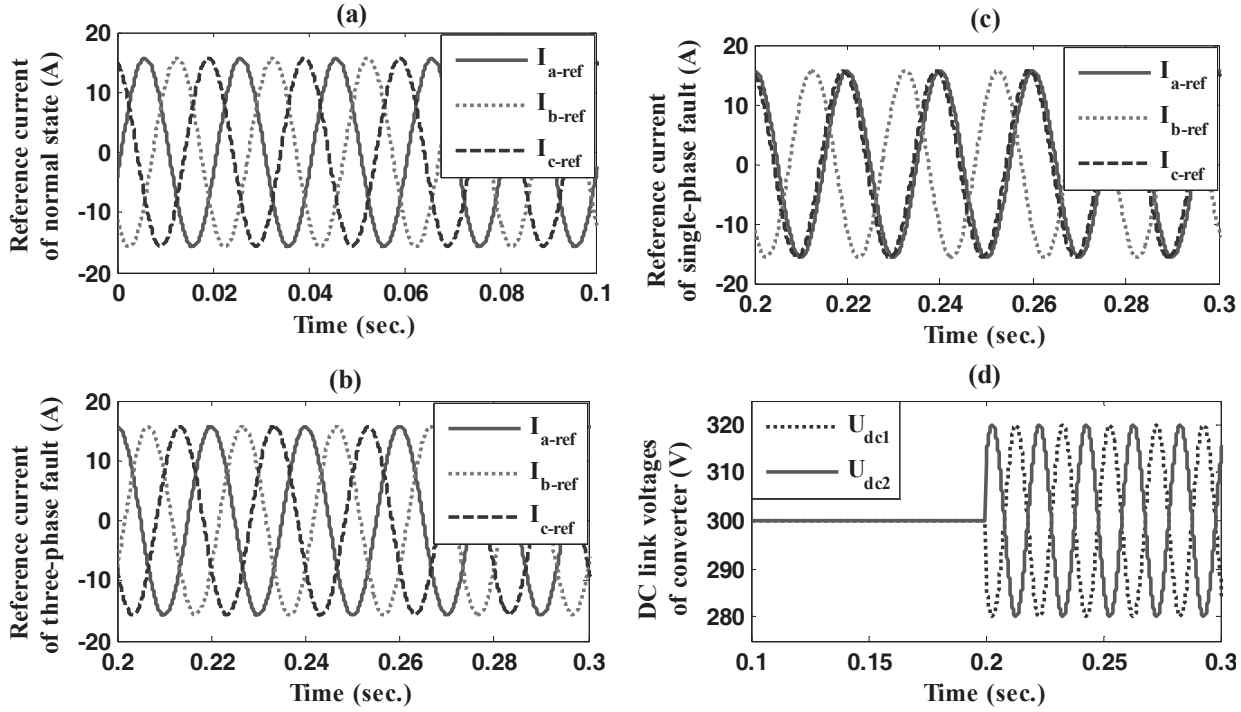

Figure 6. Reference current of normal state (a), three-phase fault (b) and single-phase fault (c), and dc link voltage of converter for single-phase fault (d)

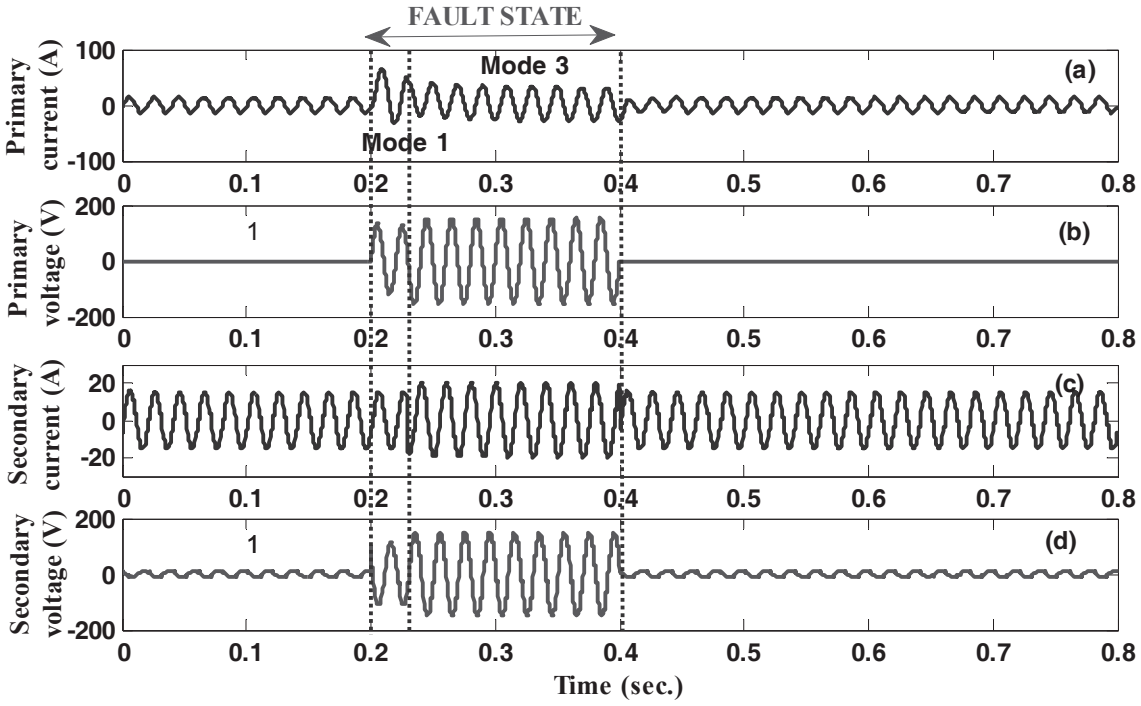

Figure 7. Waveforms of superconducting transformer: (a) primary current (I_A); (b) primary voltage (U_A); (c) secondary current (I_a); (d) secondary voltage (u_a)

Operation of OCRs

In the first state, the operation of one relay (R_6) was investigated and its appropriate setting parameters for the protective coordination in the whole modes of ASCC were calculated. Then the protective coordination of the whole relays, illustrated in Figure 4, was evaluated. For different

operating modes of ASCC, the time-current curve of the OCR is shown in Figure 8. To meet the protective coordination in modes 1 and 2, the modification of *TD* value from '0.5' to '0.1' is inevitable. The operation times of OCR in this case are reduced to 0.27 sec. and 0.3 sec. respectively. When the ASCC operates in mode 3 and *TD* is equal to '0.1', the operation time of OCR is 0.57 sec. and thus, in this mode adjusting the other setting parameter of OCR (I_{pickup}) is necessary. According to Figure 8d, when the *TD* value of OCR changes from '0.5' to '0.1' and I_{pickup} is also modified from '2.1' to '1.9', the protective coordination in three operation modes is performed. Based on equation (5), in mode 3, when the amplitude of output current of the converter is increased, the current limiting further decreases, and consequently the protective coordination cannot be achieved even by adjusting the OCR parameters to their minimum values.

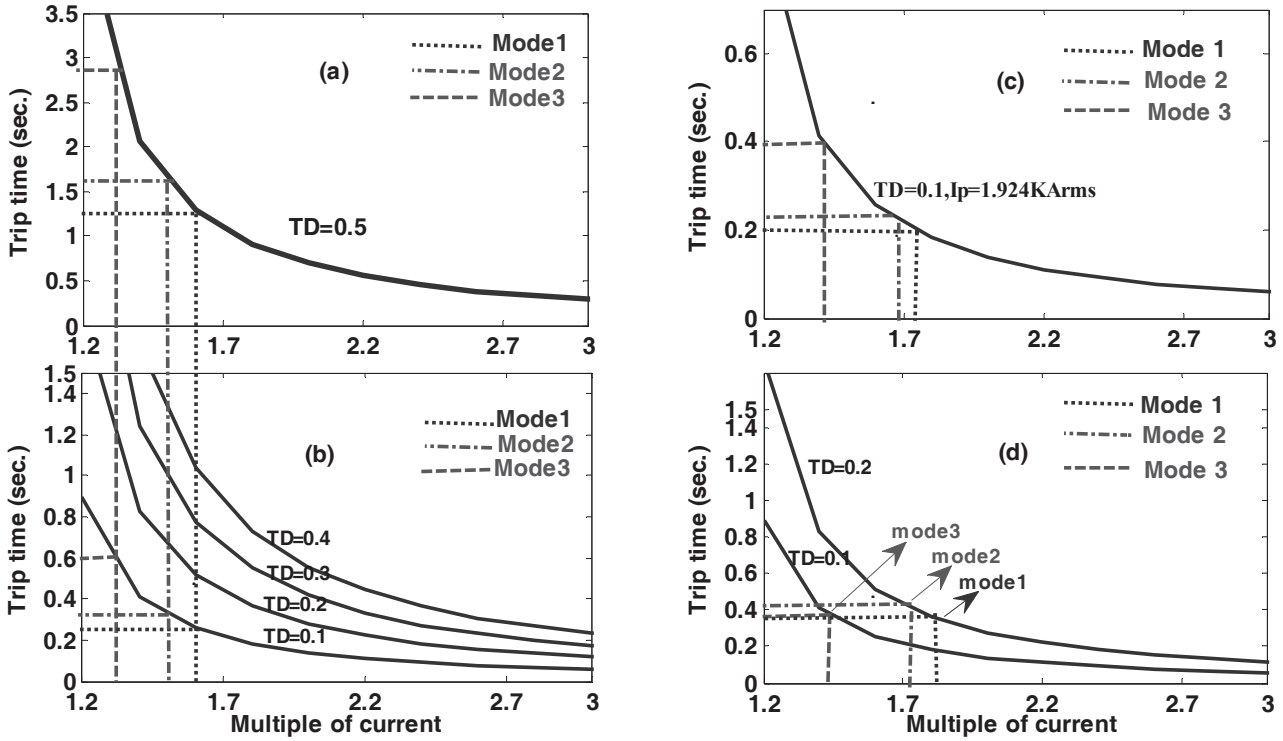

Figure 8. Time-current curve of OCR operation for the protective coordination with ASCC operation: (a) original settings of OCR; (b) Coordination with modified *TD*; (c) Coordination by modifying both *TD* and I_p for mode 3; (d) Coordination by modifying both *TD* and I_p for modes 1-3

In the second state, to study the protective coordination of the whole OCRs, simulations consisting of 27 cases of coordination (nine protective states and three modes of ASCC) were considered. The values of rated current (I_n), short-circuit current (I_{SC}), current transformer ratio and tap setting of relays as the initial setting of OCRs are tabulated in Table 3. The instantaneous relays were set based on 50% of the short-circuit current at point *F* (Figure 4). R_7 was also set based on 1.25 I_{SC} when the fault occurred in location R_6. It should be noted that R_6 is the backup protection for R_1 - R_5 and R_7 is the backup for R_6.

Figure 9 shows the time-current curves of R_1-R_5 with different values of *TD* when the ASCC operates in mode 1. The multiple currents of R_1-R_5 are shown in Table 4. Based on Figure 9, in order to meet the protective coordination of R_1 to R_5 for mode 1, the modification of *TD* value from '0.5' to '0.4' (for R_2-R_5) and to '0.3' (for R_1) is needed. Figure 10 shows time-current curves of the main and backup protection of R_6 and R_7 in mode 1 of ASCC. To perform the protective

coordination of R_6 and R_7 in mode 1, the modification of their *TD* values to '0.1' and '0.5' respectively is needed. Table 5 lists the modified values of setting parameters of R_6 and R_7 in the three operation modes of ASCC.

Table 3. Values of OCR parameters

Circuit breaker	I_n (A)	I_{sc} (A)	Current transformer ratio	Tap setting of relay
1	252.11	12560	700/5	3
2	176.48	12560	700/5	2
3	226.9	12560	700/5	3
4	201.69	12560	700/5	3
5	201.69	12560	700/5	3
6	1058.87	12560	1100/5	8
7	157.46	21240	1100/5	1

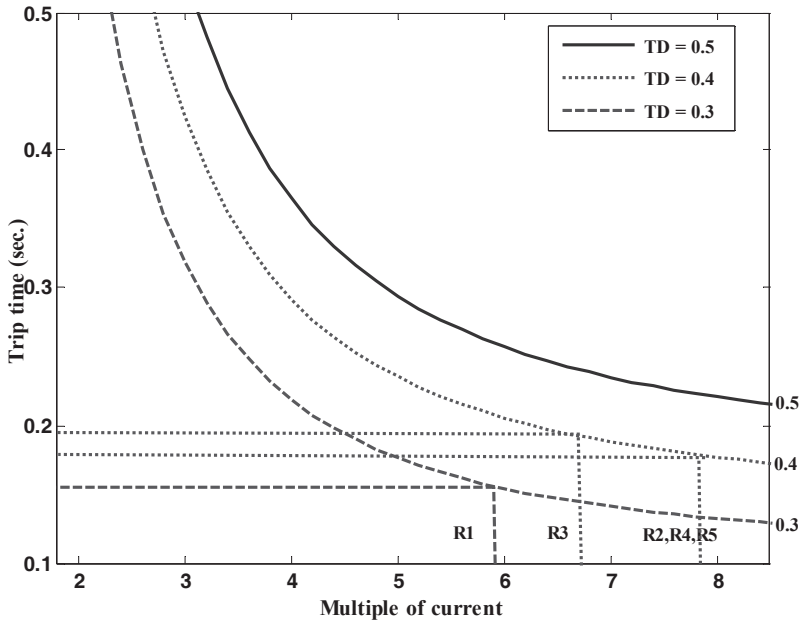

Figure 9. Time-current curves of R_1-R_5 in the case that *TD* is adjusted to meet the coordination in mode 1

According to Tables 4 and 5, if the modifications of *TD* value from '0.5' to '0.3' for R_1 and R_3 and from '0.5' to '0.4' for R_2, R_4 and R_5 are carried out, the protective coordination in mode 2 is achieved. In addition, the coordination of R_6 and R_7 in mode 2 is similar to that in mode 1. Similarly, when the ASCC operates in mode 3, the modification of *TD* value from '0.5' to '0.3' for R_1-R_5 is needed. By the same token, for the coordination of R_6 in mode 3, both setting parameters (*TD* and tap setting) need to be modified. Again, based on Table 5, the modifications of *TD* from '0.7' to '0.1' and also of the tap setting of relay from '7' to '6' are required for R_6. Finally, with the modification of *TD* from '1.7' to '0.4', the coordination of R_7 is done in mode 3.

Table 4. Setting parameters of R_1-R_5 in different modes

			R_1	R_2	R_3	R_4	R_5
Mode1	Without correction	Multiple of current	5.57	7.83	6.71	7.83	7.83
		Trip time (sec.)	0.27	0.22	0.24	0.22	0.22
	With correction	*TD* (sec.)	0.3	0.4	0.4	0.4	0.4
		Trip time (sec.)	0.16	0.18	0.19	0.18	0.18
Mode2	Without correction	Multiple of current	5.43	7.67	5.57	7.67	7.67
		Trip time (sec.)	0.27	0.23	0.27	0.23	0.23
	With correction	*TD* (sec.)	0.3	0.4	0.3	0.4	0.4
		Trip time (sec.)	0.16	0.18	0.16	0.18	0.18
Mode3	Without correction	Multiple of current	4.71	7	5.57	6.5	6.5
		Trip time (sec.)	0.31	0.24	0.27	0.24	0.24
	With correction	*TD* (sec.)	0.3	0.3	0.3	0.3	0.3
		Trip time (sec.)	0.18	0.14	0.16	0.15	0.15

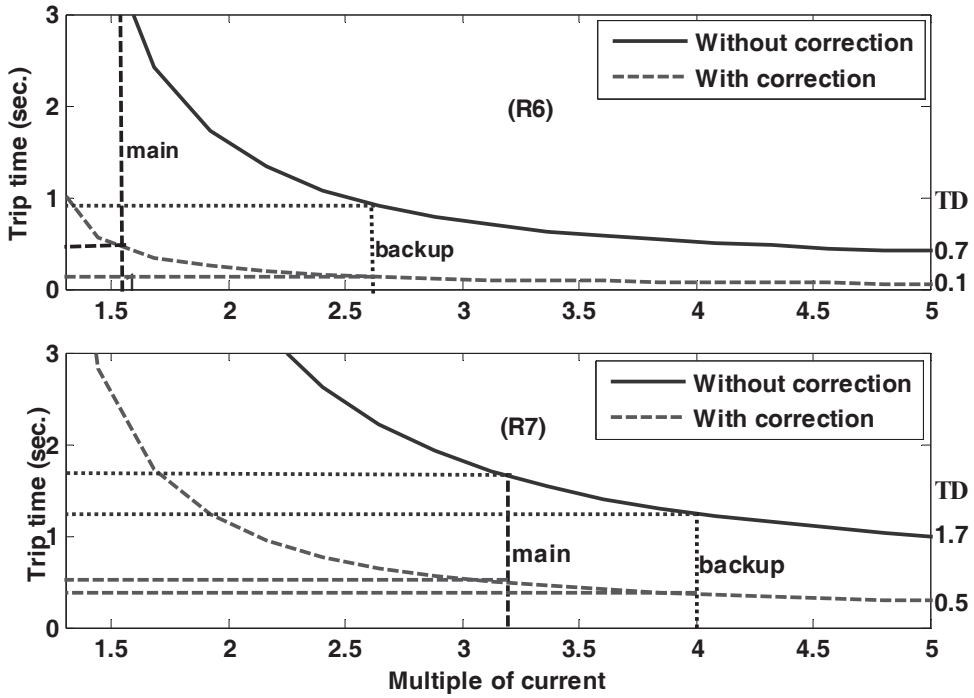

Figure 10. Time-current curves of R_6 and R_7 to meet the coordination of main and backup protection in mode 1

Table 5. Setting parameters of R_6 and R_7 in different modes

		Tap setting of relay	TD	Multiple of current as backup protection	Trip time as backup protection (sec.)	Multiple of current as main protection	Trip time as main protection (sec.)
Mode 1	R_6	7	0.1	1.55	0.59	2.61	0.13
	R_7	1	0.5	3.2	0.53	4	0.36
Mode 2	R_6	7	0.1	1.5	0.58	2.25	0.14
	R_7	1	0.5	3.04	0.54	4	0.36
Mode 3	R_6	6	0.1	1.48	0.58	2.5	0.14
	R_7	1	0.4	2.6	0.54	4	0.3

CONCLUSIONS

When an ASCC was tested through simulations in a typical three-phase circuit to evaluate its effect on fault current limiting, simulation results confirmed the appropriate performance of different operation modes and control strategy of the ASCC. In other words, this study shows that by adjusting the ASCC in different operating modes, the setting parameters of OCRs are modified to obtain the protective coordination. Also, simulation results confirmed that for mode 3, when the amplitude of output current of the converter is increased, the current limiting further decreases. Although ASCC is more effective for current limiting in this case than the other cases, the protective coordination may deteriorate because of an excessive reduction in current even when the OCR parameters are adjusted to their minimum values. Therefore, this limitation should be considered in an ASCC setting.

REFERENCES

1. J. Wang, L. Zhou, J. Shi and Y. Tang, "Experimental investigation of an active superconducting current controller", *IEEE Trans. Appl. Superconduct*., **2011**, *21*, 1258-1262.
2. K. Kajikawa, K. Kaiho, N. Tamada and T. Onishi, "Magnetic-shield type superconducting fault current limiter with high Tc superconductors", *Elec. Eng. Jap*., **1995**, *115*, 104-111.
3. I. Shimizu, Y. Naito, I. Yamaguchi, K. Kaiho and S. Yanabu, "Application study of a high-temperature superconducting fault current limiter for electric power system", *Elec. Eng. Jap*., **2006**, *155*, 20-29.
4. Y. Xin, W. Z. Gong, X. Y. Niu, Y. Q. Gao, Q. Q. Guo, L. X. Xiao, Z. J. Cao, H. Hong, A. G. Wu, Z. H. Li, X. M. Hu, B. Tian, J. Y. Zhang, Y. He, Y. Wang, J. Cui, S. Z. Ding, J. Z. Wang, A. L Ren and F. Ye, "Manufacturing and test of a 35 kV/90 MVA saturated iron-core type superconductive fault current limiter for live-grid operation", *IEEE Trans. Appl. Superconduct*., **2009**, *19*, 1934-1937.
5. M. Endo, T. Koyama, Y. Takahashi, K. Kaiho and S. Yanabu, "Study of shunt type SFCL equipped with electromagnetic repulsion switch for large capacity" *Elec. Eng. Jap.*, **2010,** *173*, 20-27.
6. L. Chen, Y. J. Tang, J. Shi and Z. Sun, "Simulations and experimental analyses of the active superconducting fault current limiter", *Physica. C. Superconduct.*, **2007**, *459*, 27-32.
7. J. Shi, Y. Tang, L. Chen, J. Wang, L. Ren, J. Li, L. Li, T. Peng and S. Cheng, "The application of active superconducting DC fault current limiter in hybrid AC/DC power supply systems", *IEEE Trans. Appl. Superconduct*., **2008**, *18*, 672-675.
8. J. Shi, Y. Tang, C. Wang, Y. Zhou, J. Li, L. Ren and S. Chen, "Active superconducting DC fault current limiter based on flux compensation", *Physica. C. Superconduct.*, **2006**, *442*, 108-112.
9. A. Ghafari, M. Razaz and S. G. Seifossadat, "Optimum coordination of overcurrent relays with active superconducting current controller in distribution systems", *J. World. Elec. Eng. Technol*., **2013**, *2*, 37-43.
10. M. Song, Y. Tang, Y. Zhou, L. Ren, L. Chen and S. Cheng, "Electromagnetic characteristics analysis of air-core transformer used in voltage compensation type active SFCL", *IEEE Trans. Appl. Superconduct*., **2010**, *20*, 1194-1198.

11. L. Chen, Y. Tang, J. Shi, Z. Li, L. Ren and S. Cheng, "Control strategy for three-phase four-wire PWM converter of integrated compensation type active SFCL", *Physica. C. Superconduct.*, **2010**, *470*, 231-235.
12. L. Chen, Y. J. Tang, J. Shi, N. Chen, M. Song, S. J. Cheng, Y. Hu and X. S. Chen, "Influence of a voltage compensation type active superconducting fault current limiter on the transient stability of power system", *Physica. C. Superconduct.*, **2009**, *469*, 1760-1764.
13. L. Chen, Y. J. Tang, J. Shi, L. Ren, M. Song, S. J. Cheng, Y. Hu and X. S. Chen, "Effects of a voltage compensation type active superconducting fault current limiter on distance relay protection", *Physica. C.Superconduct.*, **2010**, *470*, 1662-1665.
14. J. S. Kim, S. H. Lim and J. C. Kim, "Study on application method of superconducting fault current limiter for protection coordination of protective devices in a power distribution system", *IEEE Trans. Appl. Superconduct*., **2012**, *22*, 2154-2159.
15. S. H. Lim, J. S. Kim and J. C. Kim, "Analysis on protection coordination of hybrid SFCL with protective devices in a power distribution system", *IEEE Trans. Appl. Superconduct.*, **2011**, *21*, 2170-2173.
16. J. S. Kim, J. F. Moon, S. H. Lim and J. C. Kim, "Study on selection of SFCLs impedance for protective coordination with overcurrent relay in a distribution system", Proceedings of Transmission and Distribution Conference and Exposition: Asia and Pacific, **2009**, Seoul, South Korea, pp.1-4.
17. J. S. Kim, S. H. Lim and J. C. Kim, "Study on protective coordination for application of superconducting fault current limiter", *IEEE Trans. Appl. Superconduct*., **2011**, *21*, 2174-2178.

Maejo Int. J. Sci. Technol. **2014**, *8*(03), 334-347

Maejo International Journal of Science and Technology

ISSN 1905-7873
Available online at www.mijst.mju.ac.th

Full Paper

Conceptual design of heterogeneous azeotropic distillation process for ethanol dehydration using 1-butanol as entrainer

Paritta Prayoonyong

Department of Chemical Engineering, Faculty of Engineering, Mahidol University, 25/25 Puttamonthon 4 Road, Puttamonthon, Nakornpathom 73170, Thailand

E-mail: paritta.pra@mahidol.ac.th

Received: 2 May 2013 / Accepted: 15 December 2014 / Published: 24 December 2014

Abstract: The synthesis of a heterogeneous azeotropic distillation process for ethanol dehydration using 1-butanol as entrainer is presented. The residue curve map of the ethanol/water/1-butanol mixture is computationally generated using non-random two-liquid thermodynamic model. It is found that 1-butanol leads to a residue curve map topological structure different from that generated by typical entrainers used in ethanol dehydration. Synthesised by residue curve map analysis, the distillation flowsheet for ethanol dehydration by 1-butanol comprises a double-feed column integrated with an overhead decanter and a simple column. The double-feed column is used to recover water as the top product, whereas the simple column is used for recovering ethanol and 1-butanol. The separation feasibility and the economically near-optimal designs of distillation columns in the flowsheet are evaluated and identified by using the boundary value design method. The distillation flowsheet using 1-butanol is compared with the conventional process using benzene as entrainer. Based on their total annualised costs, the ethanol dehydration process using 1-butanol is less economically attractive than the process using benzene. However, 1-butanol is less toxic than benzene.

Keywords: ethanol dehydration, heterogeneous azeotropic distillation, 1-butanol, entrainer

INTRODUCTION

Bioethanol derived from biomass is gaining significance as a biofuel. However, the process for recovering ethanol from the fermentation product is energy-intensive. Usually, the dilute ethanol-water mixture with an ethanol concentration about 5-12 wt% [1] is firstly dehydrated by an ordinary

distillation to a concentration close to the azeotrope. Then the ethanol mixture is further dehydrated to highly pure ethanol by a separation technique that can break the ethanol/water azeotrope. Conventional technologies, e.g. azeotropic distillation and adsorption, are continuously improved because a demand for anhydrous ethanol has been greatly increased.

The dehydration of ethanol can be accomplished in a heterogeneous azeotropic distillation process using a third component called entrainer that induces the immiscibility of two-liquid phases to facilitate the separation. The additional component alters the thermodynamic property of the original mixture. Examples of entrainers for ethanol dehydration are benzene [2, 3], cyclohexane [4], pentane [5], isooctane [6, 7] and hexane [8]. Most of the entrainers that have been explored were selected such that they form a binary homogeneous azeotrope with ethanol, a binary heterogeneous azeotrope with water and a ternary heterogeneous azeotrope. Thus, those entrainers have similar performance with respect to ethanol dehydration [9].

The similarity of those entrainers can be seen from the residue curve map of the mixture, which is a useful graphical tool for characterising azeotropic mixtures and designing distillation processes. Figure 1 illustrates a common residue curve map and vapour-liquid-liquid equilibrium for a mixture of ethanol, water and a typical entrainer. A residue curve is generally used as an approximation of the liquid composition profile for a staged column at total reflux [10, 11]. The presence of one ternary and three binary azeotropes in the mixture induces distillation boundaries that divide the residue curve map into three distillation regions. In each region, all residue curves start at the same starting point (unstable node) and end at the same ending point (stable node). In general, the products of a simple distillation column, which is a column with one feed and two products, are restricted to be in the same distillation region [10]. However, the immiscibility of two liquid phases may allow the products in different distillation regions to be recovered, as will be described as follows.

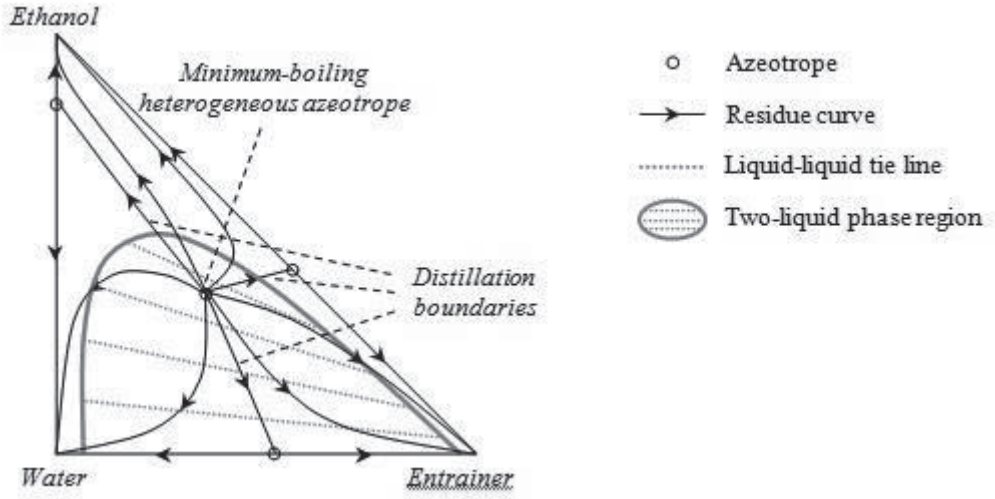

Figure 1. Vapour-liquid-liquid equilibrium and residue curve map of a ternary mixture of ethanol, water and a typical entrainer [9]

A typical heterogeneous azeotropic distillation process for ethanol dehydration using an entrainer, e.g. benzene and cyclohexane, is presented in Figure 2. The process consists of a distillation column with an integrated overhead decanter and a simple column. The ethanol/water azeotropic mixture and the entrainer are fed to the first column where highly pure ethanol is

recovered as a bottom product. At the top of the first column, the overhead vapour with a composition near the ternary minimum-boiling heterogeneous azeotrope is condensed and two liquid phases in equilibrium are formed in the decanter. The entrainer-rich phase is mixed with a part of the entrainer-lean phase before being refluxed back to the column. The entrainer-lean phase from the decanter is taken out as a top product. By using the column with an integrated decanter, the top and bottom products can be in different distillation regions. Subsequently, the top product from the first column is separated further in the simple column where highly pure water is obtained as the bottom product and the distillate is recycled to the first column.

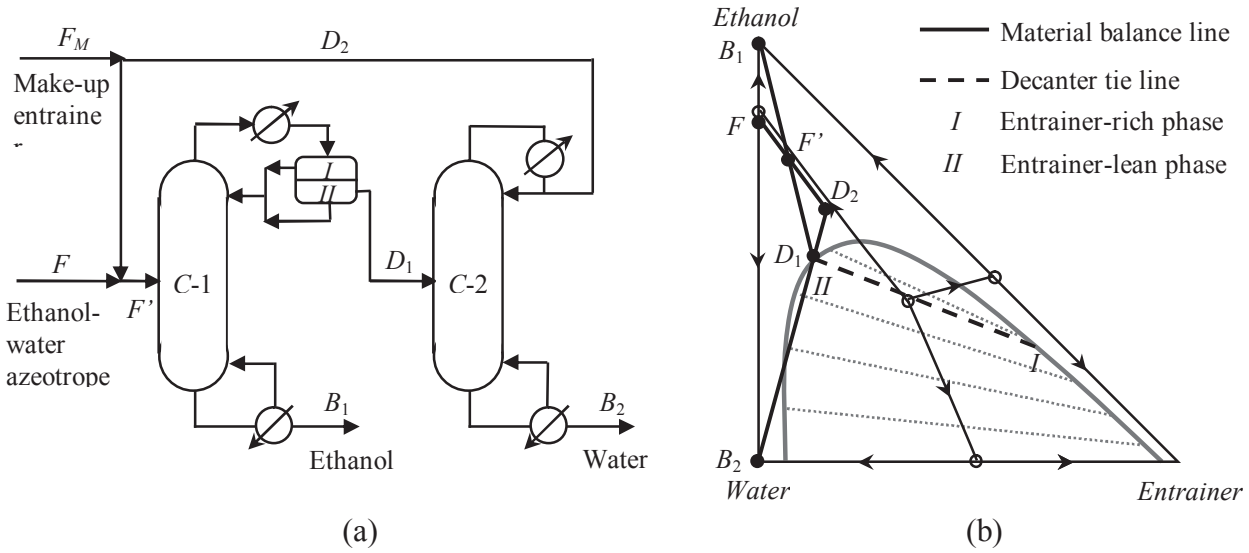

Figure 2. (a) Heterogeneous azeotropic distillation process for ethanol dehydration using a typical entrainer; (b) residue curve map showing material balance of the process [9]

In this study, the feasibility of using 1-butanol as an entrainer for the dehydration of ethanol is investigated. 1-Butanol is a biofuel that can be produced from the fermentation of biomass and it is less toxic than benzene. It is found in this work that the residue curve map of the ethanol/water/1-butanol mixture is very different from that of the mixture of ethanol, water and typical entrainers shown in Figure 1. 1-Butanol forms a heterogeneous azeotrope with water but does not form an azeotrope with ethanol. None of entrainers giving a residue curve map similar to that of ethanol/water/1-butanol mixture have been explored for ethanol dehydration.

This paper presents a synthesis of heterogeneous azeotropic distillation process using 1-butanol as entrainer for the dehydration of ethanol. The process is synthesised based on the residue curve map analysis. The distillation columns in the proposed process are assessed for their separation feasibilities and economic performance by using the boundary value method, which is a conceptual design method, developed by Prayoonyong and Jobson [12]. The proposed process using 1-butanol is compared in terms of total annualised costs with the conventional process utilising benzene as entrainer.

RESIDUE CURVE MAP OF ETHANOL/WATER/1-BUTANOL MIXTURE

A residue curve displays the change in the composition of the liquid remaining in a single stage batch distillation over a period of time. It can be used for representing an approximation of the

liquid composition profile of a staged column operating at total reflux. A residue curve can be calculated from the following differential equation [13]:

$$\frac{dx_i}{d\xi} = x_i - y_i \tag{1}$$

where x_i is the mole fraction of component i in the liquid, y_i is the mole fraction of component i in the vapour that is in equilibrium with the liquid, and ξ is dimensionless time.

The residue curve map and heterogeneous boiling envelope of the ethanol/water/1-butanol mixture at atmospheric pressure are shown in Figure 3. The residue curves generated from equation (1) and the two-liquid phase region were constructed using MATLAB [14] interfaced with Aspen HYSYS [15] from which the phase equilibrium of the mixture is obtained. The phase equilibrium was predicted using a non-random two-liquid (NRTL) model [15] for the liquid phase and the ideal gas law for the vapour phase. The NRTL interaction parameters from Aspen HYSYS [15] are shown in Table 1. Besides the binary homogeneous azeotrope of ethanol and water, the mixture has a binary heterogeneous azeotrope of water and 1-butanol, which are partially miscible. The residue curve map (Figure 3) is divided into two distillation regions. In region 2, all residue curves start from the ethanol/water azeotrope (unstable node *UN*) and end at the 1-butanol vertex (stable node *SN*2), but approach different saddle points. Distillation region 2 is thus divided further into two compartments. The residue curves in one compartment move towards and away from the water/1-butanol azeotrope (saddle point *S*1) while those in the other compartment approach ethanol (saddle point *S*2). The compartment boundary can be linearly approximated as shown by the dash line in Figure 3.

Table 1. NRTL interaction parameters (a_{ij} and α_{ij}) for ethanol/water/1-butanol mixture from Aspen HYSYS [15]. The interaction parameters b_{ij} are all zero.

Parameter	Component *i*	Component *j*		
		Ethanol	Water	1-Butanol
a_{ij}	Ethanol	-	1332.312	-32.941
	Water	-109.634	-	570.136
	1-Butanol	38.072	2794.666	-
α_{ij}	Ethanol	-	0.303	0.304
	Water	0.303	-	0.470
	1-Butanol	0.304	0.470	-

The NRTL-ideal gas model with the interaction parameters in Aspen HYSYS adequately predicts the phase equilibrium of the mixture. The predicted binary azeotropes agree well with those found from the experiments by Iwakabe and Kosuge [16]. The selected thermodynamic model also predicts well the compositions of vapour and two liquid phases corresponding to the heterogeneous azeotrope of water and 1-butanol, compared to the experimental results of Iwakabe and Kosuge [16]. However, the calculated two-liquid phase envelope is slightly different from the experimental data of Iwakabe and Kosuge [16] and Gomis et al. [17].

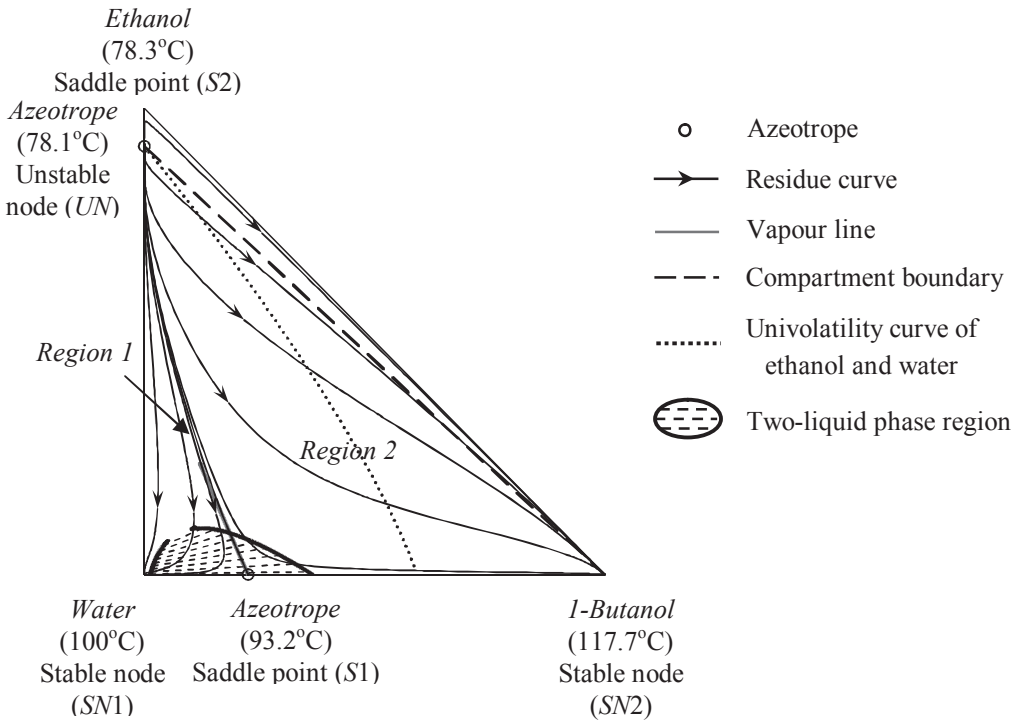

Figure 3. Residue curve map and heterogeneous boiling envelope of ethanol/water/1-butanol mixture at 101.3 kPa calculated using NRTL-ideal gas model in Aspen HYSYS [15]

DISTILLATION PROCESS SYNTHESIS

The feed to be separated consists of 89.4 mol% ethanol and 10.6 mol% water, which is a composition close to the azeotrope. The feed is a saturated liquid at 101.3 kPa and has a flow rate of 100 kmol h^{-1}. The distillation flowsheet for ethanol dehydration using 1-butanol as entrainer was synthesised based on the residue curve map and volatility-order diagram analysis. Only single- and double-feed columns integrated with overhead decanters were taken into account. The decanters were operated at the boiling point of heterogeneous liquid mixtures; operating the decanters at a sub-cool temperature was not considered. All separation units were operated at 101.3 kPa with no pressure drop.

As described in the previous section, distillation region 2 in the residue curve map of the ethanol/water/1-butanol mixture (Figure 3) has two non-adjacent saddle points (ethanol and the heterogeneous azeotrope of water and butanol) dividing the region into two compartments. Methods for identifying feasible products from a simple column in different distillation compartments (split crossing compartment boundary) have been developed [18, 19]. However, none of the methods lead to a feasible split employing a simple column to recover saddle-type products in different adjacent compartments. Generally, a pure component which is a saddle in a distillation region cannot be recovered from a simple column at high purity [20]. Typically, the separation to obtain saddle-type products in different compartments is performed in a double-feed column. A well-known example is the dehydration of ethanol using ethylene glycol as entrainer in a double-feed column in which ethanol (a saddle product) is recovered as a top product and a mixture of water and ethylene glycol is removed at the bottom [18, 21]. Subsequently, water (another saddle product) is separated from ethylene glycol using another simple column.

The residue curve map of ethanol/water/1-butanol mixture can be classified as Serafimov's class 2.0-2b [22]. For such topological structure of residue curve map, Moussa and Jiménez [21] proposed a heterogeneous extractive distillation flowsheet to recover two non-adjacent saddles as products. Their flowsheet involved using a double-feed column integrated with an overhead decanter to firstly recover one of the saddle products and using a simple column to recover another one. Moussa and Jiménez [21] assumed that the entrainer and the saddle component consist of similar chemical compounds with high affinity to each other. Thus, the heterogeneous azeotrope is firstly recovered from the double-feed column at the top as the entrainer and the saddle component flow together to the bottom of the double-feed column.

Either the saddle heterogeneous azeotrope or the saddle component to be recovered as the top product of the double-feed column can be evaluated from a univolatility curve, which is the curve showing the locus of points where the relative volatility of one component to that of the other equals unity [22]. The univolatility curve divides the residue curve map or distillation region into two regions. In one region, one component is more volatile than the other, whereas it is less volatile in the other region. For a homogeneous extractive distillation, the heavy entrainer will be a stable node in the residue curve map, whereas the two azeotropic components are saddle points. A univolatility curve of the azeotropic constituents can be generated starting from the azeotrope and ending on one of the other two edges of the residue curve map. Laroche et al. [23] found that the saddle component to be recovered as the top product of the double-feed column must lie on the edge that is intersected by the univolatility curve. This is deduced from the fact that this saddle component must be more volatile than the other saddle components in the middle and stripping sections, whereas it becomes less volatile at least at the top of the rectifying section. The intersection of the univolatility curve and an edge of the residue curve map indicates that the volatility order of the saddle components (two azeotropic components) changes along that edge, whereas there is no change in volatility order along the other edge. The method of Laroche et al. [23] is also valid for the case of heterogeneous extractive batch distillation [24].

For the ethanol/water/1-butanol mixture, the univolatility curve of ethanol and water is shown in Figure 3. The curve starts from the minimum-boiling azeotrope and reaches the edge of water-butanol, illustrating that ethanol is more volatile than water in the region below the univolatility curve and the volatility order is reversed in the region above the curve, whereas 1-butanol is always less volatile than ethanol and water in distillation region 2. Following the method of Laroche et al. [23], the heterogeneous azeotrope of water and 1-butanol (saddle point *S*1) is recovered as the top product of the double-feed column while ethanol (saddle point *S*2) is taken down the column by 1-butanol. Since the azeotrope of water and butanol is a heterogeneous one, the condenser at the top of the column allows the two liquid phases to be formed. Thus, a decanter equipped at the top of the double-feed column may be applied such that an aqueous phase can be recovered as a product and an organic-rich phase is refluxed back to the column.

From the discussion above, the ethanol dehydration process using 1-butanol is shown in Figure 4. The process comprises a double-feed column with an integrated decanter (*C*-1) and a single-feed column (*C*-2). The ethanol/water azeotropic mixture is added to the double-feed column (*C*-1) as a lower feed, whereas 1-butanol is added as an upper feed. A vapour with a composition close to the heterogeneous azeotrope of water and butanol, which is a saddle point (*S*1), is obtained from the top of the double-feed column and condensed in the decanter where an aqueous phase is recovered. A mixture of ethanol and butanol from the bottom of the column is further separated in

the subsequent simple column (*C*-2) where highly pure ethanol, which is another saddle point (*S*2), is produced. Nearly pure 1-butanol from the simple column is recycled to the double-feed column together with some of the aqueous phase from the decanter.

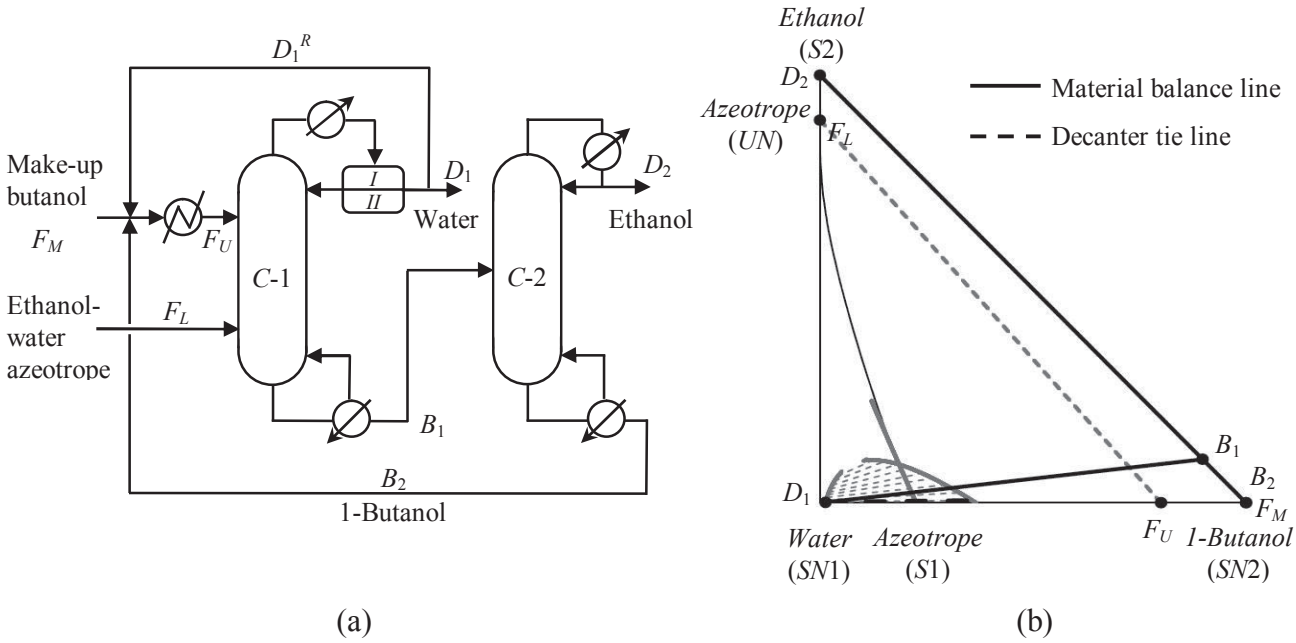

Figure 4. Distillation flowsheet for ethanol dehydration using 1-butanol (a) and triangular diagram showing mass balance of the process (b)

DISTILLATION PROCESS EVALUATION

The separation feasibility and economic performance of the proposed distillation process (Figure 4) were evaluated using the boundary value method developed by Prayoonyong and Jobson [12]. The boundary value method is a column design method for establishing separation feasibility and designing columns for separating ternary ideal and azeotropic mixtures [13]. The method requires the column product composition to be fully specified. Then the liquid composition profiles for each column section are calculated using the material and energy balance over each column section, along with the phase equilibrium at a given reflux (or reboil) ratio. A given set of column specifications is identified as feasible if the intersection of the composition profiles of each column section is found. The number of theoretical stages can then be counted from the composition profiles and the feed location is identified from the intersection of the two profiles. By applying the boundary value design method, a feasible and economically near-optimal column design can be identified systematically. The results from the design method also make possible a comparison of column designs and of distillation processes in terms of an indicator, e.g. total annualised cost. A recent development of the design method allows its application to single- and double-feed columns with integrated decanters in which the presence of two liquid phases is not limited to the decanter [12].

A process simulation software was not applied for evaluating the processes because the simulation of a heterogeneous azeotropic distillation column requires an iterative and exhaustive change in the column design parameters until a converging and/or optimal solution is found [25]. Furthermore, a multiplicity of solutions is commonly encountered in the simulation of heterogeneous azeotropic distillation columns [25, 26].

Before designing the columns in the process (Figure 4) by the boundary value method, the material balance of the process must be completed. In this step, the mole fractions of some components in the product streams of both columns were specified. Then the material balance of the process was solved using Excel to determine the compositions and flow rates of all streams in the process.

Once the material balance of the process is completed, each column in the process can then be designed individually using the boundary value method. The calculation required in applying the boundary value method was performed using MATLAB interfaced with Aspen HYSYS for enthalpy calculation and for retrieving the phase equilibrium properties of the mixture [27]. To design a column, the liquid composition profiles for each column section were calculated stage by stage starting from the specified product compositions using material and energy balances along with phase equilibrium. The composition profiles were generated for a range of key design variables, e.g. reflux ratio, reboil ratio and feed condition. The choice of design variables depends on the type of column. For a column with an overhead integrated decanter, the ratio of the molar flow rate of heavy liquid to that of total liquid in the reflux stream, called reflux phase split ratio, is also a degree of freedom. For the double-feed column, the upper-to-lower feed rate ratio and the location of the lower feed are additional design variables. The proposed separation is feasible if a rectifying profile intersects a stripping profile (for the single-feed column) or a middle section profile (for the double-feed column) in the composition space.

When a feasible column design was found from an intersection of the profiles, its column design parameters at a set of design variables, e.g. number of stages, feed location and heat duties, were obtained. The column designs were searched from a range of key design variables and a number of feasible designs for each column were generated. Those feasible designs were evaluated on the basis of their total annualised costs estimated from their column design parameters. As a result, the most attractive design with the lowest cost was identified. However, the most attractive design found from the boundary value method is the design with economically near-optimal performance because the feasible designs are generated iteratively from a range of design variables.

After the near-optimal designs for all columns have been identified, the total annualised cost of the distillation process can be estimated. The total annualised cost is the sum of operating and annualised capital costs. The capital cost includes the installed costs of the main equipment, i.e. columns, decanters and heat exchangers. They are estimated using cost models [28, 29] based on the sizes of column and decanter vessel, heat transfer area, and materials. The capital cost is annualised over a three-year period with an interest rate of 5%. The operating cost includes the costs of steam and cooling water estimated using cost models [30, 31].

For the proposed distillation flowsheet (Figure 4), the application of the boundary value method indicated that the separations in both columns are feasible. The mass balance of the process was calculated based on fully specified feed and product compositions, initially assuming an upper-to-lower feed rate ratio, as shown in Table 2. The upper-to-lower feed rate ratio was varied later on, ranging from 8 to 15. The top product composition of the double-feed column *C*-1 was specified such that two liquid phases appear in the top decanter and 98.6 mol% water is obtained. The ethanol concentration in the product stream of the process was assigned to be 99 mol% (99.5% v/v). At an upper-to-lower feed rate ratio, a feasible column design for the two columns was searched for a reflux ratio range of 2-15 for column *C*-1 and 2-20 for column *C*-2. For the double-feed column *C*-1, the reflux phase split ratio and reboil ratio were varied within the range of 0-1 and 0.4-0.8

respectively. The location of the lower feed was also changed. Note that some of the aqueous phase from the integrated decanter has to be recycled to mix with 1-butanol from the recovery column and the make-up stream so as to make the separation in the double-feed column feasible. The temperature of the upper feed was determined from the energy balance of the column and only designs that need the upper feed temperature ranging between 35-180^{o}C were accepted.

Table 2. Mass balance of distillation process for ethanol dehydration using 1-butanol in Figure 4 (upper-to-lower feed rate ratio = 8)

	F_L	F_M	F_U	D_1	D_1^R	B_1	D_2	B_2
Composition (mole fraction)								
Ethanol	0.8940[a]	0.0000	0.0001	0.0010[a]	0.0010	0.1016	0.99000[a]	0.0001[a]
Water	0.1060[a]	0.0000	0.0121	0.9860	0.9860	0.0010[a]	0.00975	0.0000
1-Butanol	0.0000	1.0000[a]	0.9878	0.0130[a]	0.0130	0.8974	0.00025[a]	0.9999
Flow rate (kmol h^{-1})	100.00[a]	0.15	800.00	9.86	9.78	880.36	90.29	790.07
Feed condition	Saturated liquid	Saturated liquid						

[a] Specified value

All feasible designs of each column in Figure 4 were evaluated in terms of total annualised costs and the economically near-optimal design was identified. The details of the near-optimal design of the two columns and the total annualised cost of the distillation process are summarised in Table 3. The corresponding composition profiles of the columns are shown in Figure 5. The near-optimal designs were found at the upper-to-lower feed rate ratio of 8. With an upper-to-lower feed rate ratio less than 8, the separation in the double-feed column is infeasible.

Table 3. Summary of near-optimal designs and total annualised costs of columns in ethanol dehydration process using 1-butanol (Figure 4)

	C-1	*C*-2
Upper-to-lower feed ratio	8	-
Reflux ratio	8	8
Reflux phase split ratio	0	-
Reboil ratio	0.5	0.95
Temperature of the upper feed, ^{o}C	43.5	-
Total number of stages	46.2	19.3
Number of stages in the rectifying section	2.7	10.3
Number of stages in the stripping section	16	-
Number of stages in the middle section	29.5	-
Condenser duty, kW	2094	8696
Reboiler duty, kW	5406	8954
Heating duty of the heat exchanger *HX*-1, kW	3567	-
Total annualised cost, million bahts per year	61	104
Total annualised cost, million bahts per year	165	

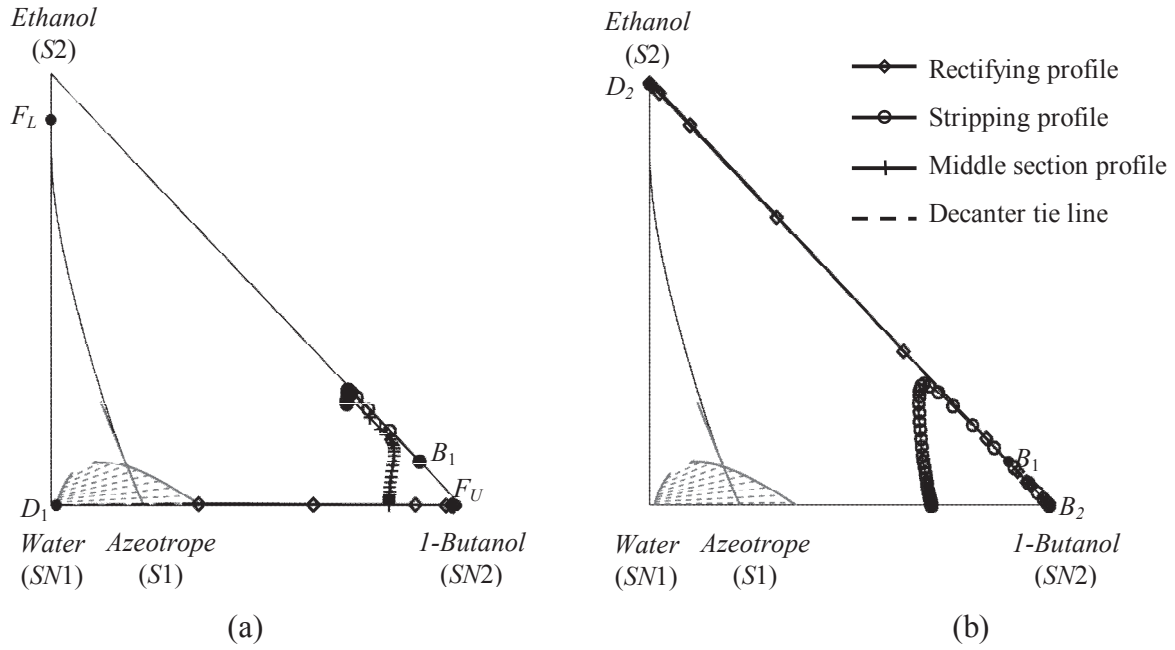

Figure 5. Liquid composition profiles of (a) the double-feed column *C*-1 and (b) the single-feed column *C*-2 in Figure 4, calculated from the boundary value method according to specifications and design results in Tables 2 and 3

COMPARISON OF ETHANOL DEHYDRATION PROCESSES

To compare with the ethanol dehydration process using 1-butanol (Figure 4), the columns in the distillation process using benzene as entrainer shown in Figure 2 were designed by applying the boundary value method and evaluated with respect to its total annualised cost. The residue curve map and the heterogeneous boiling envelope of the ethanol/water/benzene mixture at 101.3 kPa were calculated using MATLAB interfaced with Aspen HYSYS for retrieving the phase equilibrium properties of the mixture. The UNIQUAC-ideal gas model [15] and the interaction parameters in Aspen HYSYS [15] were used for predicting the phase equilibrium. The mass balance over the process and the details and costs of the near-optimal design are shown in Tables 4 and 5. The top-product composition of the first column *C*-1 was selected such that it is located in the two-phase region and a part of its corresponding tie line is in the same region as the bottom product (see Figure 6a). Feasible designs of the column with the integrated decanter *C*-1 were searched for the ranges of reflux ratio and reflux phase split ratio of 6-11 and 0-1 respectively. For the simple column *C*-2, the reflux ratio was varied from 5 to 15. The composition profiles of the columns corresponding to the process mass balance and design results in Tables 4 and 5 are shown in Figure 6.

Table 4. Mass balance of the distillation process for ethanol dehydration using benzene (Figure 2)

	F	F_M	F'	D_1	B_1	D_2	B_2
Composition (mole fraction)							
Ethanol	0.8940[a]	0.0000	0.8018	0.3800[a]	0.99000[a]	0.5000[a]	0.0060
Water	0.1060[a]	0.0000	0.1221	0.3740	0.00975	0.1751	0.9940
Benzene	0.0000	1.0000[a]	0.0760	0.2460	0.00025[a]	0.3249	1×10^{-6} [a]
Flow rate (kmol h^{-1})	100.00[a]	0.02	130.50	40.26	90.24	30.48	9.78
Feed condition	Saturated liquid	Saturated liquid					

[a] Specified value

Table 5. Summary of near-optimal designs and total annualised costs of columns in ethanol dehydration process using benzene (Figure 2)

	C-1	*C*-2
Reflux ratio	7.25	8
Reflux phase split ratio	0.29	-
Reboil ratio	3.44	24.74
Number of heterogeneous stages in the rectifying section (from the top)	2	-
Phase split ratio of the last heterogeneous stage	0.3	-
Total number of stages	17.1	8.9
Number of stages in the rectifying section	2.5	8.9
Condenser duty, kW	3309	2897
Reboiler duty, kW	3323	2905
Total annualised cost, million bahts per year	88	35
Total annualised cost, million bahts per year	123	

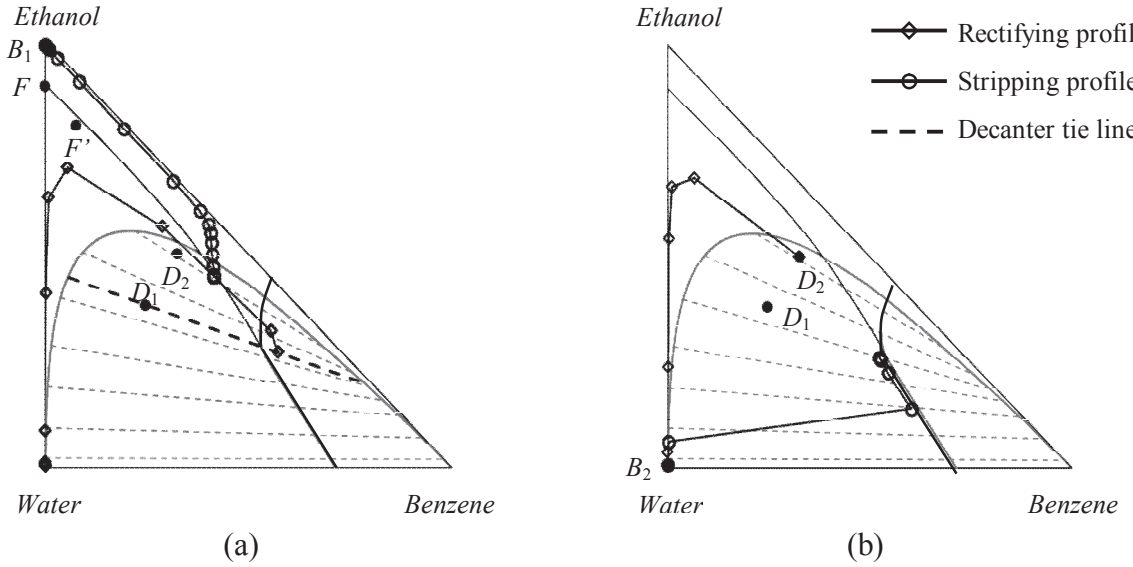

Figure 6. Liquid composition profiles of columns in Figure 2 (calculated from boundary value method corresponding to specifications and designs in Tables 4 and 5): (a) column with integrated decanter *C*-1; (b) simple column *C*-2

According to Tables 3 and 5, the proposed process using 1-butanol is more expensive than that using benzene. The columns in the proposed process (Figure 4) require more theoretical stages and heat duties than those in the process using benzene (Figure 2). In particular, the high cost of the distillation process using butanol stems from the cost of butanol recovery column (column *C*-2 in Figure 4). In column *C-2* in Figure 4, not only is nearly pure ethanol recovered at the top, but also highly pure butanol is obtained at the bottom. The butanol recovery column requires a large amount of heat duties due to the higher boiling point of 1-butanol compared to that of benzene while the prices of the two entrainers are presently close to each other.

Although the cost of ethanol dehydration process using 1-butanol may be higher than that using benzene, 1-butanol is less toxic than benzene and while there is no limitation of butanol remaining in the fuel-graded ethanol since butanol is an alternative biofuel, the level of benzene in ethanol-blended fuels is limited by laws in many countries [32, 33]. The proposed process may also be further developed and become more economically attractive by applying another entrainer that

leads to the same residue curve map topological structure as that for butanol but with a lower price. Also, in this study only single- and double-feed columns integrated with overhead decanters were considered in process design. By synthesising the process taking into account other design options, e.g. types of columns and splits, ethanol dehydration using butanol may turn out to be competitive with the conventional method.

CONCLUSIONS

From the distillation flowsheet for ethanol dehydration generated based on residue curve map analysis and assessed using the boundary value design method, the results show that 1-butanol can be used as an entrainer for ethanol dehydration, in which a double-feed column with an integrated decanter and a simple column are used. However, although environmentally favourable, the process using 1-butanol may not be as yet economically attractive compared to that using benzene.

ACKNOWLEDGEMENTS

The author gratefully acknowledges financial support from the Energy Policy and Planning Office, Ministry of Energy, Royal Thai Government. The author is grateful for the kind assistance from Assoc. Prof. Dr. Anawat Sungpet at King Mongkut's University of Technology Thonburi, where Aspen HYSYS was available. The author also thanks Warumporn Pejpichestakul, Parichat Laothong, Nakarin Chamnanpaisont and Darika Bhatia for their assistance.

REFERENCES

1. H. J. Huang, S. Ramaswamy, U. W. Tschirner and B. V. Ramarao, "A review of separation technologies in current and future biorefineries", *Sep. Purif. Technol.*, **2008**, *62*, 1-21.
2. K. Kubierschky, "Verfahren zur Gewinnung von hochprozentigen, bezw. absoluten Alkohol-Wassergemischen in unterbrochenem Betriebe", *German Patent*, *287,897* (**1915**).
3. S. Young, "LXXIII. - The preparation of absolute alcohol from strong spirit", *J. Chem. Soc. Trans.*, **1902**, *81*, 707-717.
4. I. A. Furzer, "Synthesis of entrainers in heteroazeotropic distillation systems", *Can. J. Chem. Eng.*, **1994**, *72*, 358-364.
5. C. Black, "Distillation modeling of ethanol recovery and dehydration processes for ethanol and gasohol", *Chem. Eng. Prog.*, **1980**, *76*, 78-85.
6. A. Font, J. C. Asensi, F. Ruiz and V. Gomis, "Application of isooctane to the dehydration of ethanol. Design of a column sequence to obtain absolute ethanol by heterogeneous azeotropic distillation", *Ind. Eng. Chem. Res.*, **2003**, *42*, 140-144.
7. V. Gomis, R. Pedraza, O. Francés, A. Font and J. C. Asensi, "Dehydration of ethanol using azeotropic distillation with isooctane", *Ind. Eng. Chem. Res.*, **2007**, *46*, 4572-4576.
8. V. Gomis, A. Font, R. Pedraza and M. D. Saquete, "Isobaric vapor-liquid and vapor-liquid-liquid equilibrium data for the water-ethanol-hexane system", *Fluid Phase Equilibr.*, **2007**, *259*, 66-70.
9. H. N. Pham and M. F. Doherty, "Design and synthesis of heterogeneous azeotropic distillations-III. Column sequences", *Chem. Eng. Sci.*, **1990**, *45*, 1845-1854.

10. D. B. Van Dongen and M. F. Doherty, "Design and synthesis of homogeneous azeotropic distillations. 1. Problem formulation for a single column", *Ind. Eng. Chem. Fundamen.*, **1985**, *24*, 454-463.
11. S. Widagdo and W. D. Seider, "Azeotropic Distillation", *AIChE J.*, **1996**, *42*, 96-130.
12. P. Prayoonyong and M. Jobson, "Flowsheet synthesis and complex distillation column design for separating ternary heterogeneous azeotropic mixtures", *Chem. Eng. Res. Des.*, **2011**, *89*, 1362-1376.
13. M. F. Doherty and M. F. Malone, "Conceptual Design of Distillation Systems", International Edn., McGraw-Hill, Singapore, **2001**.
14. MATLAB Release 2011, The MathWorks, Inc., Natick (MA), USA.
15. "Aspen HYSYS Simulation Basis Guide", Aspen Technology Inc., Burlington (MA), **2011**.
16. K. Iwakabe and H. Kosuge, "Isobaric vapor-liquid-liquid equilibria with a newly developed still", *Fluid Phase Equilibr.*, **2001**, *192*, 171-186.
17. V. Gomis, F. Ruiz and J. C. Asensi, "The application of ultrasound in the determination of isobaric vapour-liquid-liquid equilibrium data", *Fluid Phase Equilibr.*, **2000**, *172*, 245-259.
18. D. Y. C. Thong and M. Jobson, "Multicomponent homogeneous azeotropic distillation 1. Assessing product feasibility", *Chem. Eng. Sci.*, **2001**, *56*, 4369-4391.
19. G. Ji and G. Liu, "Study on the feasibility of split crossing distillation compartment boundary", *Chem. Eng. Process.: Process Intensificat.*, **2007**, *46*, 52-62.
20. J. J. Siirola, "Strategic process synthesis: Advances in the hierarchical approach", *Comput. Chem. Eng.*, **1996**, *20*, S1637-S1643.
21. A. S. Moussa and L. Jiménez, "Entrainer selection and systematic design of heterogeneous azeotropic distillation flowsheets", *Ind. Eng. Chem. Res.*, **2006**, *45*, 4304-4315.
22. V. N. Kiva, E. K. Hilmen and S. Skogestad, "Azeotropic phase equilibrium diagrams: A survey", *Chem. Eng. Sci.*, **2003**, *58*, 1903-1953.
23. L. Laroche, H. W. Andersen, M. Morari and N. Bekiaris, "Homogeneous azeotropic distillation: Comparing entrainers", *Can. J. Chem. Eng.*, **1991**, *69*, 1302-1319.
24. I. R. Donis, J. A. Esquijarosa, V. Gerbaud and X. Joulia, "Heterogeneous batch-extractive distillation of minimum boiling azeotropic mixtures", *AIChE J.*, **2003**, *49*, 3074-3083.
25. S. K. Wasylkiewicz, L. C. Kobylka and F. J. L. Castillo, "Optimal design of complex azeotropic distillation columns", *Chem. Eng. J.*, **2000**, *79*, 219-227.
26. R. Gani and S. B. Jørgensen, "Multiplicity in numerical solution of non-linear models: Separation processes", *Comput. Chem. Eng.*, **1994**, *18*, S55-S61.
27. P. Prayoonyong, "Synthesis and design of ternary heterogeneous azeotropic distillation processes including advanced complex column configurations", *PhD Thesis*, **2009**, University of Manchester, UK.
28. A. M. Gerrard, "Guide to Capital Cost Estimating", 4th Edn., Institution of Chemical Engineers, Rugby (UK), **2000**.
29. M. S. Peters, K. D. Timmerhaus and R. E. West, "Plant Design and Economics for Chemical Engineers", 5th Edn., McGraw-Hill, New York, **2002**.
30. R. Smith, "Chemical Process Design and Integration", John Wiley and Sons, Chichester, **2005**.
31. G. D. Ulrich and P. T. Vasudevan, "How to estimate utility costs", *Chem. Eng.*, **2006**, *113*, 66-69.

32. Department of Environment, Australian Government, "Ethanol E85 fuel quality and fuel quality information standards", **2012**, http://www.environment.gov.au/topics/environment-protection/fuel-quality/standards/ethanol-e85 (Accessed: October 2014).
33. Renewable Fuels Association, "Fuel ethanol: Industry guidelines, specifications and procedures", **2011**, http://www.ethanolrfa.org/pages/industry-resources-guidelines (Accessed: October 2014).